Three-dimensional studies of the developing mammalian cornea

A thesis submitted to Cardiff University for the degree of Doctor of Philosophy

August 2019

Eleanor Mai Feneck

Structural Biophysics Group

School of Optometry and Vision Sciences

Cardiff University

Supervisors:

Professor Keith Meek

Dr Philip Lewis

Abstract

This thesis aimed to understand the structural changes that occur during the development of the mammalian cornea. The imaging techniques used included novel three-dimensional serial block-face scanning electron microscopy, transmission electron microscopy, optical coherence tomography, X-ray diffraction and immunofluorescence. These techniques were utilised to investigate the human, mouse and the fibrillin-1 knockout mouse cornea.

The mouse cornea had no collagenous primary stroma to direct mesenchymal cell migration. Stromal cell projections associated with adjacent corneal stromal cells and the corneal epithelium, and appeared to direct collagen alignment. The mouse stroma expressed types I, II and V collagen, and later type IX collagen in the epithelium. Proteoglycans were observed before collagen deposition in the mouse stroma, associated with stromal cells and collagen fibrils.

A collagenous primary stroma was identified in the human embryonic cornea prior to mesenchymal cell migration. The corneal endothelium contained novel cell extensions that associated with the mesenchymal cells and the acellular collagenous matrix; these results suggested that the endothelium assists mesenchymal cell migration.

The human adult cornea contained true elastic fibres in the peripheral posterior cornea with fibrillin-rich microfibrils in the central posterior cornea. The elastic fibres in the mouse contained only fibrillin-rich microfibrils. In the human, elastic fibres were detected from week 12 of development and had a distribution similar to the mature human cornea. This included elastic fibre

sheets directly anterior to the endothelium and individual elastic fibres in the posterior peripheral stroma.

The fibrillin-1 knockout mouse cornea had reduced stromal thickness and a disorganised extracellular matrix. It is thought that elevated transforming growth factor-beta disrupted the corneal architecture.

This thesis has contributed novel findings of the events that develop the mammalian cornea. The results identified fundamental differences and similarities between the mouse and human models and have suggested new mechanisms in the developmental process.

Acknowledgements

First and foremost, I would like to acknowledge my supervisors Professor Keith Meek and Dr Philip Lewis for their continued support and expert knowledge throughout my PhD journey.

Following this, I would like to thank Dr Rob Young and Dr Jim Ralphs for their expertise in developmental biology and extracellular matrix and their helpful advice with laboratory work. I acknowledge Dr Sally Hayes and Dr James Bells for their assistance in the collection of the X-ray data at Diamond. I also acknowledge the technical support team on beamline I22 at Diamond, UK, which granted the collection of meaningful data for my PhD thesis.

I especially acknowledge Professor Lygia Pereira and Dr Rodrigo Barbosa for the fibrillin-1 knockout mouse model developed and collected from their laboratory in Sao Paulo, Brazil. This collaboration allowed me to undertake novel research which I believe has generated exciting results for future study.

I also thank the School of Optometry and Vision Sciences and give special thanks to the members of the Structural Biophysics group for their continued support and encouragement throughout my PhD.

I am grateful to my family and friends for their continued support. I especially thank Gregor and family for their continued support throughout my PhD journey. Lastly, I would like to give a special thanks to my parents, sister and grandparents for their continued support throughout my academic career and for always encouraging me.

List of publications

Feneck. E.M, Lewis. P.N, Ralphs. J., Meek. K.M. (2018). A comparative study of the elastic fibre system within the mouse and human cornea. *Experimental Eye Research.* Volume 11. Pages 35-44.

Feneck. E.M, Lewis. P.N., Meek. K.M. (2019). Three-dimensional imaging of the extracellular matrix and cell interactions in the developing prenatal mouse cornea. *Scientific Reports.* Volume 9: 11277.

List of Abbreviations

ARVO	Association for Research in Vision and Ophthalmology
BL	Basal lamina
BMP	Bone morphogenetic protein
CB	Ciliary body
CS	Carnegie stage
DM	Descemet's membrane
E	Embryonic day
$FBN1^{+/-}$	$mg\Delta^{LoxPneo}$ fibrillin-1 knockout mouse model
GAGs	Glycosaminoglycans
HA	Hyaluronic acid
HDBR	Human developmental Biology Resource
H_20	water
IOP	Intraocular pressure
IFS	Interfibrillar spacing
L	Lens

LE	Lens epithelium
MCs	Mesenchymal cells
OCT	Optical coherence tomography
PBST	Phosphate buffered saline-Tween-20
POAG	Primary open angle glaucoma
P	Postnatal day
PGs	Proteoglycans
ROI	Region of interest
SAXS	Small angle X-ray scattering
SBF-SEM	Serial block-face scanning electron microscopy
SC	Schlemm's canal
SE	Surface ectoderm
SLRPs	Small leucine rich proteoglycans
TA	Tannic acid
TEM	Transmission electron microscopy
TGF-β	Transforming growth factor beta

3-D	Three-dimensional
TM	Trabecular meshwork
UA	Uranyl acetate
WT	Wild type

Table of Contents

Table of Figures

Table of Tables

Chapter 1: Introduction

1.1. Cornea

The cornea is a transparent connective tissue with a curved architecture located at the front of the anterior chamber of the eye, running into the sclera at the limbus (Moore et al. 2013). Together with the lens, the cornea focuses light onto the retina. Photoreceptors then transmit impulses along the optic nerve towards the brain to yield an image with minimal distortion (**Figure 1.1**) (Remington and Remington 2012).

Posterior

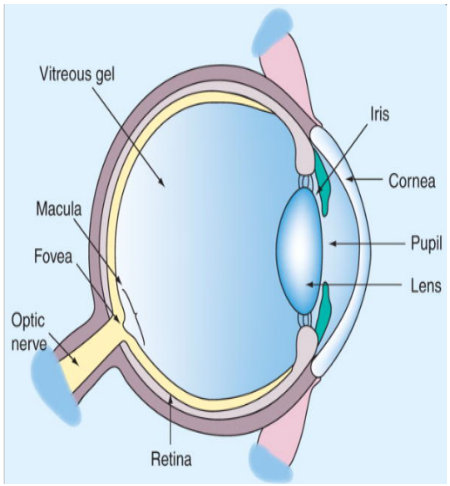

Anterior

Figure 1.1. A Schematic sagittal section of the human eye.

For vision, light must pass through the anterior portion of the eye with minimal light scatter, and be reflected onto the retina. Photoreceptors then transmit signals along the optic nerve towards the brain to generate an image. The anterior segment of the eye is composed of the cornea, lens, iris and ciliary body and they must act as a unit with the surrounding muscles and nerves to successfully allow light to focus onto the retina. Image taken from (Niederkorn 2009), with permission under the Taylor and Francis copyright policy.

1.1.1. Function and Transparency

The cornea provides two-thirds of the eyes refractive power (~43 dioptres) to direct light onto the retina with minimal light scatter (Ganguli et al. 1975, Meek et al. 2003). This is achieved by the unique shape and ultrastructure of the cornea, which provides a transparent and biomechanically strong tissue. Corneal transparency is determined by the arrangement of individual collagen fibrils within lamellae, avascularity and the presence of specialised proteins (proteoglycans and crystallins) within the cornea (Meek and Knupp 2015). Early studies demonstrated that the number density of collagen fibrils and their arrangement are vital for permitting corneal transparency. Maurice hypothesised the lattice theory, where collagen fibrils cause destructive interference of scattered light (Maurice 1957). The lattice theory was further modified by studies which proposed the distance between the collagen fibrils minimised light scatter, with the absence of fluctuations in refractive index (on the scale of the wavelength of light) between the collagen fibrils (Goldman and Benedek 1967). The arrangement of collagen fibrils forms a short-range order, and the secondary radiation scattered by the narrow collagen fibrils cumulates. This causes destructive interference of scattered light and leaves the forward radiation to carry the energy of the incoming light through the cornea. The importance of the collagen fibrillar ultrastructure has been further demonstrated by alterations reducing visual acuity. A discontinuity in the spacing between collagen fibrils and any significant increase in collagen fibril diameters enhance light scatter and reduce transparency (Goldman and Benedek 1967).

To maintain transparency the cornea must also remain avascular (Chang et al. 2001). This has the added advantage of isolating the cornea from the immune system, which delays the immune response and benefits treatment strategies for corneal transplantation (Streilein 2003). However, it also makes the cornea vulnerable to disease. To overcome this limitation, aqueous humor provides the cornea with its main protection and immune response when required (Cousins et al. 1991).

In addition to the low light scattering properties of the cornea, the tissue also acts as a shield to protect the contents located posteriorly from foreign material and damage (DelMonte and Kim 2011). The cornea must remain strong and resilient to withstand the biomechanical forces it experiences, maintaining its physiological shape and organised configuration. If the normal architecture or transparency of the cornea is disrupted, which is seen in corneal diseases, such as keratoconus, or after surgical complications, visible light is unable to focus onto the retina and clarity of the overall image is lost (Bao et al. 2016, Nishtala et al. 2016).

1.1.1.1. Structure

Traditionally, the human cornea is composed of five layers, each having different roles that contribute to tissue function (***Figure 1.2***). Different genes have been identified within the individual layers that indicate each layer has a different function to the next (Norman et al. 2004). An additional layer was recently suggested and termed ‘Dua’s layer’ (Dua et al. 2013). However, this proposed layer has been shown by further studies to be a part of the existing stroma with an enhanced elastic fibre network (Lewis et al. 2016). Even though these layers have been identified in the human cornea, the mouse cornea lacks Bowman’s layer and is therefore composed of four layers (Hendrich 2012).

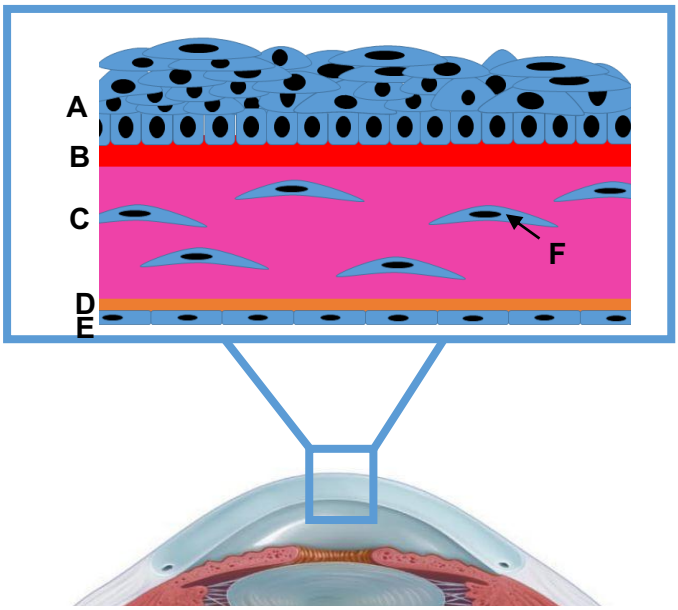

Figure 1.2. A schematic cross-section of the human cornea.

A - The epithelial layer, approximately 50-90 µm thick.
B - The approximate location of Bowman's layer that is 8-14 µm thick.
C - Corneal stroma, approximately 500 µm thick.
D - The approximate location of Descemet's membrane, which increases in thickness throughout an adult's life to approximately 12 µm.
E - The endothelial layer, around 10 µm in thickness at birth and decreasing to around 3-5 µm with age.
F – Cells (termed keratocytes) within the stroma

1.1.1.2. Epithelium

The epithelium is the outmost layer of the cornea; it is continuous with the conjunctival epithelium at the limbus and is separated from the collagenous stroma by a basal lamina. The epithelium acts as a protective barrier against foreign material and pathogens (Simon et al. 1993). The epithelium is composed of approximately four to five layers of non-keratinised stratified squamous epithelial cells and a monolayer of columnar basal cells posteriorly (Remington and Remington 2012). The co-ordinated turnover and communication of these cells is vital to maintain the corneal structure. Epithelial cells readily replenish to maintain the epithelium, with the superficial cells being continually replaced by the deeper basal cells (Wiley et al. 1991). The basal cells are attached to the basement membrane and provide the wing

cells, which stratify anteriorly to form the flattened superficial cells with projecting surface microvilli, increasing the surface area to allow close associations with the tear film (DelMonte and Kim 2011, Zieske 2004). This strong attachment is responsible for the epithelium being firmly bound to the underlying Bowman's layer (Torricelli et al. 2013).

There are many junctions between epithelial cells, which provide the epithelium with communication and strength to enhance its function as a barrier (Mantelli et al. 2013, Remington and Remington 2012). The epithelium is covered by a tear film which protects the corneal surface and provides most of the eye's refractive power at the air-tear interface (Patel et al. 1995). The tear film is composed of mucins-1, -4, and -16, which independently form a glycocalyx, a glycoprotein coating that helps bind transmembrane mucins to the corneal surface, this attracts water molecules and provides additional protection to the corneal surface (Gipson and Argueso 2003, Mantelli et al. 2013). The superficial and wing cells also have a high glycogen content that contributes a protective function and provides an energy source to the epithelium; this content decreases during repair (Bron et al. 1997).

For maintenance of the cornea, the epithelium is continually renewed by stem cells located within the limbus (Kruse 1994). Deficiency within the limbal stem cell (LSC) niche leads to complications during corneal wound repair, leading to a decreased visual acuity (Kocaba et al. 2016). Strategies to combat the use of LSCs in corneal tissue engineering are being explored to improve repair and regeneration in corneal diseases, especially where the epithelium is dysfunctional (Gonzalez et al. 2018).

1.1.2. Bowman's Layer

Bowman's layer is an acellular fibrous layer composed of collagen fibrils arranged randomly within the extracellular matrix (Bettman 1970). This layer was first identified by William Bowman in the late 19th century with its unique organisation of collagen fibrils, thought to assist the maintenance of corneal

curvature (Jacobsen et al. 1984, Patel et al. 1998). Type I collagen is the main collagen type present within Bowman's layer, but small amounts of type XII collagen have also been identified during development (Marchant et al. 2002). The Bowman's layer is described as a transition layer to the stroma as a result of the arrangement of collagen fibrils. The collagen fibrils within Bowman's layer are thinner in diameter compared to the collagen fibrils found within the stroma, with a greater organisation and increased thickness at locations closer to the stroma (Lao and Tang 2014). Even though Bowman's layer is thought to be important within the human cornea, it has been described to be much thinner or absent in electron microscopy analysis in less developed mammals, including the mouse, this suggests that it is not an essential structure within all mammalian corneas (Hayashi S. et al. 2002, Hendrich 2012).

1.1.3. Corneal Stroma

The stroma is a highly organised layer that constitutes approximately 90% of the corneal thickness (Reinstein et al. 2009). The stroma contains collagen fibrils organised in arrays of lamellae, proteoglycans, cells and ions. Collagen molecules assemble themselves into parallel collagen fibrils which in turn are arranged in lamellae that run predominantly, but not exclusively, in the superior to inferior and nasal to temporal directions in the human cornea (Meek and Boote 2004). There are around 200 to 300 lamellae lying parallel to the corneal surface through the central cornea, with packing density increasing in the anterior lamellae when compared to the posterior lamellae, and the number of lamellae increasing towards the corneal periphery (Bergmanson et al. 2005, Hamada et al. 1972). Studies have demonstrated the arrangement of lamellae within the cornea using electron microscopy and X-ray scattering techniques (Abass et al. 2015, Aghamohammadzadeh et al. 2004). These techniques have enhanced our knowledge of the organisation of proteins within the cornea, to further understand the corneal structure. The arrangement of lamellae provides the main strength to resist load-bearing forces that the cornea may experience, with lamellar interweaving enhancing corneal strength and tear resistance (Smolek and McCarey 1990). The corneal stroma

is mainly composed of heterodimeric fibrils of type I and V fibril-forming collagen molecules; these are responsible to regulate fibril assembly and fibril diameter (Birk et al. 1990, Birk et al. 1986, Wenstrup et al. 2004, Wenstrup et al. 2006). Type IX collagen is important during the early synthesis of the avian corneal stroma, for matrix stabilisation and cell migration, being absent when the tissue is mature (Fitch J. et al. 1998, Fitch J. M. et al. 1994).

The anterior and posterior stoma have a different lamellar organisation, changing the properties within these compartments. Lamellae within the posterior stroma are more organised and hydrated, with wider collagen fibril diameters compared with the anterior stromal lamellae (Komai and Ushiki 1991, Quantock A. J et al. 2007). Posterior stromal lamellae run from limbus to limbus, parallel to the corneal surface, with fibrils interweaving away from the central cornea. X-ray scattering techniques have shown that the inclination angle in the posterior peripheral cornea is increased, therefore interweaving is increased when compared to the central posterior cornea (Abass et al. 2015). As a result of the lamellar arrangement, the posterior stroma is more easily swollen and has a lower refractive index compared to the anterior stroma (Muller et al. 2001). Collagen fibrils within the anterior stroma are increasingly interwoven with frequent branching but are more randomly organised due to the interweaving of lamellae. Lamellae within the anterior stroma insert into Bowman's layer; this creates an attachment for the stroma, and additionally adds rigidity and enhances the curvature of the human cornea (Morishige et al. 2011). The organisation of the interweaving lamellae within the stroma is vital to maintain a functional cornea. This arrangement is disrupted in corneal diseases, including keratoconus, where the shape, and consequently the function of the cornea is lost (Akhtar et al. 2013).

Keratocytes occupy approximately 20% of the stroma and are responsible for extracellular matrix synthesis and deposition (Chen S. et al. 2015, Young et al. 2014). Keratocytes are mesenchymal fibroblasts, derived from cranial neural crest cells and lie between lamellae (Hay E.D. 1980). The high proliferation rate of keratocytes during embryogenesis for collagen synthesis decreases in mice between birth and the process of eyelid opening (Zieske

2004). Keratocytes remain in a cell arrest phase and do not undergo complete differentiation until required, e.g. during repair and regeneration (Zieske 2004). In repair, keratocytes become more active, transforming into myofibroblasts to remodel the extracellular matrix (Lakshman et al. 2010, West-Mays and Dwivedi 2006). Keratocytes possess long-range processes, which are thought to align the extracellular matrix in avian corneal development (Koudouna et al. 2018a, Young et al. 2014); this has not been explored in the mammalian cornea. Extracellular matrix components, including fibronectin, have also been identified to arrange stromal collagen, which identifies components other than cells to assist collagen organisation (Gordon 2014).

Keratocytes also contribute to maintaining transparency through their crystallin proteins (Jester et al. 1999). These corneal crystallins concentrate within the cell cytoplasm to minimise fluctuations in refractive index, thus reducing light scattering (Gardner et al. 2015). Throughout the corneal stroma, keratocytes display diverse morphologies at different locations and change shape during pathologies. Previous studies have identified stromal cells to be sensitive to glucose, with an altered phenotype, identifying the importance of nutrient homeostasis for keratocyte phenotype (Foster et al. 2015).

1.1.4. Descemet's Membrane

Considered the basement membrane for the endothelial layer, Descemet's membrane lies between the stroma and the endothelium (Remington and Remington 2012). Descemet's membrane is continually synthesised and laid down by endothelial cells, increasing in thickness with age (Bourne 2003).

Descemet's membrane contains two zones, the anterior banded zone and the posterior non-banded zone (Levy S. G. et al. 1995). The anterior zone contains organised collagen throughout its extracellular matrix and the posterior zone contains an amorphous matrix with different components. There is a connection formed by collagen fibrils from the posterior stroma which project into Descemet's membrane, where a pre-Descemet's layer has been

hypothesised; however, no clear evidence of this layer has yet been found (Dua et al. 2013, Lewis et al. 2016, Meek and Knupp 2015).

Type IV collagen is the main collagen of Descemet's membrane (Fitch J. M. et al. 1990). Type IV collagen allows cellular processes including adhesion, migration and differentiation to occur smoothly (Ito et al. 2015). In addition, type VIII collagen is important for Descemet's membrane formation during development, which assists corneal stability (Puk et al. 2009). Fibronectin has also been identified within Descemet's membrane to adhere the corneal endothelium to Descemet's membrane (Gordon 2014). Fibronectin also promotes successful cell migration in development and repair, indicating Descemet's membrane to have a regulatory role in corneal assembly (Levy S. G. et al. 1995). The basement membrane has also been described to maintain corneal homeostasis by controlling the release of transforming growth factor beta (TGF-β) into the stroma, thus regulating the fibrotic response during repair (Stramer et al. 2003). The identification of TGF-β and fibronectin indicates that this layer is important during wound healing and may disrupt wound healing if damaged.

1.1.5. Corneal Endothelium

The endothelial layer is the innermost layer of the cornea, composed of a single layer of cuboidal cells which forms the posterior border of the cornea (DelMonte and Kim 2011). The endothelium maintains a transparent cornea, and damage to this layer can lead to severe vision loss (Zavala et al. 2013). Without the endothelium, the hydrophilic cornea would swell and disrupt the collagen fibrils, which could result in an opaque cornea (Bourne 2003). The critical hydrated state of the stroma is maintained by the endothelium, which contains pumps that regulate nutrients and metabolic wastes. This occurs by tight junctions that generate an ion gradient and continually pump water out of the cornea (He et al. 2016, Noske et al. 1994). The corneal endothelium additionally secretes matrix components that form Descemet's membrane (Bourne 2003). Cellular components which include gap junctions (connexin

43), vimentin and N-cadherin also contribute to endothelial function and can protect cells against mechanical stress; these components may also regulate and protect the endothelial cells from intraocular pressure (IOP) fluctuations (He et al. 2016, Williams and Watsky 2002).

1.2. Corneal Extracellular matrix

The cornea is mainly composed of water (~80%), with the remainder comprising extracellular matrix proteins, salts and cellular components. Corneal stromal cells, known as keratocytes, are responsible for the synthesis of the mature stroma within the cornea and it is the extracellular matrix organisation throughout development that provides the cornea with its physiological shape and function (Young et al. 2014). Alterations to the matrix organisation may contribute to corneal diseases, where its overall shape, transparency and function is lost (Chakravarti et al. 2000, Liu C. Y. et al. 2003, White et al. 2017a).

1.2.1. Collagen

Collagen is the most abundant protein in the human body, essential in providing tissues with their biomechanical properties and tensile strength (Canty and Kadler 2005, Ricard-Blum 2011). Collagen fibrils within the cornea establish the cornea's shape, transparent nature and function in focusing incoming visual light. These fibrils also give the cornea durability and strength to maintain its architecture when forces are applied (Meek and Boote 2004). Collagen fibrils lie parallel within superimposing lamellae, with a regular diameter between individual collagen fibrils, maintaining the cornea's mechanical strength and transparency respectively (Maurice 1957).

Collagen molecules are triple helical structures composed of three polypeptide chains, known as α chains (Pauling and Corey 1951). Each α chain contains

a glycine amino acid every third residue to form a repeating Gly-X-Y structure, usually X and Y represent proline and hydroxyl-proline respectively (Kadler et al. 1996). These residues form a left-handed helical structure which, when combined with the two additional helices, forms a right-handed triple helix (tropocollagen molecule) with enhanced stability (Ramachandran and Kartha 1954, Rich and Crick 1961, Shoulders and Raines 2009). Within a cross-section of a corneal collagen fibril, approximately 300-400 triple-helical molecules exist (Meek and Leonard 1993). Within most connective tissues including tendons and the sclera, collagen molecules are staggered to produce a D-periodicity of ~67 nm. Within the cornea, the microfibrils within fibrils are tilted to ~15° to the fibrils long axis in a right-handed helix (Holmes et al. 2001). The subsequent tilt within the cornea reduces the axial periodicity to a smaller value of ~65 nm (Yamamoto et al. 2000) (**Figure 1.3**).

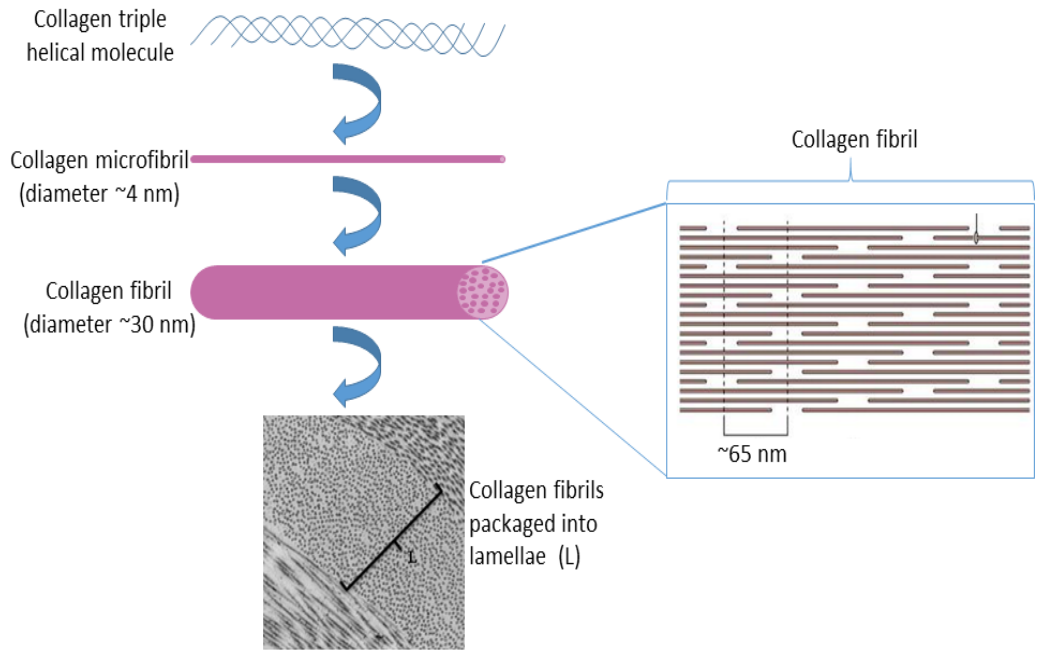

Figure 1.3. Collagen Structure.

Collagen molecules assemble into a left-handed triple helix, which further self-assemble into a staggered array to form microfibrils which coil together to form a collagen fibril. There are ~70 microfibrils within each collagen fibril, which are subsequently tilted by 15° to the fibril long axial. This tilt reduces the axial periodicity to 65 nm in the cornea. The alternating twists at each hierarchical level enhances strength within the corneal collagen fibrils. The collagen fibrils are then packaged into lamellae which maintain corneal shape, strength and corneal birefringence (Meek and Knupp 2015).

1.2.1.1. Collagen Biosynthesis

Initially, procollagen genes are transcribed into mRNA and translated in the cytosol into pro-α polypeptide chains, protruding into the lumen of the rough endoplasmic reticulum with the help of a signal recognition domain by the corresponding receptors (Gelse 2003). Selected prolyl and lysyl residues are then hydroxylated, with the addition of a hydrogen and oxygen element. Hydroxylysine residues are further glycosylated with glucose and galactose. Three pro-α chains assemble in the endoplasmic reticulum, which forms a triple helix. Procollagens are translocated to the Golgi apparatus and packaged into secretory vesicles that fuse with the cell membrane, being released into the extracellular matrix after post-translational modifications (Gelse et al. 2003). Once secreted extracellularly, procollagens are then processed depending on the collagen type. Pro-collagen contains an N- and C-terminal pro-peptide which are cleaved by the N- and C- proteinases to produce a resultant tropocollagen molecule. Cleavage of the C-pro-peptide on the pro-collagen by a metalloproteinase initiates collagen fibrillogenesis, and further allows the molecules to aggregate into fibrils (Canty and Kadler 2005, Shoulders and Raines 2009). Oxidation of lysine side chains via lysyl oxidase (LOX) leads to the formation of hydroxylysyl pyridinoline and lysyl pyridinoline cross-links. Collagen molecule cross-linking occurs in the terminal step of collagen synthesis to increase the tensile strength of collagen fibrils (Hassell and Birk 2010). Once collagen fibrillogenesis is complete, mature collagen fibrils are packaged into lamellae and organised to provide the cornea with strength and transparency (**Figure 1.4**).

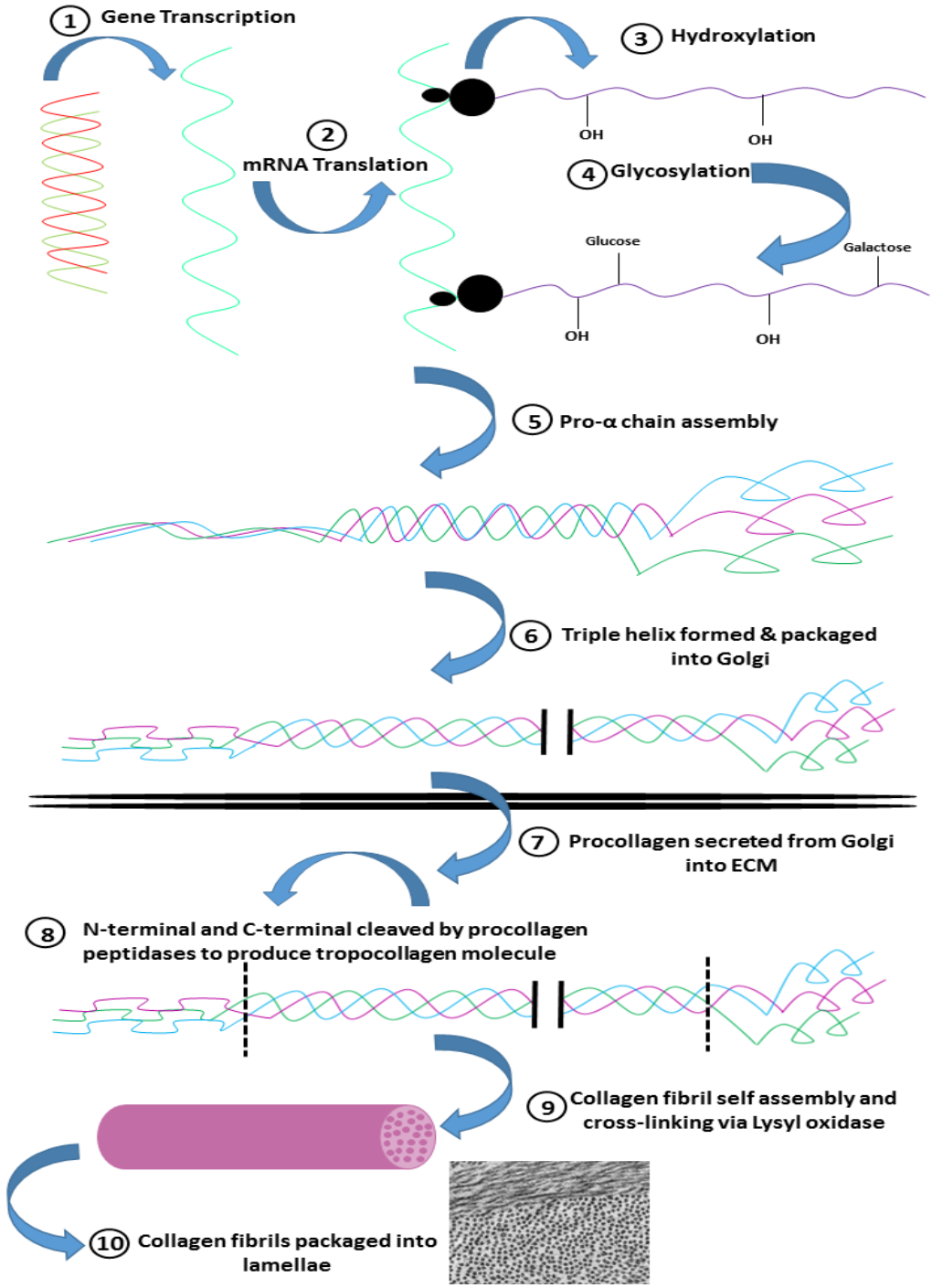

Figure 1.4. Collagen biosynthesis and fibrillogenesis.

Procollagen genes are initially transcribed into mRNA before being translated in the cytosol to produce polypeptide chains. The chains are hydroxylated and glycosylated and assemble into three polypeptide chains to produce the triple helix. The triple helix is then secreted into the extracellular matrix, cleaved by pro-peptides at the C and N terminal regions to produce a tropocollagen molecule, in the direction from C to N. Fibrillogenesis is then initiated, proceeding with nucleation, fibre growth and crosslinking to assemble collagen fibrils. Within the cornea, the collagen fibrils are packaged into lamellae and organised to provide the cornea with tensile strength and transparency (Shoulders and Raines 2009).

1.2.1.2. Corneal Collagen

Twenty-eight collagens have been identified, each with different roles within connective tissues. The specific collagen type within the helical structure confers a tissue with its specific properties (Ricard-Blum 2011). The cornea is mainly composed of type I collagen, but other collagen types are present within the cornea to contribute different properties (**Table 1**) (Birk et al. 1990, Newsome et al. 1982). Fibril-forming collagens are the most prevalent, some include types I, II, III, V and XI. FACIT collagens (fibril-associated collagen with interrupted triple helix) are found associated with collagen fibril surfaces and modify their interactive properties, these may include type IX, XII, XIV and XX collagen. Finally, other non-fibril-forming collagens can include type IV, VI and VII. These collagens localise in connective tissues and with cell surfaces, with some collagen types forming extracellular networks.

Most fibrils within the cornea are heterotypic, therefore they have more than one fibrillar collagen type within their triple helix. Heterotypic fibrils within the stroma are composed of both types I and V collagen, which mainly enhances the biomechanical properties of the cornea (Birk et al. 1990, Fitch J. M. et al. 1994). Type V collagen also limits fibril growth and is theorised to shorten corneal D-periods (Jastrzebska et al. 2017). These properties were demonstrated by studies that identified a reduction of collagen fibril diameter when type V collagen was increased (Birk et al. 1990). In addition, deletion of the type V collagen gene in a mouse model permitted an increase in fibril diameter, lack of fibril assembly and enhancement of corneal opacity (Sun et al. 2011).

Table 1. The main collagens found within the cornea. **The roles of specific collagens and their association with other molecules and cells, which help maintain a functional cornea (Chen S. et al. 2015, Fitch J. M. et al. 1994, Gelse et al. 2003, Massoudi et al. 2016, Puk et al. 2009)**

Type of collagen	Role	Associations
I	Tensile strength & transparency	Type V collagen (heterotypic fibrils)
II	Corneal stroma development, assembly of collagen fibrils	Type IX collagen
III	Increased during corneal wound healing and inflammation, increased in corneal scarring	Corneal stroma, enhanced in elastic tissues.
IV	Maintains the structure and function of basement membranes	Corneal epithelial cells
V	Regulates fibril diameter, initiates fibril assembly & important for transparency	Type 1 collagen
VI	Regulates stroma development; influences cell processes	Collagen type I, II, IV and XIV. Elastin
VII	Component of anchoring fibrils, important for the stroma adhering to the epithelium, expressed during corneal wound healing and decreased during corneal diseases.	Laminin
VIII	Present within Descemet's membrane, assembles into a hexagonal lattice, altered in many corneal endothelial pathologies.	Produced by endothelial cells
IX	Present in the corneal stroma during development	Type II collagen
XII	Involved in the organisation & interactions of fibrils, corneal scarring	Protrude the surface of collagen fibrils to interact with stromal proteins
XIII	Binds with other proteins e.g. fibronectin and type IV collagen	Posterior two-thirds of the corneal stroma
XVIII	Anti-angiogenic role	C-terminal non-triple helical domain endostatin – angiogenesis inhibitor. Only known collagen to carry heparin sulphate glycosaminoglycan side chains

1.2.2. Proteoglycans

Proteoglycans (PGs) are extracellular matrix molecules that maintain corneal homeostasis by regulating collagen fibrillogenesis, collagen fibril spacing, and allow collagen fibril maturation and organisation of the extracellular matrix (Lewis et al. 2010, Rada et al. 1993). PGs are composed of a protein core with covalently bound sulphated glycosaminoglycan (GAG) side chains. GAG's are negatively charged repeating disaccharide units that are strongly hydrophilic and especially abundant in tissues that retain water. There are three families of GAG side chains that attach to the protein cores of PGs: chondroitin/dermatan sulphate, keratan sulphate and heparan sulphate (Massoudi et al. 2016). Different PGs have diverse roles within tissues, being identified by their distinct gene products (Iozzo and Schaefer 2015). Early studies that used cuprolinic blue contrasting and electron microscopy techniques originally identified PGs to associate with corneal stromal collagen fibrils (Scott and Haigh 1988a). Small leucine-rich proteoglycans (SLRPs) are a family of PGs that have been identified to be ubiquitously expressed within the cornea, especially throughout development. The SLRPs interact with fibrillar collagens to regulate collagen fibrillogenesis, signalling, matrix assembly and organisation (Chen S. and Birk 2013).

1.2.2.1. Corneal Proteoglycans

PGs have been well documented to regulate corneal transparency through their interactions with collagen fibrils. Changes to PGs reduce corneal transparency and exert detrimental effects on corneal structure and function. Keratan sulphate PGs make up approximately half of the PGs present within the cornea and provide the cornea with an organised stroma. Keratan sulphate PG synthesis is important to achieve corneal transparency, with the abnormal synthesis of these PGs leading to corneal opacity (Hassell et al. 1980, Midura et al. 1990, Pellegata et al. 2000). This GAG chain is N-linked to asparagine residues in PG core proteins. Different variants of PGs contain the sulphated keratan sulphate GAG side chains are identified in the cornea. These PG variants include lumican, keratocan, mimecan and fibromodulin (Carlson et al.

2005, Chakravarti et al. 2000, Funderburgh et al. 1997). Interestingly, even though all these PGs are found in various other tissues, they are only glycosylated with sulphated keratan sulphate side chains in the cornea, which suggests an important role for transparency (**Table 2**).

Lumican limits collagen fibrillogenesis in the cornea, with thinner collagen fibrils in the presence of lumican (Rada et al. 1993). The GAG side chains of lumican become sulphated during embryonic development when transparency increases, which further supports the argument for its role in corneal transparency (Cornuet et al. 1994). Lumican-null mice exhibit altered collagen fibril organisation and loss of corneal transparency (Chakravarti et al. 1998). The role of lumican in corneal fibrillogenesis has been demonstrated in lumican-null mice, which exhibit larger collagen fibrils in the posterior corneal stroma in comparison with the anterior stroma (Saika et al. 2000). Lumican also regulates other corneal PGs at the transcription level. For example, overexpression of lumican results in an increase in keratocan mRNA, whilst a decrease in lumican expression results in a reduction of keratocan mRNA (Carlson et al. 2005). Lumican also contains a collagen-binding site that is homologous to the binding site on the keratan sulphate PG fibromodulin. This SLRP regulates corneal collagen fibrillogenesis in postnatal mouse development, localised within the peripheral cornea and limbal regions; this PG ceases to exist in the mature cornea (Chen S. et al. 2010). Other than its involvement in collagen fibrillogenesis, lumican is also thought to have an involvement in cell migration, epithelium-mesenchyme transition and wound healing (Kao and Liu 2002).

Keratocan is expressed throughout the corneal stroma and is a subsequent marker for keratocytes (Musselmann et al. 2005). Keratocan helps maintain transparency by regulating collagen fibril spacing and thus extracellular matrix organisation (Liu C. Y. et al. 2003). Keratocan-null mice exhibit corneal stromal thinning, collagen fibril thinning and abnormal collagen fibril spacing, but its effects on transparency are not as severe as a loss of lumican demonstrated (Kao and Liu 2002). In addition, keratocan is overexpressed in keratoconus,

where the central cornea thins and bulges outwards (Wentz-Hunter et al. 2001).

Mimecan is also expressed throughout the cornea and can regulate type 1 collagen fibrillogenesis (Ge et al. 2004). However, the collagen fibril network is not disrupted in mimecan-null mice, which suggests that mimecan has a less dominant role in the regulation of corneal collagen fibrils and corneal extracellular matrix in comparison to the other keratan sulphate PGs, lumican and keratocan (Beecher et al. 2005).

The chondroitin sulphate PGs contain both chondroitin and dermatan sulphate GAG side chains. An important chondroitin sulphate PG within the cornea is decorin (Axelsson and Heinegard 1980). Decorin maintains corneal transparency by regulating interfibrillar spacing and collagen fibril diameter (Rada et al. 1993, Scott 1988). The important role these PGs play in corneal morphogenesis was clearly demonstrated by gene mutations in decorin that resulted in irregular collagen fibrillogenesis, which led to corneal opacity (Bredrup et al. 2005). Some chondroitin sulphate and dermatan sulphate GAG side chains also associate with fibrillin microfibrils, an important component of elastic fibres (Chan and Choi 1995, Kielty et al. 1996).

It should also be noted that mouse corneas mainly contain dermatan sulphate GAG side chains, with low and under-sulphated levels of keratan sulphate compared to human corneas (Parfitt et al. 2010, Young et al. 2005). These studies identified large structures unique to the mouse cornea with chondroitin sulphate and dermatan sulphate side chains to predominate. Keratan sulphate is thought to replace dermatan sulphate GAGs in the cornea when oxygen levels are low. The mouse cornea is very thin, therefore oxygen deprivation is less likely to occur than within a thicker cornea, e.g. in the human eye (Scott and Haigh 1988b), which could explain why the mouse cornea has mainly under-sulphated GAGs.

***Table 2. The main proteoglycans within the cornea and their specific roles in maintaining a functional cornea* (Carlson et al. 2005, Massoudi et al. 2016).**

Glycosaminoglycan	Variant Proteoglycan	Role	Associations
Chondroitin/ Dermatan sulphate	Decorin	Growth, assembly, inhibition and stability of collagen fibrils.	Dermatopontin TGF-β Collagens Fibronectin EGF-R
Keratan sulphate	Lumican	Growth, assembly, inhibition and stability of collagen fibrils.	Collagen keratocan TGF-β
Keratan sulphate	Keratocan	Regulation of collagen fibrils diameter and spacing.	Lumican
Keratan sulphate	Mimecan	Collagen fibril organisation and prevents thickening of collagen fibrils.	
Keratan sulphate	Fibromodulin	Collagen fibrillogenesis	Lumican

1.2.3. Elastic fibres

Elastic fibres are important extracellular matrix components that provide elasticity and structural support to tissues, whilst regulating growth factors and signalling molecules to maintain extracellular matrix homeostasis (Baldwin et al. 2013, Kielty et al. 2002b, Neptune et al. 2003, Sengle et al. 2008). Elastic fibres provide elastic properties to tissues, which can return tissues to their original configuration when subjected to external forces (Kielty et al. 2002b). The properties elastic fibres provide are crucial in dynamic tissues which undergo repeated cycles of extension and recoil, including arteries, skin, ligaments and lung tissue (Dick 1947, Magrath 1898). Elastic fibres are also crucial in non-elastic tissues, which includes ciliary zonules and bone, where the fibrillin-rich microfibrils strengthen tissues (Hansson 1970, Sherratt et al. 2003).

Elastic fibres differ in their ratio of elastin and microfibril components to provide tissues with different properties. Oxytalan fibres, the most immature elastic fibre are composed of bundles of fibrillin-rich microfibrils (Fullmer and Lillie 1958, Sawada et al. 2006). Fibrillin-rich microfibrils are predominantly composed of fibrillin-1 glycoproteins in the adult system. Each fibrillin-1 molecule contains domains that permit fibrillin-1 to interact with the extracellular matrix. Elaunin fibres mature from oxytalan fibres as an intermediate elastic fibre type and contain small quantities of amorphous elastin (Carrington et al. 1984). True elastic fibres, the most mature elastic fibre type develop from oxytalan fibres and contain an elastin protein core surrounded by fibrillin-rich microfibrils (Baldwin et al. 2013).

Fibrillin microfibrils form stable structures to maintain tissue architecture, whilst modulating TGF-β availability (Sengle and Sakai 2015). Fibrillin can also act as a scaffold in true elastic fibre formation, where tropoelastin uses fibrillin as a scaffold for deposition, forming a fibre with an elastin core surrounded by fibrillin-rich microfibrils (Baldwin et al. 2013, Kielty et al. 2002b). The

amorphous elastin component of elastic fibres permits elasticity, returning tissues to their original shape after deformation (Debelle and Tamburro 1999, Green et al. 2014).

Many other components associate with the elastin-microfibril and elastic fibre-cell interfaces to support the function of elastic fibres. These components include microfibril-associated glycoproteins (MAGPs), fibulins, EMILIN-1, fibronectin and PGs (Baldwin et al. 2013, Kielty et al. 2002b). Microfibril-associated glycoproteins (MAGPs) contribute to elastic fibre formation, as well as mediating type VI collagen interactions with fibrillin microfibrils, where type VI collagen is thought to anchor elastic fibres into the extracellular matrix (Gibson et al. 1998, Kielty et al. 1991). In addition, the PGs decorin and biglycan interact with tropoelastin and MAGPs during elastic fibre assembly (Reinboth et al. 2002). The variety of components found associated with the fibrillin and elastin components of elastic fibres indicates the complexity of the elastic fibre network.

1.2.3.1. Elastic Fibre Biosynthesis

The assembly of mature elastic fibres is dependent on the deposition of tropoelastin on an aligned fibrillin-rich microfibrillar scaffold, which forms a parallel insoluble elastic fibre with an elastin core surrounded by microfibrils (Kielty et al. 2002b, Sherratt 2009).

Fibrillin, a cysteine-rich glycoprotein initially constructs a scaffold of beaded transglutaminase-crosslinked microfibrils (Qian and Glanville 1997, Sakai et al. 1986). This beaded appearance results from the 148 nm long fibrillin monomer, which assembles close to the cell surface, with fibrillin-1 and microfibril-associated glycoprotein components that interact with integrin receptors via RGD sequences (Keene et al. 1991, Sakai et al. 1991, Sakamoto et al. 1996). The fibrillin monomers bundle into fibrils with a bead to bead

periodicity of 56 nm (Wess et al. 1997). There have been two main theories of how this packaging occurs. The first states that one fibrillin monomer is folded every inter-bead distance, this is known as the intramolecular pleating model (Baldock et al. 2001, Baldock et al. 2006, Kielty et al. 2002a, Lu et al. 2005). The second model states that the fibrillin monomers extend over two or more inter-bead distances, overlapping (Kuo et al. 2007). The fibrils subsequently form a one-third stagger arrangement with maturation from a parallel head-to-tail alignment, with a complex folded arrangement in un-tensioned state (Baldock et al. 2001). Throughout connective tissue, fibrillin-1 is the main fibrillin present within mature elastic fibres. Fibrillin-2 has an increased presence in embryonic development (Zhang H. et al. 1994, Zhang H. et al. 1995). The development of elastic fibres in embryogenesis is crucial, due to the inability of organised elastic fibres to develop in the adult system.

Tropoelastin molecules are the soluble precursors that bind together with crosslinks to form elastin (Mithieux and Weiss 2005). Initially, tropoelastin is secreted from fibroblasts into the extracellular matrix space. Tropoelastin contains an N-terminal which provides the elastic properties and a C-terminal that interacts with cells via integrins (Baldwin et al. 2013, Yeo et al. 2012). Tropoelastin then deposits onto the microfibril scaffold and undergoes self-aggregation (coacervation) to form a fibrillar structure that represents the elastin core (Cox et al. 1973). The elastin core is further stabilised via cross-linking with lysyl oxidase (LOX), with contributions from fibulin-4 and fibulin-5 which is thought to aid the deposition of elastin onto fibrillin microfibrils (Choi et al. 2009, Siegel et al. 1970).

Microfibril assembly also relies on fibronectin, integrins and heparan sulphate PGs (Cain et al. 2008, Kinsey et al. 2008, Tiedemann et al. 2001). Latent TGF-β binding protein 4 (LTBP-4) has been shown to interact with fibulin-4 and fibulin-5 to form elastic fibres, a tropoelastin binding protein necessary for elastic fibre production (Bultmann-Mellin et al. 2015, Noda et al. 2013, Sinha et al. 1998). Fibulins also regulate the organisation of the elastic fibres by

communicating with cells of the extracellular matrix (Midwood and Schwarzbauer 2002). Fibrillin maintains tissue homeostasis and interacts with regulatory growth factors including TGF-β and BMPs (Jensen et al. 2012). ADAMTS10 has also been shown to have a high affinity to fibrillin-1, participating in the synthesis of microfibrils (Kutz et al. 2011). The sulphation of PGs is also important for elastic fibre assembly; inhibition of sulphation has prevented microfibrillar protein incorporation into the extracellular matrix of cultured cells (Schaefer et al. 2007).

1.2.3.2. Corneal Elastic Fibres

Elastic tissue initially identified to associate with Descemet's membrane and Schlemm's canal, is closely affiliated with the ciliary zonules of the eye (Kolliker 1860). Further studies carried out collagen digestion with acetic acid and further identified elastic fibres to predominate in the posterior peripheral cornea (M'Ilroy J 1906). The previously described elastic fibres resisted acid hydrolysis and were further identified as oxytalan fibres in studies carried out in periodontal membranes (Fullmer and Lillie 1958). This led to studies that identified oxytalan fibres in the cornea (Alexander and Garner 1983, Carrington et al. 1984). These oxytalan fibres were described in the skin to be composed of many microfibrils ~10-12 nm in diameter, which was further classified as the glycoprotein, fibrillin (Cotta-Pereira et al. 1976, Sakai et al. 1986). Fibrillin microfibrils were further morphologically identified by their beaded morphology with a periodicity of ~56 nm, which structurally alter with extension of the microfibrillar component (Baldwin et al. 2013, Keene et al. 1991). Studies have also provided evidence of ~8 fibrillin molecules contained within a microfibril cross-sectional diameter (Baldock et al. 2001).

Studies in different species have identified elastic fibres to localise within the cornea. In the avian species, oxytalan fibres predominate in the corneal stroma and Descemet's membrane, which increases in density towards the periphery (Bruns et al. 1987, Daga Gordini et al. 1990). In mammalian models, elastic fibres have been described in the rabbit cornea, which was sensitive to

elastase digestion and stained with tannic acid (Carlson and Waring 1988). In addition, microfibrils were also described in the mouse cornea (Hanlon et al. 2015). Studies directed at the human cornea further localised elastic fibres within the posterior peripheral cornea (Kamma-Lorger et al. 2010). These studies led to investigations using electron microscopy methods, which demonstrated a complex elastic fibre network to be concentrated within the posterior corneal stroma, directly anterior to Descemet's membrane (**Figure 1.5**) (Lewis et al. 2016). This study demonstrated the presence of elastic fibres in week 13 of foetal corneal development, which suggested the elastic fibre system to support corneal development. The role of elastic fibres in the cornea was additionally shown to influence corneal shape and structure by an abnormal elastic fibre architecture and corneal structure in keratoconus and Marfan syndrome tissue (White et al. 2017a, White et al. 2017b).

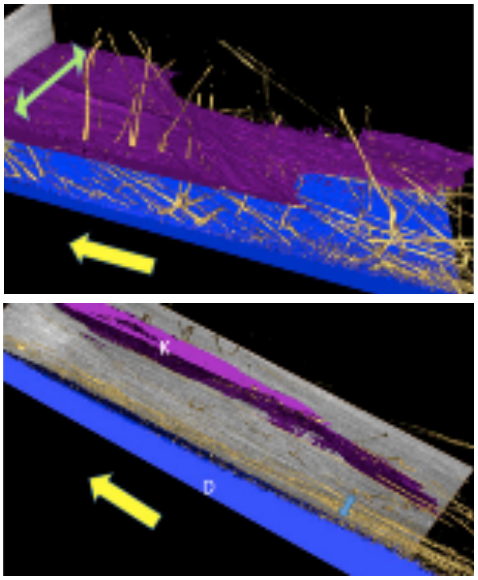

Figure 1.5. The elastic fibre system in the adult human cornea.

Three-dimensional reconstructions of elastic fibres using a tannic acid-uranyl acetate based method with serial block-face scanning electron microscopy imaging show elastic fibres (yellow) concentrated above Descemet's membrane (blue) and surrounding keratocytes (purple). Images were taken from (Lewis et al. 2016) with permission under the creative commons user license (https://creativecommons.org/licenses/by/4.0/).

1.2.3.3. Elastic fibres in Corneal Diseases

Genetic conditions where elastic fibre proteins are mutated have demonstrated the importance of a functional elastic fibre system across biology. Mutations in the FBN1 gene, which encodes fibrillin-1 lead to fibrillinopathies, which have consequential clinical and phenotypic disruptions to skeletal and ocular tissues. To understand the pathogenesis of fibrillinopathies across tissues, researchers have developed a fibrillin-1 knockout mouse model (Lima et al. 2010). The fibrillin-1 mutations represent Marfan syndrome (MFS), which allows us to analyse the elastic fibre system when the fibrillin-1 glycoprotein is impaired (Fernandes G. R. et al. 2016, Lima et al. 2010). Marfan syndrome patients present with a thinner and flattened cornea, with a disruption in the ciliary processes that hold the lens in suspension (Konradsen and Zetterstrom 2013, Maumenee 1981, Sultan et al. 2002). The clinical corneal disruptions described in MFS patients led to studies that further identified structural alterations in the cornea of an MFS mouse model (White et al. 2017a).

A loss of corneal structure with alterations in the elastic fibre network has also been described in patients with keratoconus (White et al. 2017b). Lysyl oxidase (LOX) cross-links collagen and elastin during their synthesis within the cornea (Siegel et al. 1970). LOX is also reduced by at least 63% in corneas affected by keratoconus, a corneal disease where the curvature of the cornea is enhanced. This suggests that an abnormal assembly and maintenance of elastic fibres and collagen is implicated in the pathology of keratoconus, with a consequent loss of function (Dudakova and Jirsova 2013).

The remodelled corneal structure with alterations to the elastic fibre system in both keratoconus and MFS tissue suggests the elastic fibre system maintains corneal structure and function.

1.2.4. Communication

1.2.4.1. Integrins

To allow the successful synthesis and organisation of the extracellular matrix proteins there must be effective communication between cells and the surrounding extracellular matrix. This communication relies on cell adhesion molecules known as integrins, allowing cells to communicate with the acellular matrix to direct its synthesis and organisation (Kadler et al. 2008). Integrins are heterodimeric cell surface receptors composed of alpha (α) and beta (β) subunits. These components regulate cell migration and adhesion during the development, maintenance and healing of the cornea (Stepp 2006). The integrins on the cell surface communicate with the outside environment by binding to extracellular proteins including fibronectin, laminin, collagen and tenascin-C. This link then directs extracellular matrix synthesis and organisation within the cornea via detecting mechanical stimuli. If this communication system is dysfunctional an abnormal turnover of extracellular matrix may occur and result in a loss of corneal architecture, which may see the development of corneal diseases (Carter 2009).

1.2.4.2. Gap Junctions

Cells must also be able to communicate with surrounding cells and this is achieved via gap junctions, which notify and regulate cells to synthesise and organise the corneal extracellular matrix. Gap junctions form a large intercommunicating network via projections, which connect the cytoplasms of adjacent cells (McNeilly et al. 1996). The ability of cells to communicate is essential for protein synthesis and the successful organisation of the extracellular matrix in development, which provides and maintains a functional cornea (Spanakis et al. 1998). Gap junctions are composed of connexin proteins which are vital for cell processes to occur, maintaining corneal homeostasis (Yuan et al. 2009). In particular, connexin 43, enhances corneal repair and has been shown to be a critical component during corneal development (Grupcheva et al. 2012, Williams and Watsky 2002).

1.3. Trabecular meshwork

Aqueous humor conserves normal vision by flowing against resistance to maintain a physiological intraocular pressure (IOP). As the cornea lacks vascularity, aqueous humor provides the eye with nutrients, removes unwanted wastes and permits the inflow of inflammatory cells when required (Goel et al. 2010, Llobet et al. 2003). Aqueous humor is produced by the ciliary processes on the ciliary body via active secretion, ultrafiltration and diffusion, with active secretion being the main process of production (Mark 2010). The aqueous humor accumulates within the posterior chamber before crossing the pupil to enter the anterior chamber, both located within the anterior portion of the eye. It is the homeostasis of the fluid volume within these chambers via a monitored outflow which maintains a physiological IOP, an important process to protect the eye from corneal disease. A disruption in the outflow of aqueous humor can lead to an increased IOP, a contributing risk factor for glaucoma, which can potentially result in blindness (Carreon et al. 2016).

1.3.1. Outflow Pathways

Studies have identified two main outflow pathways located in the iridocorneal angle of the eye that regulate IOP (**Figure 1.6**) (Goel et al. 2010). The conventional pathway filters the majority of aqueous humor outflow through the trabecular meshwork (TM) and Schlemm's canal (SC). The TM is composed of extracellular matrix components and is positioned on the anterior portion of the eye, and is further divided into the uveal, corneoscleral and juxtacanalicular meshwork (Carreon et al. 2016). The outflow pathway through the TM is affected by the organisation and turnover of the extracellular matrix and can affect the biomechanical properties of the cornea (Vranka et al. 2015). When aqueous humor is filtered through the TM it continues through Schlemm's canal, a channel created by the TM that passes over the scleral sulcus (Goel et al. 2010). After passing through this channel, the aqueous humor drains into the episcleral veins and is recycled back into the circulation.

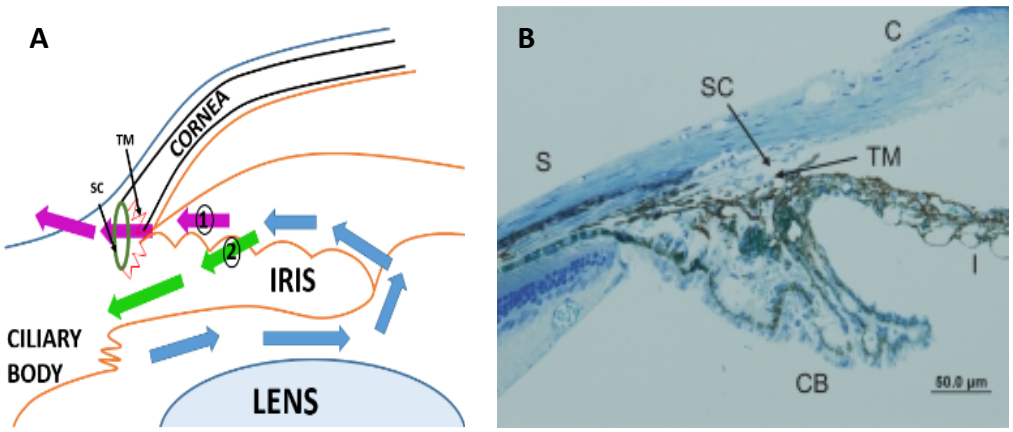

Figure 1.6 The outflow pathways of the trabecular meshwork

Fig. 1.6A: Identifies the conventional route (Pathway 1 – purple arrows) which travel through the trabecular meshwork (TM) and Schlemm's canal (SC). The unconventional pathway (pathway 2 - green arrows) allows aqueous humor to bypass the TM and SC (Adapted from Goel el al., 2010). **Fig.1.6B:** A toluidine blue stained image of the irido-corneal angle in the mouse eye showing the trabecular meshwork (TM) and Schlemm's canal (SC) and their association with the iris (I), Ciliary body (CB) cornea (C) and Sclera (S). Permission to use image was granted from (Kang et al. 2011), ARVO is the copyright holder.

The uveoscleral or unconventional pathway allows aqueous humor to exit the anterior chamber by diffusion through intercellular spaces within the ciliary muscle fibres, which avoids the TM and SC (Carreon et al. 2016). The unconventional pathway passes approximately 4-27% of aqueous humor outflow, independent of IOP. Even though the unconventional pathway is independent of IOP, many pharmaceutical interventions target this pathway to treat conditions that result from an increased IOP (Carreon et al. 2016).

1.3.2. Trabecular Meshwork Related Pathologies

The extracellular matrix of the TM is continually remodelled in response to pressure changes and forces applied. Studies have shown an abnormal organisation of matrix components within the cornea delays aqueous humor outflow and increases IOP (De Groef et al. 2016). This increase in IOP presents a major risk factor for developing glaucoma, a disease where damage to the optic nerve leads to irreversible blindness (Kwon et al. 2009).

Pharmaceutical interventions have been undertaken to target the permeability of the TM in an attempt to decrease IOP and reduce the progression of glaucoma (Overby et al. 2014). Studies have identified genetic mutations that result in glaucoma by disrupting the organisation of the extracellular matrix. Some of the mutations that have been linked to glaucoma include variants within the CYP1B1, LTBP2 and MYOC genes (Lim et al. 2013). Genetic mutations to particular proteins disrupt TM organisation and pose a risk factor for corneal disease development. Mutations to the MYOC gene within TM-cells disrupts the protein myocilin, which initiates glaucoma progression via increased IOP, enhancing the expression of fibronectin, laminin, elastin, type I collagen and type IV collagen (Kasetti et al. 2016). ADAMTS10 and ADAMTS17 are also mutated in some incidences of glaucoma; these polymorphisms have also been related to fibrillinopathies. This has shown the involvement of the elastic fibre system in glaucoma progression (Morales et al. 2009). These studies have also indicated the importance of matrix homeostasis to allow the TM to function effectively, maintain a physiological IOP and prevent the development of glaucoma.

To further reduce the risk factor associated with high IOP, other strategies to lower IOP have been undertaken; targeting ciliary muscle contraction, TM-cell regulation and extracellular matrix turnover. The TM-cells detect IOP changes and alterations within the TM environment, which can further regulate gene transcription alterations and signals to other cells and matrix components. TGF-β signalling in particular associates with protein expression patterns of TM-cells in glaucoma and could be targeted as a treatment intervention (Han et al. 2011). As mentioned previously, the TGF-β signalling could increase elastic fibres within the TM to increase IOP. Elastic fibres in the TM are further surrounded by type VI collagen in association with aqueous humor outflow resistance, which significantly increases in the advancement of glaucoma (Tektas and Lutjen-Drecoll 2009). Strategies to lower IOP have included targeting signalling pathways, oxidative stress and vascular damage (Maddala et al. 2016, Zhao et al. 2016). In addition, elastase administrations were found to digest elastin in the TM and could be a potential method to treat glaucoma,

this further indicates elastic fibres could have an involvement in glaucoma progression (Segawa 1995, Umihira et al. 1994).

1.4. Corneal Development

Successful corneal development requires sequentially controlled events that induce structural changes and interactions between cells and the surrounding extracellular matrix. The precise secretion and alignment of extracellular components within mammalian corneal development remains poorly understood, even though its role is imperative for the development of a physiological cornea (Young et al. 2014). Many previous studies have directed corneal research to understand the developmental events that occur in the avian model system. This research has greatly enhanced our knowledge of corneal development, however, a gap remains in the events that develop the mammalian cornea, which many studies have shown differs in comparison to avian development.

1.4.1. Avian Corneal Development

Corneal development has been widely documented in the avian model organism. Initially, a cup-shaped structure forms in the optic vesicle inducing the development of the lens placode from the overlying ectoderm (Fuhrmann 2010). On the 3rd day of chick development, the primitive lens detaches from the surface ectoderm, followed by the differentiation of the ectodermal layer to form the corneal epithelium. The epithelium proceeds to synthesise an acellular primary stroma composed of type I, II and IX collagen under the basal lamina, which increases the stromal thickness to 10 μm (Hendrix et al. 1982). Neural crest cells from the lip of the optic cup migrate centrally between the primary stroma and the lens capsule to form the endothelium (Bard et al. 1975, Beebe and Coats 2000). Towards the end of day 5, the primary corneal stroma swells to approximately 60 μm and the endothelium secretes large amounts of hyaluronic acid. Following this, presumptive corneal fibroblasts derived from the neural crest migrate into the centre and posterior primary stroma to

synthesise the extracellular matrix and develop the secondary corneal stroma (Hay E.D. 1980). This secondary stroma is mainly composed of type I collagen which forms heterotypic fibrils with type V collagen (Birk et al. 1986). Even though the exact mechanism of cell migration into the primary stroma is unknown, the primary stroma is thought to act as a template for the biosynthesis of the secondary stroma, which initially directs the second migration of mesenchymal cells that proceed to develop and organise the collagenous extracellular matrix (Bard and Hay 1975, Hay E. D. and Revel 1969, Trelstad and Coulombre 1971). The endothelial cells proceed to develop Descemet's membrane by day 9, as well as the development of corneal curvature. The enhancement of corneal curvature is thought to be initiated by an increase in intraocular pressure, the interaction between the cornea and sclera as well as the organisation of the stromal matrix. The corneal stroma reaches its optimum thickness at day 9 (190 – 220 μm). Bowman's layer is seen to develop from the anterior 1 μm region of the acellular stroma between day 12 and 14. By day 14, the synthesis of the secondary stroma is complete with its thickness decreased by half, enhancing transparency from ~40% to 95% by day 19 (Coulombre and Coulombre 1958, Quantock A. J. et al. 1998). The dehydration process is thought to remove water by the breakdown of hyaluronic acid and thyroxine acting on the endothelium to pump sodium from the secondary stroma to the anterior chamber of the eye, resulting in curvature changes (Hay E.D. 1980, Toole and Trelstad 1971). The cornea continues to package collagen fibrils, further increasing corneal organisation and thus transparency.

The primary stroma is thought to be important for the initiation of cell migration to synthesise the secondary stroma. Evidence of a primary stroma is absent within mammalian development, which leaves questions concerning the control of the migration of cells that develop the corneal stroma and how the collagen is further laid down and organised.

1.4.2. Mammalian Corneal Development

1.4.2.1. Stages of Mammalian Corneal Development

One of the most well studied mammalian species in development is the mouse, which has a rapid developmental time frame and is easy to access and handle. For these reasons, plus the ability to analyse corneal development at the genesis of the eye, the mouse model will be the main mammalian model analysed throughout this thesis.

Mice develop over three weeks, divided into twenty-six prenatal and two postnatal stages (Theiler 1989). The first sign of ocular development in mammals is when the optic vesicle presents as a lateral outgrowth of the prosencephalon (forebrain). The optic vesicle is present between days E8.5 to E9 in mouse embryos and day 22 in human embryos (Vecino and Acera 2015, Zavala et al. 2013). The neuro-ectoderm of the optic vesicle grows laterally to contact the overlying surface ectoderm, which forms a local thickening (**Figure 1.7**) (Pei and Rhodin 1970). The thickening of the optic vesicle forms the retinal disc and the thickening of the surface ectoderm forms the lens placode (Cvekl and Tamm 2004). The proximal aspect of the optic vesicle constricts and elongates to form the optic stalk, this acts as the main communication network between the optic vesicle and the forebrain (Pei and Rhodin 1970).

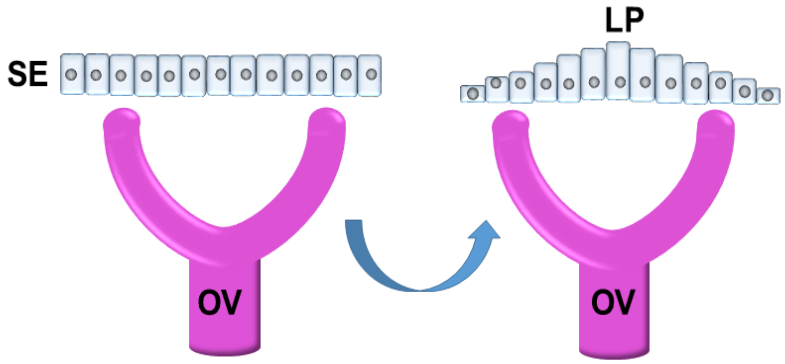

Figure 1.7. The initial stages of mammalian ocular development.

The surface ectoderm (SE) overlies the optic vesicle (OV), the surface ectoderm thickens to become the lens placode (LP).

The distal part of the optic vesicle is invaginated into its more proximal part and forms a double-layered optic cup (**Figure 1.8**) (Barishak 2001). The inner layer of the optic cup forms the neural retina, whilst the outer layer will differentiate into the retinal pigment epithelium. In parallel to the development of the optic cup, the lens placode enlarges and sinks below the level of the surface ectoderm to form the lens pit. Subsequently, it forms the lens vesicle, which remains connected to the surface ectoderm and invaginates into the optic cup (**Figure 1.8**) (Pei and Rhodin 1970). The optic cup is incomplete inferiorly at the choroidal fissure, allowing the hyaloid artery to pass through this fissure, this provides an arterial supply to the optic cup and lens vesicle (Cvekl and Tamm 2004).

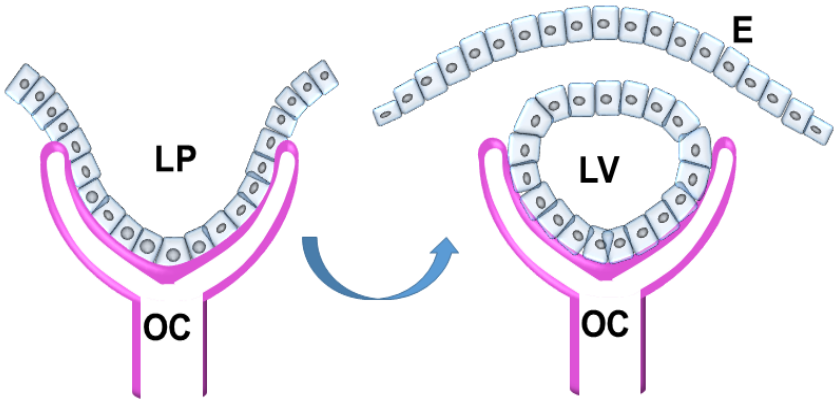

Figure 1.8. Corneal development.

The lens placode (LP) invaginates to develop the optic cup (OC). The lens placode has enlarged and sunk below the ectoderm to form the lens pit, forming the lens vesicle (LV) invaginated into the optic cup. The lens vesicle then becomes detached from the surface ectoderm. The corneal epithelium (E) derived from the surface ectoderm is overlying the optic vesicle. The space between these two structures following detachment initiates the first mesenchymal cell migration.

The overlying surface ectoderm proceeds to form the corneal epithelium in the mouse at day E8.5 and in the human embryo at around week 5. The epithelium's basement membrane is also established by week 9 of human development, even though the distinct Bowman's membrane is not complete until month 4 of development (Sevel and Isaacs 1988). The basement membrane is thought to fulfil critical roles in the early stages of corneal development (Tisdale et al. 1988). The basement membrane in some tissues can act as a scaffold to allow cell migration processes to occur (Vracko 1974). As previously mentioned, the avian corneal epithelium secretes the primary stroma (Hay E. D. and Dodson 1973). Thus, the avian epithelium increases in height to compensate for the enhanced secretory organelles in the basal cell layer (Hay E. D. and Revel 1969). The epithelium within the mammalian cornea has not been currently identified to secrete a primary stroma, supported by an absence of secretory organelles within the corneal epithelium as well as no acellular collagenous layer (Haustein 1983, Pei and Rhodin 1971). Within mouse development, the epithelium remains approximately 1-2 cell layers thick until stratification following cell detachment and further post-natal modifications. In human embryogenesis, the corneal epithelium further forms a layer three to four cells thick in the seventh week of development (Remington and Remington 2012, Zieske 2004). The epithelium continues to proliferate in the mouse to reach maturity after eyelid opening during the 2nd week of development, similar to what is seen in human corneal development. The age that corneal epithelium maturation is reached is species dependant. In the mouse cornea, full maturation is not seen until 3-7 months after birth, when the corneal epithelial stem cells localise into the limbus. Cell proliferation after eyelid opening decreases dramatically in the stroma and the endothelium, which then remains constant throughout the life of the cornea.

The lens vesicle proceeds to detach from the surface ectoderm, which initiates mesenchymal cells to migrate into the space between the anterior epithelium of the lens vesicle and the surface ectoderm (Rones 1932). In mouse development, a single influx of multipotent mesenchymal cells will develop the corneal stroma, keratocytes and the endothelium (Dublin 1970, Pei and Rhodin 1971, Reneker et al. 2000). It has been observed that 4-7

mesenchymal cell layers are present at embryonic day E12, with a stellate, star-shaped phenotype and long cytoplasmic processes. Cell numbers continue to increase and condense to form several layers of separated flattened cells. This initial mesenchymal cell migration occurs at week 6 in the human embryo. However, in human embryogenesis, the initial mesenchymal cell migration only gives rise to the corneal endothelium (Zieske 2004). An additional second migration of neural crest-derived mesenchymal cells becomes the stromal keratocytes. This second migration which also occurs in chick development is not present in mouse or rabbit development (Cintron et al. 1983, Hay E. D. and Revel 1969, Kao 2010) (**Figure 1.9**).

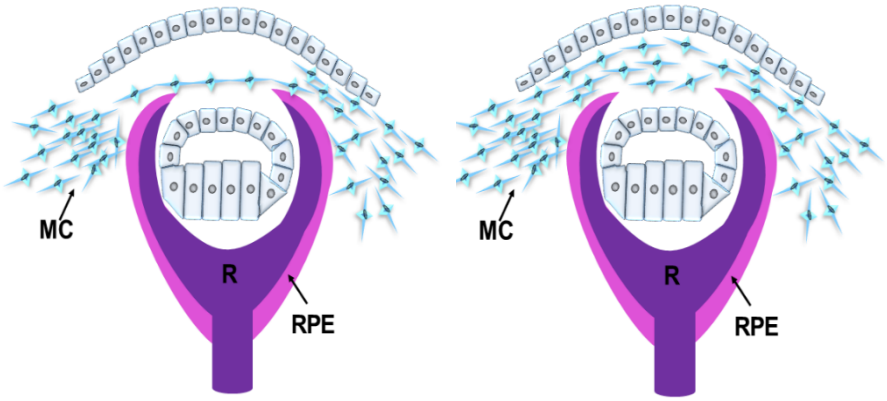

Figure 1.9. Mesenchymal cell migrations that develop the cornea.

The initial migration of mesenchymal cells in the human (left image) and mouse (right image) cornea. In the mouse model mesenchymal cells (MC) migrate into the presumptive corneal stroma, which have the differentiation potential to become the endothelium, stroma and keratocytes. The first wave of mesenchymal cells in the human embryo becomes the endothelium, a second wave of mesenchymal cells differentiates into the corneal stromal fibroblasts. The retina (R) and retinal pigment epithelium (RPE) surrounds the developing lens.

During days E14.5-15.5 of mouse prenatal development, the posterior mesenchymal cells condense to produce the corneal endothelium, which distinguishes a distinct anterior chamber between the lens and the cornea (**Figure 1.10**). Further differentiation of endothelial cells allows the cells to detach from the immature cornea and form a fluid-filled area for the iris and ciliary bodies to develop. In human embryogenesis, the endothelial layer of the

cornea is formed by the first wave of migrating mesenchyme as a double layer of cuboidal cells. Differentiation of the corneal endothelium is required for anterior chamber formation. Mutated mouse strains, where the endothelium fails to form, result in the lens not detaching from the cornea, and the anterior chamber fails to form (Kidson et al. 1999, Reneker et al. 2000).

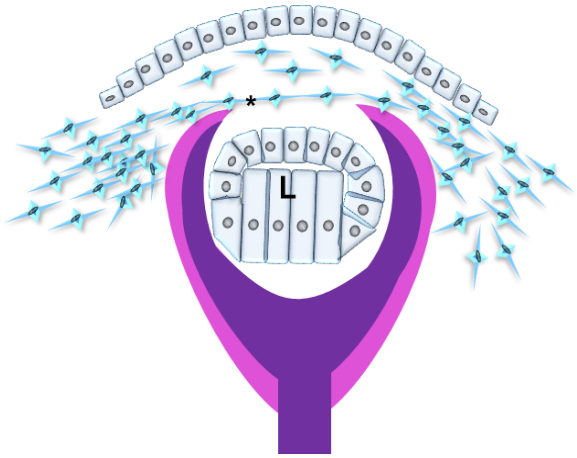

Figure 1.10. Mouse corneal endothelium development.

Within the developing mouse cornea the posterior mesenchymal cells (asterisk) which originate from the first mesenchymal cell migration condense to form the corneal endothelium. The lens (L) is well defined.

The remaining mesenchymal cells in the mouse stroma differentiate into corneal stromal fibroblasts. Initially, these stromal cells synthesis the extracellular matrix of the corneal stroma (Haustein 1983). The proliferative potential of these corneal fibroblasts diminishes during development from birth to eyelid opening, with cells which have arrested in the G0 phase of the cell cycle, but retain the potential to differentiate for corneal repair and wound healing (Zieske et al., 2001). Within human development, the second migration of mesenchymal cells into the space between the newly formed endothelial layer and the surface ectoderm differentiates into corneal fibroblasts, which are thought to develop the stroma. Even though the cell migrations have been well documented, the mechanisms that secrete and organise collagen fibrils within the cornea remains elusive. Previous studies have demonstrated that tendon fibroblasts have fibripositors that direct extracellular matrix secretion

and alignment (Canty et al. 2004). However, studies have failed to show conclusively that corneal fibroblasts also secrete collagen through fibripositors.

The structure of the cornea continues to mature after birth to achieve transparency. In the mouse cornea, increased proliferation of the epithelium, increased corneal stroma thickness as well as a decrease in stromal cell density, all contribute to accomplishing corneal transparency (Song et al. 2003). Once these changes are complete, the mouse eyelids begin to open at approximately postnatal day P12 (Beecher. N. 2003). After the eyelids open in the mouse model the annulus of the cornea forms, a structure that supports corneal curvature in humans (Newton and Meek 1998). It is thought that the development of the annulus may prevent corneal shape changes once eye growth is complete. Even though collagen fibrils have been shown to organise around this annulus to enhance stability, elastic fibres may also have a role to enhance stability (Kamma-Lorger et al. 2010, Sheppard et al. 2010).

The final ocular structures to develop include the trabecular meshwork with aqueous humor outflow, which commences around days E17-E19 in the mouse and is complete by P21. In human embryogenesis, a third migration of cells has also been described to create the stroma of the iris and ciliary bodies (Cvekl and Tamm 2004). The ocular structures associated with aqueous humor drainage (trabecular meshwork and Schlemm's canal) are the final structures to develop. These structures begin to develop between weeks 15-20 of human development and are completed around the time of birth. The chamber angle is occupied by a dense mass of mesenchymal cells, which elongate, flatten and become separated from each other by open spaces that are partially filled with the extracellular matrix. To provide nutrition and a blood supply to maintain the anterior chamber and aqueous humor during development, an extensive capillary network is present, termed the tunica vasculosa lentis.

Evidence of a primary stroma is absent within the mammalian model, and it has been proposed that instead, blood vessels, mesenchymal cells and the lens all fulfil its role in to guide cells in corneal development (Cintron et al. 1983). However, the exact mechanisms that direct cell migration into the presumptive cornea as well as the understanding of how the mature stroma is synthesised and organised remain unknown. An aim of this thesis will be to investigate these events in the mammalian cornea.

1.4.2.2. Developmental Control Mechanisms

The specific time points where cell migrations occur to develop the mouse cornea have been determined. However, the mechanisms that initiate cell migration and guide cells to their specific location remain elusive (Cvekl and Tamm 2004). However, a small understanding of the mechanisms that control some of the events in corneal development has been made clearer by the analysis of human heritable diseases, pathologies and mouse mutant genetic models (Cvekl and Tamm 2004).

The lens exerts an important regulatory influence upon corneal development, with the cornea overlaying this structure (Coulombre 1965). Studies have identified signalling from the anterior epithelium of the lens to maintain a healthy cornea; its removal causes the cellular arrangement within the cornea to be disorganised (Beebe and Coats 2000). On account of this, many studies have analysed signalling molecules associated with the lens. Defects to the lens have led to a failure of corneal mesenchyme differentiation and endothelium formation that results in corneal opacity (Reneker et al. 2000). The chemoattractant TGF-α has been shown to alter the developmental fate of mesenchymal cells, which leads to ocular abnormalities (Reneker et al. 1995). Mutations in transcription factors and genes expressed in the lens have led to corneal developmental and anterior segmentation abnormalities, often developing cataracts and opaque corneas (Cvekl and Tamm 2004, Doward et al. 1999, Kidson et al. 1999, Kume et al. 1998, Nishimura et al. 2001, Perveen et al. 2000, Reneker et al. 2000). TGF-β is thought to be involved in the

proliferation of the mesenchymal cells into corneal fibroblasts. TGF-β2 deficient mice contain fewer keratocytes with a decreased accumulation of lumican and keratocan and an overall thinner corneal stroma. This evidence indicates SLRPs could regulate TGF-β in development, as well as being involved in wound healing and corneal scarring. In addition, lumican is critical for developing a physiological cornea with transparency, as deficiencies often lead to corneal opacity (Carlson et al. 2005, Song et al. 2003). Additional signalling pathways involved in development that prove crucial for achieving corneal maturation are: Paired box protein Pax-6 (Pax6), Epidermal growth factor (EGF) and Fibroblast growth factor (FGF), and have various roles that contribute to eyelid opening, cellular migration and proliferation (Collinson et al. 2003, Vecino and Acera 2015, Xie W. et al. 1999, Zhang J. et al. 2015).

Other than signalling molecules, cell fate determination and morphogenesis are also thought to be regulated through adhesion proteins, specifically cadherin molecules. Cadherin molecules connect neighbouring cells, which form strong cell-cell adhesions and intercellular junctions for signalling (Gumbiner 1996; Kleminckx and Kemler 1999). It is thought that the possible expression of N-cadherin in mesenchymal cells establishes the corneal endothelium and maintains a permeability barrier.

1.5. Murine Model

The mouse proves a good animal model to study mammalian corneal development due to its similarities to the structure and function of the human cornea (Overby et al. 2014). The small size and easy to handle nature of the mouse, as well as its economic effectiveness, has made the mouse an attractive mammalian model to study (Henriksson et al. 2009). The mouse has ~99% genetic similarity to humans, and with the ability to carry out genetic defect studies, models of ocular diseases can easily be analysed within mice models and compared to the human situation for the investigation of disease aetiologies, pathophysiologies and treatment strategies (Fernandes K. A. et al. 2015, Puk et al. 2006). The mouse reaches developmental adulthood at

around eight weeks old, therefore, experimentally the mouse model is time and cost-efficient for developmental studies (Hanlon et al. 2011). There have also been many antibodies that react with mouse tissue, making it a good model to carry out immunohistochemistry experiments to specifically identify components (Liu H. S. and Kao 2009).

However, anatomical variations exist between the human and mouse cornea. The Bowman's layer within the mouse cornea is thin in comparison to the human, measuring 0.7 um with scanning electron microscopy methods, but some studies dispute its presence (Hayashi S. et al. 2002, Smith et al. 2002). There is also a structural variation, with the human corneal centre being thinner compared to the periphery and in contrast, the mouse cornea being thicker in the centre compared to the periphery (**Figure 1.11**) (Henriksson et al. 2009). The organisation of collagen within the stroma is also different compared to the human, with an annulus of highly aligned collagen surrounding the cornea at the limbus, thought to increase corneal strength (Sheppard et al. 2010). Overall, however, the mouse model is a viable model to study mammalian corneal development and compare to the human scenario, but the differences that do exist between these species should be appreciated.

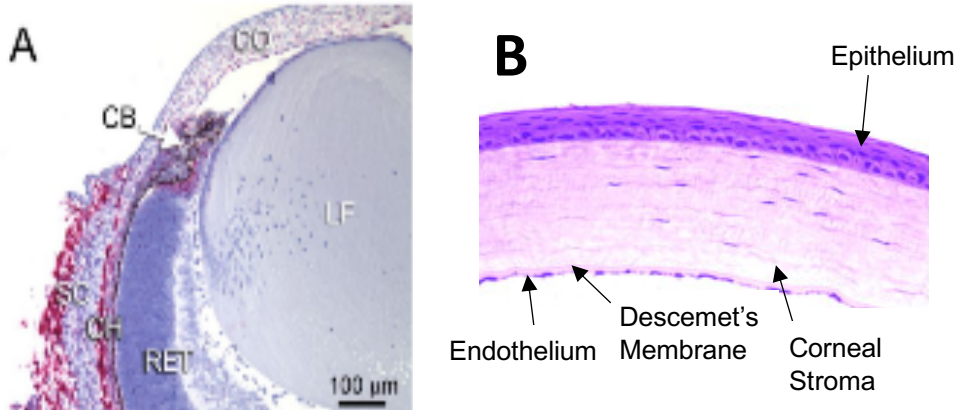

Figure 1.11. The Mouse Cornea.

Fig. 1.11A: A histological image of the normal architecture of a mouse eye. The cornea (CO) is thicker in the centre and becomes progressively thinner towards the periphery. The cornea can be seen to run into the sclera (SC) in the region of the limbus. **Fig. 1.11B:** A histological image of the cornea at a higher magnification. Images are modified from (Cui et al. 2005, Shi et al. 2013) with obtained permission.

This thesis will use the mouse as its main model for investigation. The adult and developing mouse will be analysed between gestation days 10-18. In addition to this, a developmental mouse model of Marfan syndrome between gestation days 12.5-18.5 will be analysed. The development of the human foetal cornea will also be investigated. Standard imaging has been used, supplemented by more recent developments in electron microscopy, X-ray scattering and ocular coherence tomography.

1.6. Electron Microscopy

The resolving power of a microscope is limited by the wavelength of its energy source. Therefore, light microscopes can only generate images within the wavelengths of visible light, which vary between ~400-700 nm. This limitation to light microscopes was overcome with the advancement of using electrons as an energy source in electron microscopy. The wavelength of electrons is much smaller than the wavelength of light and this allows the visualisation of samples that would be beyond the resolution capabilities of a light microscope. To allow the visualisation of structures, a contrast is established by staining samples with heavy metals (Watson 1958). This increases the density of the sample, which interacts with the electron beam, either scattering, transmitting or backscattering electrons to generate differences in contrast, to permit imaging of the desired structure, depending on which electron microscopy technique is being used.

1.6.1. Transmission Electron Microscopy

The first electron microscope technique developed was transmission electron microscopy (TEM). The transmission electron microscope transmits a high energy beam of focused electrons through a thin sample (~90 nm) stained with heavy metals, usually uranyl acetate and lead. Because the samples are thin, electrons are transmitted through, being further magnified, focused and conveyed into an image.

Experiments in this thesis use conventional TEM to analyse the ultrastructure of the developing mammalian cornea at high magnification in two-dimensions. In addition, labelling techniques to analyse the distribution of specific tissue components, including PGs by cuprolinic blue staining and immunogold electron microscopy were employed.

1.6.2. Serial Block-Face Scanning Electron Microscopy

Advances in electron microscopy techniques led to the development of serial block-face scanning electron microscopy (SBF-SEM) (Starborg and Kadler 2015). SBF-SEM provides a tool to reconstruct three-dimensional models of structures at a high magnification (Starborg and Kadler 2015, Tafti et al. 2015). In SBF-SEM imaging, a beam of electrons is rastered across the surface of a sample *en bloc*, then the backscattered electrons are collected and portrayed as an image. To enhance the backscatter electron signal, the samples are stained with heavy metals during processing. In addition, the automated serial sectioning capability of an in-chamber ultramicrotome within the microscope allows sections repeated renewal of the sample face for multiple imaging, providing a large dataset for three-dimensional reconstruction (**Figure 1.12**).

Throughout this thesis, SBF-SEM will be used for three-dimensional structural analysis. It will be used to analyse the interactions of the developing cells and surrounding deposited extracellular matrix. In addition, this technique will be

used to reconstruct developing and adult elastic fibres within the embryonic and adult mammalian cornea.

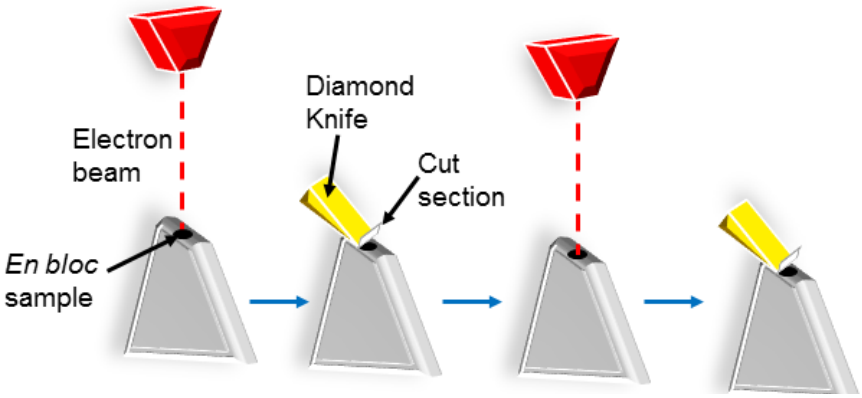

Figure 1.12. ***Serial block-face scanning electron microscopy.***

Once the desired area of a sample is selected, electrons are fired at the block face surface with an electron beam and the backscattered electrons are detected and conveyed into an image. Once imaged, a diamond knife cuts the top of the sample to remove a section (50 nm), to expose a new surface and allow another image to be taken. This process is repeated until a dataset of images are collected. The dataset is then reconstructed into a three-dimensional model.

1.7. X-ray Scattering Techniques

X-ray scattering experiments have proved imperative for gaining structural information of the cornea. The corneal stroma contains a highly ordered system of collagen molecules and fibrils, which allows an X-ray scatter pattern to be formed when X-rays pass through its thickness (Meek and Quantock 2001). Depending on whether a small-angle X-ray scattering (SAXS) or a wide-angle X-ray scattering (WAXS) technique is selected will provide quantitative data from different hierarchical levels within the collagen structure. SAXS produces both meridional and equatorial X-ray reflections. It is the ordered collagen fibrils within the cornea that give a series of meridional X-ray reflections that arise from the D-periodicity of the axial ordering of the collagen fibrils (Bear 1942). The equatorial reflection allows measurements of collagen fibril diameter and interfibrillar spacing to be collected (Meek and Quantock, 2001). When the scattering angle is increased to give a WAXS scattering pattern, the orientation and distribution of the collagen molecules within fibrils can be calculated (North et al. 1954).

SAXS techniques allow the analysis of fresh samples; this means that tissue ultrastructure is not altered compared with the fixed tissue imaged with electron microscopy (Fullwood and Meek 1993). Therefore, the tissue is closer to its physiological structure *in vivo*. In addition, an average measurement of the scattering by every fibril in the X-ray beam path throughout the volume of tissue and across different samples is measured, this improves the reliability of the data. However, interfibrillar spacing results are dependent on tissue hydration and the values obtained are very sensitive to any alterations to the water content of tissues.

Research presented in this thesis used X-ray diffraction techniques to analyse collagen fibril ultrastructure. Specifically, SAXS was used to measure collagen fibril spacing and collagen fibril diameters. To interpret the SAXS results, it was important to understand the corneas overall shape and structure. To do

this, optical coherence tomography was used to measure corneal thickness and curvature before the SAXS data was collected.

1.8. Optical Coherence Tomography

Optical coherence tomography (OCT) imaging provides a non-invasive technique to analyse tissue in cross-section without causing any damage or ultrastructural changes (Huang et al. 1991). OCT is analogous to ultrasound imaging techniques but replaces sound for near-infrared light to receive an image. The near-infrared light can penetrate through the scattering medium to obtain a series of two-dimensional images through different axis at a micron-scale resolution over the depth of several millimetres. Thus, the datasets can be combined to reconstruct three-dimensional images to accurately measure structures. An advantage of the relatively non-invasive method that the OCT provides is that the tissue can be further prepared for experiments to give information that the OCT cannot obtain.

Mouse corneal curvature and thickness was measured using OCT before the ultrastructure of the tissue was further investigated with electron microscopy and X-ray scattering techniques.

1.9. Aims

The overall aim of this thesis was to structurally analyse the developing mammalian corneal stroma with imaging techniques. Novel three-dimensional imaging techniques were used to analyse cells and extracellular matrix components within the corneal stroma during mouse and human corneal development. The emphasis was placed on three-dimensional structural interactions between cell migrations and the surrounding extracellular matrix during early prenatal development that synthesise and secrete a physiological corneal stroma. The second aim of the thesis was to analyse human corneal

development, with a focus on the initial development of the corneal stroma and elastic fibres. In addition, the importance of elastic fibres in the embryonic cornea was explored by comparing the wild type cornea with a Marfan syndrome mouse model, where fibrillin-1 is disrupted.

The specific chapter aims:

Chapter 3: A 3-D structural study of the developing mouse corneal stroma.

To use three-dimensional serial block-face scanning electron microscopy and transmission electron microscopy techniques to analyse cell and extracellular matrix interactions in the developing mouse cornea. The specific aim was to elucidate the poorly understood sequence of mouse corneal development compared to the chick model.

Chapter 4: Collagen and proteoglycan distributions in the developing mouse cornea.

To characterise the distribution of types I, II, V and IX collagen in the prenatal mouse cornea using immunofluorescence techniques. To analyse proteoglycan structures and their associations with cells and collagen during extracellular matrix deposition in the developing mouse cornea using transmission electron microscopy.

Chapter 5: A structural study to compare the elastic fibre system between the adult mouse and human cornea.

To localise and compare the adult human and mouse elastic fibre systems using immunofluorescence and electron microscopy techniques and test the hypothesis that elastic fibres are concentrated within the posterior peripheral cornea of the human and mouse.

Chapter 6: A 3-D structural study of the developing human corneal stroma.

To analyse the developing human corneal stroma in three-dimensions, with a focus on the elastic fibre system using serial block-face scanning electron microscopy and transmission electron microscopy. To test the hypothesis that elastic fibres are present within the developing human cornea and that human corneal development follows a similar pattern to that in the mouse.

Chapter 7: A Structural study of the developing fibrillin-1 knockout mouse cornea.

To test the hypothesis that a disruption to the fibrillin-1 network perturbs corneal development in a Marfan syndrome mouse model using 3-D reconstructions from serial block-face scanning electron microscopy, transmission electron microscopy, optical coherence tomography and small-angle X-ray scattering techniques.

Chapter 2: General Methods

2.1. Tissue Collection

2.1.1. Mouse tissue collection and embryo ageing

All mouse tissue was ordered from Charles Rivers, Margate, United Kingdom. For all experiments that analysed developing mice, time-mated maternal mice were ordered at the developmental embryonic age's day (E) 10, 11, 12, 13, 14, 15, 16, 17 and 18. The maternal parent was sacrificed when the embryos reached the required developmental stage via cervical dislocation at a Schedule 1-approved designated establishment in accordance with Animals (scientific procedure) Act 1986 (United Kingdom) and Home Office (United Kingdom) guidance rules. All research carried out on animal tissue followed the rules and regulations concerning animals in research under the Association for Research in Vision and Ophthalmology (ARVO) statement. The impregnated mice were aged where the appearance of a plug (Day 0) was first apparent after fertilisation.

The embryos were dissected from the impregnated mouse and removed from the uterus (**Figure 2.1**). The embryos were dissected and staged using a combination of the Theiler stage definition as well as the use of a mouse timeline atlas (**Figure 2.2**) (Theiler 1989, Wong et al. 2015). The age of the embryo was determined by the analysis of their size as well as their surface and developmental morphological characteristics.

At E10, the embryos had no sign of limb formation, characterised by the presence of a deepened lens pit and the initial appearance of the umbilical hernia. By E11 the lens vesicle closed, cervical somites diminished and the brain was clearly visible. The first early signs of hind-limb digits appear at E12 and the hand-plate develop angles which represent the presumptive digits of

the limbs. The retina showed pigmentation at E12, as there were no coverings over the eyes. At E13 the footplates were indented and the location and thickness of the digits were visible. By E14, the digits had separated in the distal aspect of the forelimb as well as the presence of indentations, which indicated the hind-limb digits. At E14 the bones of the limbs were present and hair follicles were seen in the trunk, pectoral and pelvic areas. At E15 the toes separated and hair follicles were now identified in the cephalic regions. By E16 the eyelids had formed and fused over the eyes, the umbilical hernia had disappeared and there was an increase in the overall size of the peritoneal sac. The skin had thickened with a wrinkled texture by E17. The digits in the forelimb and hind-limb had also become parallel within E17. By E18, one day before birth, the whiskers were present with an exponential increase in skin thickness.

Once the age of the tissue was determined, the whole eyes were dissected out of the embryos, excluding the younger ages (E10-E11), where the eyes were left *in situ* due to their small size and fragile nature. To reduce tissue wastage, the adult mouse eyes used throughout this thesis, unless stated otherwise, were taken from the maternal adult mice. Tissue was then divided for different experiments; being placed in the necessary fixative, snap-frozen for cryosectioning or processed for its specific use. The specific preparation of tissue will be outlined in every experiment undertaken throughout this thesis.

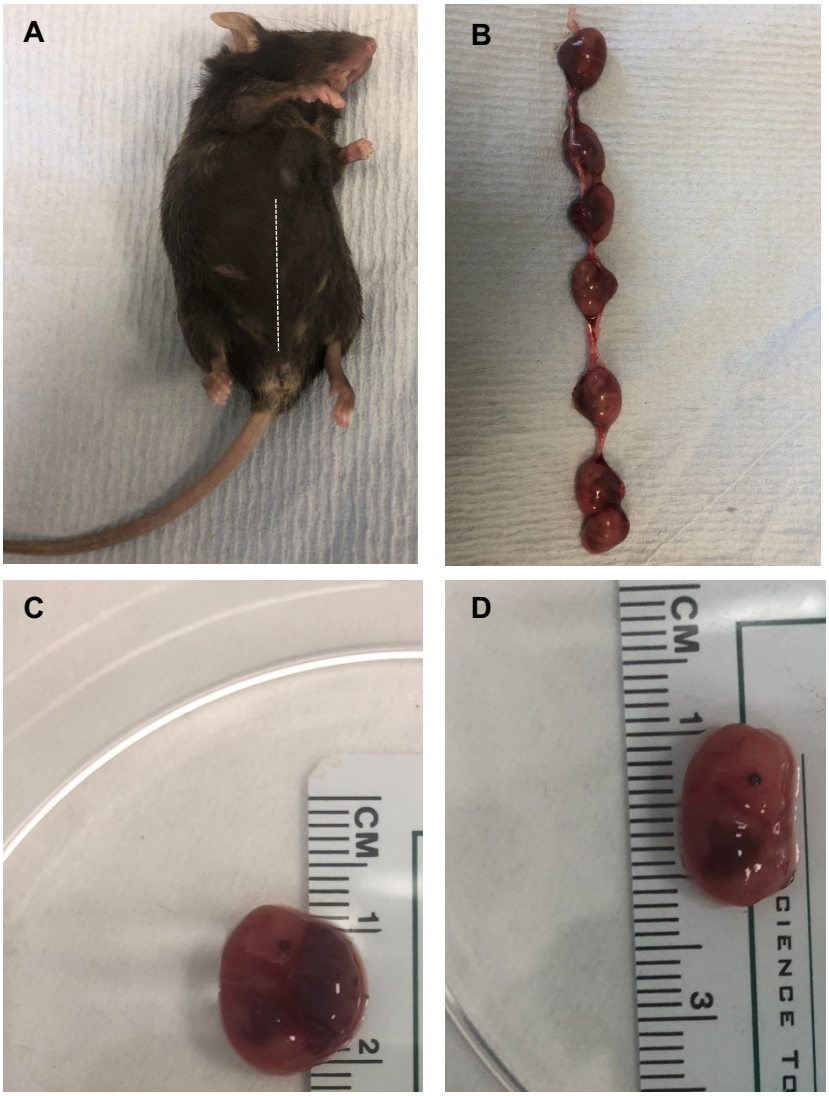

Figure 2.1. ***Method to dissect mouse embryos from impregnated maternal mouse.***

Fig. 2.1A: An incision was made vertically along the lower abdomen (white dotted lines). **Fig. 2.1B:** The embryos were dissected out of the uterus using a dissecting microscope, removing all membranous tissue. **Fig. 2.1C and Fig. 2.1D:** The embryos were dissected one at a time. The embryos were carefully removed from the placenta and aged accordingly.

The ages E10, E11, E12, E13, E14, E15, E16, E17 and E18 post-fertilisation were obtained. The embryo ages were determined by the analysis of the size, surface and developmental morphological characteristics of the embryos (**Figure 2.2**).

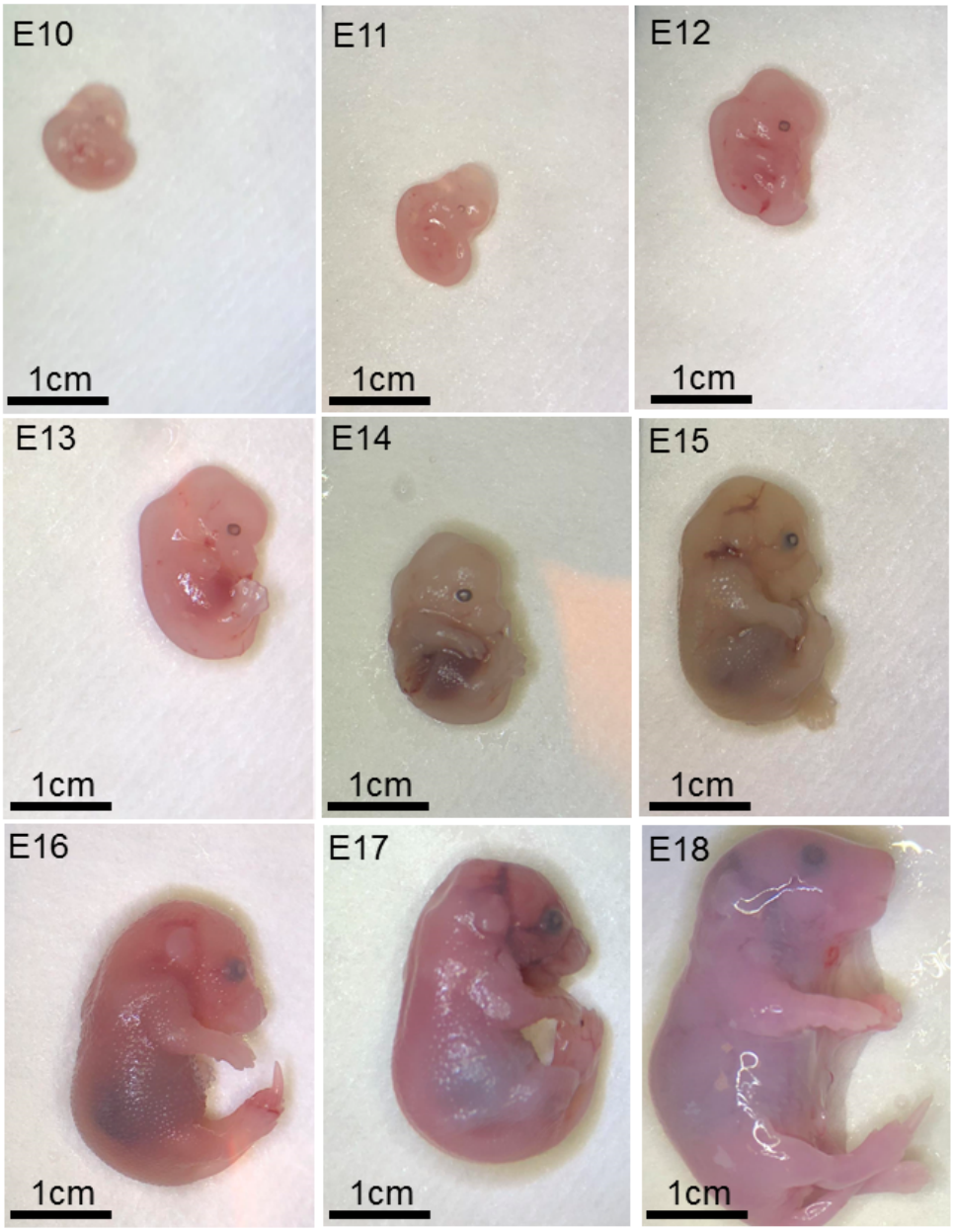

Figure 2.2. Embryonic tissue aged E10-E18.

Embryos were aged based on morphological features and size using the Theiler stage definition and a mouse timeline atlas. Once the ages of the embryos were determined, the eyes of embryos E12-E18 were dissected and prepared for a specific experiment. The eyes of embryos E10 and E11 were too small to dissect, therefore the eyes were left *in situ* for experiments. The tissues for all embryonic ages were either placed in 0.5% paraformaldehyde, 4% paraformaldehyde, cuprolinic blue or frozen in optimal cutting temperature for cryo-sectioning.

2.1.2. Human Tissue Collection

All adult human tissue used in this thesis was obtained from the NHS Blood and Transplant (NHSBT), UK and was used in accordance with the human tissue act 2004 legislation.

All foetal human tissue used for experiments in this thesis was obtained from the Human Developmental Biology Resource (HDBR), Newcastle, UK and was used in accordance with the human tissue act 2004.

Throughout this thesis where human tissue was used the specific methodology and preparation techniques have been outlined in each chapters' methodology.

All experiments carried out throughout this thesis followed the Declaration of Helsinki guidelines and ethical principles developed by the World Medical Association.

2.2. Electron Microscopy

Serial block-face scanning electron microscopy (SBF-SEM) was used to investigate the 3-D ultrastructural organisation of developing cells, extracellular matrix components and elastic fibres. Transmission electron microscopy (TEM) was used to determine the fine ultrastructure detail of samples at a higher magnification, beyond the capabilities of the SBF-SEM.

2.2.1. Serial block-face scanning electron microscopy

2.2.1.1. Sample preparation: En bloc staining

Two different en block processing methods were used. One specifically to enhance the contrast of elastic fibres and the other for general ultrastructural morphology of cells and tissues.

Elastic fibres were stained using an SBF-SEM processing method that combined tannic acid-uranyl acetate and en block lead electron microscopy staining procedures. The combination of uranyl acetate and lead stains the microfibrillar component of elastic fibres whereas tannic acid specifically stains the amorphous core (Simmons and Avery 1980). These EM processing techniques were incorporated into a single SBF-SEM en-block processing method specifically developed to enhance elastic fibres by (Lewis et al. 2016). This method has subsequently been used in a number of publications on elastic fibre (White et al. 2017a, White et al. 2017b).

2.2.1.1.1. The elastic fibre staining procedure

Samples were fixed in Karnovsky's fixative (2.5% glutaraldehyde, 2% paraformaldehyde, 0.1 M cacodylate buffer pH 7.2) for 3 hours at 4°C. Samples were then washed in cacodylate buffer 3 times over 10 mins and in distilled water (H_20) for 5 mins. Samples were immersed in 1% osmium tetroxide for 1 hour. Samples were washed with distilled H_20 3 times over 20 mins before 0.5% of filtered tannic acid (TA) was added to distilled H_20 for 2 hours. Samples were washed with distilled H_20 3 times over 30 mins and left overnight in 2% aqueous uranyl acetate (UA).

The samples were dehydrated through an ethanol series of increasing concentrations every 20 mins (70%, 90%, 100% and 100%). They were then placed in 1% UA in 100% ethanol for 2 hours and washed with 100% ethanol twice over 20 mins and transferred to 1:1 ethanol-acetone for 10 mins.

Samples were then washed in 1:1 ethanol-acetone twice over 15 mins. Lead acetate was added in excess to 25 ml of 100% ethanol and shaken for 15 mins. The mixture was shaken and 25 ml of 100% acetone was added and shaken for a further 15 mins. The mixture was filtered twice before the samples were added for 2 hours. The samples were washed with 1:1 ethanol acetone twice over 20 mins and then washed 3 times over 20 mins with 100% acetone.

Araldite resin (50%) and acetone 50% (1:1) were added to the samples for 1 hour. 100% Araldite resin was made up with 98 ml of Araldite monomer CY212 and 112ml of DDSA hardener and left overnight. 2.4 ml of BDMA accelerator was added to 120 ml of pre-made Araldite resin. The resin mixture was added to the samples every 2 hours until 6 changes had been made and were left overnight with the caps off. The samples were embedded into a mould, which contained resin and was polymerised at 60°C for 48 hours. The resin blocks were then prepared for transmission electron microscopy (TEM) or serial block-face scanning electron microscopy (SBF-SEM).

2.2.1.1.2. General morphology cell and tissue staining procedure

A “modified Deerinck” method was employed to stain the general morphology of structures (Deerinck 2010). The samples were washed in cacodylate buffer 3 times over 10 mins and added to 1.5% potassium ferricyanide/1% osmium tetroxide in 0.1M cacodylate for one hour. They were washed 5 times over 30 mins with distilled H_20 before being added to 1% thiocarbohydrazide for 30 mins. They were then washed 5 times over 30 mins before adding a solution of 1% osmium tetroxide to the vials for 1 hour, after which they were washed with distilled H_20 5 times over 30 mins before being added to 1% uranyl acetate for 1 hour. After uranyl acetate staining, they were washed with distilled H_20 5 times over 30 mins before being added to excess lead aspartate made up with 25 ml acetone and 25 ml ethanol for 1 hour.

The samples were then washed with distilled water 5 times over 30 mins before going through a dehydration series of rising concentrations of ethanol every 25 mins (70%, 90%, 100% and 100%). They were immersed in 1:1 acetone (50%) and ethanol (50%) before being introduced to 100% acetone for 25 mins twice, then added to 1:1 acetone and Araldite resin (98 ml Araldite and 112 ml DDSA hardener) and left overnight. The samples were then embedded in resin and processed into blocks as previously described in the elastic fibre staining method (section 2.2.1.1.1).

2.2.1.2. Semi-thin sectioning

A resin block was secured into the Leica UC6 ultra-microtome trimmed with a razor blade and cut using glass knives which were prepared on a Leica EM KMR2 glass knife maker (Leica Microsystems, Wetzlar, Germany). Once the correct orientation of the sample was determined, semi-thin sections (0.25 µm) were cut in order to identify the precise region of interest (ROI) for imaging. Sections were collected from a small water collecting reservoir "boat" which was attached to the glass knife. These cut sections were picked up with a loop and transferred onto a microscope slide (Thermo Fisher Scientific, Waltham, MA, USA) (Rieder 1981). The samples were dried on a heat plate before toluidine blue was added to the sections using a pipette. The toluidine blue dye was washed off with distilled H_20 and analysed under a microscope to confirm the ROI of the sample.

2.2.1.3. Pin preparation

Once the samples ROI was established, the resin block was further trimmed with a razor blade to create a cube approximately 1-2 mm^2. This was then mounted onto a Gatan specimen pin using super glue and left to dry for 2 hours. Silver conductive epoxy (TAAB laboratories, Aldermaston, England) was used to cover the sides of the specimen cube in contact with the pin in order to negate charging in the SEM during image acquisition. The pin was

then left to dry for a further 24 hours. The surface of the specimen block was then polished using a Leica UC6 ultramicrotome.

2.2.1.4. SBF-SEM imaging, data acquisition and 3-D analysis

The pin was gold-sputtered coated with 8 nm gold using the Leica ACE 200 (Leica Microsystems, Wetzlar, Germany) and placed within the chamber of a Zeiss Sigma VP FEG SEM equipped with a Gatan 3View system (**Figure 2.3**). The block face ROI of the specimen was then imaged on the SEM at 3.5 KV at a pixel resolution of 4 nm and a dwell time of 8 µs and approximately 1000 images slices were acquired from the specimen block every 50 nm by automated serial sectioning. All SBF-SEM data sets were recorded at 4096 x 4096 (4K) in Gatan format dm4 files then batch converted to TIFF format and were 3-D reconstructed using Amira 6.4 software (FEI, Mérignac, France). The large number of samples and the complexity of 3-D data generated required different image analysis strategies.

Corneal ultrastructure at the tissue and cell level were reconstructed and 3-D rendered with Amira 6.4 using a combination of semi-automated 3-D volume generation (Volren) and surface generation (isosurface). Manual segmentation was used to segment out specific ultrastructural elements from 3-D data sets with a variety of segmentation tools. 3-D reconstructions using Volren and isosurface functions were created by manually choosing a threshold to reconstruct all of the 3-D components within the data set in their entirety.

For 3-D reconstructions of the elastic fibre network. A combination of both manual and semi-automated 3-D rendering techniques using Amira 6.4 software was used to reconstruct the complex fibre network. The staining intensity of the SBF-SEM electron microscopy protocol allowed for most of the complex elastic fibre network to be rendered in 3-D using Amira 6.4

semi-automated isosurface rendering tools. The grey scale values of the elastic fibres allowed for most of the fibres to be identified from the surrounding matrix.

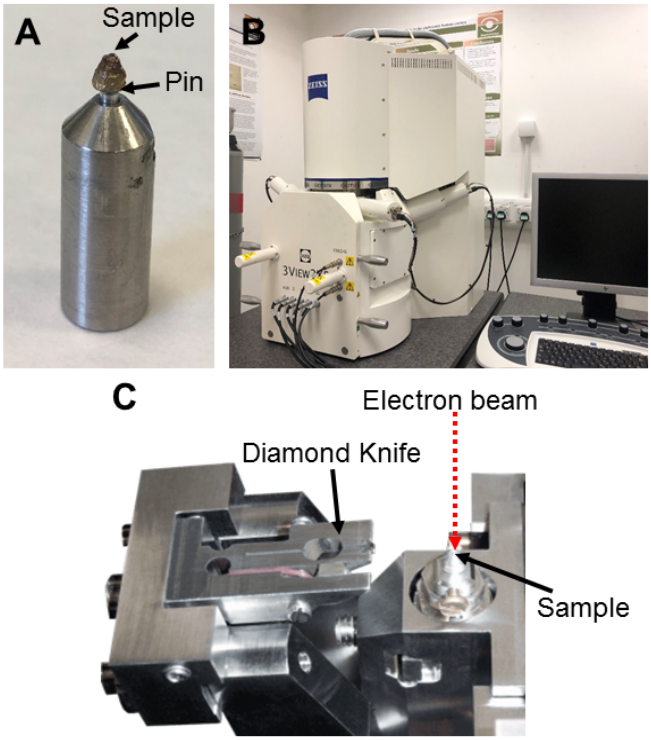

Figure 2.3. Serial Block-Face Scanning Electron Microscopy (SBF-SEM).

Fig. 2.3A: A SBF-SEM sample mounted onto an aluminium pin. **Fig. 2.3B:** The pin is placed into the serial block-face scanning electron microscope unit. **Fig. 2.3C:** The microscope is equipped with a 3-view system to allow serial sectioning of the sample. An electron beam is used to direct electrons to the sample, where an image is collected from the backscattered electrons. The stage containing a diamond knife then moves over the block face surface to remove a 50 nm slice of the sample before another image is taken. This occurs until up to 1000 images are collected, which are then reconstructed into a three-dimensional dataset.

2.2.2. Transmission electron microscopy (TEM)

2.2.2.1. Sample Preparation: Elastic fibre and general cell and tissue staining

Please refer to SBF-SEM sample preparation en bloc staining (section 2.2.1), which are the same staining methods used for TEM.

2.2.2.2. Ultra-thin sectioning

The orientation of the block was identified and trimmed using a razor blade to a (~1-2 mm x 1-2 mm) ROI. Gold ultrathin sections (90 nm) were then cut using a diamond knife (Diatome, Nidau, Switzerland) and sections collected into the water-filled reservoir within the knife. Chloroform was used to decompress and smooth out the sections which floated on the surface of the water reservoir. Ribbon sections were collected using a loop and placed on 300 hexagonal copper TEM grids.

2.2.2.3. Imaging and analysis

A JEOL 1010 transmission electron microscope with a Gatan Orius 1000 TEM camera (Gatan, Abingdon, England) was used to image the samples on TEM grids at an accelerating voltage of 80 KV at set magnifications ranging from 1k-50K (**Figure 2.4**). Transmission electron microscopy generates higher-magnification images approximately <4 nm, which allowed for resolving fine ultrastructural details of the cells and extracellular matrix components that could not be resolved using the SBF-SEM technique. The images collected on the TEM were saved as TIFF files and analysed in Image J.

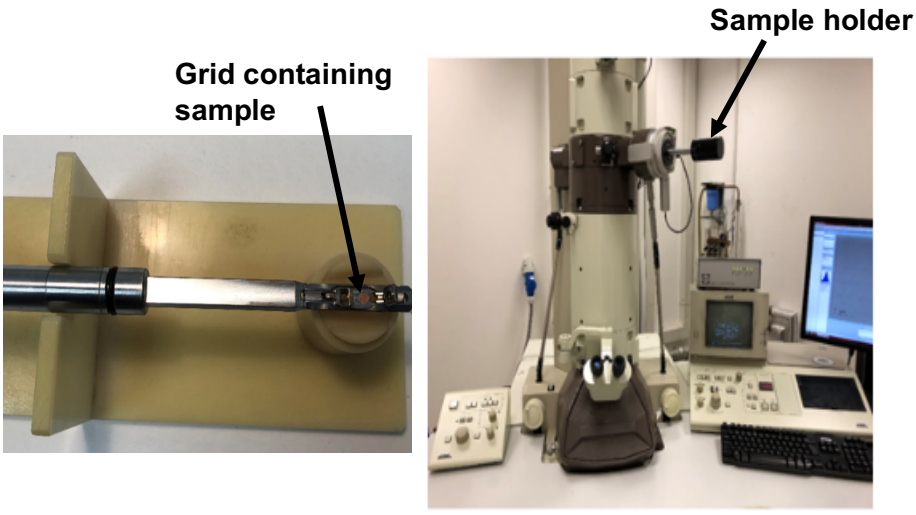

Figure 2.4. Transmission electron microscopy imaging.

Fig. 2.4A: Samples collected on hexagonal copper grids were placed into a sample holder. **Fig. 2.4A:** Samples were imaged using the JEOL 1010 transmission electron microscope.

2.2.2.4. Proteoglycan processing protocol for TEM imaging

2.2.2.4.1. Cuprolinic blue staining method

The Quinolinic phthalocyanate (cuprolinic blue) method was used to visualise glycosaminoglycan chains of proteoglycans with TEM imaging. The staining initiated a cationic metachromatic reaction, which reacted with the anionic glycosaminoglycan side chains that attach to the proteoglycan core protein (Juarranz et al. 1987). To increase the specificity of the dye, a critical electrolyte concentration method is used, which visualises proteoglycans as electron-dense elongated, filament-like components with electron microscopy imaging (Scott 1980, Scott and Haigh 1988a). This method included the addition of negatively charged magnesium chloride, which takes up the binding sites of poly-anions; this means that only the sulphate groups which are only prevalent on the proteoglycans in the cornea bind to the dye. To enhance the contrast of proteoglycans for electron microscopy imaging sodium tungstate is then added, with the tungstate binding to the poly-anionic-dye complex to enhance electron density (Scott 1980).

Fresh mouse tissue was dissected as required and immersed in vials overnight in 2.5% glutaraldehyde in 25 mM sodium acetate buffer, pH 5.7, which contained 0.1M magnesium chloride and 0.05% cuprolinic blue (American Elements, Los Angeles, USA). The 25mM sodium acetate buffer was made from 0.205 g/100 ml sodium acetate, 2.03 g/100 ml of 0.1M magnesium chloride with the pH being adjusted to 5.7 with 0.1M hydrochloric acid. The samples were rinsed in sodium acetate buffer 3 times over 5 mins and washed 3 times over 10 mins in aqueous 0.5% sodium tungstate.

The samples were dehydrated in an ethanol series at increasing concentrations every 15 mins. Initially 50% ethanol with 0.5% sodium tungstate and thereafter 70%, 90%, 100% and 100% ethanol. The samples were then added to 1:1 acetone (50%) and ethanol (50%) for 15 mins, before being added to acetone twice over 30 mins. The samples were further added

to 50% acetone and 50% Araldite resin mixture (98 ml Araldite and 112 ml DDSA hardener) for one hour, three 100% resin changes were then made every 2 hours, with vials being left on a rotator with no lids, which allowed acetone to evaporate overnight. 2.4 ml of BDMA accelerator was added to 120 ml 100% Araldite resin with continuous resin changes made every 2 hours throughout the day. Samples were orientated and embedded into moulds and then placed into an oven at 60°C to allow polymerisation of the resin blocks.

2.2.2.4.2. Ultrathin sectioning and imaging

Samples were cut, sectioned and imaged as previously described in the SBF-SEM ultrathin sectioning and imaging section of this chapter.

2.3. Optical Coherence Tomography (OCT)

2.3.1. Data Collection

OCT was used to analyse corneal thickness and corneal curvature. All OCT results were collected with a near-infrared (NIR) bespoke OCT microscope. The light source had a central wavelength of 1040 nm with a bandwidth of 70 nm (1-M-ASE-HPE-S; NP Photonics, Tucson, AZ, USA) connected through a 2 x 2 optical fiber coupler (FC; FOBC-2-64+/−100-20-L-H64f-2; AFW Technologies, Hallam, Victoria, Australia) which connected with an imaging head and reference arm. The imaging head contained an achromatic off-axis parabolic reflector to collimate the fiber output beam to 2 mm diameter (RC02APC-P01; Thorlabs, Ely, UK) with 2-D (XY) optical scanners (6210HBM60/6102103R; Cambridge Technology Division, GSI Group GmbH, Muenchner, Germany) and a broad-band near-infrared telecentric scan lens (LSM02BB; Thorlabs). The reference arm contained a polarization controller (PC; FPC560, Thorlabs), a reflecting collimator (RC08APC-01; Thorlabs), an adjustable aperture, a precision near-infrared retroreflector (RR; 1 Arcsec Gold, Edmund Optics, York, UK) and a glass compensation block (CB;

LSM02DC; Thorlabs) to correct for dispersion in the scan lens. Reflected light from the specimen and reference arm was combined in a spectrometer. The camera within the OCT microscope was a 47 kHz Goodrich SU-LDH-1.7 (UTC Aerospace Systems, Arlington, VA, USA).

Each eye globe analysed was placed onto a glass slide secured by Blu Tack® with the corneal surface facing upwards for scanning (**Figure 2.5**). Datasets of 1000 images were collected at a 1024 x 1024 pixel resolution at different scanning angles. The collected data of reflected infrared light from every 2-D (XY) scan were processed into a 3-D volume imaged by spectral resampling and Fourier transformation. The OCT was controlled by LabView (National Instruments, Newbury, UK) software and spectra. Datasets were then processed using MATLAB (Mathworks, Cambridge, UK) and ImageJ/Fiji software (Wayne Rasband, U.S. National Institutes of Health, Maryland, USA). The collected datasets recorded as FDN files were converted into TIFF files using a MATLAB OCT FD1 data processing script. The datasets were then in the correct file type to be read into ImageJ/Fiji and analysed.

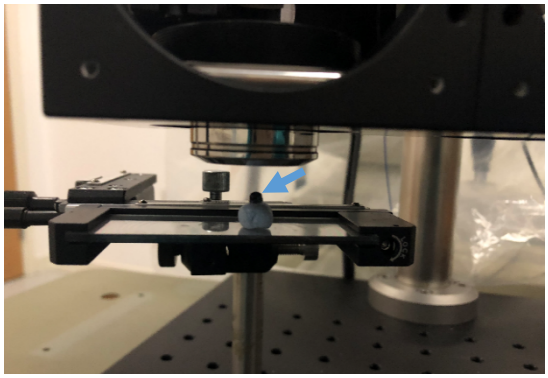

Figure 2.5. OCT imaging.

A sample, in this case a whole mouse eye (blue arrow), is placed on Blue-Tac®, which is placed onto a glass slide. When the cornea is imaged, it is vital that the cornea is facing directly upwards towards the infrared light source. The sample was moved into the correct position by moving the slide through the x and y positions. In addition, the slide can be tilted for the cornea to be positioned correctly.

2.3.2. Data Analysis

The datasets were imported into ImageJ, being re-spliced to give an *en face* view and sectioned into five images at different degrees (0°, 10°, 75°, 90°, 135°). The 90° image was selected for analysis throughout each calculation for different samples. Initially, the datasets were scaled due to various scans being taken at a different scan angle. To scale an image the μm per pixel was calculated as following for a 1024 image:

$$\mu m\ per\ pixel = \frac{\text{Angle of Scan}}{1024} \times\ 283.207$$

Lateral scaling is required to scale an obtained image and was calculated by dividing the pixels per micron value by the pixel height of the tissue. The pixel height in the adult mouse cornea was calculated by dividing the pixel height (2.66) by the refractive index of the cornea (1.376) (Hughes 1972, Massof and Chang 1972), leading to a pixel height in the adult mouse cornea of 1.933. The pixel height and width were input into ImageJ properties, followed by scaling by adding lateral scaling in the x plot, whilst keeping the y plot as 1 (voxel depth). The pixel height for the developmental tissue was assumed to be the same. Unfortunately, due to the small size of the corneal tissue, the refractive index could not be accurately calculated. With the images scaled, corneal thickness and curvature calculations were carried out using a measuring tool in ImageJ.

To calculate corneal thickness the following method was used:

$$Actual\ Thickness\ (\mu m) = \frac{\text{Number of pixels x} - \text{axial scaling}}{\text{Refractive index of the cornea}}$$

The “Straight” tool was used to measure the thickness of the curvature by drawing a line from the anterior to the posterior cornea at the most central point, due to the image being scaled the value measured was directly comparable to μm.

The radius of curvature was measured from the arc formed at the anterior surface of the cornea using the following equation:

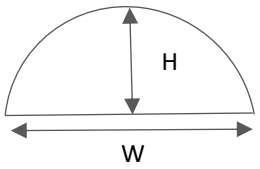

$$r = \frac{H}{2} + \frac{W^2}{8H}$$

Where,

H = Height

W = Width

r = radius

In ImageJ, a box was drawn with a constant height when calculating corneal curvature within comparable tissue samples. The width of the box varied depending on the curvature of the cornea, the edges of the box always ended on the surface of the cornea. The height and width values were taken from the box drawn and were input into the above equation to calculate the radius of curvature at the centre of the cornea.

2.4. Small-Angle X-Ray Scattering (SAXS)

2.4.1. Sample Preparation

Small-angle X-ray scattering patterns were obtained at the I22 beamline (Diamond Light Source, Oxfordshire, UK). Each sample was stored in 4% PFA and just before being placed into the sample holder the sample was wrapped tightly in one sheet of cling film to prevent sample dehydration. The samples were placed into a Perspex sample holder that contained two transparent Mylar sheet windows. The sample holder was positioned on the beamline with the anterior surface central cornea perpendicular to the incident X-ray beam (**Figure 2.6**). The resultant X-ray scatter pattern was recorded as grid scans 0.3 x 0.3 µm with a 0.1 second exposure time on a multi-wire gas detector, using an X-ray beam measuring 200 x 200 µm with a wavelength of 0.1 nm.

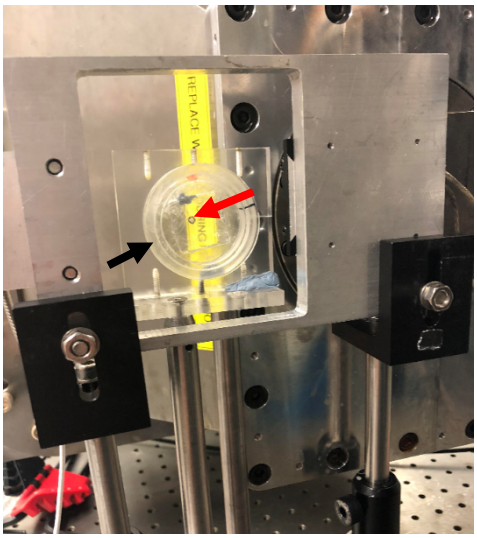

Figure 2.6. Small angle X-ray diffraction sample set up.

One whole cornea was placed into a Perspex sample holder that contained two transparent Mylar sheet windows (black arrow). The sample holder was positioned on the beamline with the anterior surface central cornea perpendicular to the incident X-ray beam red arrow). A grid scan was taken across the whole cornea.

2.4.2. Analysis

The SAXS datasets initially collected in NSX files were converted into TIFF files using DAWN (Diamond Light Source, Oxfordshire, UK). The converted TIFF files were then uploaded into SAXS4COLL for analysis (Abass et al. 2017). To use this software, initially, the images needed to be centred using a powdered silver behenate diffraction pattern. Using a MATLAB script which improves the accuracy of pixel resolution, five points were manually selected around the circumference of the X-ray scatter image to precisely determine the x and y co-ordinates of the centre of the pattern. Calibration of the X-ray set-up is necessary as it is very difficult to measure the distance from the specimen to the detector accurately, and hence determine the scatter angle 2θ. Calibration of the patterns is carried out using the known periodicity of the powdered silver behenate. This is done by manually selecting the first order peak of the silver behenate reflection corresponding to its 58.380 Å crystal spacing. These values are then input into SAXS4COLL which uses the known values of the wavelength of the X-rays, and the Bragg spacing, to determine the scatter angle from Bragg's law:

$$2d \sin\theta = n\lambda$$

Where,

d = Bragg spacing

θ = half the angle between incident X-ray beam and reflection

n = order of reflection

λ = radiation wavelength

The specimen-film distance is then given by:

$$Detector\ distance = \frac{radius\ of\ calibrated\ reflection\ (r)}{tan2\theta}$$

The X-ray scatter patterns from the cornea included scatter from all tissue components, therefore the residual background scatter needed to be deducted from this to retrieve the diffraction scatter from the collagen. Once calibration had been carried out, a SAXS dataset, which included a whole grid scan was loaded into SAXS4COLL, automatically radially integrated and then presented as a double logarithmic plot. A power function background was accurately fitted to the dataset by manually selecting three points (**Figure 2.7A**), which equates to general power function in linear space:

$$I = aR^b$$

Where,

I = Integrated SAX intensity

R = Radial pixel

a = Constant

b = Constant

From the SAXS pattern with the now subtracted background signals, the collagen equatorial interference function peak is selected by clicking the top of the peak (**Figure 2.7B**). By selecting the peak, the interfibrillar Bragg spacing (d) is determined, and the centre-to-centre collagen interfibrillar spacing is calculated on the assumption that fibrils are packed in a liquid-like manner

(Inouye 1983). To calculate the average collagen fibril diameter, a Bessel function representing the equatorial fibril transform is fitted over the first subsidiary maximum in the equatorial scatter pattern (**Figure 2.7C**) (Meek and Quantock 2001). The meridional D-period is calculated by selecting the peak of the third order meridional reflection (**Figure 2.7C**).

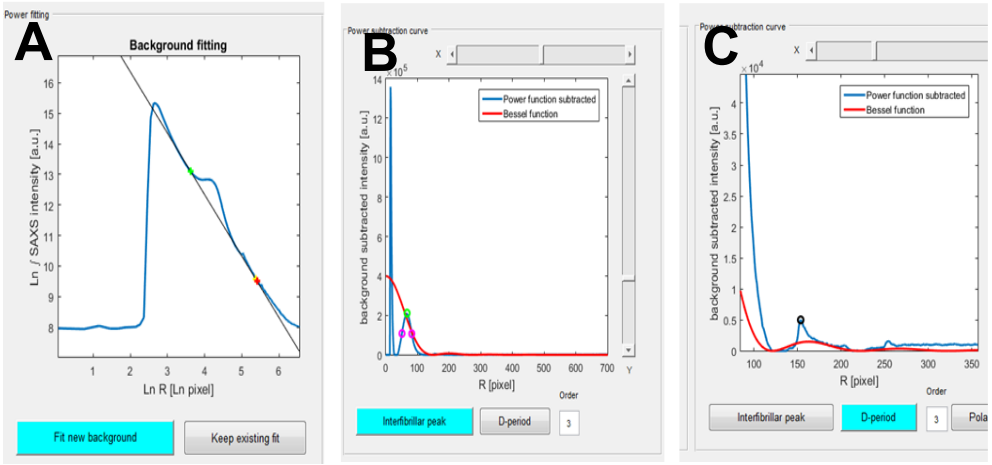

Figure 2.7. Small angle X-ray diffraction analysis with SAXS4COLL.

Fig. 2.7A: With the SAX4COLL software, a power function background was fitted by selecting three points along an input dataset. Once a power function was fitted, the software subtracted the background from the dataset. **Fig. 2.7B:** The background subtracted data allowed the selection of the interfibrillar peak (green circle) to calculate interfibrillar spacing. **Fig. 2.7C:** A Bessel function (red curve) is then fitted over the first subsidiary maximum (blue peak) in the equatorial pattern to calculate average collagen fibril diameter. The peak is then selected (black circle) to calculate the D-period. R = radial distance from the centre of the pattern.

2.5. Immunofluorescence

All the samples that were examined with immunofluorescence were snap frozen in optimal cutting temperature compound over isopentane which was placed over liquid nitrogen, cryo-sectioned (Leica CM3050 S cryostat) and collected on Superfrost Plus Slides (Thermo Scientific, UK). The plane of the sample when cryo-sectioned is stated in each chapter.

All cryo-sections were circumscribed with a water-repellent delimiting pen (ImmEdge Hydrophobic Barrier PAP pen, Vector labs) before being rehydrated with phosphate buffered saline-Tween-20 (PBST) made up of 0.1% Tween-20 and 0.05M phosphate buffer saline solution. 5% horse serum in PBST was applied to cryo-sections for 20 mins to prevent non-specific antibody binding (Levy E. M. 1980). Primary antibodies were added to the cryo-sections and incubated for 24 hours at 4°C (the antibodies used are listed in the specific chapters). The antibodies were tested at different concentrations (1:10, 1:100, 1:200 and 1:1000), the specific concentrations that the antibodies were used at are stated in each chapter. PBST was used to wash off the primary antibodies 3 times over 10 mins before the secondary antibodies (specific to the primary antibody used) were added. Cryo-sections were incubated for 5 hours at room temperature before the secondary antibodies were washed off with PBST. Coverslips (VWR International) were then added to the cryo-sections using VECTASHIELD HardSet Antifade Mounting Medium with 4',6-diamidino-2-2-phenylindole (DAPI) (Vector Laboratories), emitting a blue fluorescence when bound to deoxyribonucleic acid (DNA) for cell nuclei detection. Cryo-sections were imaged with the Olympus BX61 epifluorescence microscope, equipped with an F-view Digital camera at x10, x20 and x40 objectives.

For all experiments, controls were carried out. To test the efficacy of the primary antibodies, a specific immunoglobulin control was used which matched the immunoglobulins in the specific primary antibody. Any label that was present in the immunoglobulin applied controls was known to be unspecific staining. To test the secondary antibody, no primary antibody was applied and the section only contained the secondary antibody. Any labelling that was detected in these controls were identified as background stain. Finally, to test if there was any autofluorescence, a slide which contained a cryosection was imaged that had no primary or secondary stain. In addition to negative controls, positive controls were carried out where the antibody was tested on a tissue that was known to contain the protein of interest.

Chapter 3: 3-D Structural Study of the Developing Mouse Corneal Stroma

3.1. Introduction

The successful development of a functional tissue relies on the finely tuned alignment of cells and the deposition of an organised extracellular matrix. Within the mammalian cornea, the precise mechanisms that align cells and organise collagen are poorly understood, even though the development of an organised extracellular matrix within the corneal stroma is imperative to establish corneal strength and transparency (Young et al. 2014). It is well known that, in the avian cornea, the primary stroma secreted from the epithelium initiates neural crest cell migration into the presumptive corneal stroma, whose cells subsequently secrete the mature secondary stroma (Hay E. D. and Dodson 1973). It is further hypothesised that the stromal cells are responsible for aligning collagen within the extracellular matrix of the avian cornea (Koudouna et al. 2018a, Young et al. 2014). However, a primary stroma has not been identified in the embryonic mammalian cornea, therefore different mechanisms are thought to drive the migration of cells compared with the avian developmental model (Haustein 1983). In addition to this, intercellular–relationships and the deposition and alignment of extracellular matrix has not previously been described in the mammalian cornea.

The mechanisms of cell movement have been well known since the late 1600s, following Van Leeuwenhoek's observation of cells moving across a microscope slide (Hoole 1798). Peripheral cell protrusions commonly referred to as lamellipodia initiate cell locomotion along a substrate by a front-to-back polarity (Svitkina 2016). A polarised cell can then move in a specified direction by directing their protruding lamellipodia driven by rearrangements of the actin cytoskeleton. The cells initially adhere to a substrate, de-adhesion of the cell body and rear follows, the cell body then contracts to cause the rear of the cell to retract, which initiates the forward movement of the cell (Pollard and Borisy

2003, Ridley et al. 2003). The lamellipodia protrusions can change direction, causing the cell to change its position in relation to the substrate. Cells protrude multiple lamellipodia and exhibit a random direction of migration via actin polymerisation through active *Rac* levels (Pankov et al. 2005). To direct cell migration in a specified direction, single axial lamellipodia protrusions form; this appears to be implemented by lowering the activity of *Rac (Pankov et al. 2005)*. Even though our understanding of the mechanisms by which cells move physically is established, the mechanisms that underlie the orientation and guidance of the cells to the correct position within mammalian cornea remains elusive and are likely to involve a combination of interacting factors. Some of those described in the literature involve chemoattractants and signalling molecules, as well as extracellular matrix components**,** such as hyaluronic acid and fibronectin**,** which have been shown to guide cells and initiate cell dispersal for matrix deposition across different tissues (Doane et al. 1996, Pratt et al. 1975, Zhu et al. 2006).

As described previously, the extracellular matrix can act as a mechanical scaffold to assist cell migration and alignment, providing chemical and mechanical cues (Friedrichs et al. 2007, Kadler et al. 1996). Cells exert forces onto an extracellular matrix substrate to alter their migrating direction and morphology. Further studies have revealed that cells co-align with ordered arrays of collagen fibrils, which suggests that fibrils provide a signalling cue for cell alignment (Friedrichs et al. 2007). Structural and mechanical anisotropy of collagen matrix initiates cells to bundle collagen fibrils, developing unidirectional cell traction along the fibrils, leading to cell polarisation, and thus movement. The theory of extracellular matrix alignment of cells is further supported by the observation that, when the mechanical strength of collagen fibrils is reduced, cells cannot align correctly within the matrix (Friedrichs et al. 2007). The migration of cells along collagen fibrils is clearly evident in the developing teleost fin and in the developing blastocoel roof of the amphibian gastrula, illustrating the impact collagen fibrils can exert on cells during cell migration in development (Nakatsuji and Johnson 1983, Wood and Thorogood 1984). In vitro studies of corneal cells, keratocytes, have also been shown to

align with extracellular matrix, demonstrating that collagen alignment with keratocytes could have an important relationship within corneal development (Kivanany et al. 2018). The collagen matrix also supports cell migration by altering its tensile strength and stiffness, with a greater stiffness supporting cell migration (Zaman et al. 2006). When the load placed on a matrix is reduced, collagen is cleaved and degrades, reducing in concentration, this study demonstrates the collagen matrix to be dynamic, which can also impact and alter cell migration (Ruberti and Hallab 2005). When collagen is cleaved by enzymes, reducing the amount of collagen within a matrix, This relationship between the cells and extracellular matrix means alterations in the expression of cell-cell and cell-extracellular matrix communication molecules can impact cell migration and alignment (Doane and Birk 1994).

It also remains unknown where the collagen fibrils are being secreted from and how the collagen fibrils are aligning within the mammalian corneal stroma to form an organised network, crucial for functional transparency. Early studies that have analysed the developing mouse cornea initially showed the appearance of collagen fibrils around E14, associating with the differentiation of mesenchymal cells to fibroblasts, with secretory organelles. Collagen fibrils then increased in diameter by E16 (Haustein 1983). Observations showed the secretion of collagen fibrils parallel to the cell membranes, which led to the hypothesis that stromal fibroblasts synthesise the mouse corneal collagen matrix (Haustein 1983). Even though collagen secretion has been seen in the developing mouse cornea, the organisation and alignment within the matrix remain to be investigated.

Within tendon and skin, fibripositors extrude collagen in a given direction and align collagen fibres in the matrix (Birk and Trelstad 1985, Birk and Zycband 1993, Canty et al. 2004). Collagen fibrils are initially synthesised in the Golgi apparatus, being transported to fibripositors for deposition within the extracellular matrix (Canty et al. 2004). Canty et al., were the first group to describe fibripositors, initially in chick tendon, demonstrating invaginations of

plasma membrane containing bundles of collagen fibrils that projected and co-aligned to the tendon's long axis. Further studies demonstrated the fibripositors require actin, which prolonged into intercellular channels stabilised by junctions expressing cadherin-11 to support cell condensation and morphology (Canty et al. 2006, Richardson et al. 2007). Previous studies have shown keratocytes to be involved with collagen alignment in chick corneal development, with the assistance of the extended filopodia, termed keratopodia, directing corneal stroma development (Birk and Trelstad 1984, Young et al. 2014). Currently, no studies have shown fibripositors to direct collagen fibril organisation in the developing mammalian cornea.

Further experiments identified that avian corneal stromal cells exhibit rotation of orientation with the alignment of collagen fibrils, consistent with the theory that the stromal cells organise the corneal stromal collagen in the avian cornea (Koudouna et al. 2018a). Collagen fibrils in avian corneas lie at 90° to those within adjacent lamellae and provide the cornea with an orthogonal arrangement (Trelstad and Coulombre 1971). This arrangement of collagen differs in the mammalian cornea, with lamellae being randomly orientated in a single plane together with lamellar branching (Aghamohammadzadeh et al. 2004, Morishige et al. 2011, Newton and Meek 1998). The difference in the organisation of lamellae in the mammalian cornea is thought to be responsible for variations to the biomechanical stiffness of the cornea, with consequent implications for corneal shape. The differences highlighted in the organisation of collagen lamellae in avian and mammalian corneas could result from different mechanisms that control collagen alignment.

To further understand mammalian corneal morphogenesis, the prenatal mouse cornea was investigated using novel serial block-face scanning techniques to analyse the developing stroma in 3-D. Initially, the focus was directed to analyse the migration of cells that construct the cornea and determine if a primary stroma was present to direct cell migration. Secondly, cell distribution and subsequent collagen deposition were analysed, to

determine if fibripositors were present, and if not, what alternative mechanism might direct the assembly and organisation of the extracellular matrix. The nature of the specific collagen types that are present in fibrils during mouse corneal development will be covered in the next chapter. However, type VII collagen was explored to identify the collagen fibrils that presented as anchoring fibrils posterior to the corneal epithelium, these have been previously seen to be type VII collagen rich with immunofluorescence and appear as “banded strands” posterior to the rabbis corneal epithelium (Gipson et al. 1987). To further understand the communication mechanisms between the corneal cells and their differentiation potential, the distribution of gap junction connexin 43 was investigated (Beyer et al. 1989, Matic et al. 1997). In addition, fibronectin and hyaluronic acid guide cells in developing tissues, acting as a substrate (Gomes J. A. et al. 2004, Pankov and Yamada 2002). The distribution of fibronectin and hyaluronic acid was investigated to provide information into the potential role of these components in mouse corneal development.

3.2. Methods

3.2.1. Electron Microscopy

The modified Deerinck protocol described previously in the general methods of this thesis (section 2.2.1, specifically 2.2.1.1.2) was the processing technique used throughout all electron microscopy experiments used in this chapter (Deerinck 2010). For all electron microscopy techniques conducted, six un-paired eyes were analysed at each embryonic age between E10-E18.

3.2.1.1. Analysis

Datasets of approximately 1000 images were collected on the SBF-SEM at different low magnifications and a high magnification of x4.33K. The datasets were reconstructed into 3-D models using Amira 6.4 software. The

reconstructions were made using manual segmentation as well as automated segmentation with the use of the volren and isosurface functions. The larger structures were mainly reconstructed using manual techniques, whilst the finite and more detailed structures were reconstructed using automated techniques.

3.2.2. Immunofluorescence

Refer back to chapter 2 general methods (section 2.5) for the general immunofluorescence method used in this section.

Six unpaired embryonic eyes of ages E12-E18 and 3-month adults were snap frozen in optimal cutting temperature compound and cryo-sectioned transversely to obtain sections of 5 µm thickness. The primary antibodies applied to the embryonic tissue in this chapter can be found in **Table 3**. For hyaluronic acid labelling a hyaluronic acid-binding protein, bovine nasal cartilage, biotinylated (Merck, Darmstadt, Germany) was applied in the same step as the primary antibodies. The secondary antibody Dylight 594 Horse Anti-Rabbit was applied at a concentration of 1:200 to stain the protein of interest red to the slides that contained the primary antibodies. A NeutrAvidin, Protein, Dylight 594, Invitrogen (Fisher Scientific, Waltham, Massachusetts, USA) was added to the slides containing the hyaluronic acid-binding protein in the same step as the secondary antibodies were added.

Table 3. ***Primary Antibodies***

Antibody	**Mono/ Poly-clonal**	**Target**	**Concentration**	**Source**	**Reference**
Anti-Fibronectin	Rabbit Polyclonal	Fibronectin	1:100	Abcam	(Solanas et al. 2008)
CNX43	Rabbit Polyclonal	Connexin 43	1:100	Abcam	(Pradeepa et al. 2014)
Type VII Collagen	Rabbit Polyclonal	Type VII Collagen	1:100	Abcam	NA

3.3. Results

3.3.1 Electron Microscopy

The modified Deerinck method employed in this study provided good preservation and contrast of cells and extracellular matrix components (**Figure 3.1-3.17**). The data-sets were reconstructed into 3-D models, revealing large-volume structural information of the associations and organisations of the cells and extracellular matrix within the developing cornea. Ultrathin sections from the same sample blocks were then cut for high-magnification imaging with transmission electron microscopy (TEM) reveal intricate details of cell and matrix ultrastructure.

E10

All samples imaged at E10 revealed the surface ectoderm overlying the lens with mesenchymal cells situated between both structures (**Figure 3.1A**). The 3-D reconstructions were used to classify the mesenchymal cells by their small cell bodies with few processes and round prominent nuclei (**Figure 3.1B-D and supplementary video 1**). Extracellular matrix strands penetrated through the basal lamina of the surface ectoderm, connecting cells in the surface ectoderm with the mesenchymal cells (**Figure 3.2 and supplementary video 1**).

High-magnification imaging revealed the mesenchymal cells to have close associations, with their cell membranes and cell extensions in close contact (**Figure 3.3**). The mesenchymal cells also contained secretory organelles and small vesicles (**Figure 3.3**). Thin strands extended from the surface ectoderm into the extracellular matrix. No orthogonally organised acellular collagenous matrix was present posterior to the surface ectoderm or through the thickness of the presumptive corneal stroma (**Figure 3.3**).

Supplementary video 1 link: *https://figshare.com/s/3324e911142af83a5aa0*

Figure 3.1. Serial block-face scanning electron microscopy datasets and three-dimensional reconstructions of the E10 mouse eye.

Fig. 3.1A: SBF-SEM image of the eye at E10 with mesenchymal cells (black asterisks) situated between the surface ectoderm (SE) and the lens epithelium (LE). The anterior (red box) and peripheral posterior (blue box) areas of the presumptive cornea were further analysed at a high magnification. **Fig. 3.1B and Fig. 3.1C**: The anterior (red box) reconstruction of the surface ectoderm (SE) and migrating neural crest cells (black asterisks) showed extracellular extensions. The extensions travelled through the basal lamina and hung from the surface ectoderm (black arrows). **Fig. 3.1D and Fig. 3.1E**: In the posterior area, between the lens (L), surface ectoderm (SE) and inner optic cup (IOC), many round cells resided with no evidence of cell projections or extracellular matrix strands.

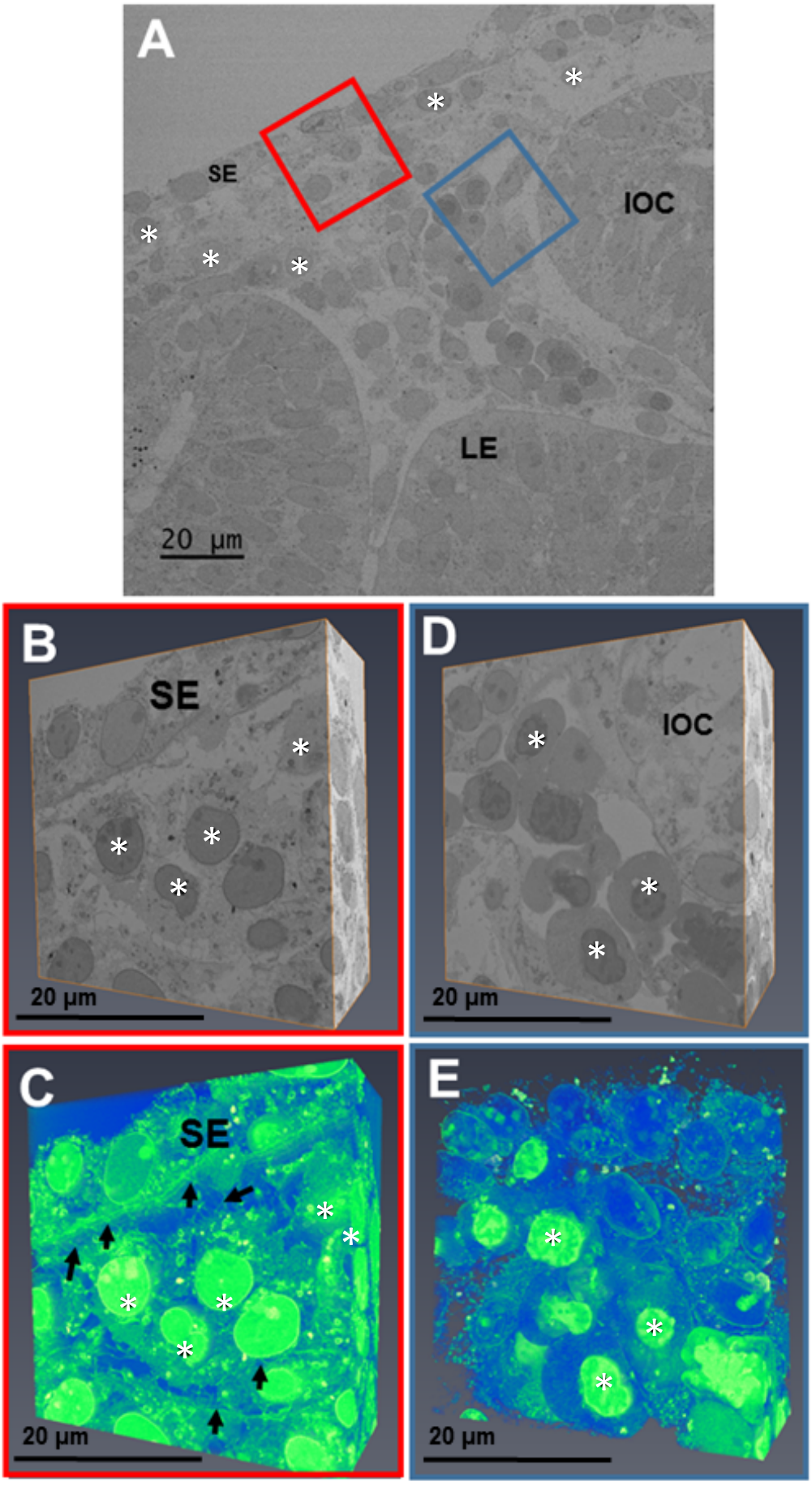
A
SE
IOC
LE
20 µm
B
SE
20 µm
D
IOC
20 µm
C
SE
20 µm
E
20 µm

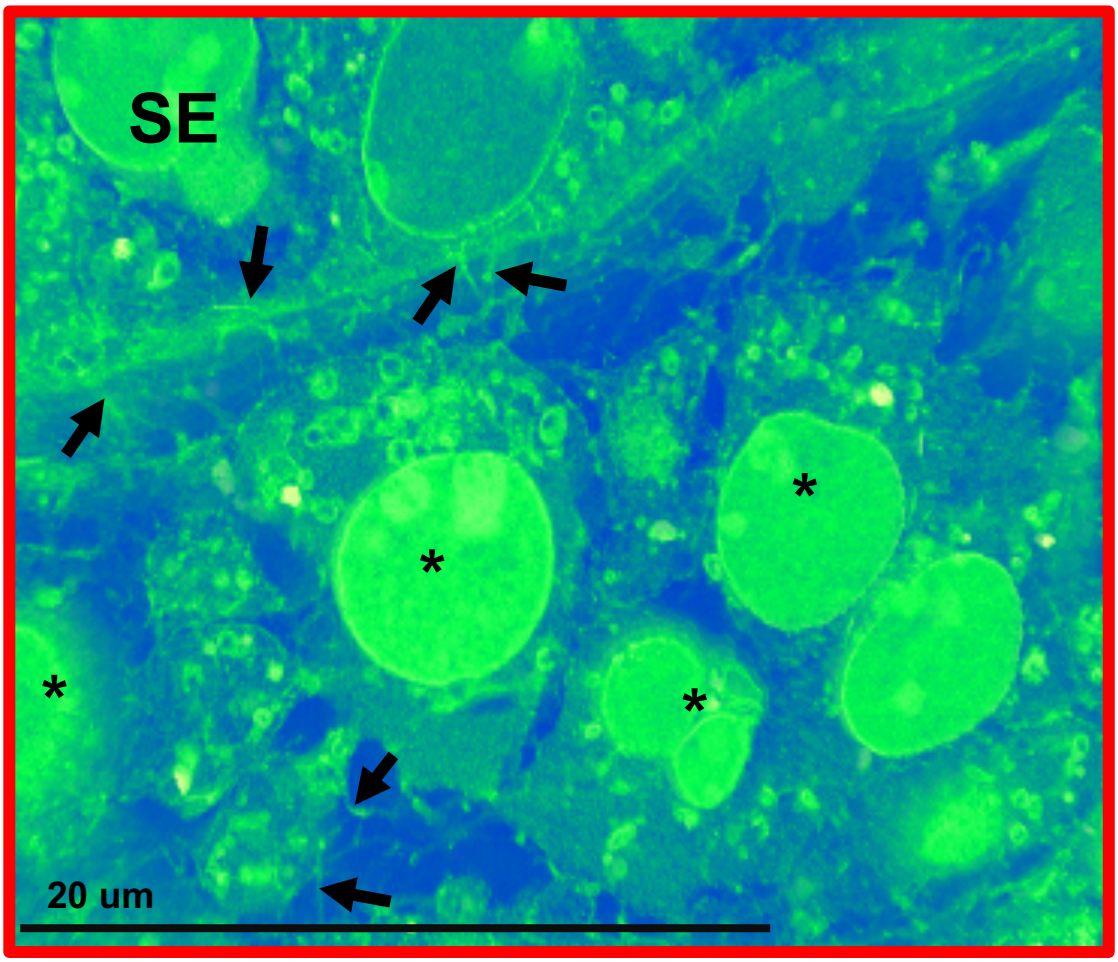

Figure 3.2. Three-dimensional reconstructions of the E10 mouse cornea (anterior cornea).

High magnification SBF-SEM dataset from the anterior cornea at E10 was reconstructed into a 3-D volren model. The 3-D reconstruction showed extracellular matrix strands (black arrows) extended from the surface ectoderm (SE), which penetrated through the basal lamina and communicated with the cells of the surface ectoderm and with the migrating mesenchymal cells (black asterisks). The mesenchymal cells were characterised by a small cell body, a small amount of lengthened cell extensions and the presence of a round and prominent nucleus. (scalebar 20 um).

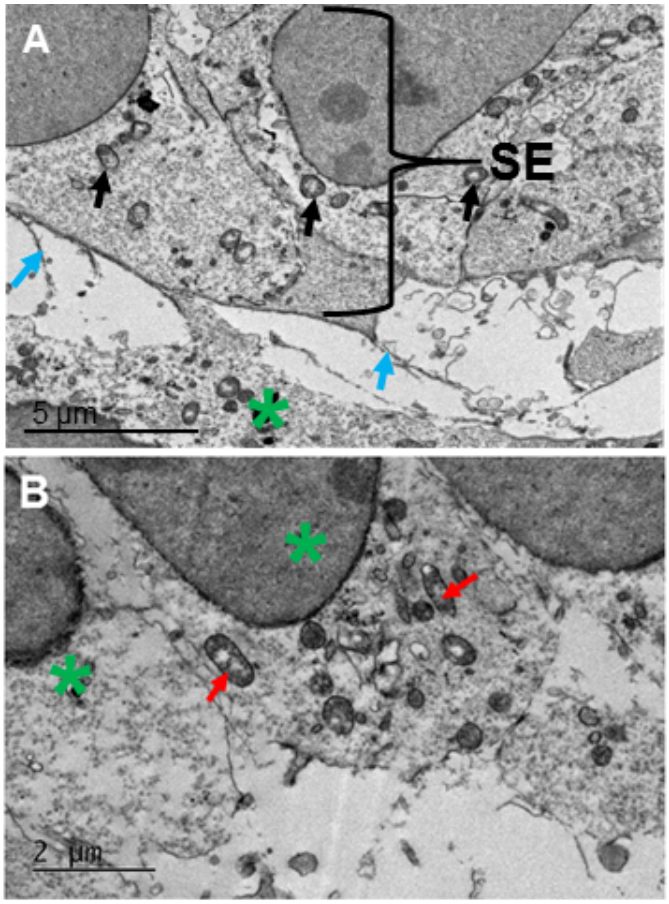

Figure 3.3. Transmission electron microscopy images of the E10 mouse cornea.

Fig. 3.3A: Imaging of the surface ectoderm (SE) showed extracellular strands (blue arrows) that had extended from the SE and projected through the extracellular space to mesenchymal cells (green asterisk) posterior to the surface ectoderm. **Fig. 3.3B:** Mesenchymal cells were found in close proximity to neighbouring mesenchymal cells (green asterisks). **Fig. 3.3B**: Organelles, including mitochondria, were inside the mesenchymal cells (red arrows). **Figs. 3.3A-C**: No organised collagen fibrils were present throughout the corneal stroma at E10.

E12

At E12 many mesenchymal cells populated the area between the lens and the surface ectoderm, with a condensation of cells compared to E10 (**Figure 3.4A**). Some of the mesenchymal cells were situated posteriorly between the optic cup and lens vesicle (**Figure 3.4A**). The 3-D models of the central and peripheral aspects of the cornea revealed the cells to be in close proximity to neighbouring cells (**Figure 3.4B-E and supplementary video 2**).

Analysing the E12 cornea at a higher magnification confirmed the close associations between the neighbouring mesenchymal cells, with cell plasma membranes and extensions in contact (**Figure 3.5C**). Within these cells, a large number of mitochondria was present, indicating a high level of metabolic activity. In addition, secretory organelles including Golgi apparatus and rough endoplasmic reticulum were identified, establishing their potential role in the synthesis of extracellular matrix molecules (**Figure 3.5**). Small bleb-like structures were also present inside and outside of the mesenchymal cells, these structures could be involved in the transport of material outside of the cells (**Figure 3.5B**). The surface ectoderm was also shown to contain small vesicles, but no synthesising organelles were identified (**Figure 3.5A**).

Supplementary video 2 link: *https://figshare.com/s/ce6f8b3bf626b1f51a8e*

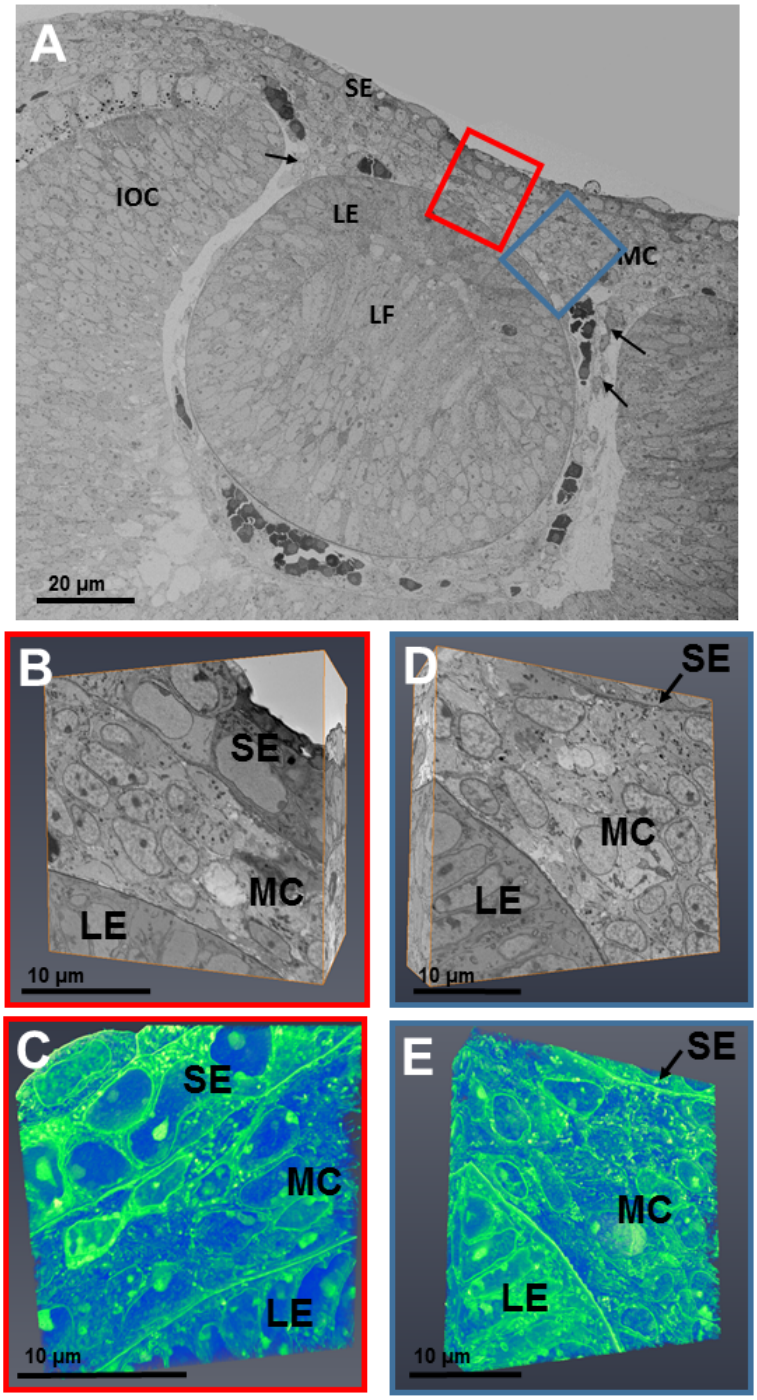

Figure 3.4. Serial block-face scanning electron microscopy images and three-dimensional reconstructions of the E12 mouse eye.

Fig. 3.4A: Low magnification SBF-SEM image of the eye at E12. The inner layer of the optic cup (IOC) surrounded the lens vesicle. Within the lens vesicle, the lens epithelium (LE) and lens fibres (LF) were clearly visible. The overlying surface ectoderm presented next to the lens. Mesenchymal cells (MCs) were located between the lens epithelium and the surface ectoderm (SE); some of the mesenchymal cells were in the cavity between the optic cup and the lens vesicle (black arrows). **Figs. 3.4B-E**: 3-D reconstructions within the central (red box) and peripheral (blue box) presumptive cornea showed mesenchymal cells to be in close proximity.

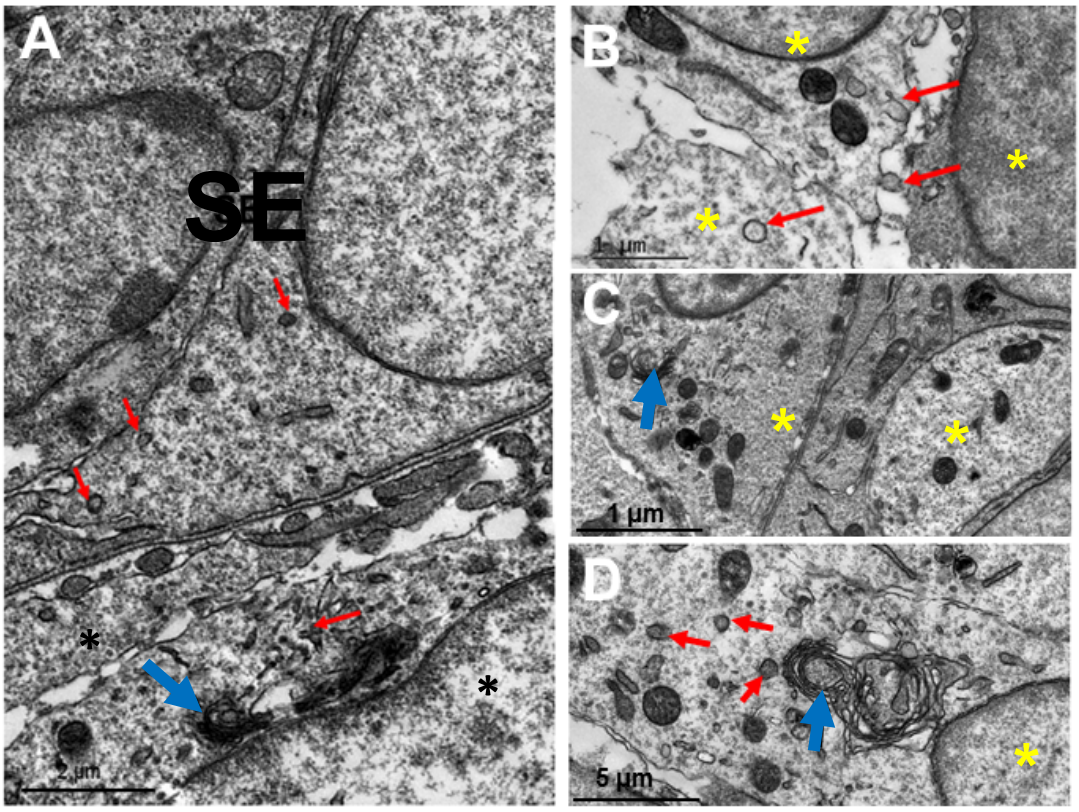

Figure 3.5. Transmission electron microscopy images of the cornea at E12

Figs. 3.5A, C and D: The mesenchymal cells are in very close proximity to neighbouring mesenchymal cells (yellow asterisks) and contain many mitochondria and synthesising organelles, which include endoplasmic reticulum and Golgi apparatus (blue arrows). **Figs. 3.5A-D**: Small intra- and extra-cellular bleb-like structures (red arrows) were also present, sometimes located close to the cell membrane. **Figs. 3.5A**: These structures (red arrows) were also seen within the surface ectoderm (SE), but no synthesising organelles were present.

E13

The eye at E13 was analysed with SBF-SEM at the central anterior and posterior cornea (**Figure 3.6**). Electron microscopy showed a definitive anterior chamber (**Figure 3.6A**). Cells were flat and elongated within the posterior and peripheral aspects of the cornea, associating close to the surrounding cells (**Figure 3.6D-E**). Cells within the anterior aspect of the cornea had a stellate morphology compared to the cells in the posterior cornea (**Figure 3.6B-C**). The cells located within the anterior cornea were surrounded by extracellular space, most probably containing pro-collagen and other extracellular matrix molecules, which are transparent with electron-optical imaging (**Figure 3.6**). However, there was only very little extracellular matrix deposition. The 3-D reconstructions identified corneal stromal cells to extend projections to neighbouring corneal stromal cells as well as projecting anteriorly towards the basal lamina (**Figure 3.7 and supplementary video 3**).

Higher magnification observations revealed collagen fibrils deposited throughout the corneal stroma. Below the basal lamina, the fibrils accumulated in a disordered array (**Figure 3.8A**). Some of the fibrils posterior to the corneal epithelium were arranged perpendicularly from the basal lamina (**Figure 3.8B**). Cells were present throughout the corneal stroma, with those in the anterior cornea having a round morphology with a greater amount of space around the cells (**Figure 3.8**). By comparison, cells within the posterior cornea were compacted, with a flatter morphology (**Figure 3.8D**). Cells throughout the stroma had cellular projections that communicated with adjacent cells, with the cell processes touching (**Figure 3.8).** The collagen fibrils appeared to be deposited from the stromal cells and contained to remain in close proximity to the cell membranes (**Figure 3.8**).

Supplementary video 3 link: *https://figshare.com/s/9773959e1d99835bcd3b*

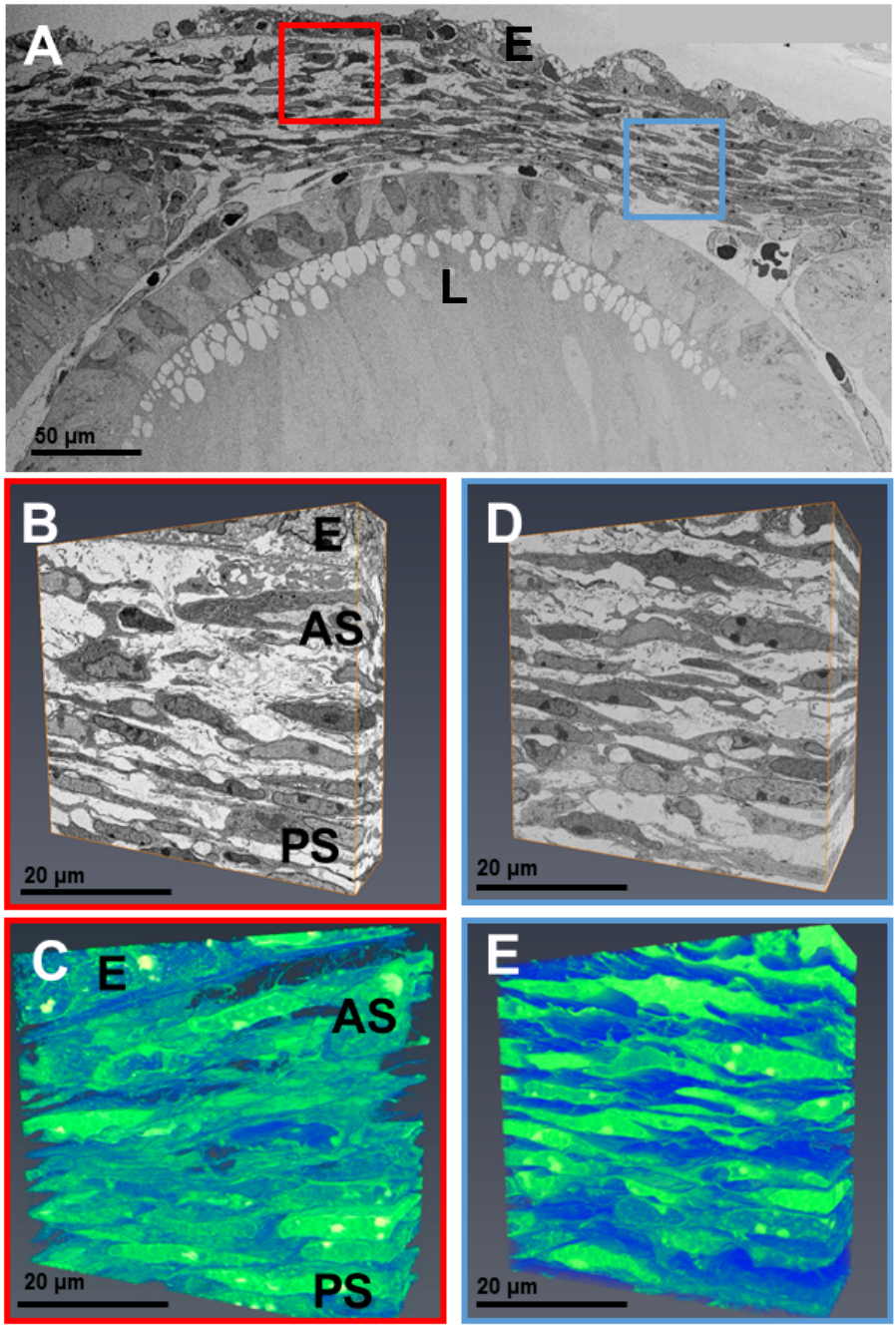

Figure 3.6. Serial block-face scanning electron microscopy images and three-dimensional models of the E13 developing mouse eye.

Fig. 3.6A: SBF-SEM imaging of the cornea and lens (L) at E13. Mesenchymal cells were situated throughout the corneal stroma, with the anterior chamber bounded by the corneal epithelium (E) and lens (L). **Fig. 3.6B and Fig. 3.6C**: High magnification SBF-SEM data-sets generated 3-D models of the anterior (red box) corneal cells sparsely organised with a stellate morphology, surrounded by extracellular matrix. **Fig. 3.6D and Fig. 3.6E**: The posterior (blue box) corneal cells were densely packed and condensed within the posterior cornea (PS), with cells having a flatter morphology within the peripheral and posterior corneal stroma compared to the anterior cornea. **Fig. 3.6C**: The corneal stromal cells had projections that interacted with adjacent corneal stromal cells and projected anteriorly to interact with the basal lamina.

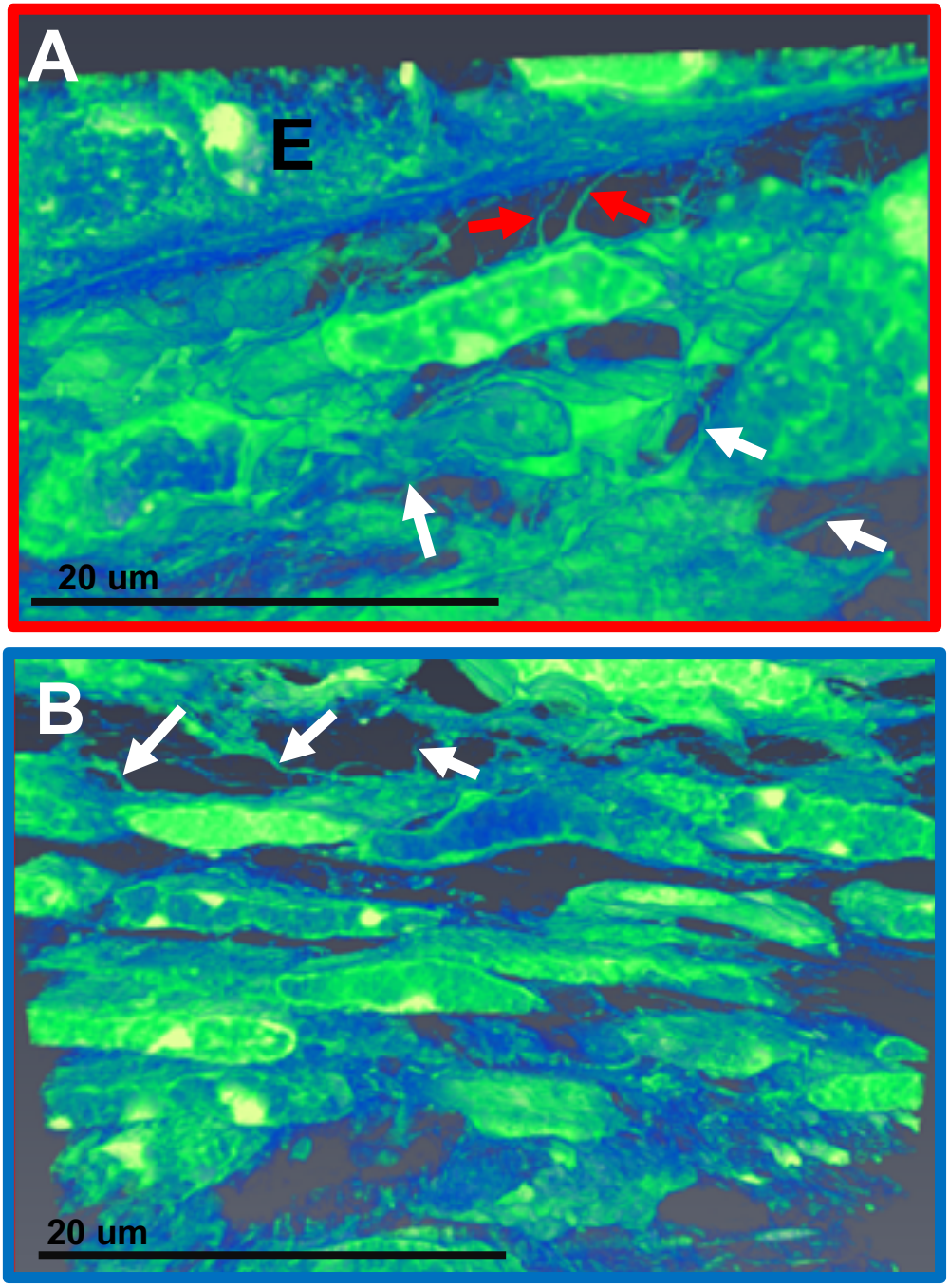

Figure 3.7. Serial block-face scanning electron microscopy three-dimensional models of the E13 mouse eye.

Fig. 3.7A: 3-D reconstructions of cells in the anterior cornea reveal a stellate morphology with cell extensions branching to adjacent cells (white arrows). The anterior corneal cells also projected towards the corneal epithelium and further interacted with the basal lamina (E) (red arrows). **Fig. 3.7B**: In the posterior cornea, cell extensions branched to neighbouring corneal stromal cells (white arrows). Refer to supplementary video 3 for greater detail of the 3-D cell extensions in the anterior cornea.

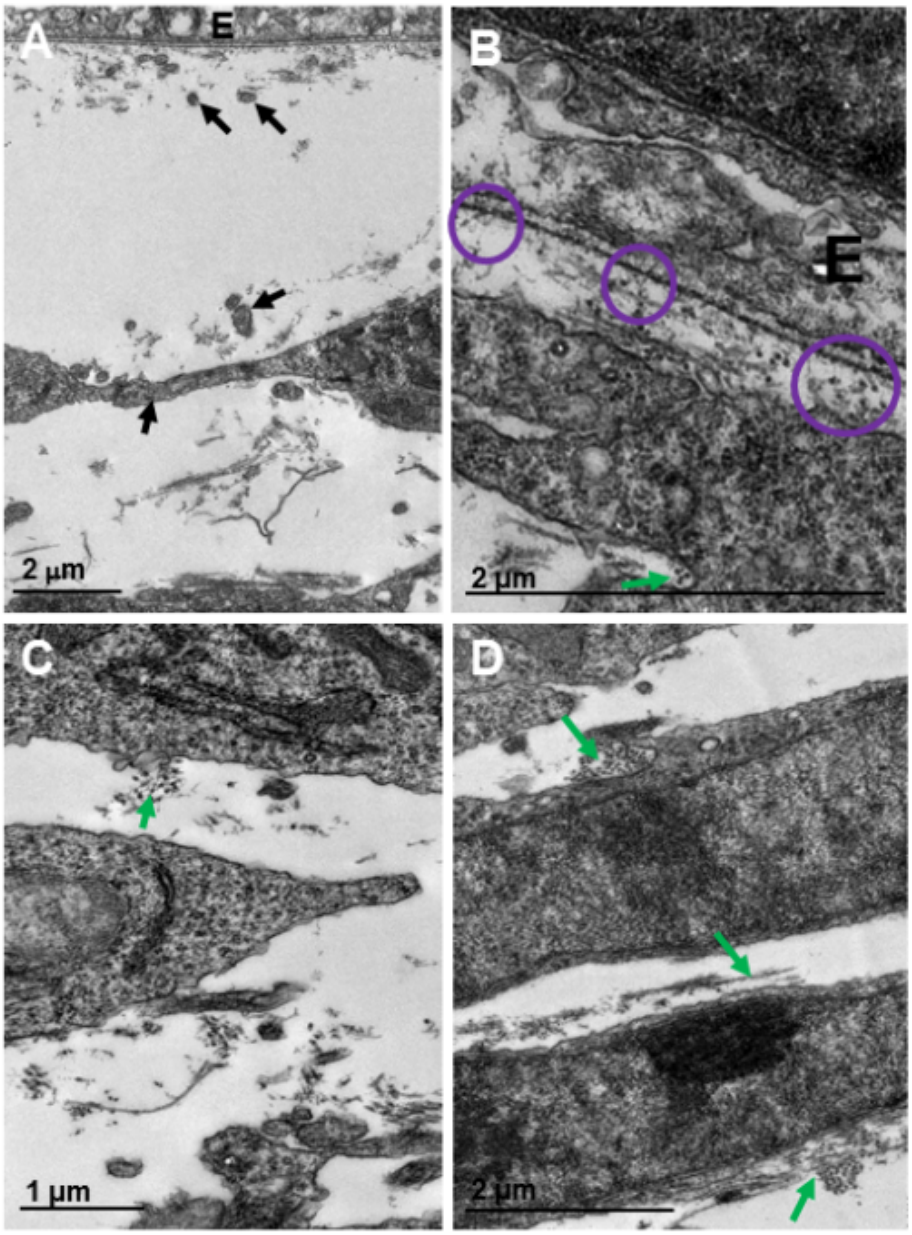

Figure 3.8. Transmission electron microscopy of the developing E13 mouse cornea, anterior (Figs 3.8A-C) and posterior corneal stroma (Fig. 3.8D).

Fig. 3.8A and Fig. 3.8B: Collagen fibrils accumulated directly posterior to the corneal epithelium (E), with some single fibrils (purple circle) extending from the basal lamina; these fibrils may represented anchoring filaments. **Figs. 3.8A-D**: Collagen fibrils within anterior and posterior stroma associated close to cell membranes (green arrows). **Fig. 3.8A and Fig. 3.8B**: Cells of the anterior cornea had a stellate morphology with membranous extensions, directed towards neighbouring cells, anteriorly towards the corneal epithelium, and within areas of collagen deposition (black arrow). **Fig. 3.8D**: Cells in posterior locations had a lengthened and flatter morphology compared to cells in the anterior corneal stroma.

E14

The developing cornea at E14 was analysed with SBF-SEM within the central anterior and central posterior aspects of the cornea (**Figure 3.9**). The corneal stroma was populated with cells with increased cell density in the peripheral and posterior areas. In these heavily populated areas, cells possessed a slender and lengthened morphology. Within the central and anterior cornea, cells had a stellate morphology (**Figure 3.9B-C**). Several layers of flattened mesenchymal cells occupied the posterior aspect of the cornea (closest to the lens) (**Figure 3.9D-E**). Again, cell extensions were identified to communicate with adjacent cells (**Figure 3.10**). In addition, more space and extracellular matrix deposition was evident within the central anterior cornea (**Figure 3.11**). Extracellular matrix was increased within the corneal stroma compared with earlier stages (**Figure 3.9-Figure 3.11 and supplementary video 4**).

Within the spaces between the cells of the developing stroma, collagen was orthogonally organised, lying in close proximity to cell membranes (**Figure 3.11**). In the central stroma, collagen fibrils were increased in abundance compared to the posterior cornea and were arranged into bundles organised orthogonally with respect to each other.

Supplementary video 4 link: *https://figshare.com/s/88f95a8b80cb5cc72191*

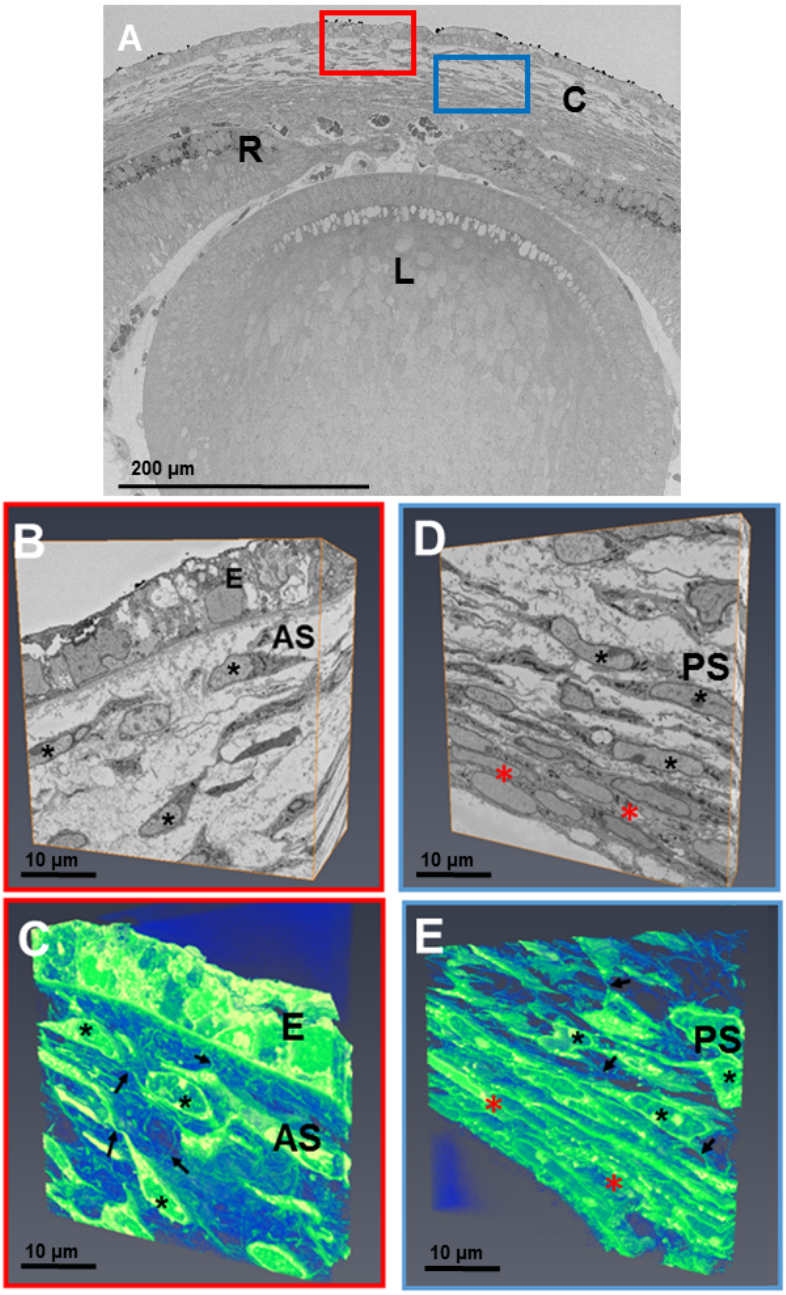

Figure 3.9. Serial block-face scanning electron microscopy datasets of E14 developing mouse eye.

Fig. 3.9A: Low magnification SBF-SEM imaging of the cornea (**C**), lens (**L**) and retina (**R**) at E14. Mesenchymal cells (black asterisks) are distributed throughout the corneal stroma. **Fig. 3.9B-C:** The anterior cornea (red box) in 3-D showed collagen fibrils deposited directly posterior to the corneal epithelium and around corneal stromal cells. The cells in the anterior corneal stroma had a stellate and large morphology, surrounded by extracellular space. **Fig. 3.9D and Fig. 3.9E:** The posterior cornea (blue box) was reconstructed in 3-D and showed cells were more densely packed within the posterior corneal stroma (red asterisk), with a flatter and lengthened morphology. The condensed cells in the posterior cornea will form the corneal endothelium (red asterisks). Anterior stroma (**AS**), Posterior stroma (**PS**) and epithelium (**E**).

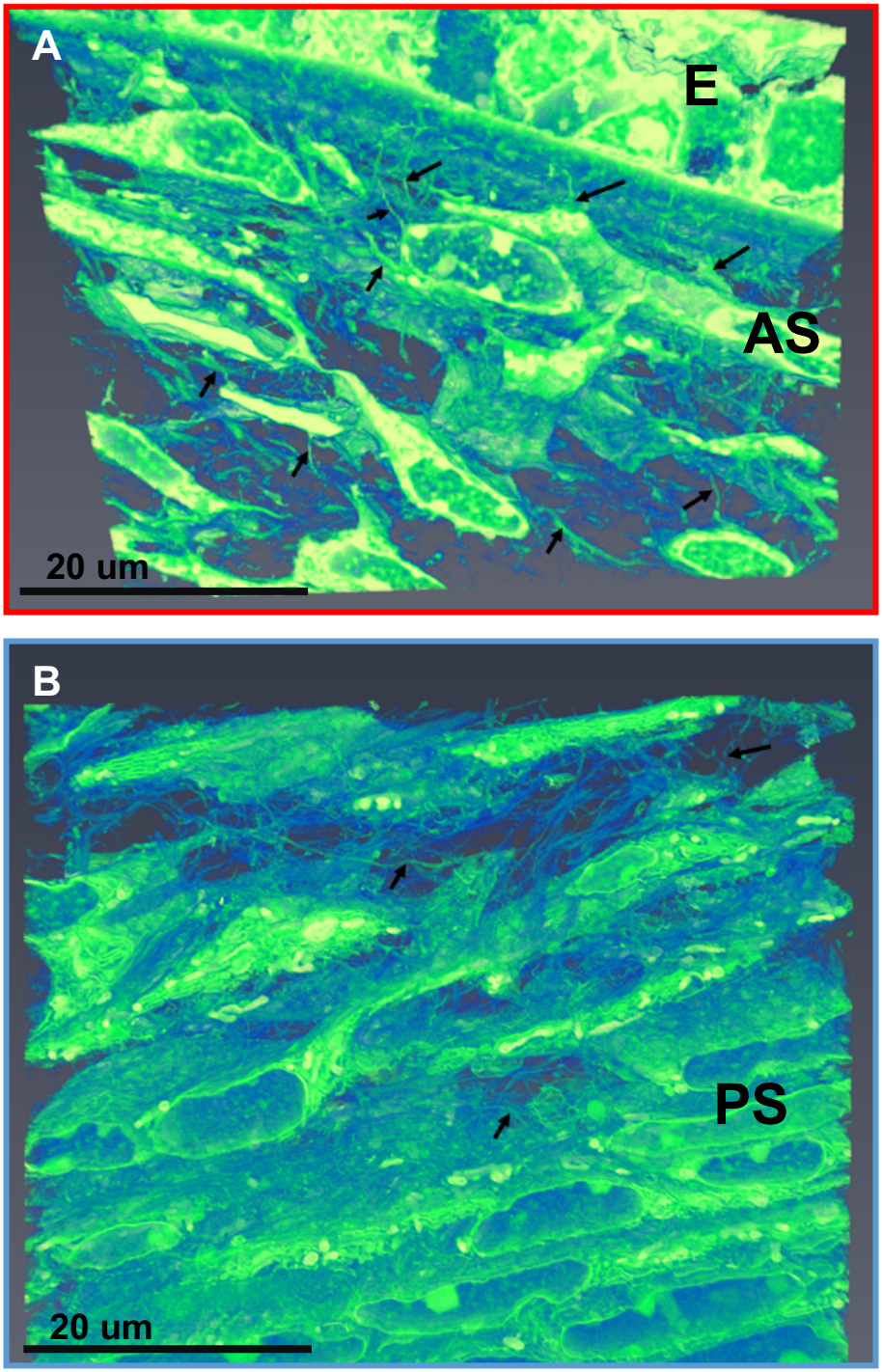

Figure 3.10. Serial block-face scanning electron microscopy three-dimensional reconstructions of the E14 developing mouse eye.

Fig. 3.10A: The anterior cornea 3-D reconstructions identified mesenchymal cell extensions branching between neighbouring mesenchymal cells (black arrows) and projecting anteriorly towards the corneal epithelium (E). **Fig 3.10B**: The posterior cornea 3-D reconstructions also showed mesenchymal cell extensions to branch towards neighbouring cells (black arrows). Cells within the posterior cornea were more densely packed compared to the anterior cornea. Further condensation of cells occurred within the most posterior cornea and contained the presumptive corneal endothelium. Anterior stroma (AS), posterior stroma (PS).

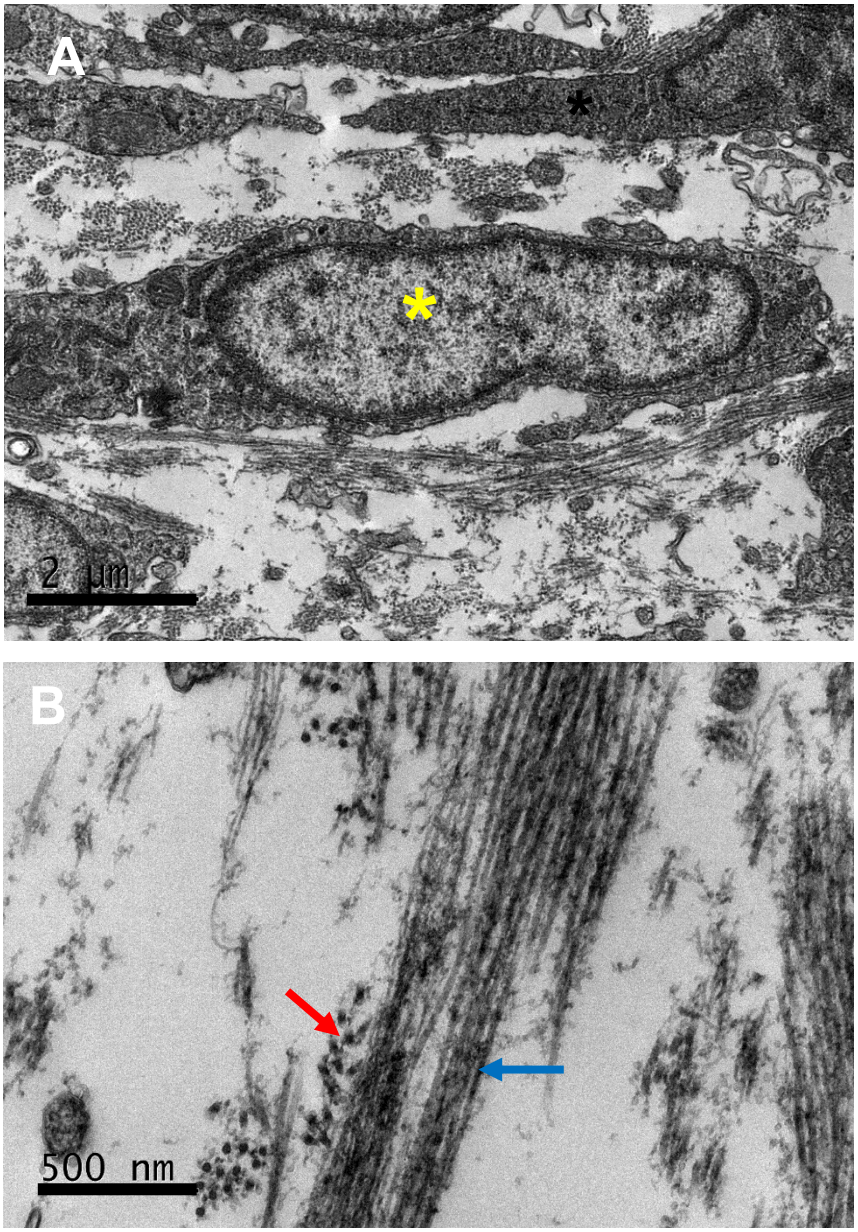

Figure 3.11. Transmission electron microscopy images of the E14 mouse cornea, central corneal stroma

Fig. 3.11A: Within the central cornea, stromal cells (yellow asterisk) appear stellate with cytoplasmic extensions, associated with the extracellular matrix. Collagen fibrils in bundles organised in an orthogonal array are identified within the extracellular space, closely associated with cells. **Fig. 3.11B**: Analysis of the collagen bundles at high magnification demonstrates the oblique and transverse organisation of the collagen fibrils. Blue and red arrows indicate the 2 different orientations of the collagen fibrils and represent an orthogonal orientation.

E15

The cornea at embryonic day E15 was analysed in the anterior central and posterior central cornea (**Figure 3.12**). The corneal stromal cells in the posterior cornea had further condensed to form the corneal endothelium (**Figure 3.12D-E**). Collagen deposition filled in the extracellular matrix spaces, with collagen fibril bundles organised into lamellae between the cells of the corneal stroma (**Figure 3.12**). The cells within the corneal stroma were elongated and appeared to organise within rows of aligned keratocytes (**Figure 3.12 and supplementary video 5**).

High-magnification analysis of the cornea at E15 identified collagen fibrils randomly deposited posterior to the basal lamina. These collagen fibrils had a smaller collagen fibril diameter compared to the collagen fibrils in the deeper stroma. The collagen fibrils within the corneal stroma also aligned with the direction of a cell projection. Fibril bundles appeared to organise into lamellae, arranged orthogonally (**Figure 3.13**). A high abundance of fibrils was evident associated with cell membranes, with the alignment along the direction of the cell processes (**Figure 3.13**).

Supplementary video 5 link: *https://figshare.com/s/75b3de09e4dccb3bf926*

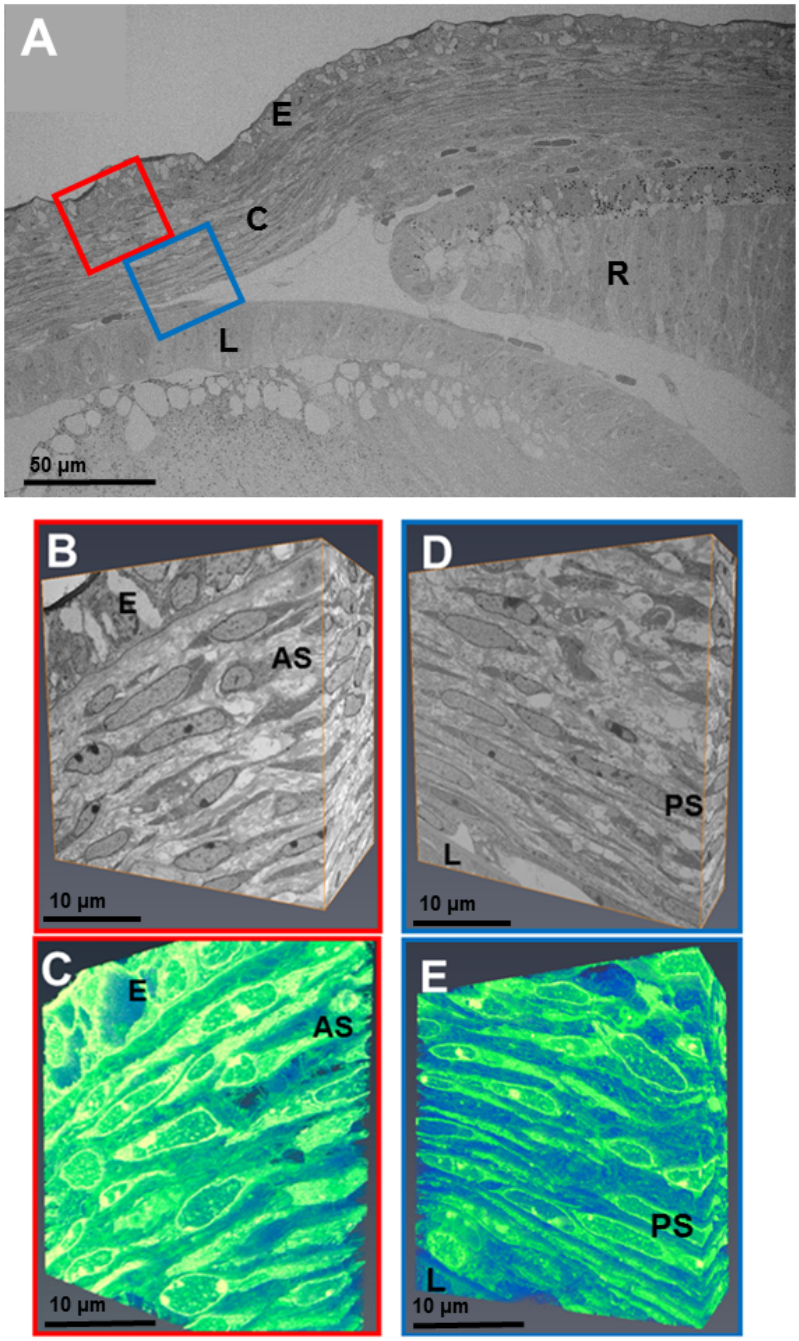

Figure 3.12. Serial block-face scanning electron microscopy three-dimensional reconstructions in the E15 developing mouse cornea.

Fig. 3.12A: SBF-SEM imaging of the eye at E15 of the cornea (C), corneal epithelium (E), lens (L) and retina (R). The anterior (red box) and posterior (blue box) areas of the cornea were further analysed. **Fig. 3.12B and Fig. 3.12C**: 3-D reconstructions of the anterior cornea identified collagen fibrils within fibril bundles to constitute the extracellular matrix between the stromal cells. Cells become flat and elongated, orientated in the same plane, with extended projections that communicated with adjacent cells. **Fig. 3.12D and Fig. 3.12E**: The posterior cornea displayed a similar morphology to the anterior cornea, with elongated cells in parallel rows that lay between collagen fibril bundles. Anterior stroma (AS), posterior stroma (PS).

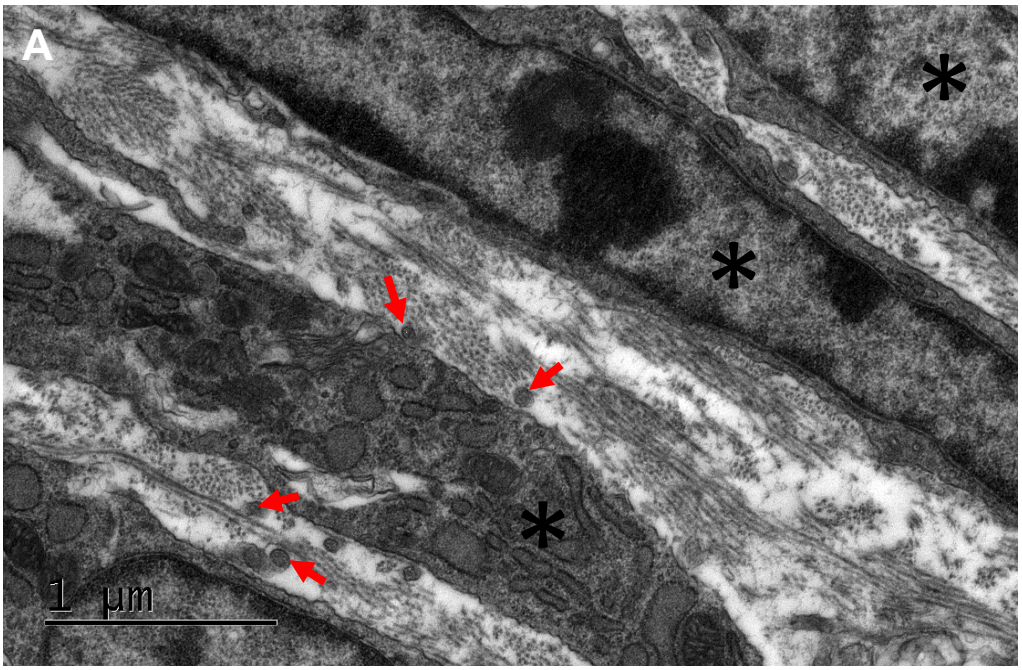

Figure 3.13. Transmission electron microscopy images of the developing E15 mouse corneal stroma

Fig. 3.13A: Collagen fibril bundles form lamellae organised orthogonally to adjacent collagen bundles and between the corneal stromal cells (black asterisk). Corneal stroma cells possess cell extensions, with some that appeared to run in the same direction as adjacent collagen fibril bundles (red arrows). However, as the TEM images are 2D it is difficult to confirm where these cell extensions are arising from, but the cell extensions were consistent with the 3D SBF-SEM data.

E16

The cornea was examined in the anterior central and posterior aspects of the cornea at E16 (**Figure 3.14**). The images displayed a defined epithelium, endothelium and stroma. Reconstructions of high magnification datasets revealed corneal stromal cells to be aligned in parallel rows, with cells in close proximity to neighbouring cells (**Figure 3.14**). The reconstructions identified organised collagen lamellae between corneal stromal cells (**Figure 3.14**).

High-magnification images of the corneal stroma at E16 showed collagen fibrils packed within lamellae, with fibrils arranged in different orientations in adjacent lamellae, some oblique and others longitudinal (**Figure 3.15**). Extensions of stromal cells aligned with the arrangement of collagen fibrils (**Figure 3.15C**). The cells contained a high quantity of synthesising organelles and mitochondria, which implies that the cells continue to be very active at E16. The density of cells within the corneal stroma is relatively high, with a larger quantity of cells compared to collagen lamellae in the corneal stroma (**Figure 3.15A**).

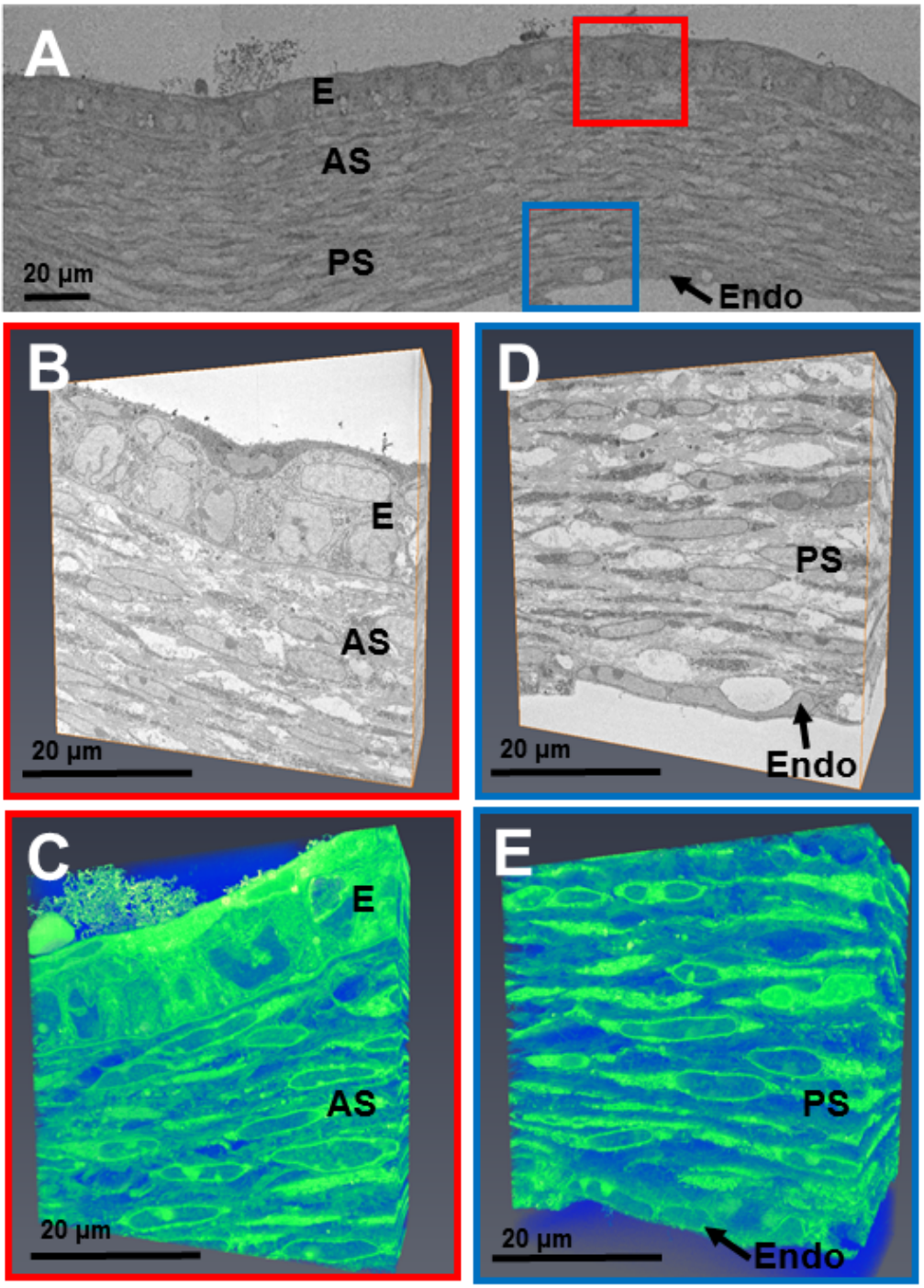

Figure 3.14. Serial block-face scanning electron microscopy three-dimensional models of the E16 mouse cornea.

Fig. 3.14A: Low magnification images of the cornea showed a well-developed structure with an epithelium (E), anterior stroma (AS), posterior stroma (PS) and endothelium (Endo). **Fig. 3.14B and Fig. 3.14C**: The anterior (red box) cornea 3-D reconstructions showed cells aligned in parallel rows with collagen fibrils in-between the rows of cells. **Fig.3.14D and Fig.3.14E:** The posterior (blue box) cornea 3-D reconstructions showed the corneal endothelial monolayer, which represents the posterior boundary of the cornea. Corneal stromal cells now have a similar arrangement and morphology to the anterior corneal stromal cells.

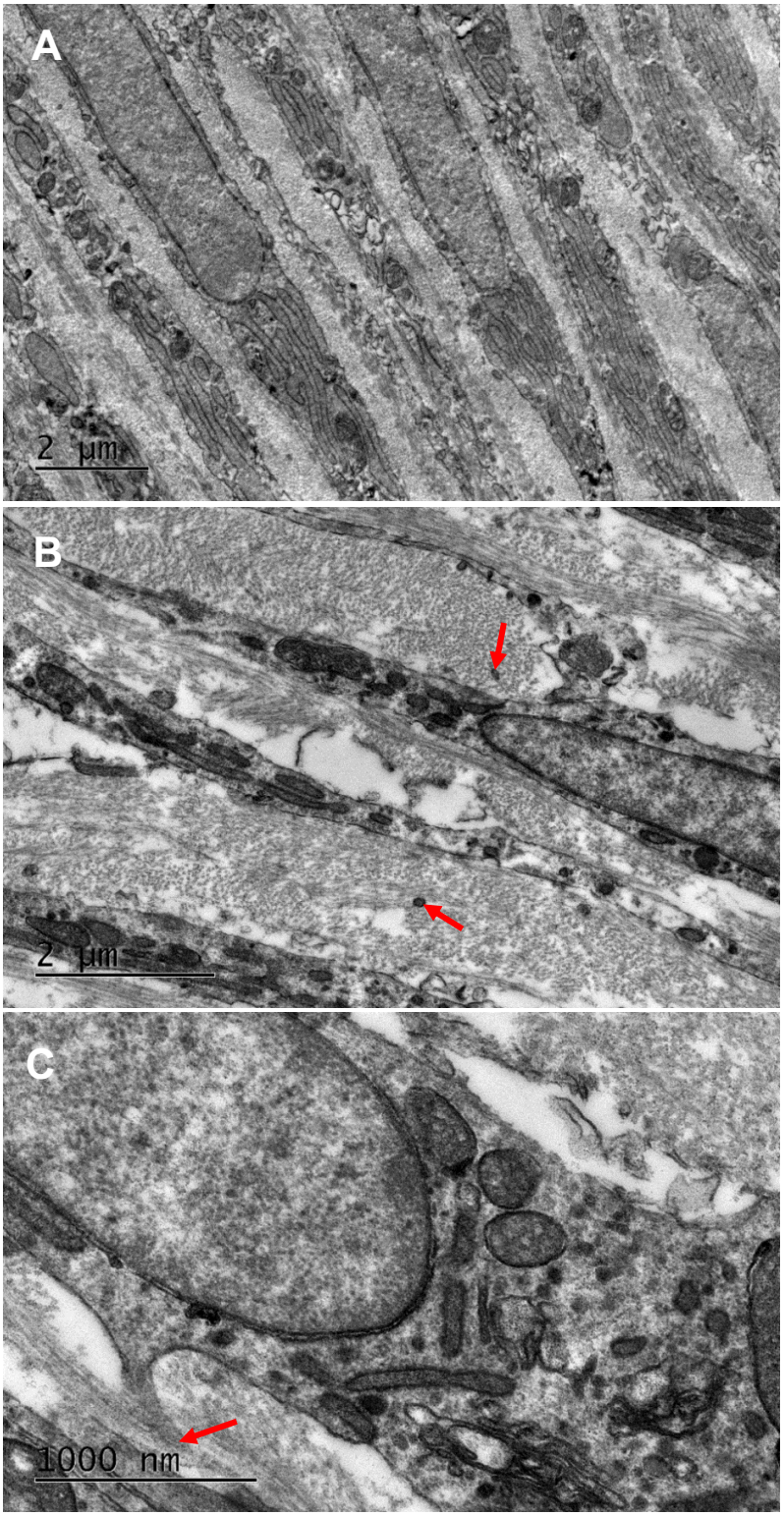

Figure 3.15. Transmission electron microscopy images of the developing E16 mouse cornea, anterior corneal stroma

Fig. 3.15A: Cells within the corneal stroma were long, slender and arranged within longitudinal rows. **Fig. 3.15B**: Collagen lamellae lie between the corneal cells in an orthogonal arrangement. **Fig. 3.15B and Fig. 3.15C:** Cells exhibited cytoplasmic projections, longitudinally and as dots (red arrows), that were consistent with the features seen with SBF-SEM. Some of the collagen fibrils aligned with the cell extension.

E18

3-D reconstructions of the cornea at E18 showed an organised corneal stroma composed of well-developed collagen lamellae (**Figure 3.16**). The keratocytes within the corneal stroma were organised between consecutive lamellae. These cells appeared to be lengthened and communicated with each other via cell processes (**Figure 3.16**).

High-magnification analysis of the E18 mouse cornea showed a densely populated cornea with many flat and elongated cells organised in longitudinal rows (**Figure 3.17A**). Collagen fibrils were organised into orthogonal lamellae between the cells of the corneal stroma. The cells throughout the corneal stroma contained high amounts of mitochondria, Golgi apparatus and rough endoplasmic reticulum, which implied a high level of activity and synthesis (**Figure 3.17B**). Some cell processes appeared to align in the same direction to the most adjacent collagen fibrils (**Figure 3.17C**).

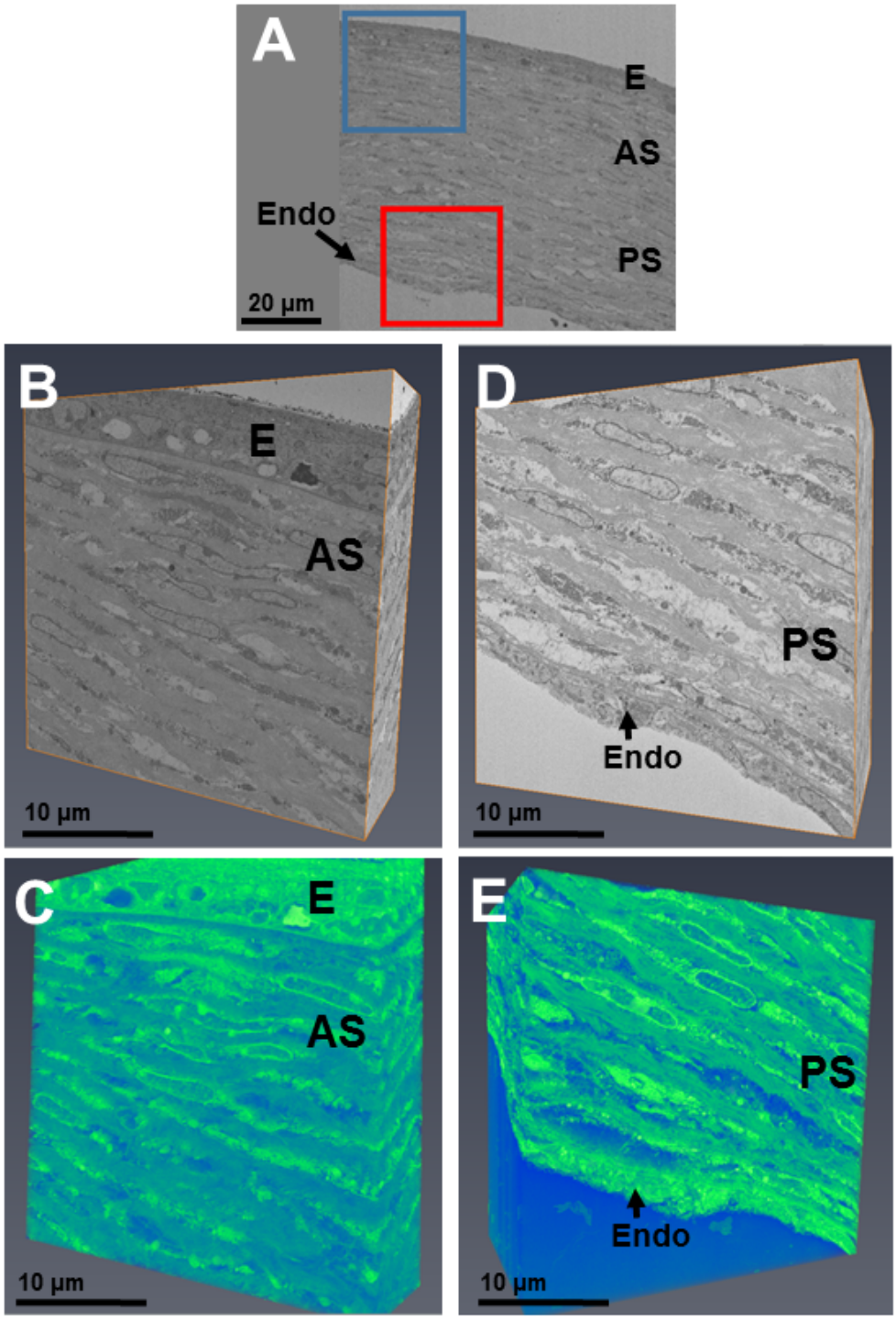

Figure 3.16. Serial block-face scanning electron microscopy three-dimensional reconstructions of the E18 mouse cornea.

Fig. 3.16A: SBF-SEM images of the cornea at E18. Anterior (AS) and posterior corneal stroma (PS), epithelium (E) and endothelium (Endo) are all well-developed. **Fig. 3.16B and Fig. 3.16C**: 3-D reconstructions of the anterior cornea showed cells aligned within longitudinal rows of cells with cell projections communicating to neighbouring cells. Cells are longitudinal, densely packed and appear to run in between collagen lamellae. F**ig. 3.16D and Fig. 3.16E**: The posterior cornea 3-D reconstructions displayed a similar morphology to the anterior cornea.

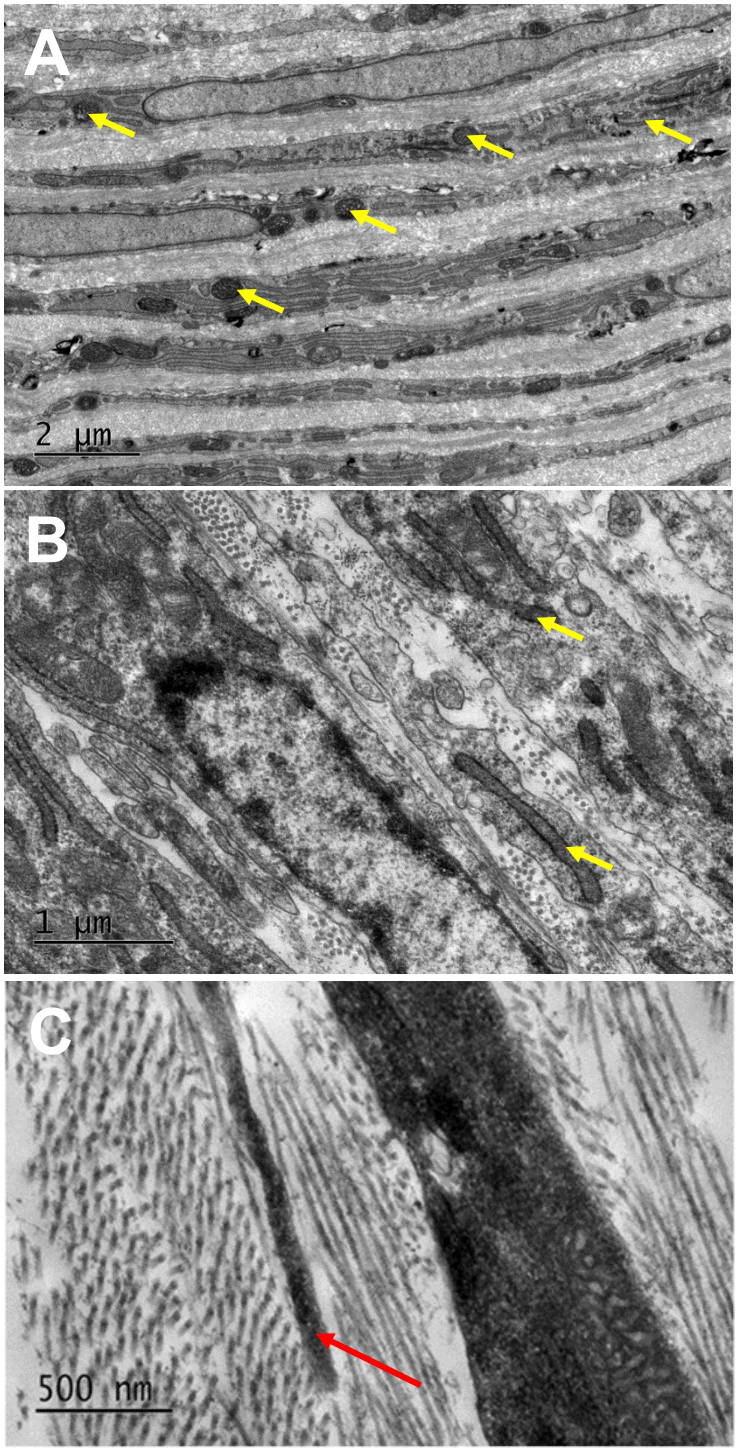

Figure 3.17. Transmission electron microscopy images of the E18 mouse corneal stroma.

Fig. 3.17A: Corneal stromal cells were flattened and elongated in parallel rows, closely associated with neighbouring corneal stromal cells. **Fig. 3.7A and Fig. 3.17B**: Collagen fibrils were laid down within orthogonally arranged lamellae between the cells. Cells contained many mitochondria and synthesising organelles, which indicates a high level of activity (yellow arrows). **Fig. 3.17C**: Cell processes extended from the keratocytes aligned in the same direction as collagen fibril orientation (red arrow).

3.3.2. Immunofluorescence

3.3.2.1. Fibronectin

Fibronectin was associated with the migrating mesenchymal cells, developing lens and surface ectoderm from E12. (**Figure 3.18**). Labelling becomes localised under the corneal epithelium from E14 to E16, with a small level within the corneal stroma from E14 to E18. By E18 fibronectin was enhanced as a band anteriorly to the corneal endothelium (**Figure 3.18**).

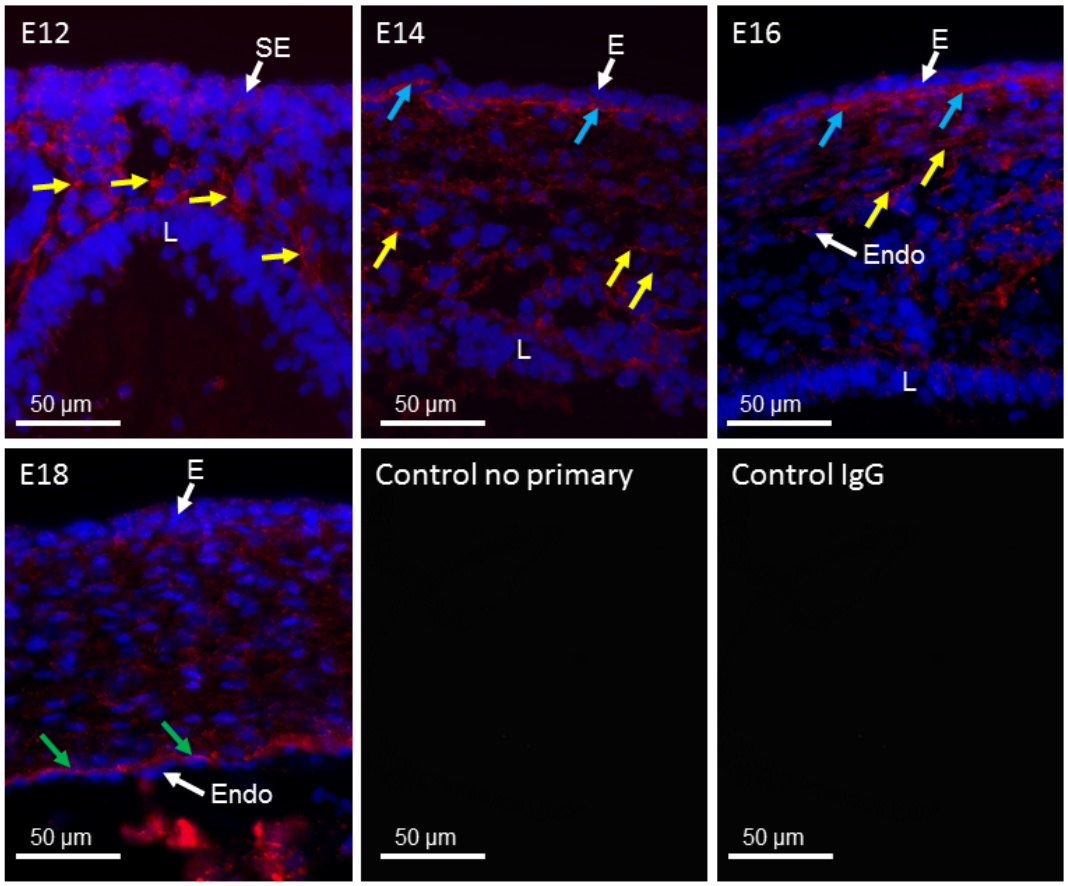

Figure 3.18. Fibronectin (red) in mouse corneal development.

Fibronectin associated with the migrating mesenchymal cells at E12 (yellow arrows). In addition, staining was present around the lens (L), surface ectoderm (SE) and presumptive corneal stromal cells. Fibronectin localised posterior to the corneal epithelium (E) from E14 to E16 (blue arrows). Fibronectin became localised directly anterior to the corneal endothelium (endo) (green arrows) at E18. Controls included IgG rabbit and no primary antibody, showing no positive labelling. Blue (DAPI – cell nuclei), red (fibronectin). For orientation, the corneal epithelium is faced upwards in all images.

3.3.2.2. Type VII Collagen

Type VII collagen first presented within the corneal epithelium at E14 (**Figure 3.19**). Type VII collagen increased from E16 and was localised to the epithelial basement membrane from E16 to E18 of corneal development (**Figure 3.19**).

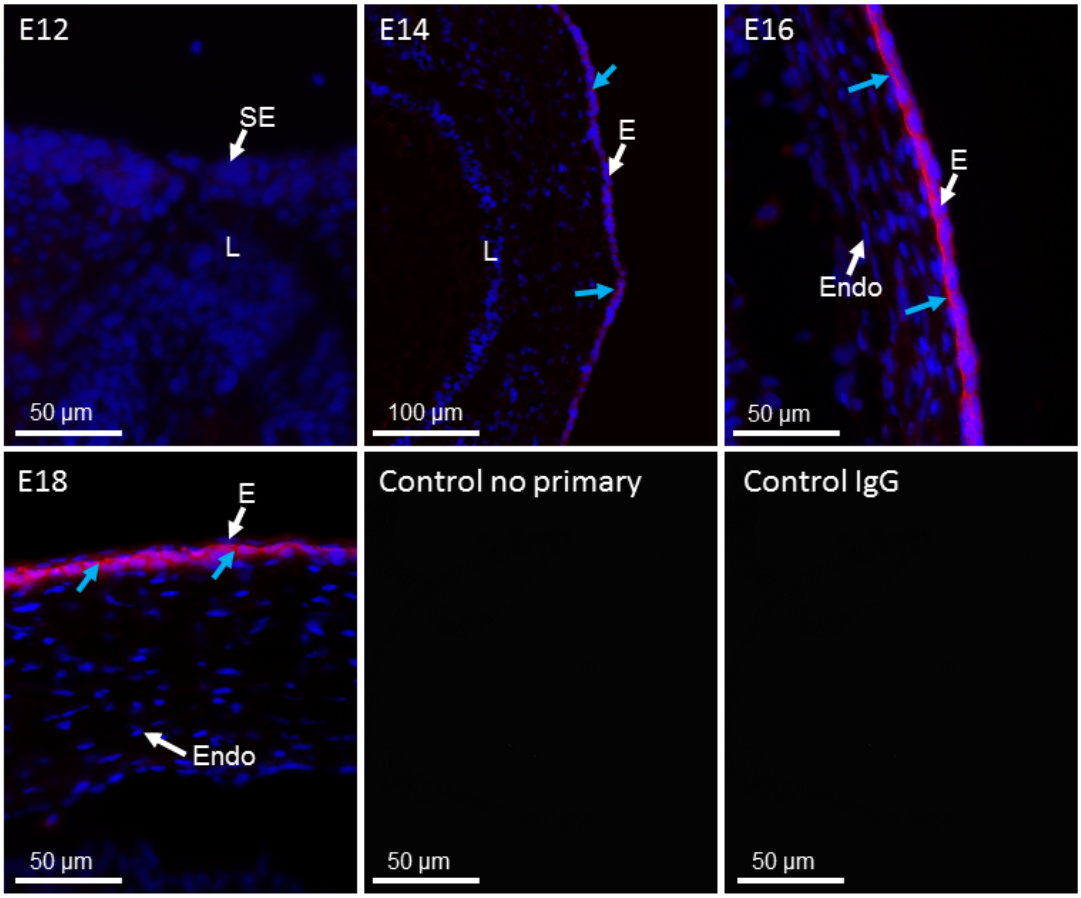

Figure 3.19. Type VII collagen junction labelling in mouse corneal development.

Type VII collagen initially appeared as a faint signal in the corneal epithelium (E) at E14 (blue arrows). By E16 type VII collagen was localised along the epithelium basement membrane (blue arrows) and continued throughout development to E18. No positive labelling was localised with the corneal endothelium (endo), surface ectoderm (SE) or the lens (L). No labelling appeared in the no primary antibody control and the rabbit IgG control images. Blue (DAPI – cell nucleus), red (type VII collagen). For orientation, the corneal epithelium is facing anteriorly or to the right of the image.

3.3.2.3. Connexin 43

CNX43 denotes gap junctions in corneal development. Connexin 43 was present as punctate dots during all ages analysed (**Figure 3.20**). The majority of labelling was localised to the lens and presumptive retina throughout all of the ages analysed as well as the surface ectoderm from E12. CNX43 presented within the corneal epithelium from E14 to E18. Small punctate dots also presented throughout the corneal stroma, which associated with cells from E14 to E18 (**Figure 3.20**).

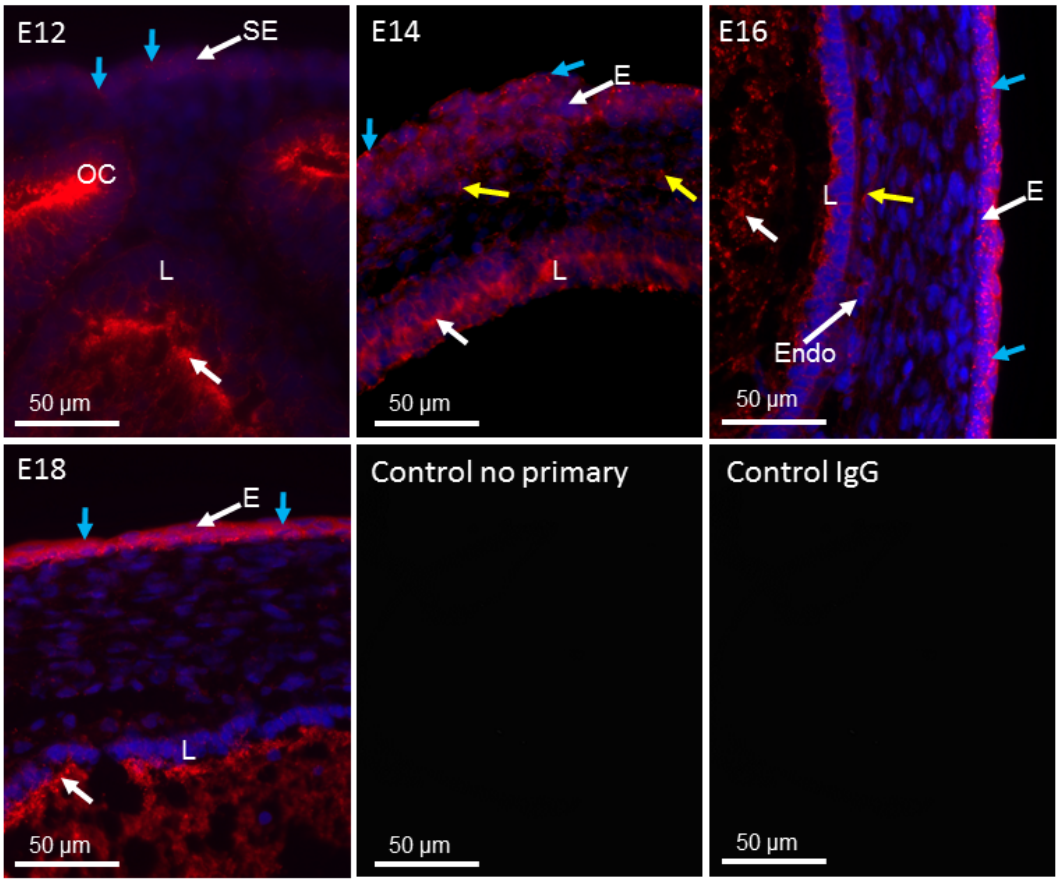

Figure 3.20. CNX43 (red) in mouse corneal development.

CNX43 denotes connexin 43 gap junctions in corneal development. Connexin 43 expressed within the surface ectoderm (SE) (blue arrows), lens (L) (white arrows) and optic cup (OC) at E12. With increased development the corneal epithelium (E) (blue arrows) and lens (L) (white arrows) had a strong staining profile of CNX43 from E14 to E18. CNX43 was also found between corneal stromal cells (yellow arrows) from E14 to E18. There was no protein labelling in controls of no primary antibody application and with a rabbit IgG control. Blue (DAPI – cell nuclei), red (connexin 43 gap junction protein). For orientation, corneal epithelia are facing upwards or to the right of the image.

3.3.2.4. Hyaluronic Acid

Hyaluronic acid (HA) was present from the earliest age analysed, which enhanced to E14 (**Figure 3.21**). The protein labelling at E11 appeared to associate with cell migration. From E11, cells around the lens are migrating as well as cells entering the presumptive corneal stroma anteriorly, the protein was seen in both of these locations. At E14 HA is amplified throughout the corneal stroma. HA decreased after E14, being completely absent at E15 and in all ages analysed older than E15. At E15 the HA is most probably replaced by collagen fibrils and other extracellular matrix proteins (**Figure 3.21**).

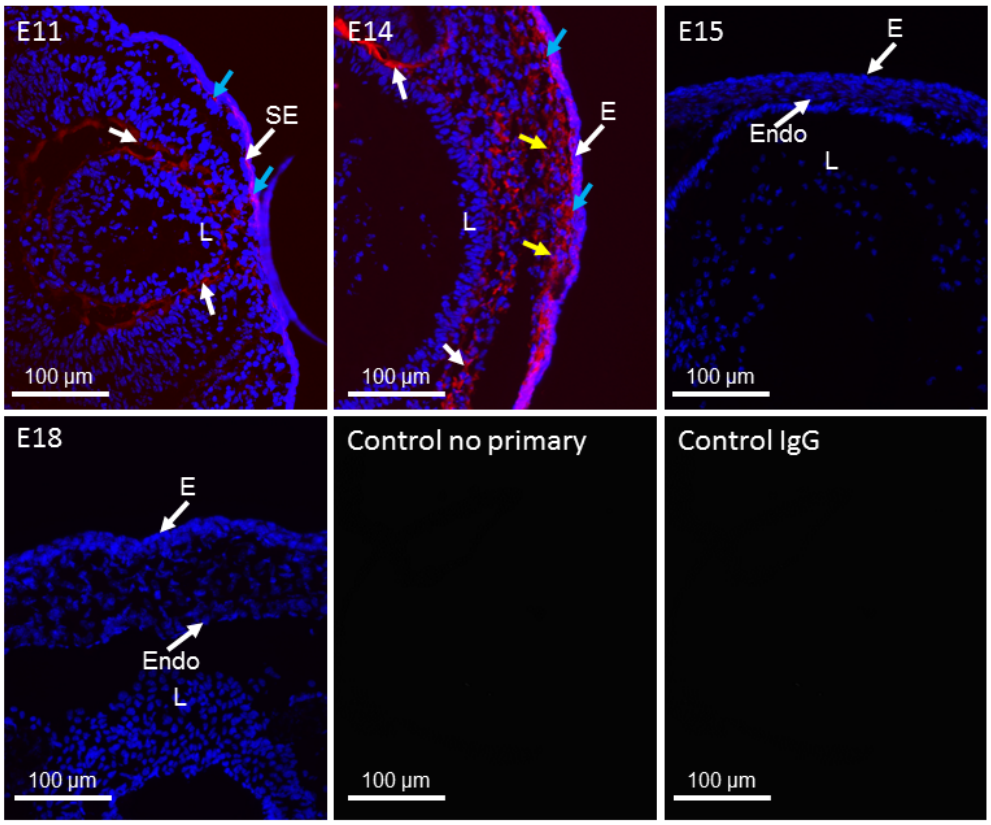

Figure 3.21. Hyaluronic acid (HA) labelling (red) in mouse corneal development.

HA was found from E11 and associated with the migrating cells around the lens (L) (white arrows) and the surface ectoderm (SE) (blue arrows). Staining increased at E14 within the corneal stroma (yellow arrows) and appeared directly posterior to the corneal epithelium (E) (blue arrows) and around the lens. HA disappeared by E15 and was not seen in any other ages analysed between E15 and E18. No labelling was seen in controls of no primary antibody application and with a rabbit IgG control. Blue (DAPI – cell nuclei), red (HA binding protein). For orientation, the corneal epithelium is faced upwards or to the right of the image.

3.4. Discussion

This study investigated the interaction between the developing corneal cells and collagen fibrils using electron microscopy and histochemical techniques. The youngest age analysed within this study (E10) showed the lens vesicle to be invaginated into the optic cup, with the overlying surface ectoderm. At E10 small vesicles were seen in the migrating mesenchymal cells, which indicated the transport of extracellular matrix content into the surrounding environment. Thin strands of extracellular matrix projected from the cells of the surface ectoderm and extended down to connect with the underlying mesenchymal cells. With increased development, the surface ectoderm becomes the corneal epithelium shortly after E12 (Pei and Rhodin 1970). If the separation of the lens vesicle from the surface ectoderm is delayed or fails, the subsequent migration of mesenchymal cells is abnormal (Cook et al. 1987). TEM analysis showed close cell-cell contacts between the condensed mesenchymal cells at E12, which had been previously been described in the mouse model (Kidson et al. 1999). These intercellular connections could represent a communication system for the initial development of the cornea and potentially be involved in the guidance of cells in migration. Cells of the presumptive corneal stroma contained synthesising organelles, including Golgi apparatus and endoplasmic reticulum, where collagen is known to be synthesised before deposition into the extracellular space (Last and Reiser 1984, Lodish 1988). Intra- and extra-cellular vacuoles were also identified, associating with the cell membranes. These vacuoles could transport collagen from the Golgi apparatus to cell membranes before the collagen is deposited extracellularly through exocytosis. Vacuoles were also identified in the surface ectoderm, however, no secretory organelles were seen and the vacuoles did not associate with the cell membrane, therefore it did not appear that the surface ectodermal cells were responsible for matrix deposition as they are within the avian corneal model (Hay E. D. and Dodson 1973). The presence of the connexin 43 gap junction protein early on in corneal development indicated the importance of communication within the epithelium, stroma, lens and retina. Disruption to this communication system could impact the success of corneal development (Nicholson and Bruzzone 1997).

Corneal stroma cells had fully populated the presumptive stroma by E13. Within the anterior aspect of the cornea, cells exhibited a stellate morphology with a large amount of space around each cell. Reduced cell density together with a greater extracellular matrix space after E12 has previously been described in the mouse cornea (Kidson et al. 1999). Within the posterior cornea, cells were in close proximity to neighbouring cells and possessed a longer and thinner morphology. The large quantities of extracellular space in the anterior corneal stroma combined with the phenotypes of the cells suggest extracellular matrix is initially deposited from the stromal cells in the anterior aspect of the embryonic cornea. Pro-collagen is secreted into the extracellular space but remains undetectable by conventional electron microscopy analysis until cleavage of procollagen and its subsequent self-assembly into collagen fibrils (Kadler et al. 1996). It is thought that the extracellular space is rich in pro-collagens as well as proteins crucial for development; these may include hyaluronic acid and proteoglycans, both of which remain unstained by the preparation method of Deerinck used here. However, with immunofluorescence techniques hyaluronic acid, a glycosaminoglycan known to regulate cell migration in development was associated with the migrating cells that develop the cornea (Pratt et al. 1975, Zhu et al. 2006). The labelling pattern observed for hyaluronic acid confirms the suggestion that hyaluronic acid is present within the extracellular spaces between E10-E14. By E15 there was no hyaluronic acid, which implied that cell migration into the corneal stroma had ceased. Hyaluronic acid is most probably replaced by collagen fibrils and matrix components for the development of a transparent cornea, similar to what is described in avian development (Hassell and Birk 2010).

3-D reconstructions of the E13 dataset showed cell processes to branch from the cell bodies in different directions and connect with adjacent cells. The cell projections within the anterior cornea directed anteriorly towards the epithelium and basal lamina, suggest a potential communication mechanism between the stromal cells and the epithelium. Mesenchymal cells migrating

into the rabbit corneal stroma from the peripheral cornea have also been shown by previous studies to interact with the corneal epithelium through cell extensions, proposed to help maintain a stem cell niche (Yamada et al. 2015). In addition, the literature states that mesenchymal cells communicate with the surface ectoderm through transcription factors; if this interaction fails, the anterior eye does not segment or form correctly (Cvekl and Tamm 2004). The results in this study identify another mechanism by which these cells could interact, which may also result in anterior eye abnormalities if faulty.

Collagen fibrils first presented at E13, with enhanced deposition of collagen fibrils posterior to the basal lamina, showing the initial synthesis of Bowman's layer. Because of the fine filamentous structure and the position of some of the fibrils arranged perpendicular to one another, it was postulated that these represented anchoring filaments. Immunofluorescence labelling identified type VII collagen posterior to the epithelium as a localised band, an important component of anchoring filaments (Lunstrum et al. 1986). Similarly, previous studies have shown the rabbit and human cornea to express type VII collagen localised to the basal lamina, with the presence of anchoring filaments suggested to be precursor filaments for the development of Bowman's layer (Tisdale et al. 1988). These anchoring structures have been previously identified to be type VII collagen rich with immunofluorescence and appear as "banded strands" posterior to the rabbis corneal epithelium, the results shown in this chapter did not show any punctate stain, to reveal this pattern a higher magnification microscope could be used (Gipson et al. 1987). In addition, the mouse structure would be thinner than the rabbit and could make the punctate staining more difficult to detect compared to the larger rabbit. The anchoring filaments could provide a substratum along which cells migrate, or to facilitate adhesion of the epithelium to the stroma (Gipson 1992, Leivo et al. 1996). The migration of cells along collagen fibrils via contact-guidance is a common mechanism to migrate and align cells in development (Dunn and Heath 1976, Ebendal 1976, Nakatsuji and Johnson 1983, Provenzano et al. 2008, Wood and Thorogood 1984). Fibronectin was found to be expressed in a similar pattern to that in developing rabbit and human corneas, localised to the

epithelial basement membrane and Descemet's membrane; this showed a similarity between the mouse with other mammalian developmental models (Cintron et al. 1984, Tervo et al. 1986). Fibronectin regulates cell-extracellular matrix interactions and is thought to govern tissue morphogenesis (Pankov and Yamada 2002).

By E14 the posterior mesenchymal cells condense to form apicolateral contacts with adjacent cells, which develop the corneal endothelium. Collagen fibrils were found to associate with cells and plasma membranes, similar to previous results, which supports evidence that the corneal stromal cells play a role to synthesise and deposit collagen fibrils (Haustein 1983). The distribution of collagen fibrils within corneal development could disrupt cell traction less, helping cells migrate. However, the cells could also generate mechanical forces to displace collagen fibrils and organise the extracellular matrix (Provenzano et al. 2008). The fact that cells within the corneal stroma appeared before collagen fibrils further implies that collagen fibrils do not regulate the initial migration of cells, which is considered to occur by the deposition of a primary stroma in the avian cornea (Hay E. D. and Revel 1969). However, as development proceeds, collagen fibrils may have a role in organising the cells within the corneal stroma.

The flattened posterior mesenchymal cells formed a monolayered endothelium by E15 to create the posterior boundary of the cornea. This event is different within other species. In the avian and human cornea, the first wave of neural crest cells migrate over the lens and develop into the endothelium before the 2nd wave of mesenchymal cells migrate and differentiate to form the corneal stromal keratocytes (Bard et al. 1975, Coulombre and Coulombre 1958, Dublin 1970, Hay E.D. 1980, Hay E. D. and Revel 1969, Johnston et al. 1979). The differences highlighted in this chapter between different species could result from evolutionary aspects, the chick and mouse eye have been previously described to be evolutionary divergent, which could be a reason as to why the chick and mouse develop differently (Koudouna et al. 2018b). The

maturation of the endothelium will be crucial to pump water from the stroma to allow stromal thinning and generate transparency (Zieske 2004). The morphology of the corneal stromal cells changes from stellate to long and slender at E15, characteristic of stromal fibroblasts. The cells gradually elongate into parallel rows between collagen lamellae, this observation has been previously described (Reneker et al. 2000). In addition, collagen fibril maturation increased as the developmental age-progressed with an increase in collagen fibril organisation. The increase in collagen fibril packaging would start to generate the structure and biomechanical properties of the cornea (Boote et al. 2003). However, even at E18, a significant amount of secretory organelles persist, which suggests that matrix biosynthetic activity is still high. Within the mouse model, many post-natal alterations occur simultaneously with eye-opening and maturation. One of these events will be the reduction of secretory organelles, with an increase in collagen fibril packing to enhance the light scattering properties of the cornea (Quantock A. J. et al. 1998, Song et al. 2003).

Extracellular matrix studies in tendon and skin have identified fibripositors to deposit and align collagen fibrils in a given direction, regulating collagen fibril organisation in tissues (Canty et al. 2004). Fibripositors were not visualised to deposit collagen fibrils in the mouse corneal stroma, which suggests collagen alignment proceeds with a different mechanism. As development progressed, the collagen fibrils become gradually more organised within lamellae, orthogonally orientated within the corneal stroma. The corneal stromal cell projections associated with the direction of aligned collagen fibrils indicate that the cell projections could orientate the collagen bundles within the corneal stroma. Previous studies have demonstrated cell protrusions to align with collagen fibrils, which provides an anchorage to propel a cell forward, with the membrane protrusions assisting cell movement and alignment within the matrix (Friedrichs et al. 2007). The mechanical forces generated from the cell migrations could directly align the collagen fibrils. Studies have also shown an association between the rotation of cell orientation and the organisation of collagen fibrils within the avian cornea (Koudouna et al. 2018a). As the rotation

of cells occurs before collagen fibril orientation, it was suggested that the cells of the corneal stroma organise the orthogonal collagen lamellae (Koudouna et al. 2018a). However, understanding how collagen fibrils organise needs more investigating. Koudouna *et al.,* 2018 further outlined the need to understand the underlying mechanisms that are responsible for collagen fibril alignment in the avian cornea. A schematic summarising the main events in the prenatal mouse cornea is presented in **Figure 3.22**

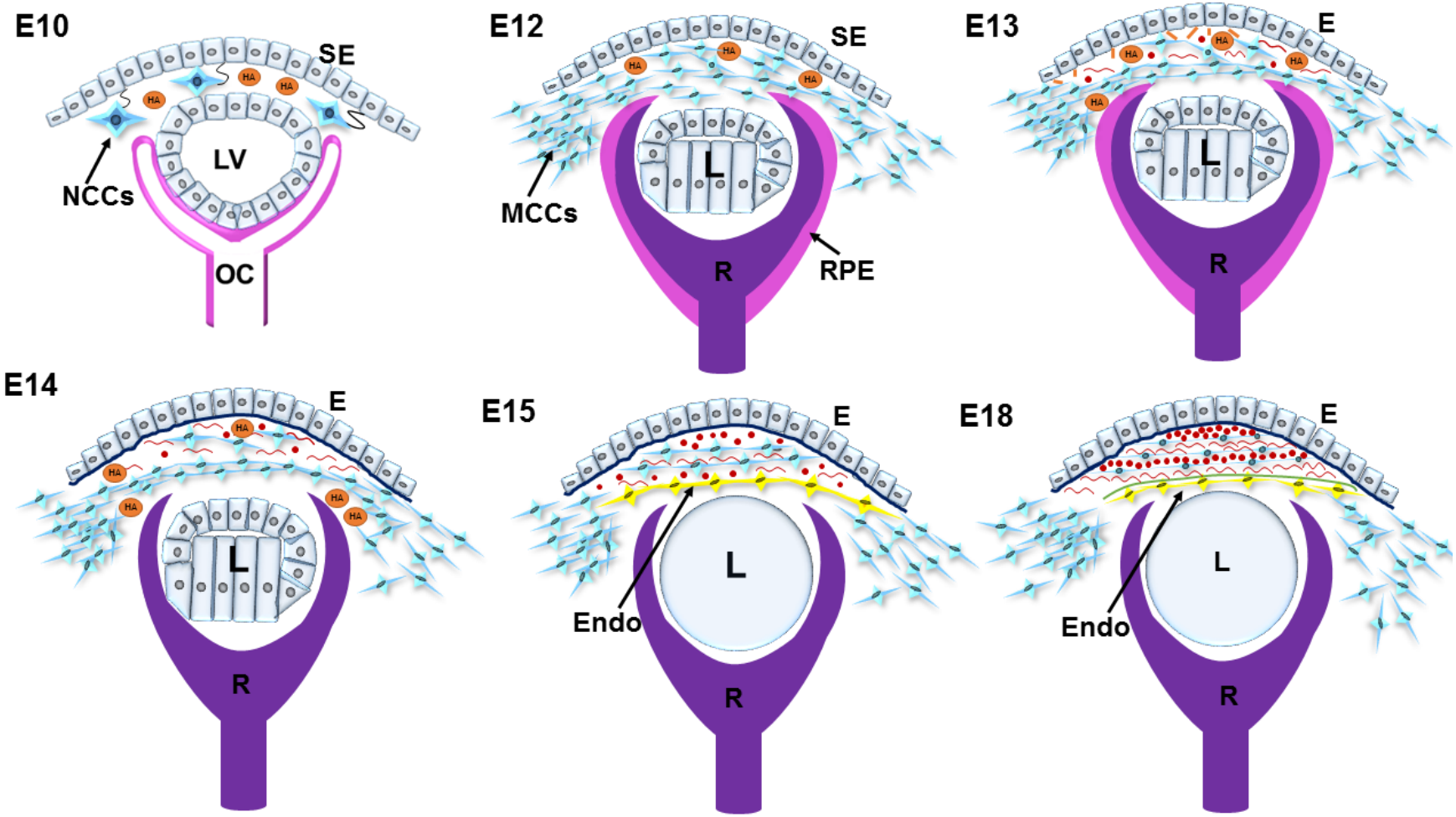
E10
SE
HA
LV
NCCs
OC
E12
SE
HA
L
MCCs
R
RPE
E13
E
HA
L
R
E14
E
HA
L
R
E15
E
L
Endo
R
E18
E
L
Endo
R

Figure 3.22. Events in the developing mouse cornea.

From E10 of corneal development the surface ectoderm (SE) overlays the lens vesicle (LV) which sits on top of the optic cup (OC). Some neural crest cells (NCCs) migrate between the SE and LV (blue cells). Strands appeared to emerge from the surface ectoderm and contact the underlying cells (black lines). The matrix contained hyaluronic acid (HA), which appeared to increase in concentration to E14 before disappearing by E18 (orange circles). By E12 the mesenchymal cells (MCCs) infiltrated the area between the surface ectoderm (SE), the lens (L), retina (R) and retinal pigment epithelium (RPE) in large numbers. The space surrounding these cells increased at E13, with small amounts of collagen fibril deposition between the cells. From the basement membrane directly posterior to the epithelium (E) anchoring filaments (orange lines) were seen to branch. The posterior mesenchymal cells have started to condense at E13, and continue to condense before forming the endothelium (endo) at E15 (yellow cells). By E14 the basement membrane had fully developed with type VII collagen clearly displayed as a bright band posterior to the corneal epithelium and for every age above E14. The amount of collagen (red) deposition increased with the number of cells decreasing. Collagen fibrils are identified as dots (red) and longitudinal fibrils (red) to show the orthogonal arrangement of the fibrils through development. By E15 the cells aligned into parallel rows, with collagen starting to bundle into lamellae. This organisation of cells and collagen fibrils appeared to further increase until E18, where corneal stromal cells were found in longitudinal rows which lay between collagen lamellae and contained collagen fibrils orthogonally arranged.

3.5. Summary

This study has mapped using 3-D imaging techniques the cell arrangements and associations from E10-E18 of mouse corneal development. The results showed extensive cell projections of the corneal stromal cells to associate with neighbouring cells and deposited collagen fibrils, which were unidentified in mammalian corneal development prior to this study. Collagen fibrils appeared to be initially synthesised and secreted through the cells of the corneal stroma in early development, which were found to align in the same direction as the cell projections. There was no organised acellular collagen layer identified posteriorly to the surface ectoderm, which confirmed that a primary stroma is not required to assist cell migration in the development of the mouse cornea. This study was the first to identify anchoring filaments within the mouse cornea, showing similarity to other mammalian developmental models, including the rabbit and human. In addition, a clear divergence of events was evident within the prenatal mouse cornea in comparison to the avian species. The similarities between the mouse model compared to other mammalian developmental models supports the mouse as an appropriate model to direct corneal developmental research. However, the divergence of some events, particularly in the cell migration steps in both the avian and human cornea, suggests more models require investigation to grant a better understanding of the corneal developmental events that occur across mammalian species.

Chapter 4: Collagen and Proteoglycan Distribution in the Developing Mouse Cornea

4.1. Introduction

The physiological cornea relies on collagen fibrils to assemble into organised lamellae, influenced by proteoglycans (PGs) that control collagen fibril diameter and organisation (Meek and Knupp 2015, Rada et al. 1993). The distribution of collagen types and extracellular matrix molecules changes in development for successful morphogenesis. Current research to understand the distribution of matrix components within the developing cornea has mainly focused on studying the avian species, with a paucity of information about the composition of the embryonic mouse cornea.

The avian cornea initially develops by the corneal epithelium laying down the primary stroma (Hay E. D. and Revel 1969). The main collagen types that reside in this primary stroma include types I, II, V and IX collagen (Hay E. D. and Revel 1969, Hayashi M. et al. 1988). The main collagen type found within the adult mammalian corneal stroma is type I, responsible for the maintenance of a transparent and biomechanically strong cornea (Birk et al. 1990, Newsome et al. 1982). The amount of collagen has been shown to increase in the later stages of development in the avian cornea in X-ray diffraction studies, increasing with maturity and transparency (Quantock A. J. et al. 2003). This study showed the initial collagen deposition was orthogonally arranged between days 13-18 but was less well-orientated later from day 16 of development. X-ray studies in mice have also shown the importance of collagen fibril deposition and development in corneal development by demonstrating the collagen fibril orientation and distribution is highly dynamic through development (Sheppard et al. 2010). In addition, type V collagen

forms heterotypic fibrils with type I collagen, where type V regulates collagen fibril diameters (Birk 2001, Birk et al. 1990, Birk et al. 1986). Type IX collagen preserves the primary stroma, and when type IX collagen breakdown is activated, the migration of mesenchymal cells into the presumptive corneal stroma to synthesise the secondary stroma is initiated (Cai et al. 1994, Fitch J. et al. 1998, Fitch J. M. et al. 2005). Type IX collagen forms heterotypic fibrils with type II collagen, and both are often found to associate together in tissues (Fitch J. M. et al. 1994). After the invasion of mesenchymal cells, prior to stromal swelling, type IX collagen depletes until being undetectable. As development continues, the secondary stroma is mainly composed of heterotypic fibrils composed of type I and V collagens (Birk et al. 1986). Minor collagen types III, IV, VI, VIII and XIII have also been identified to distribute within the secondary stoma, which regulates the development of the avian cornea (Fitch J. M. et al. 1990, 1991, Grant and Leblond 1988, Linsenmayer et al. 1986). As a result of their abundance in chick development, it was considered that types I, II, V and IX collagens may also be present in mouse prenatal corneal development (Hendrix et al. 1982).

PGs are key components of the corneal extracellular matrix that control collagen fibril diameter, spacing and synthesis, and confer the tissue with transparency (Rada et al. 1993). Keratan sulphate PGs are the main PGs initially synthesised in the avian cornea, which are sulphated around day 14 (Funderburgh et al. 1986). The keratan sulphate PG keratocan expresses within the cells that migrate into the primary stroma. Keratocan levels decrease from E9 when lumican proceeds to increase in concentration (Conrad and Conrad 2003). Keratan sulphate has also been shown in mammalian corneal development, which is elevated in the early development of rabbit corneas (Cintron and Covington 1990). When keratocan is removed from mammalian corneas, the corneal stroma thins and collagen fibrils increase in diameter; these results demonstrated the importance of keratocan in the development of a functional mammalian cornea (Liu C. Y. et al. 2003, Meek et al. 2003). Sulphated keratan sulphate increases in chick development, alongside collagen interfibrillar distance decreasing to further demonstrate its importance

in the generation of transparency in corneal development (Liles et al. 2010). Lumican associates with new collagen fibrils near the cell surface and within embryonic corneas. Mice deficient in lumican lose collagen fibrillar structure and overall thickness of the corneal stroma, which results in opacity (Chakravarti et al. 2000, Kao and Liu 2002, Song et al. 2003). These knockout models have demonstrated the importance of PGs to maintain corneal structure in mammalian development. However, their organisation and distribution in the prenatal mammalian cornea remain to be investigated. Importantly, it should be noted that, compared to other mammalian species, the adult mouse cornea possesses predominantly under-sulphated keratan sulphate, with large chondroitin sulphate/dermatan sulphate extensions; this is unique to the mouse cornea (Young et al. 2005).

The different types of PGs and collagens within developing tissues each provide a specific role for successful development. Identifying the components that are present at different developmental stages will elucidate which extracellular matrix components are crucial for mouse corneal morphogenesis. The main aim of this chapter was to investigate for the first time the distribution of types I, II, V and IX collagens and type I pro-collagen within the developing mouse cornea. The second aim was to examine the distribution and structural interactions of PGs at different ages in the prenatal mouse cornea.

4.2. Methods

4.2.1. Immunofluorescence

Immunofluorescence labelling was carried out on 6 un-paired mouse eyes at ages E10-E18. The complete protocol of tissue collection and immunofluorescence is described in chapter 2 general methods (sections 2.1 and 2.5).

For this chapter, mouse eyes were cryo-sectioned transversely to the anatomical position of the eyes *in vivo,* before being collected on Superfrost Plus Slides (Thermo Scientific, Waltham, MA, USA). The primary antibodies added in this experiment were rabbit polyclonal or mouse monoclonal antibodies. Information on the antibodies used can be found in **Table 4**. The secondary antibody Dylight 594 Horse Anti-Rabbit secondary (Abcam, Cambridge, England) was added to the slides which contained the rabbit polyclonal primary antibodies, and Dylight 594 Horse Anti-Mouse antibody (Abcam, Cambridge, England) was applied to the slides that contained the mouse monoclonal primary antibodies. Both secondary antibodies were used at a concentration of 1:200.

Table 4. **Primary Antibodies used to Analyse Collagens in Developing Cornea**

Primary Antibody	Description	Target	Concentration	Source	Reference
Anti-Type I Collagen	Rabbit Polyclonal	Type I collagen	1:100	Abcam (Cambridge, England)	(Kalash et al. 2014)
Anti-Type II Collagen	Rabbit Polyclonal	Type II collagen	1:100	Abcam (Cambridge, England)	(Mo et al. 2009)
Anti-Type V Collagen	Rabbit Polyclonal	Type V collagen	1:100	Abcam (Cambridge, England)	(Guillen-Ahlers et al. 2008)
Anti-Type IX Collagen	Rabbit Polyclonal	Type IX collagen	1:100	Abcam (Cambridge, England)	(Liu W. et al. 2015)

Pro-Collagen I	Monoclonal Mouse	Type 1 pro-peptide (N-terminal residues)	1:100	Developmental Studies Hybridoma Bank (Iowa City, Iowa, USA)	(Foellmer et al. 1983)

4.2.2. Transmission Electron Microscopy

4.2.2.1. Proteoglycan Staining Protocol

The complete methodology is described in section 2.2.2.4 of the general methods chapter. 6 unpaired eyes from each age (E10-E18) were immersed in vials overnight in 2.5% glutaraldehyde in 25mM sodium acetate buffer, pH 5.7 containing 0.1M magnesium chloride and 0.05% cuprolinic blue (American Elements, Los Angeles, USA). For the embryonic stages E10-E11, the eyes were left *in situ* with the whole head being immersed. The whole eyes of the embryonic samples from E12-E15 were processed and the corneas were dissected from the whole eye for embryonic tissue E16-E18.

Each copper grid was analysed on the JEOL 1010 transmission electron microscope at different magnifications (x1000, x2000, x5000, x6000, x7500, x10000, x20000).

4.3. Results

4.3.1. Immunofluorescence

The staining patterns of type I, II, V, IX collagen and type I-procollagen were imaged in embryonic mouse corneas from E10-E18 at x20 and x40 magnifications (**Figure 4.1-4.9**). Low magnification images of the cornea showed the cornea in relation to other aspects of the embryonic eye. Higher magnification images of the cornea captured increased details of the extracellular matrix components. All negative controls included no primary antibodies, IgG controls (rabbit) and IgM controls (mouse) and unless stated otherwise showed no positive labelling, which indicated that the positive fluorescence was true staining.

4.3.1.1. Type I Collagen

Type I collagen was seen throughout the lens capsule from the earliest ages analysed (E10-E12) (**Figure 4.1 and Figure 4.2**). A very distinct line was present which associated with the surface ectoderm (E10-E12). Labelling was found posterior to the corneal epithelium from E13 to E16. Type I collagen was evident in the anterior corneal stroma by E14, and was enhanced throughout the corneal stroma by E16 to E18. Type I collagen was increased directly anterior to the corneal endothelium from E17-E18.

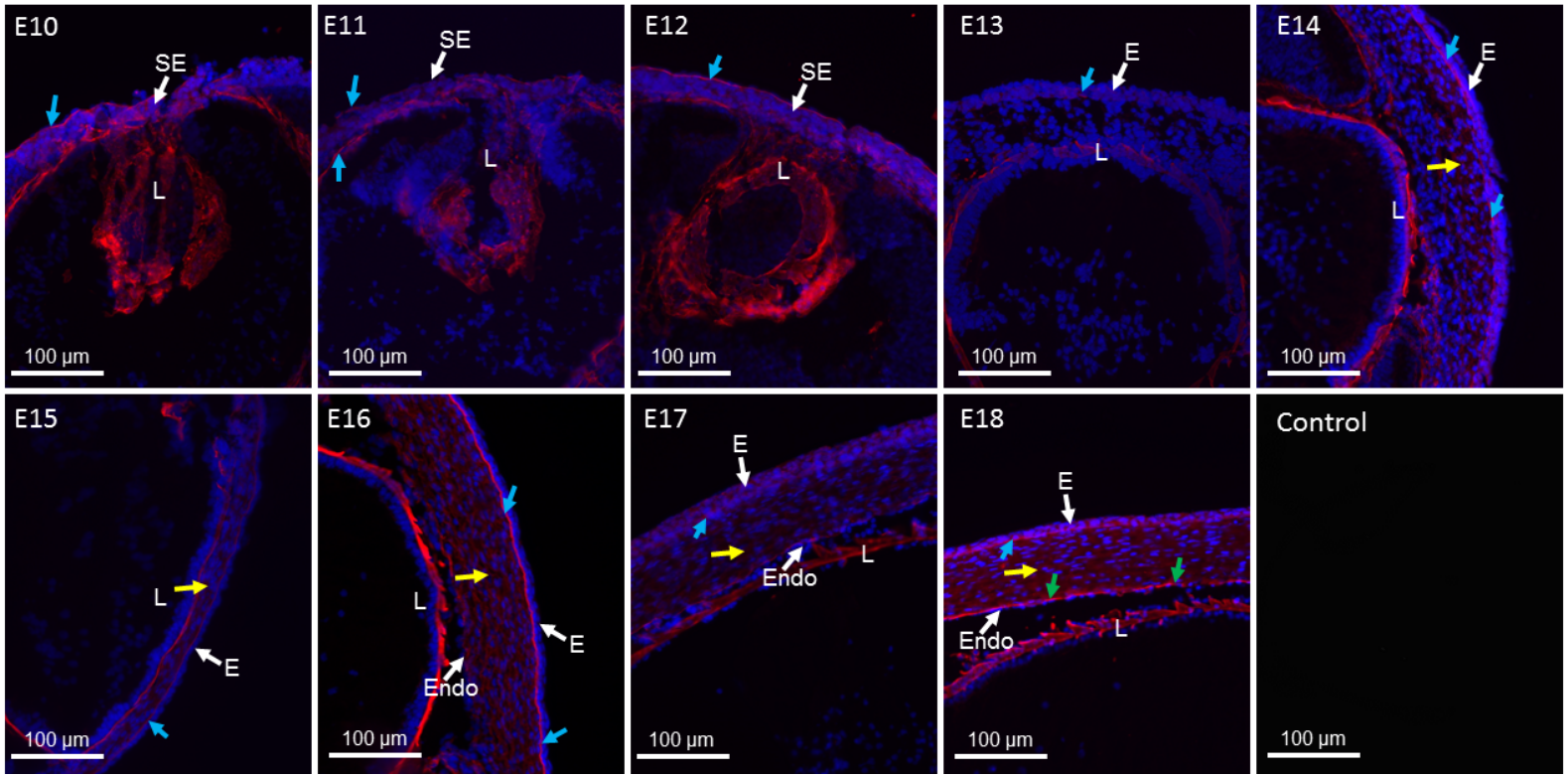

Figure 4.1. ***Type I collagen in the developing mouse cornea x20 magnification.***

Type I collagen associated with the surface ectoderm (SE) and lens (L) (E10-E12). Throughout all ages analysed, the lens capsule Type I collagen expanded within the anterior corneal stroma (yellow arrow) by E14, and was posterior to the corneal epithelium (blue arrow). Type I collagen was present throughout the corneal stroma with maturation, which appeared anteriorly to the corneal endothelium (endo) by E18 (green arrows). No positive labelling was observed within all of the negative controls: without primary antibodies (shown) and with rabbit immunoglobulin controls (not shown). Blue (DAPI -cell nucleus), red (type I collagen). To orientate the eye, the corneal epithelium is facing to the top or to the right of the image. Images are representative of n=6 for timepoints.

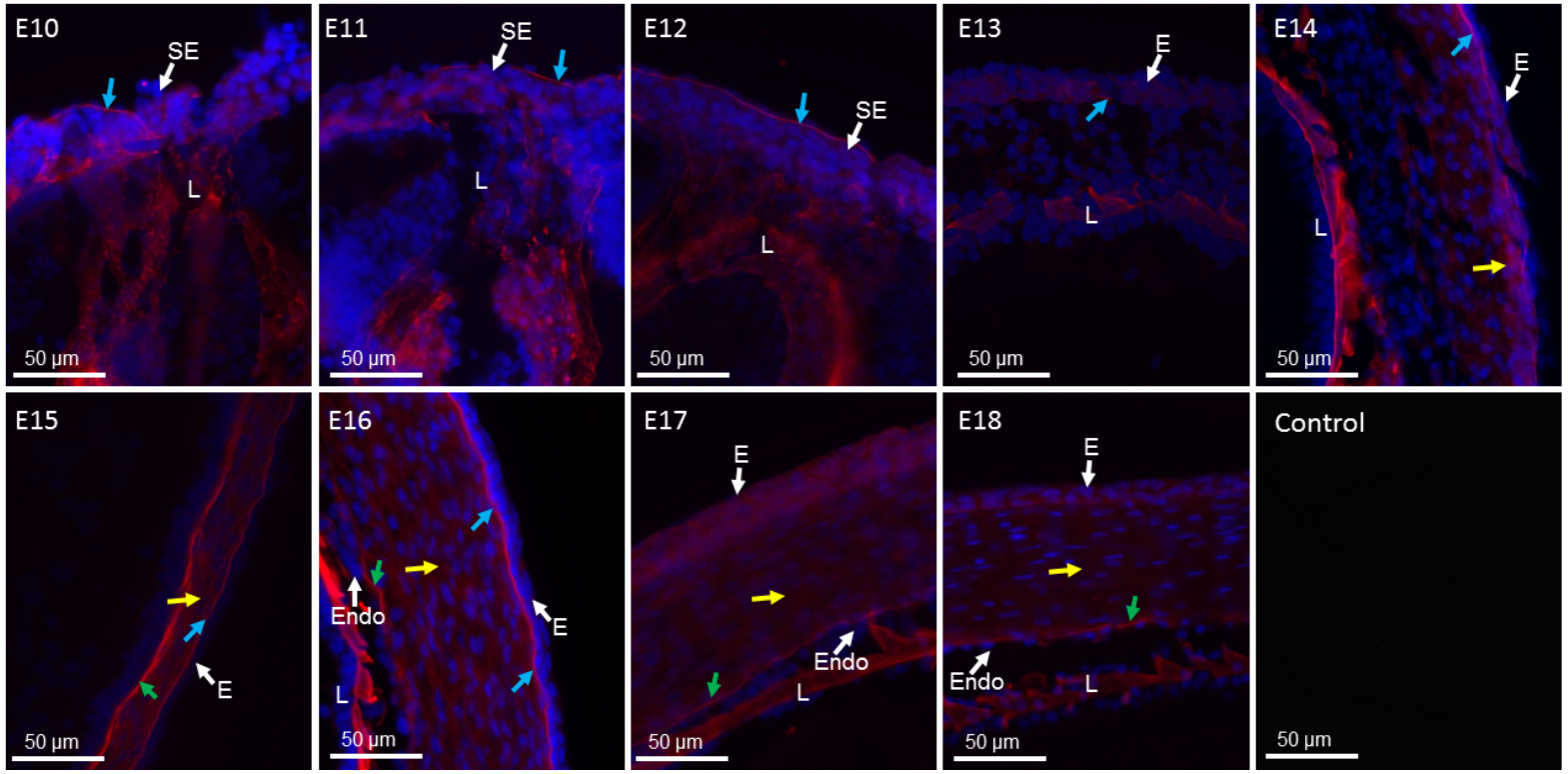

Figure 4.2. Type I collagen in the developing mouse cornea x40 magnification.

Imaging showed a localised line of type I collagen along the surface ectoderm (SE) in addition to being enhanced within the developing lens (L) (E10-E12). From E13-E14 labelling presented beneath the corneal epithelium (E) (blue arrow), with faint labelling within the anterior corneal stroma (yellow arrows). From E15 type I collagen was throughout the corneal stroma and increased along the corneal epithelial basement membrane at E16 (blue arrows). From E17-E18 the label expressed anterior to the endothelium (endo) (green arrows) and throughout the corneal stroma (yellow arrows). Blue (DAPI – cell nucleus), red (type I collagen). Negative controls showed no positive staining without primary antibody (not shown) and rabbit immunoglobulin (shown). Images are representative of n=6 for timepoints.

4.3.1.2. Type II Collagen

Weak labelling of type II collagen was evident around the lens and posterior to the surface ectoderm between E11 and E12 (**Figure 4.3 and Figure 4.4)**. Type II collagen was found within the corneal stroma at E13, increased at E14 within the anterior corneal stroma (yellow arrow). Between E13 and E14, labelling was enhanced directly posterior to the corneal epithelium and was observed throughout the whole thickness of the corneal stroma from E15 to E18 (**Figure 4.3 and Figure 4.4**).

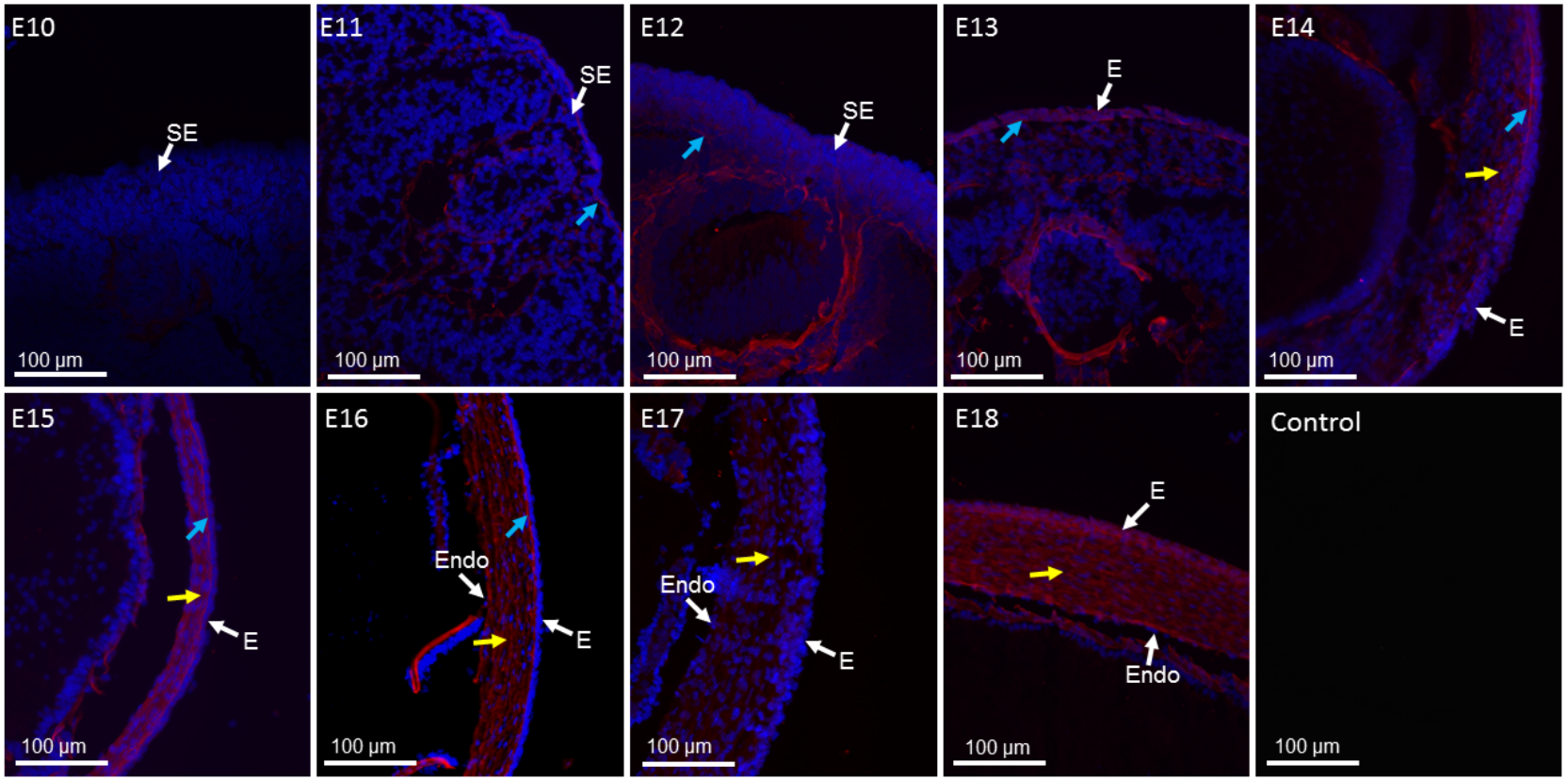

Figure 4.3. Type II collagen in the developing mouse cornea x20 magnification.

Type II collagen was present from E11 to E12 within the surface ectoderm (SE) (blue arrows) and posterior to the corneal epithelium from E13 to E16 (blue arrows). Type II collagen started to show in the corneal stroma from E13, localised within the anterior corneal stroma from E14 (yellow arrows). Type II collagen was identified throughout the whole thickness of the corneal stroma between E15-E18 (yellow arrows). No positive labelling was evident in the no primary control (shown) and immunoglobulin control (not shown). Blue (DAPI – cell nucleus), red (type II collagen). Endothelium (Endo). Images are representative of n=6 for timepoints.

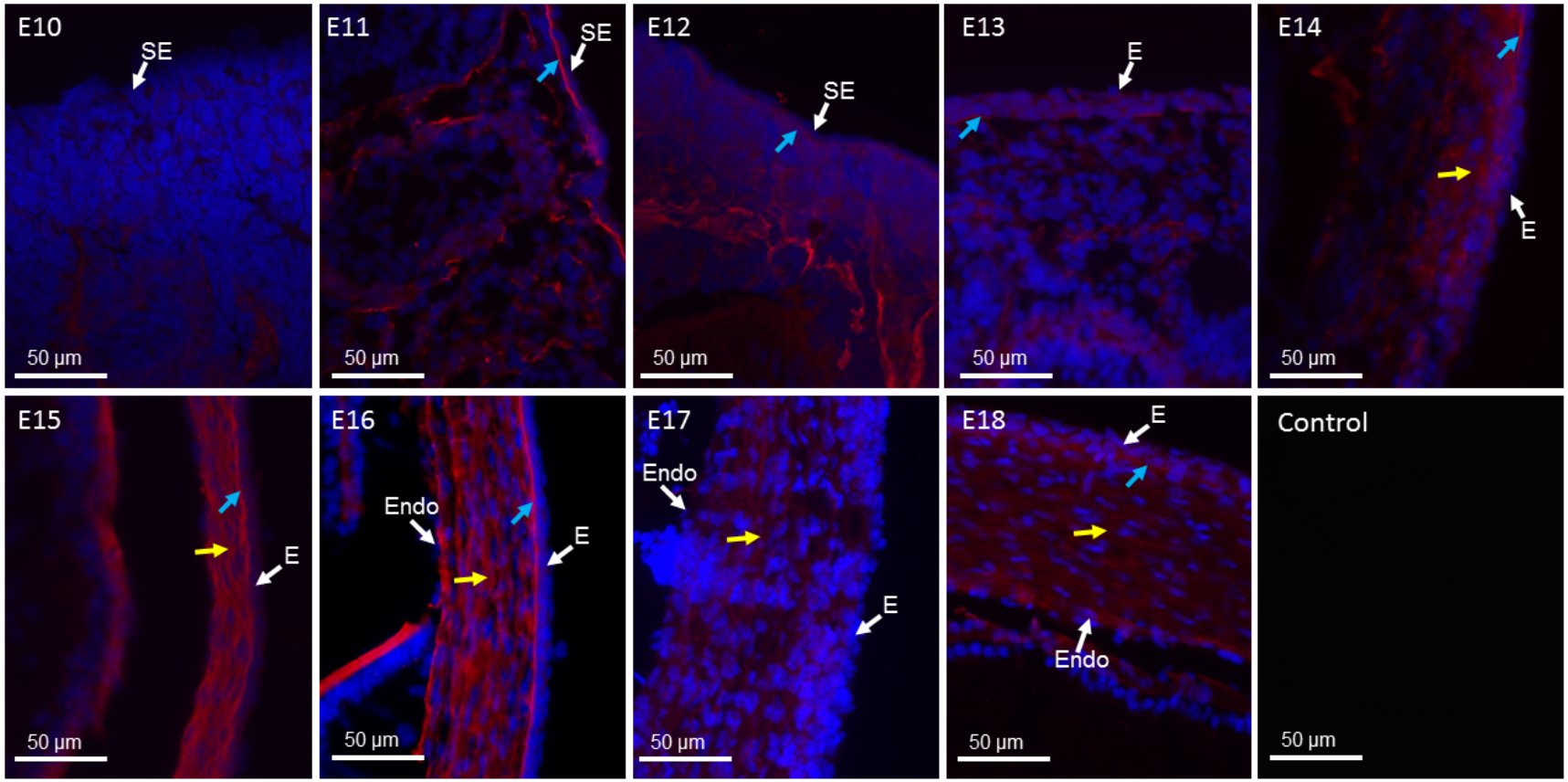

Figure 4.4. Type II collagen in the developing mouse cornea x40 magnification.

Type II collagen expressed from E11 to E12 within the surface ectoderm (SE) (blue arrows) and around the lens (L). Type II collagen first was observed in the corneal stroma from E13, and was clearly localised within the anterior corneal stroma from E14 (yellow arrows). Type II collagen was distributed throughout the whole thickness of the corneal stroma between E15-E18 (yellow arrows). No labelling was present in the no primary control (not shown) and the immuno-globulin control (shown). Blue (DAPI – cell nucleus), red (type II collagen). Images are representative of n=6 for timepoints.

4.3.1.3. Type V Collagen

Type V collagen associated with the surface ectoderm between E10-E12. Type V collagen appeared within the anterior corneal stroma at E13, which spread throughout the corneal stroma by E16. Labelling was positive within the corneal stroma and within the basement membrane of the corneal epithelium. Type V collagen appeared within the anterior corneal stroma at E14. At E15, the protein appeared throughout the whole corneal stroma, being enhanced directly posterior to the corneal epithelium and anterior to the corneal endothelium **(Figure 4.5 and Figure 4.6)**.

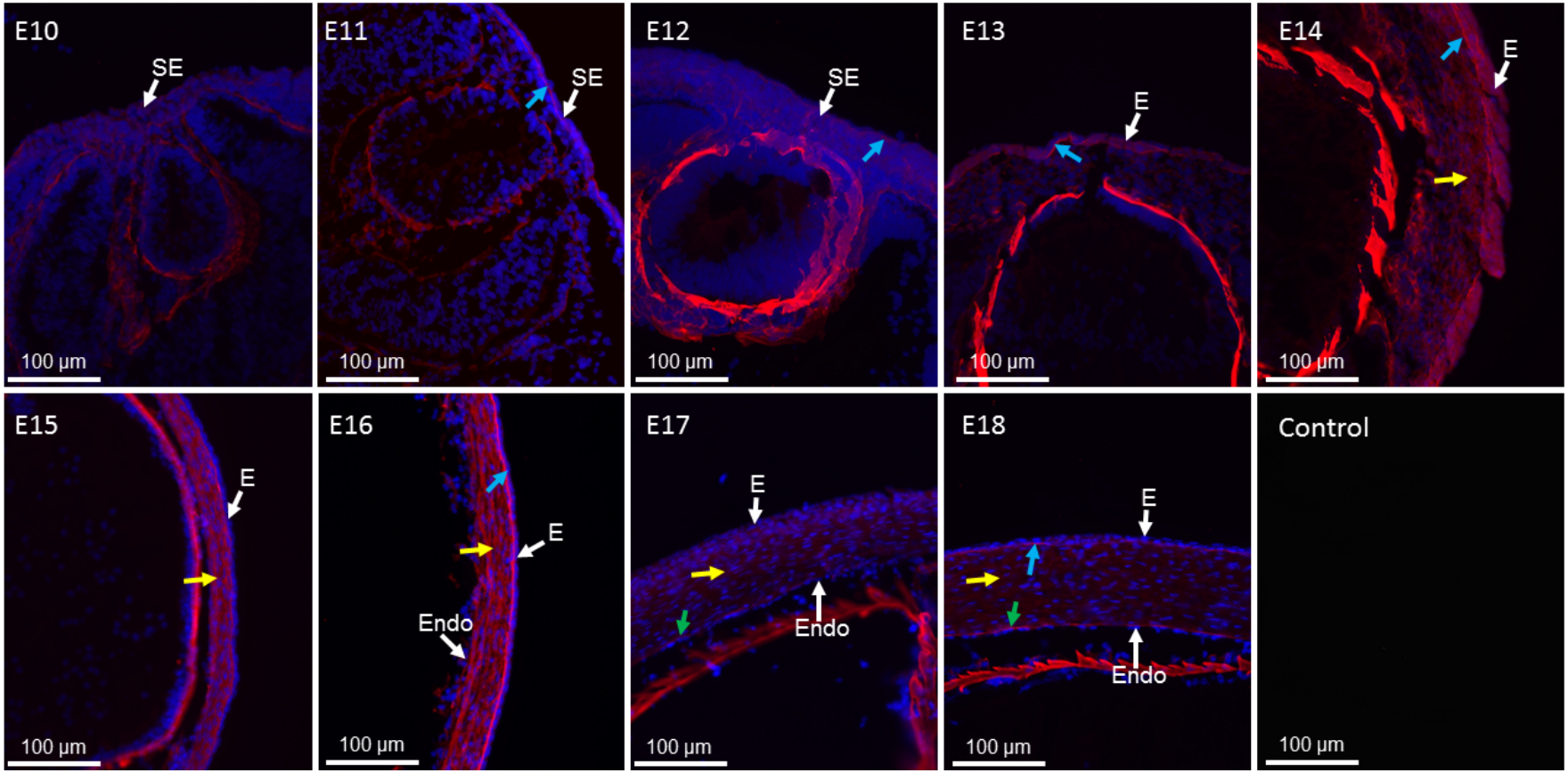

Figure 4.5. Type V collagen in the developing mouse cornea x20 magnification.

Type V collagen was present along the cells of the surface ectoderm from E10-E12 (blue arrows). Positive labelling was initially seen in the anterior corneal stroma at E14, which dispersed through the thickness of the corneal stroma between E15 and E18. Labelling was also enhanced anterior to the corneal endothelium between E17 and E18 (green arrows). There was no positive label in the no primary (shown) and immunoglobulin (not shown) controls. Blue (DAPI – cell nucleus), red (type V collagen). Images are representative of n=6 for timepoints.

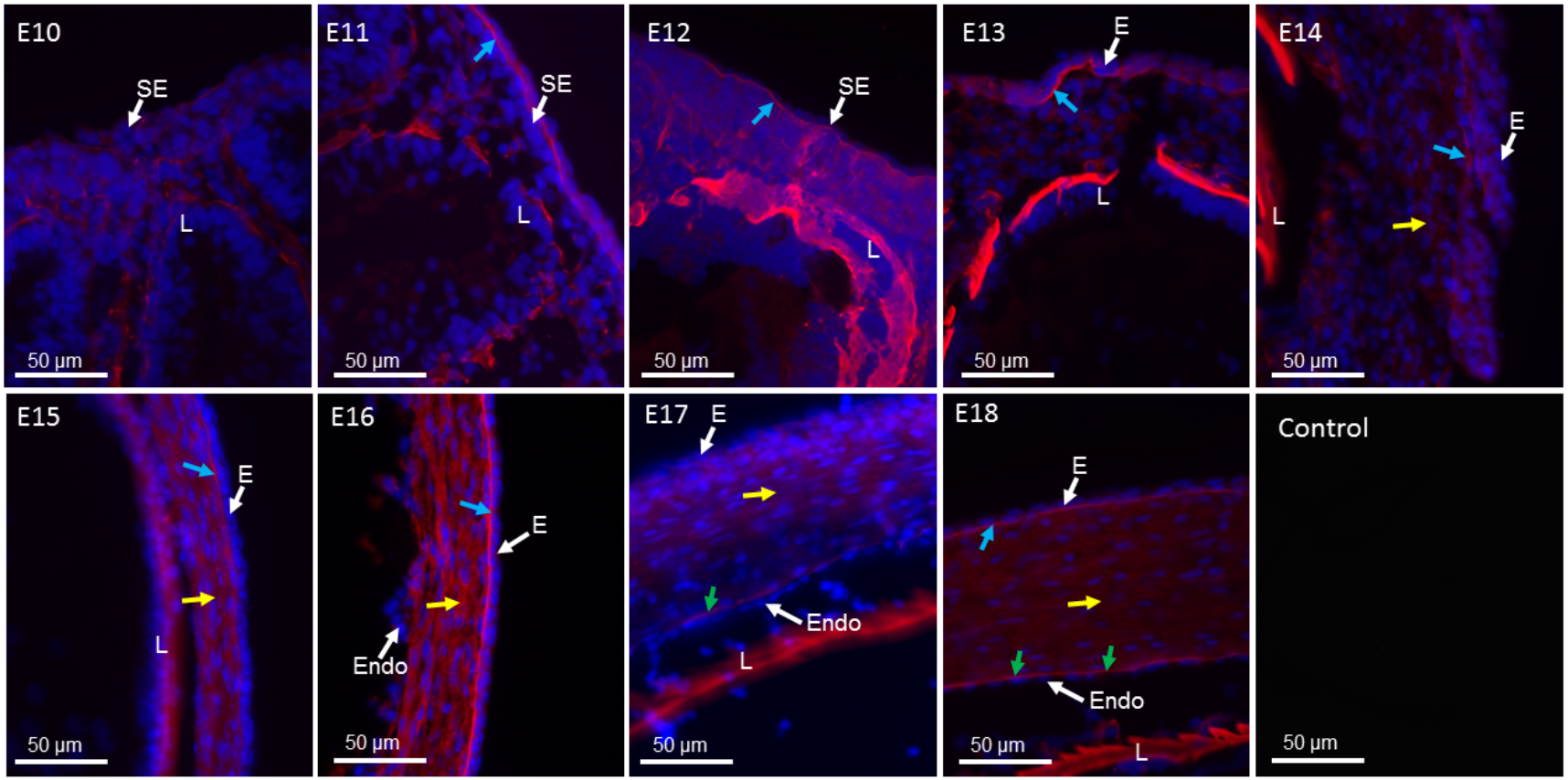

Figure 4.6 Type V collagen in the developing mouse cornea x40 magnification.

Type V collagen was present along the cells of the surface ectoderm from E10-E12 (blue arrows). Staining also occurred posterior to the corneal epithelium from E13 to E18 (blue arrows). Type V collagen was initially seen in the anterior corneal stroma at E14, and had increased by E18 through the full thickness of the corneal stroma. Increased labelling was also identified anterior to the corneal endothelium between E17 and E18. No primary (not shown) and immunoglobulin (shown) controls presented with no positive labelling. Blue (DAPI – cell nucleus), red (type V collagen). Images are representative of n=6 for timepoints.

4.3.1.4. Type IX Collagen

Type IX collagen was not present in the initial stages of corneal development (E10-E13) (**Figure 4.7 and Figure 4.8**). Type IX collagen became localised within the corneal epithelium later in corneal development (E14-E18), with some staining within the corneal stroma from E17.

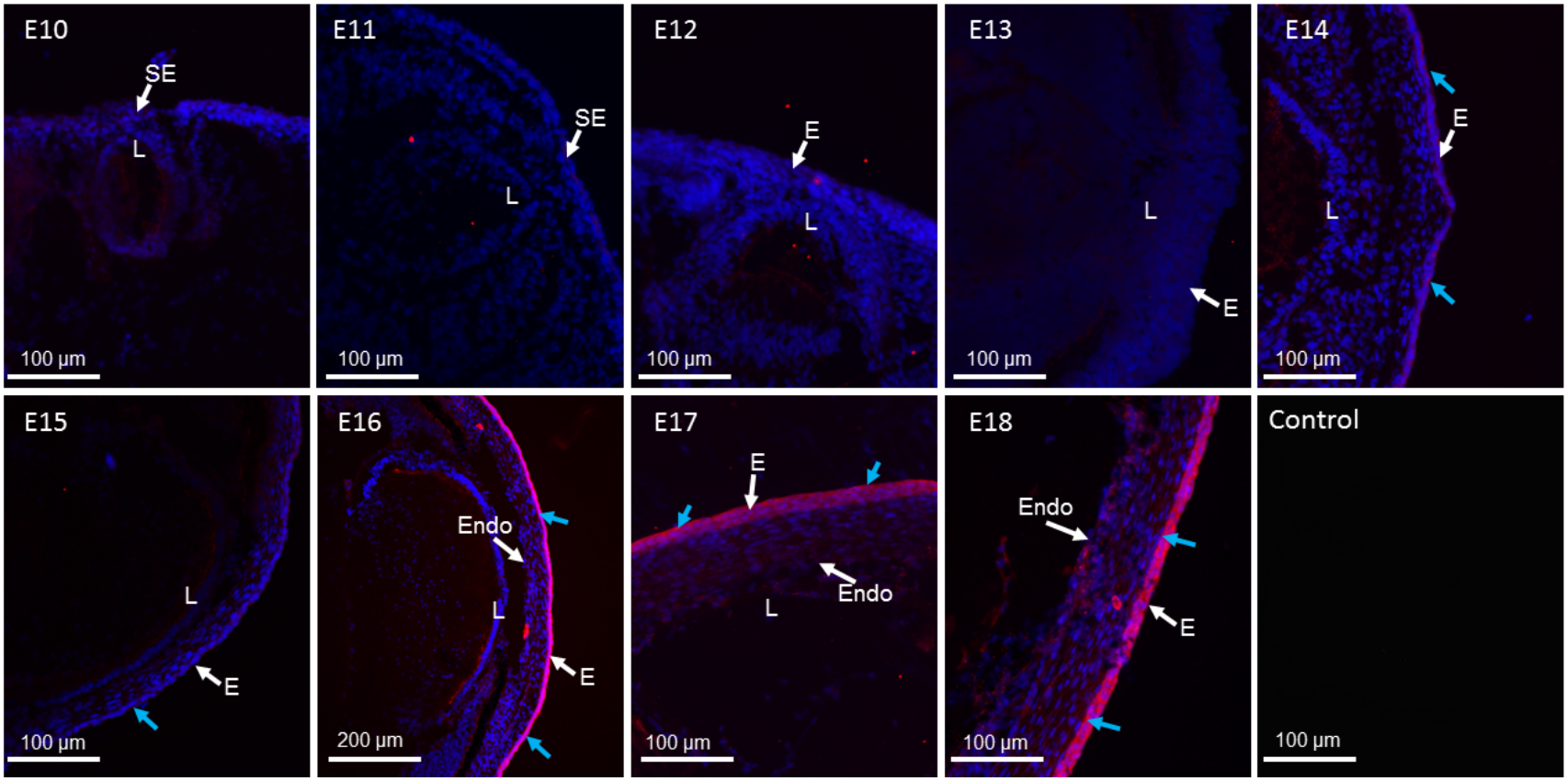

Figure 4.7. Type IX collagen in the developing mouse cornea at x10 and x20 magnifications.

Type IX collagen first appeared associated with the corneal epithelium (E) at E14 and continued to be expressed within the corneal epithelium up to E18 (blue arrows). Type IX collagen was found at low levels within the corneal stroma between E17 and E18. Type IX collagen was not expressed within both negative controls (no primary control, shown, and immuno-globulin control, not shown). Blue (DAPI – cell nucleus), red (type IX collagen). Surface ectoderm (SE), lens (L), endothelium (Endo). Images are representative of n=6 for timepoints.

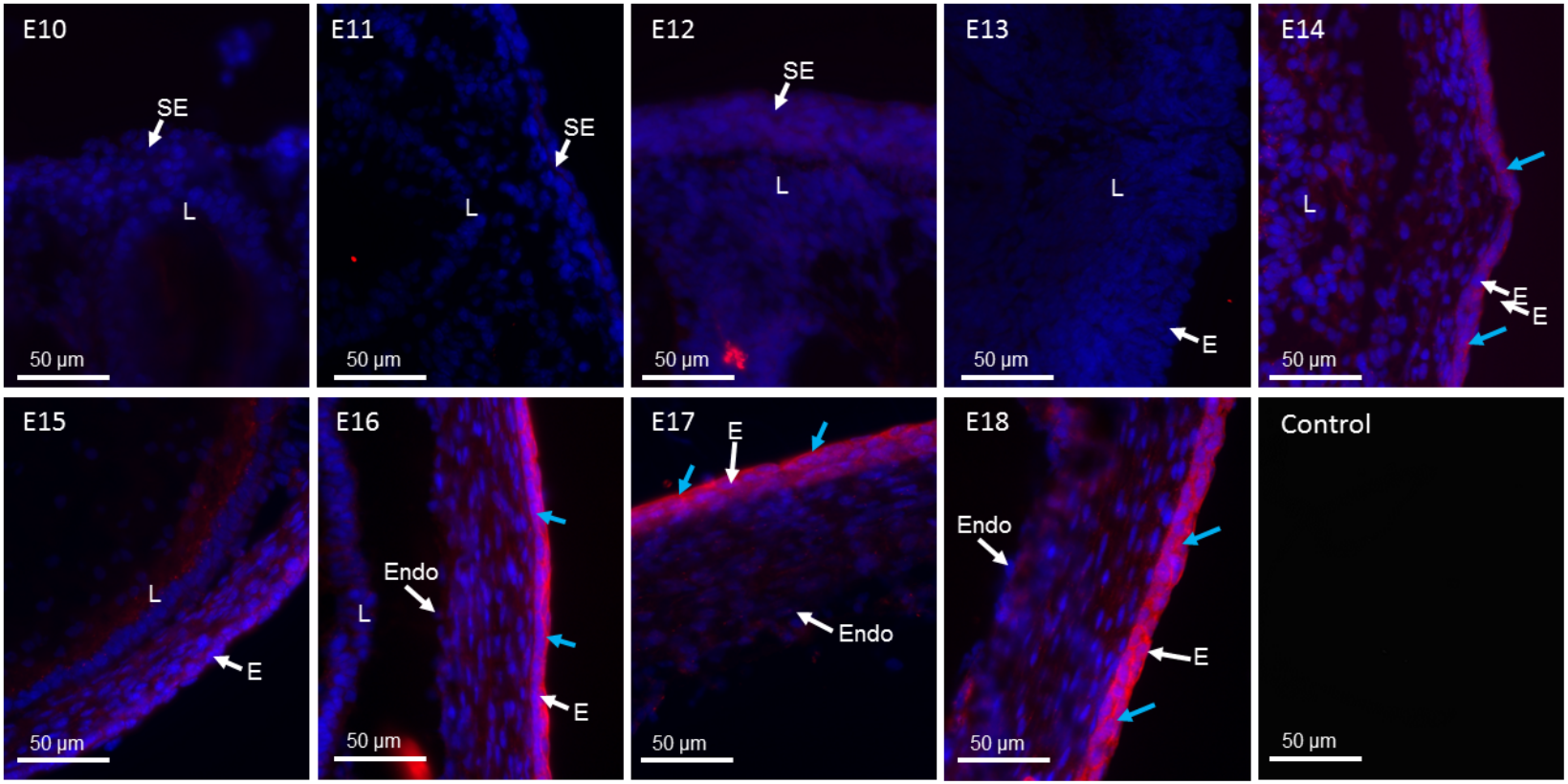

Figure 4.8. Type IX collagen in the developing mouse cornea x40 magnification.

Type IX collagen first appeared in the corneal epithelium (E) at E14 and continued to be expressed up to E18 (blue arrows). High magnification images revealed little labelling within the corneal stroma from E17-E18 (yellow arrows). Blue (DAPI – cell nucleus), red (type IX collagen). To orientate the eye, the corneal epithelium (E) is facing at the top or to the right of the image, apart from E15 where the epithelium is facing towards the bottom-right of the image. The negative controls of no primary control (not shown) and immunoglobulin control (shown) contained no positive stain. Surface ectoderm (SE), lens (L), endothelium (Endo). Images are representative of n=6 for timepoints.

4.3.1.5. Type 1 pro-peptide

Type I pro-collagen was imaged as punctate dots throughout the corneal stroma, increased in the anterior stroma (**Figure 4.9**). It was seen between the presumptive corneal stromal cells from E12, which associated posteriorly to the corneal epithelium within the anterior corneal stroma from E14. Labelling increased within the anterior corneal stroma and then appeared throughout the corneal stroma from E16-E18. Between these ages, labelling was stronger in the anterior corneal stroma than in the posterior corneal stroma.

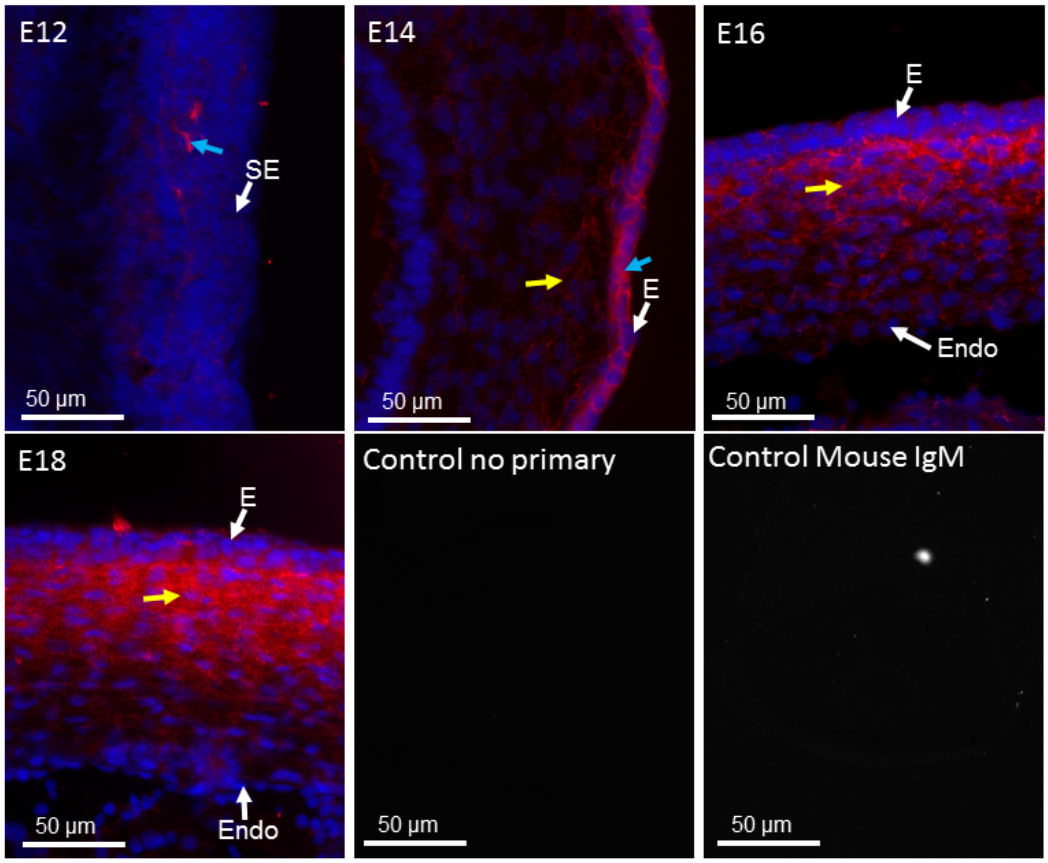

Figure 4.9. Type I collagen pro-peptide in the prenatal mouse cornea x40 magnification.

Type I collagen pro-peptide was present in the corneas of all ages analysed. The protein was initially found between the presumptive corneal stroma cells from E12 (blue arrow). Labelling was then identified within the corneal epithelium and anterior corneal stroma from E14. Labelling continued across the whole thickness of the corneal stroma between E16 and E18, but was stronger within the anterior corneal stroma than the posterior corneal stroma. Blue (DAPI – cell nucleus), red (type I collagen pro-peptide). No positive type I collagen was seen in no primary control, with a small label in the immunoglobulin control. To orientate the eye, surface ectoderm (SE) and corneal epithelium (E) is always facing anteriorly or to the right of the image. Endothelium (Endo). Images are representative of n=6 for timepoints.

4.3.2. Proteoglycan Staining

Prior to TEM, low magnification images of semi-thin sections of the tissues demonstrate the prenatal mouse corneal morphology for the different developmental stages **(Figure 4.10).**

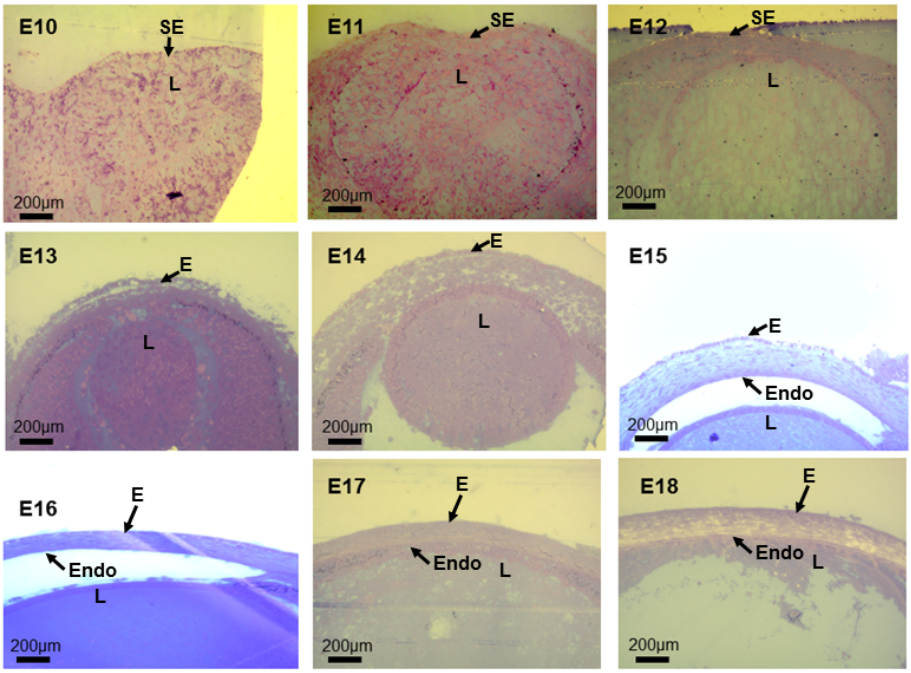

Figure 4.10. Semithin Sections of the Developing Mouse Cornea x20.

Semi-thin sections of the mouse cornea stained with Toluidine Blue dye. The sections represent the block-face surface before being cut smaller for transmission electron microscopy sectioning. Surface ectoderm (SE), corneal epithelium (E), endothelium (Endo), and lens (L).

The glycosaminoglycan (GAG) chains of proteoglycan (PG) proteins associated with the surface ectoderm and cell membranes from the earliest age analysed, prior to collagen fibril deposition (**Figure 4.11**). By E13, the GAGs accumulated posteriorly to the corneal epithelium with a regular arrangement along the basement membrane, which accumulated with increased age throughout development (**Figure 4.12**). At E13 many GAGs surrounded the mesenchymal cells in the central and peripheral corneal stroma. GAGs displayed as longitudinal filaments and punctate dots, arranged in different directions. This organisation could suggest some relationship with the orthogonally arranged collagen fibrils within the stroma (**Figure 4.13 and**

Figure 4.14). As development continued, there was a further increase in PGs within the stroma. The GAG filaments were also connected with adjacent collagen fibrils and between collagen fibrils and the corneal stromal cells. This arrangement identified an intermediate between the corneal stromal cells and collagen fibrils (**Figure 4.14**).

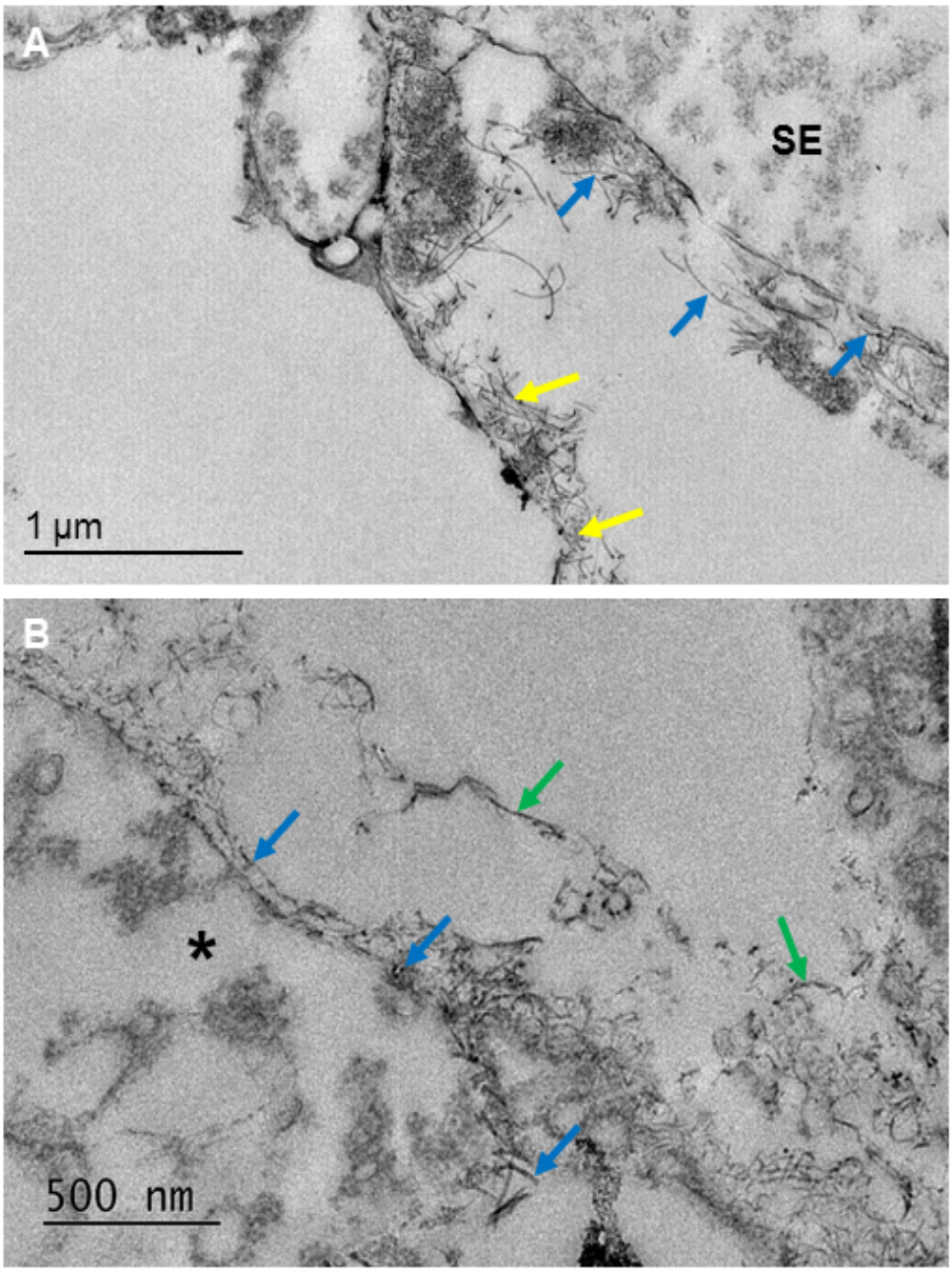

***Figure 4.11. Transmission* electron microscope images of the proteoglycans (PGs) in the E11 (Fig. 4.11A) and E12 (Fig. 4.11B) mouse cornea.**

Fig. 4.11A: GAG's on PGs (blue arrows) associated with the surface ectoderm (SE) at E11. The GAGs were imaged in a dense area below the surface ectoderm (yellow arrows). **Fig. 4.11B:** At E12 PGs (blue arrows) accumulated around the mesenchymal cell (black asterisk) membranes of the presumptive corneal stromal cells. PGs were also observed in the corneal stromal extracellular matrix (green arrows).

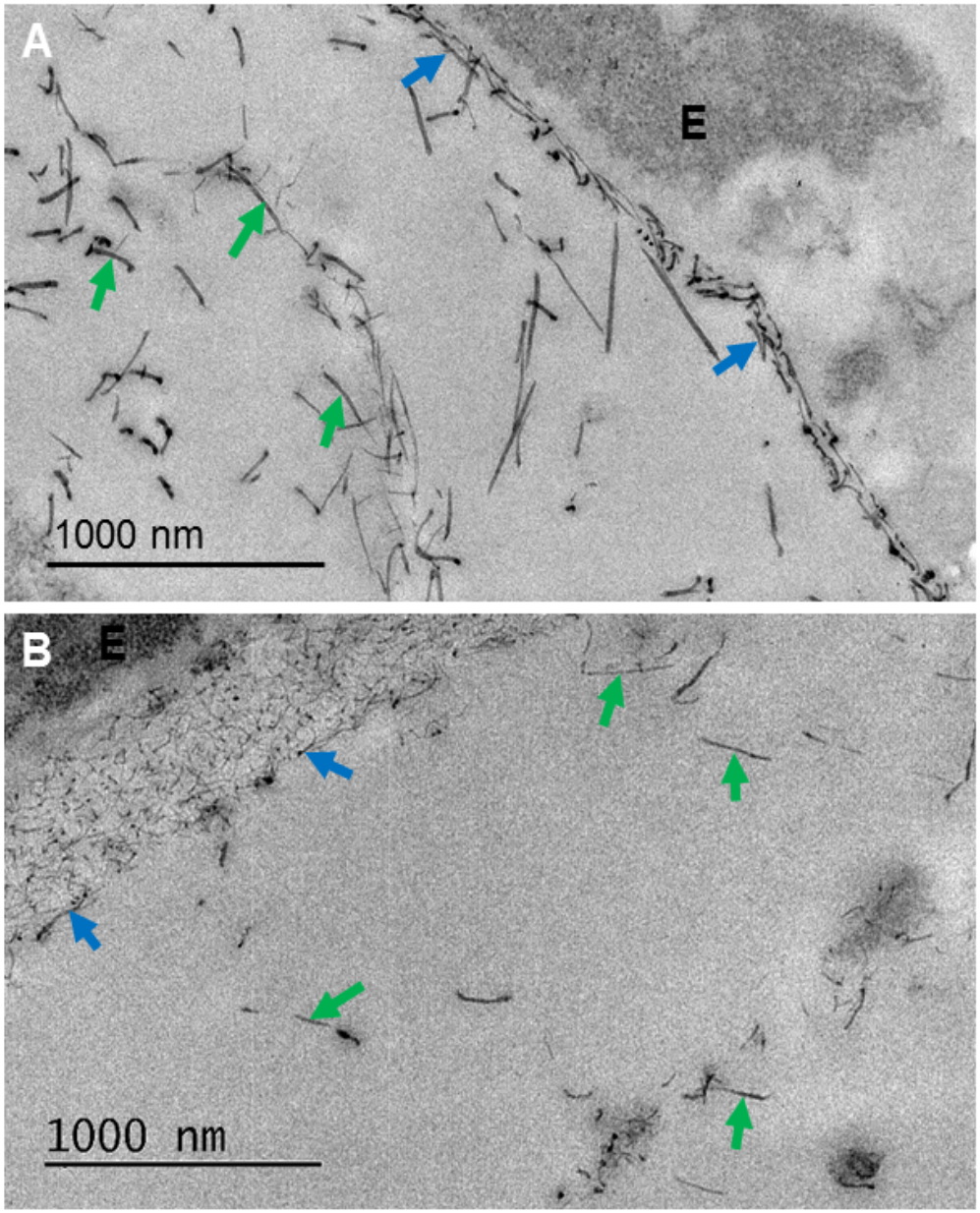

Figure 4.12. Transmission **electron microscopy images of the proteoglycans (PGs) in the E13 (Fig. 4.12A) and E14 (Fig. 4.12B) mouse cornea (sub-epithelial).**

Fig. 4.12A: GAGs (blue arrows) were found continuously along the basal lamina, posterior to the corneal epithelium (E) from E13. **Fig. 4.12B:** At E14 GAGs accumulated in association with the basement membrane. **Fig. 4.12A and Fig. 4.12B:** GAGs (green arrows) were present within the extracellular matrix space of the developing corneal stroma.

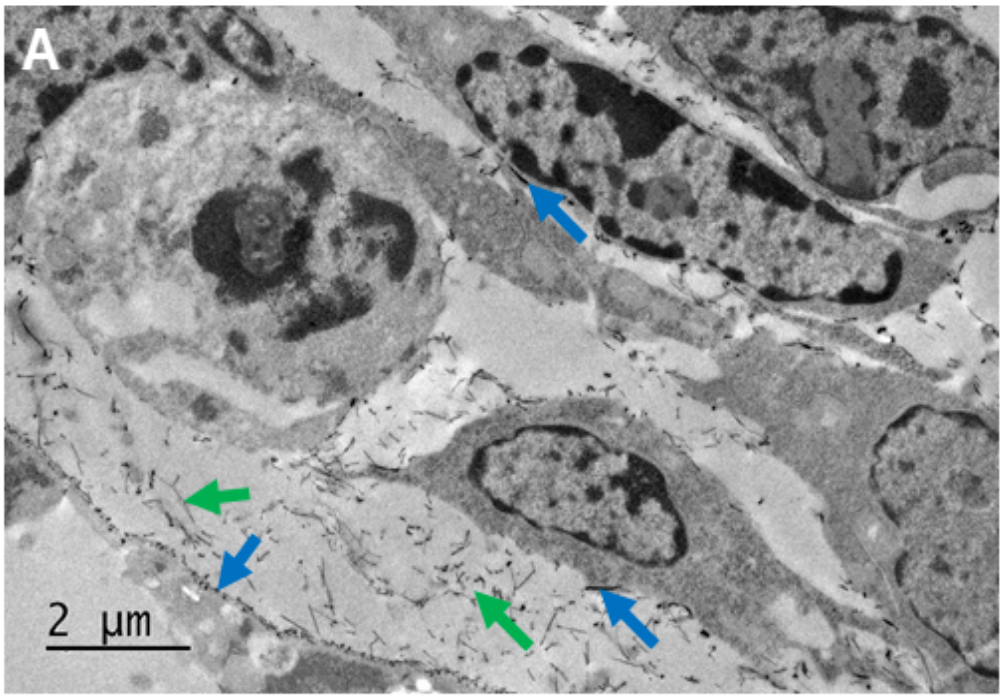

Figure 4.13. Transmission electron microscopy images of the proteoglycans (PGs) in the E13 central (Fig. 4.13A) mouse corneal stroma.

Fig. 4.13A: GAGs (blue arrows) associated around the corneal stromal cell membranes in the central and peripheral cornea. The GAGs ran in a longitudinal direction around the cells as well as being present as punctate dots. This identified the GAGs to run in different directions. **Fig. 4.13A**: GAGs (green arrows) were also found in the extracellular matrix of the central corneal stroma.

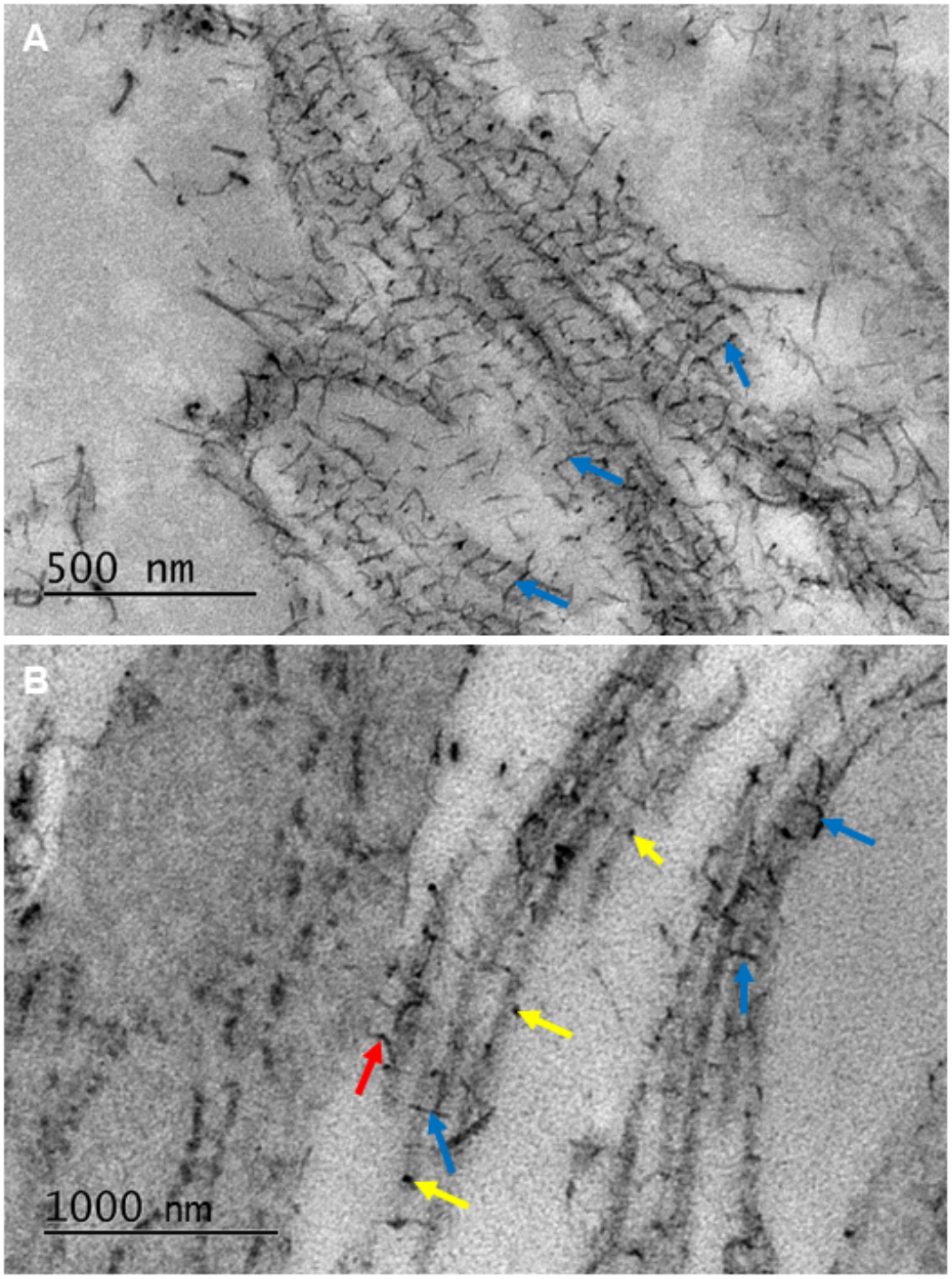

Figure 4.14. Transmission electron microscopy images of the proteoglycans (PGs) in the E16 mouse corneal stroma.

Fig. 4.14A and Fig. 4.14B: GAGs bridged between longitudinal collagen fibrils (blue arrows). **Fig. 4.14B**: GAGs appeared to be linked to the corneal stromal cells and the longitudinal collagen fibrils (red arrows). Some GAGs appeared as punctate dots representing a different orientation to the longitudinal filaments (yellow arrows).

4.4. Discussion

Types I, II and V collagen was visualised as a localised line associated with the surface ectoderm from E10-E12. A similar staining pattern was found in the avian cornea where types I and II collagen were initially laid down by the corneal epithelium (Hayashi M. et al. 1988). However, no evidence in the mouse cornea showed the synthesis of a primary stroma from the corneal epithelium. The results represented in ***Chapter 3*** of this thesis showed the corneal stromal cells to be responsible for the initial synthesis and deposition of collagen fibrils, with no organised acellular primary stroma. This identification of collagen between the cells of the surface ectoderm shows potential evidence of the surface ectoderm synthesising small quantities of collagen in the early stages of development. Future studies should be conducted to understand the distribution of types I, II and V collagen within the surface ectoderm at this early stage. Using a monoclonal antibody with immunogold electron microscopy techniques to localise the specific collagen types at a high magnification would be more suitable to increase the accuracy to locate the collagen fibril types and determine if types I, II and V collagen are secreted by the surface ectoderm between E10-E12 of mouse development.

Type I collagen appeared directly posterior to the corneal epithelium between E15-E16, before being present throughout the corneal stroma with increased age. The assembly of type I collagen is crucial to provide the cornea with structural support and transparency. Type I collagen knockout studies in the mouse have shown that collagen fibrils from E16 are thinner in comparison to the wild type cornea, and that the structure of the corneal stroma is disrupted (Bard et al. 1988). These results suggest that, from an early stage in mouse corneal development, the structure of the corneal stroma is already being established and relies on the assembly of type I collagen.

Type V collagen showed a similar pattern of labelling to type I collagen, with a localised band along the surface ectoderm between E10 and E13. Type V

collagen associated with migrating cells in early development. From E14 to E16, type V collagen was enhanced posterior to the corneal epithelium and was then expressed anterior to the endothelium from E17. The similarities in the localisation of type I and V collagen suggests that they may have formed heterotypic fibrils, as seen in the chick species (Birk et al. 1986). However, dual labelling studies were not undertaken to confirm this. A similar staining profile of type V collagen is also found in the human foetal cornea, which associates with the corneal stroma and basement membranes (Herwig et al. 2013). Knockout mouse studies have also demonstrated type V collagen to be important in early collagen fibrillogenesis (Sun et al. 2011).

Type II collagen increased within the corneal stroma between E14-E18, from being localised to the surface ectoderm between E11-12. Type II collagen was first apparent in the stroma at E13, which localised to the anterior corneal stroma at E14 before appearing throughout the corneal stroma between E15-E18. Type II collagen correlated with the early development of the avian cornea, as well as within cartilaginous growth plates (Chen Q. et al. 1993). Type II collagen is thought to direct corneal growth within the avian cornea and a similar developmental regulation could explain the early labelling of type II collagen in the mouse cornea (Linsenmayer et al. 1990). The presence of type II collagen in early ages implies an important role in the initial development of tissues and extracellular matrix.

Type IX collagen did not show a similar distribution in the mouse compared to the avian cornea (Fitch J. et al. 1998). Type IX collagen was not present in the initial stages of development between E10-E13, with its presence first associated with the corneal epithelium at E14 and continued to express localised to the epithelium at E18. Even though the staining profiles appeared different between type IX and II collagen, as type II collagen appeared earlier than type IX collagen, the enhanced label associated with the corneal epithelium at E14 could indicate an interaction of type IX collagen with the fibrils of type II collagen, where collagen II was seen to also increase in the

corneal stroma at E14. Type IX collagen labelling is usually found in tissues rich in type II collagen, with both fibril types associating together. Type IX collagen is thought to stabilise the fibrils through interactions of the triple helical domain (Muller-Glauser et al. 1986). Type IX collagen has also been previously identified within the corneal epithelium of the human foetal cornea (Herwig et al. 2013), similar to the mouse development results shown in this study. These results indicate that type IX collagen plays a role within the corneal epithelium in mammalian development and is different from the avian cornea. Type IX collagen is expressed within the corneal epithelium in early avian development when the primary stroma is being synthesised, but levels drop by E11 (Svoboda et al. 1988). Within the avian cornea, type IX collagen coincides with corneal swelling and the secondary influx of mesenchymal cells (Fitch J. et al. 1998, Fitch J. M. et al. 2005). As the subsequent swelling and second mesenchymal cell migration does not occur in the mouse cornea, type IX collagen may not be required within the mouse corneal stroma. Its role in the mouse most likely stabilises collagen fibrils and associates with the type II collagen fibrils. Results in the previous chapter demonstrated hyaluronic acid to be present at E11, which increased in labelling at E14 and was not found present after this age. Hyaluronic acid is associated with corneal swelling and could assist mesenchymal cell migration, this protein could provide this role to the mouse cornea as type IX collagen is not expressed between E11-E14.

Type I procollagen labelling recognised the N-terminus of type I procollagen fibrils, and was found mainly within the anterior corneal stroma (Gealy et al. 2009). This coincides with the location where the majority of extracellular matrix space and the initial deposition of fibres was identified by electron microscopy in ***Chapter 3***. In addition, collagen fibril deposition was increased within the anterior corneal stroma, especially in the initial stages. These results indicate that collagen is initially laid down within the anterior corneal stroma as smaller fibrils that increase in diameter with development, and then distribute throughout the corneal stroma. Type I procollagen is intracellular prior to collagen N-terminal pro-peptide cleavage, before extracellular matrix deposition, however, studies have shown this antibody to persist as an

extracellular matrix component after extracellular matrix deposition (Gealy et al. 2009).

TEM imaging of cuprolinic blue stained samples displayed PGs between the collagen fibrils and the stromal cells as well as among the collagen fibrils. PGs were initially found below the corneal epithelium before collagen deposition commenced. Within lung tissue, PGs accumulate below the epithelium and were suggested to regulate epithelial cell function (Frevert 2005). The PGs posterior to the mouse corneal epithelium suggests their potential role in regulating the function and development of the epithelial cells. Previous studies have suggested PGs regulate mesenchymal cell migration and their differentiation into keratocytes (Doane et al. 1996). These studies, combined with the results of PGs present from an early age, indicate that PGs provide an important role in the initial development of the mouse cornea and impact the development of an organised corneal collagen matrix. Specific labelling of PGs was not undertaken. However, PGs in the adult mouse are predominantly under-sulphated, which contain larger chondroitin sulphate and dermatan sulphate rich structures that are unique to rodent corneas. So it is likely the PGs imaged in the prenatal cornea are precursors of PGs found in mature mouse corneas.

Previous studies have demonstrated the importance of PGs in the regulation of a transparent cornea. Lumican knockout mice have increased interfibrillar spacing and thinner fibrils within mouse cornea development, which demonstrates that PGs have a role of controlling physiological collagen fibril development (Beecher et al. 2006). Lumican has also been shown to affiliate with newly formed fibril intermediates near the keratocyte surface to prevent lateral fibril growth within the mouse (Chakravarti et al. 2000). The subsequent swelling prior to eye-lid opening followed by thinning of the stroma is absent in the lumican deficient mouse model, which further suggested that lumican sulphation is crucial in mouse corneal development (Song et al. 2003). The results in this study show PG filaments before collagen fibril deposition, with

PGs organised orthogonally that connected corneal stromal cells to collagen fibrils. These results coincide with the previous structural distribution of collagen fibrils and cell alignment in the prenatal mouse cornea. PGs could have a regulatory role between the stromal cells and collagen fibrils, which suggests that PGs could play a role in the alignment of the collagen fibrils directed by corneal stromal cells.

4.5. Summary

This chapter has demonstrated the distribution of types I, II, V and IX collagen through the stages of prenatal mouse corneal development from E10-E18 post-fertilisation. Types I, II and V collagen were the main collagens within the presumptive corneal stroma, with type IX collagen localised to the corneal epithelium at a later stage of prenatal development. The staining of collagen in this chapter was similar to previous studies that analysed collagen in human foetal corneas. In addition, PGs were present before collagen was laid down and were deposited around cells as well as associating with newly formed collagen fibrils. This suggests that PGs may play an important role in the regulation of developmental events.

Chapter 5: A Structural Study to Compare the Elastic Fibre System between the Adult Mouse and Human Cornea

5.1. Introduction

As previously described, elastic fibres were first detected in the cornea in the late 1800s (Kolliker 1860). Since then, advancements in equipment and technology have enhanced our understanding of elastic fibres in different tissues. These techniques were also applied to investigate elastic tissue in the cornea, across a number of different species. This included the localisation of fibrillin-rich microfibrils in the chicken, rabbit and mouse cornea (Alexander and Garner 1983, Bruns et al. 1987, Carlson and Waring 1988, Hanlon et al. 2015). Since elastic tissue was identified in the mammalian cornea, recent studies have examined the localisation of elastic tissue in the human cornea (Kamma-Lorger et al. 2010, Lewis et al. 2016). These investigations found fibrillin-rich microfibrils and an extensive elastic fibre system concentrated within the human posterior peripheral cornea. Initially, mature elastic fibres were identified in the posterior human cornea using two-photon excitation fluorescence (TPEF) microscopy (Kamma-Lorger et al. 2010). A second study then incorporated tannic acid-and orcein- based processing methods with electron microscopy imaging to investigate the distribution of elastic fibres in three dimensions. *Lewis et al.,* identified elastic fibres in the posterior 200 μm of the human cornea that were highly concentrated within the posterior 8 μm, immediately above Descemet's membrane (Lewis et al. 2016). However, even though these studies showed where elastic fibres were located, there are different types of elastic fibres, and the localisation of the different types of elastic fibres within the cornea remains to be investigated.

Elastic fibres have a range of functions in tissues and provide important roles to elastic and non-elastic tissues (Baldwin et al. 2013). Elastic fibres differ in

their ratio of elastin and fibrillin microfibril components, conveying tissues with different properties. The fibrillin component of the fibres provide structural support and interact with growth factors and signalling molecules to regulate tissue homeostasis (Sengle and Sakai 2015). Fibrillin also supports true elastic fibre formation; to act as a template for tropoelastin deposition, which forms fibres with an amorphous core surrounded by fibrillin-microfibrils (Baldwin et al. 2013). These true elastic fibres then provide elastic properties to tissues, with the capability to return tissues to their original shape after deformation with minimal energy loss (Debelle and Tamburro 1999, Green et al. 2014, Kielty et al. 2002b).

This chapter aims to compare and localise the distribution of fibrillin-rich microfibrils and true elastic fibres in the adult mouse and human cornea. This will then provide a foundation of knowledge to further study the foetal elastic fibre system in chapter 6 of this thesis. 3-D reconstructions of the elastic fibre system were made with serial block-face scanning electron microscopy. Elastic fibres were further analysed at high rmagnification with conventional transmission electron microscopy. Immunofluorescence was used to localise elastin and fibrillin-1.

5.2. Methods

5.2.1. Tissue Collection

10 adult mice aged 9 weeks old (Charles Rivers, C57BL/6) were collected as described in section 2.1 of this thesis. 12 of the mouse eyes were carefully removed with forceps. The corneas were further dissected into quadrants and immersed in Karnovsky's fixative for 3 hours at 4°C. The remaining 8 eyes were snap frozen, cryo-sectioned (Leica CM3050 S cryostat) transversely (10 µm) and collected on Superfrost Plus Slides (Thermo Scientific, UK).

Eight human corneas which contained the scleral ring were obtained from the NHS Blood and Transplant (NHSBT), UK (see **Table 5** for human cornea information). All corneal tissue was dissected into quadrants, snap frozen, cryo-sectioned (Leica CM3050 S cryostat) transversely (10 μm) and collected on Superfrost Plus Slides (Thermo Scientific, UK). Cornea 1 was dissected into quadrants and immersed in Karnovsky's fixative for 3 hours at 4°C.

Table 5. **Information on adult human donor corneas.**

Cornea Number	Age (years)	Gender	Left/Right
1	50	Male	N/K
2	66	Male	Left
3	66	Male	Right
4	31	Male	N/K
5	69	Male	N/K
6	69	Male	N/K
7	77	Female	N/K
8	75	Male	N/K

5.2.2. Electron Microscopy

The elastic fibre processing technique was undertaken as described previously in chapter 2 (section 2.2.1, specifically 2.2.1.1.1).

5.2.3. Immunofluorescence

The immunofluorescence experiment was undertaken as described in section 2.5 of the general methods chapter.

5.2.3.1. Single protein labelling

Cryo-sections were circumscribed with a water-repellent delimiting pen (ImmEdge Hydrophobic Barrier PAP pen, Vector labs) before being

rehydrated with phosphate buffered saline-Tween-20 (PBST) made up of 0.1% Tween-20 and 0.005M phosphate buffer saline solution. 5% horse serum in PBST was applied to cryo-sections for 20 min to prevent non-specific antibody binding (Levy E. M. 1980). Primary antibodies were added to the cryo-sections and incubated for 24 hours at 4°C (see **Table 6** for antibody list). PBST was used to wash off the primary antibodies 3 times over 10 mins before adding secondary antibodies. Dylight 594 Horse Anti-Mouse IgG antibody (Vector Labs) was applied to the monoclonal mouse primary antibodies and Dylight 594 Horse Anti-Rabbit for the polyclonal rabbit primary antibodies. Cryo-sections were incubated for 5 hours at room temperature before secondary antibodies were washed off with PBST. Coverslips (VWR International) was added to the cryo-sections using VECTASHIELD HardSet Antifade Mounting Medium with 4',6-diamidino-2-2-phenylindole (DAPI) (Vector Laboratories), emitting a blue fluorescence when bound to deoxyribonucleic acid (DNA) for cell nuclei detection. Cryo-sections were imaged using the Olympus BX61 epifluorescence microscope, equipped with an F-view Digital camera at x10, x20 and x40 magnifications.

5.2.3.2. Dual protein labelling

The dual labelling methodology mirrored the method undertaken for single labelling described in section 5.2, except two primary antibodies with different host species were applied to the cryo-section. Both Dylight 594 Horse Anti-Mouse and Dylight 488 Horse Anti-Rabbit were applied as secondary antibodies. The secondary antibodies contained different fluorescent tags, fluorescing red for Dylight 594 and green for Dylight 488.

Table 6. **Antibodies used during the immunohistochemistry staining**

Antibody	Monoclonal (M)/ Polyclonal (P)	Target	Concentration	Source	Reference
Anti-Elastin (ab11370)	Rabbit P	Elastin	1:100	Abcam	(Raghavan et al. 2009)
Anti-Fibrillin-1 (ab124334)	Mouse M	Fibrillin-1	1:100	Abcam	(Pan et al. 2015)
Anti-Tropoelastin (ab21600)	Rabbit P	Tropoelastin	1:50	Abcam	(Mondrinos et al. 2007)
Anti-type VI Collagen (ab6588)	Rabbit P	Type VI Collagen	1:100	Abcam	(Guillen-Ahlers et al. 2008)

5.3. Results

5.3.1. Electron Microscopy

5.3.1.1. Mouse Cornea

The tannic acid-uranyl acetate method revealed an extensive elastic fibre system within the mouse peripheral corneal stroma and trabecular meshwork (**Figure 5.1**). 3-D reconstructions showed a concentrated elastic fibre sheet anterior to Descemet's membrane, with individual elastic fibres throughout the corneal stroma in longitudinal and transverse directions between collagen lamellae (**Figure 5.1B and Figure 5.1C**). The elastic fibres anterior to Descemet's membrane were integrated with those within the trabecular meshwork, which indicated a continuous fibre system across the transition

from the trabecular meshwork to the cornea (**Figure 5.2A and Figure 5.2B**). Descemet's membrane terminated anterior to the trabecular meshwork, with the trabecular meshwork elastic fibre system merging into Descemet's membrane (**Figure 5.2A and Figure 5.2B**). High-magnification analysis of the elastic fibre system found microfibrils bundles together to form larger fibres, with no amorphous core in the centre of the elastic fibres, a morphology characteristic of fibrillin-rich microfibrils (**Figure 5.3A and Figure 5.3B**).

5.3.1.2. Human Cornea

The human corneal elastic fibre system was concentrated in the posterior peripheral region of the cornea in the 3-D reconstructions (**Figure 5.2C and Figure 5.2D**). The elastic fibres from the trabecular meshwork had an insertion anterior to Descemet's membrane, which connected with the elastic fibre system in the posterior peripheral cornea (**Figure 5.2C and Figure 5.2CD**). High-magnification analysis of the elastic fibres showed an elastin-amorphous core in the centre of the fibres, identified with a reduced contrast compared to the surrounding fibrillin-rich microfibrils; this is characteristic of true elastic fibre morphology (**Figure 5.3C and Figure 5.3D**).

The videos for all 3-D videos can be accessed at an online publication (Feneck et al. 2018).

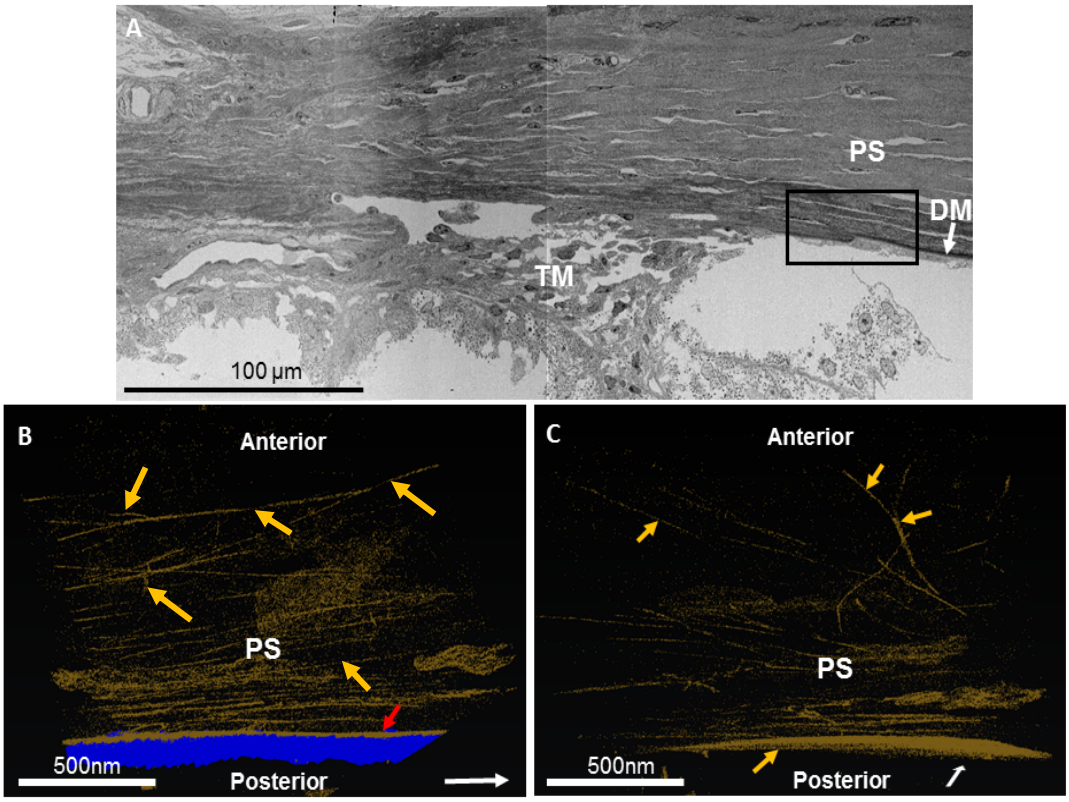

Figure 5.1. Elastic fibre serial block-face scanning electron microscopy (SBF-SEM) reconstructions within the adult mouse posterior peripheral cornea.

Fig. 5.1A: SBF-SEM image of the mouse trabecular meshwork (TM) and posterior peripheral cornea stroma (PS). Higher magnification SBF-SEM datasets within the area of Descemet's membrane (DM) termination (black square) were collected. **Fig. 5.1B**: An elastic fibre system (gold) was detected throughout the posterior peripheral corneal stroma, with a highly stained sheet (red arrow) of elastic fibres anterior to Descemet's membrane (blue) and individual fibres appearing throughout the corneal stroma (yellow arrows). The white arrow indicates the direction towards the central cornea **Fig. 5.1C:** The 3-D dataset was rotated 90° to Fig. 5.1B. Elastic fibres (gold) occasionally bifurcated and continued within the same plane (yellow arrows). The white arrow indicates the direction towards the central cornea.

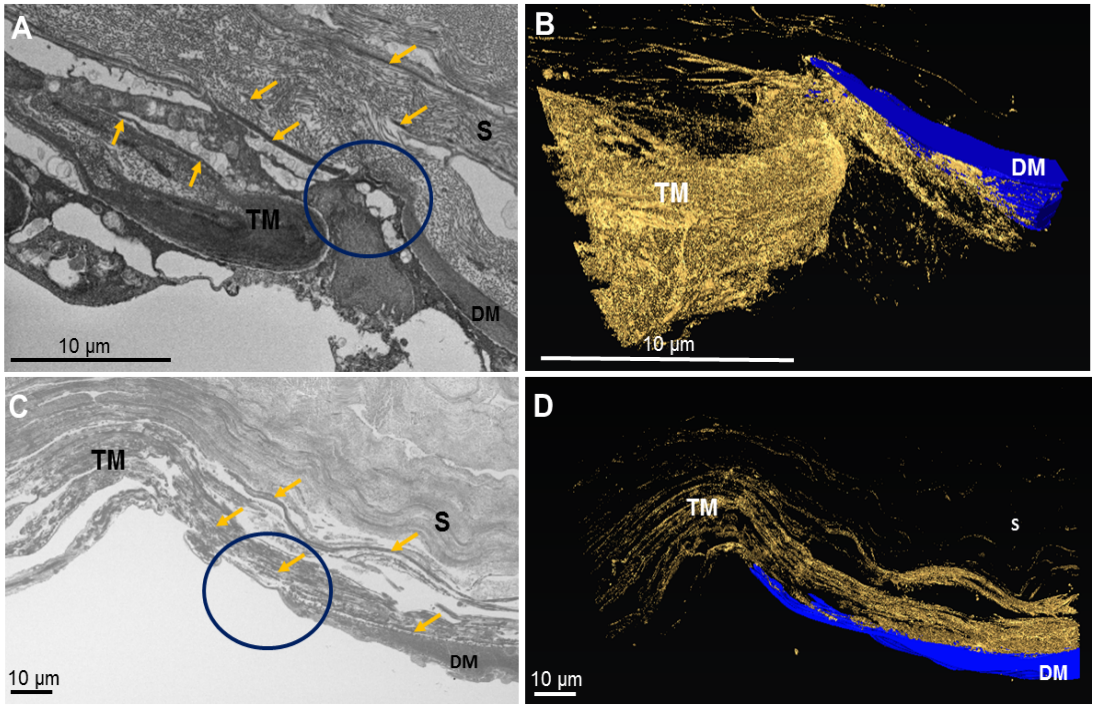

Figure 5.2. A comparison of the elastic fibre network at Descemet's membrane (DM) termination within the adult mouse (Fig 5.2A and Fig. 5.2B) and adult human cornea (Fig. 5.2C and Fig. 5.2D) with serial block-face scanning electron microscopy (SBF-SEM) imaging.

Fig. 5.2A: The termination of DM within the mouse cornea appeared to run anterior to the trabecular meshwork (TM) (blue circle). Elastic fibres are present within the TM and within the stroma (S) (yellow arrows). **Fig. 5.2B**: SBF-SEM 3-D reconstruction of the mouse cornea shows the elastic fibre system (gold) anterior to the trabecular meshwork and DM (blue), with no clear insertion point of the trabecular meshwork into the posterior peripheral cornea. **Fig. 5.2C**: The TM within the human cornea showed a clear insertion of the trabecular meshwork, which ran anterior to DM. **Fig. 5.2D**: The 3-D reconstruction of the human elastic fibre system shows the TM to run anterior to DM, which further connected with the elastic fibre system within the posterior peripheral aspect of the cornea.

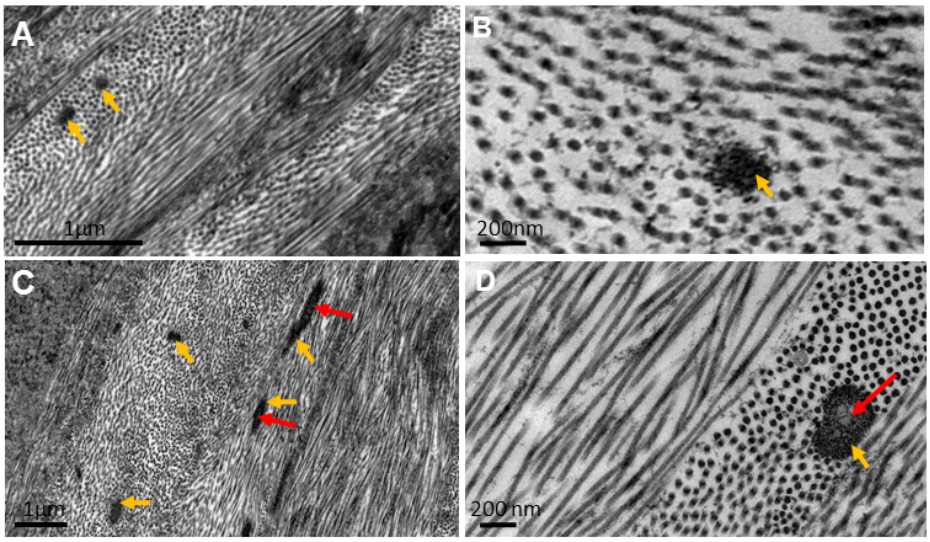

Figure 5.3. Transmission electron microscopy images of tannic acid stained elastic fibres (yellow arrow) within the adult mouse cornea (Fig. 5.3A and Fig. 5.3B) and adult human cornea (Fig. 5.3C and Fig. 5.3D).

Fig. 5.3A: Fibres within the posterior peripheral cornea in oblique and longitudinal section show the different directions the fibres which run within the plane of the cornea. **Fig. 5.3B**: High magnification cross-section of a mouse elastic fibre had no clear amorphous core with only bundles of microfibrils (yellow arrow) displayed. **Fig. 5.3C:** Fibres within the human posterior peripheral cornea in oblique and longitudinal section (yellow arrow). Within the centre of the elastic fibres an elastin-amorphous core is seen (red arrows) with a reduced contrast to the surrounding fibrillin-rich microfibrils **Fig. 5.3D**: High magnification image of a human elastic fibre cross-section within the peripheral cornea shows an amorphous core (red arrow) surrounded by microfibrils (yellow arrow).

5.3.2. Immunofluorescence

To localise proteins associated with true elastic fibres and fibrillin-rich microfibrils, antibodies to label type VI collagen, elastin, tropoelastin and fibrillin-1 were employed. All controls for the immunofluorescent results showed no background label, which indicated that all positively stained images localised the primary antibody applied (**Figure 5.4 and 5.5**).

5.3.2.1. Mouse Cornea

Type VI collagen displayed throughout the corneal stroma, but was enhanced within the posterior peripheral corneal stroma and anterior sclera (**Figure. 5.4A and Figure 5.4B**). Fibrillin-1 was also present throughout the mouse corneal stroma, but enhanced within the anterior stroma and along Descemet's membrane (**Figure 5.4E and Figure 5.4F**). Elastin did not positively express within the mouse cornea, however, tropoelastin was found within the posterior peripheral and anterior central corneal stroma (**Figures 5.4 I-J & Figures 5.4M-N).**

5.3.2.2. Human Cornea

Type VI collagen was found throughout the corneal stroma, enhanced within the trabecular meshwork, Descemet's membrane, posterior to the epithelium and the posterior peripheral cornea (**Figures 5.5A-C**). Fibrillin-1 was seen within the trabecular meshwork and peripheral cornea (**Figure 5.5F and Figure 5.5G**). It was present anterior to Descemet's membrane, but decreased towards the central cornea, with only small staining within the posterior stroma of the central cornea (**Figure 5.5H**). Elastin labelling was high within the trabecular meshwork and peripheral posterior cornea of all corneas analysed (**Figure 5.5K-L**). Elastin continued from the trabecular meshwork, anterior to Descemet's membrane, but gradually decreased until no elastin was detected within the central corneal stroma (**Figures 5.5K-M**). Tropoelastin did not label within the human corneal tissue analysed, which indicated that all tropoelastin

had been cross-linked to become elastin (results not shown). Dual labels of fibrillin-1 and elastin showed a co-localisation of the proteins in the trabecular meshwork and peripheral posterior cornea (**Figures 5.5P-R**).

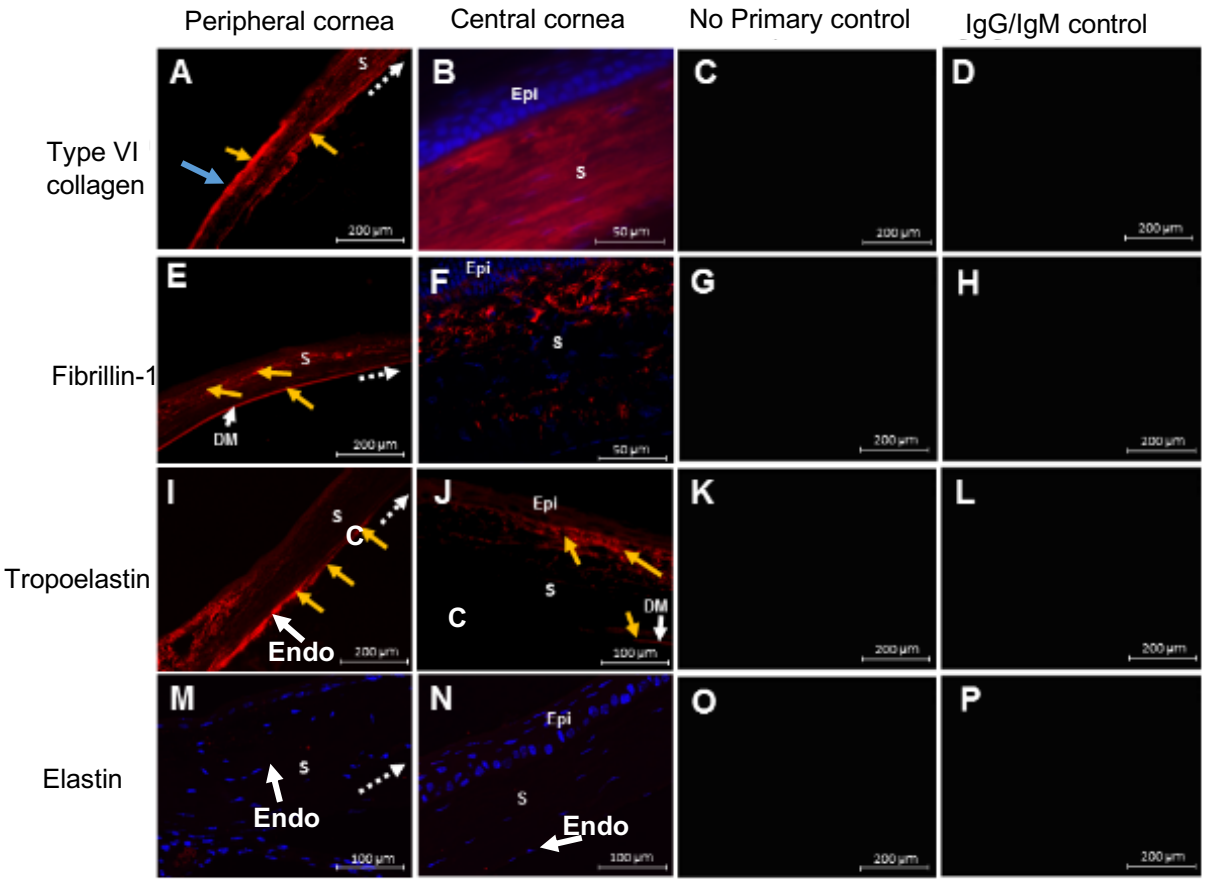

Figure 5.4. Adult mouse cornea immunofluorescence.

DAPI in blue represents cell nuclei; Epi: epithelium; s: stroma; DM: Descemet's membrane; Endo: Endothelium. White broken arrows indicate the direction towards the central cornea. **Fig. 5.4A and Fig. 5.4B**: Type VI collagen expressed throughout the corneal stroma, and was enhanced within the anterior sclera (blue arrow) and posterior peripheral cornea (yellow arrow). **Fig. 5.4C and 5.4D**: No positive type VI collagen was present in the no primary control and the IgG controls. **Fig. 5.4E and Fig. 5.4F**: Fibrillin-1 was seen throughout the corneal stroma, enhanced within the anterior stroma and Descemet's membrane (yellow arrows). **Fig 5.4G and Fig. 5.4H**: No positive staining of fibrillin-1 was seen in the no primary control and the IgM control. **Fig. 5.4I**: Tropoelastin was in the posterior peripheral corneal stroma (yellow arrows). **Fig. 5.4J:** Tropoelastin was labelled within the anterior central corneal stroma (yellow arrow), however, staining in both the posterior cornea terminated before reaching the central cornea (c) (yellow arrow). **Fig 5.4K and Fig. 5.4L**: No positively labelled tropoelastin was seen in the no primary control and with an IgG control. **Fig. 5.4M and 5.4N:** Elastin was not detected throughout the mouse corneal stroma. **Fig. 5.4O and Fig. 5.4P**: No positive labelling was seen in elastin no primary control and with an IgG control.

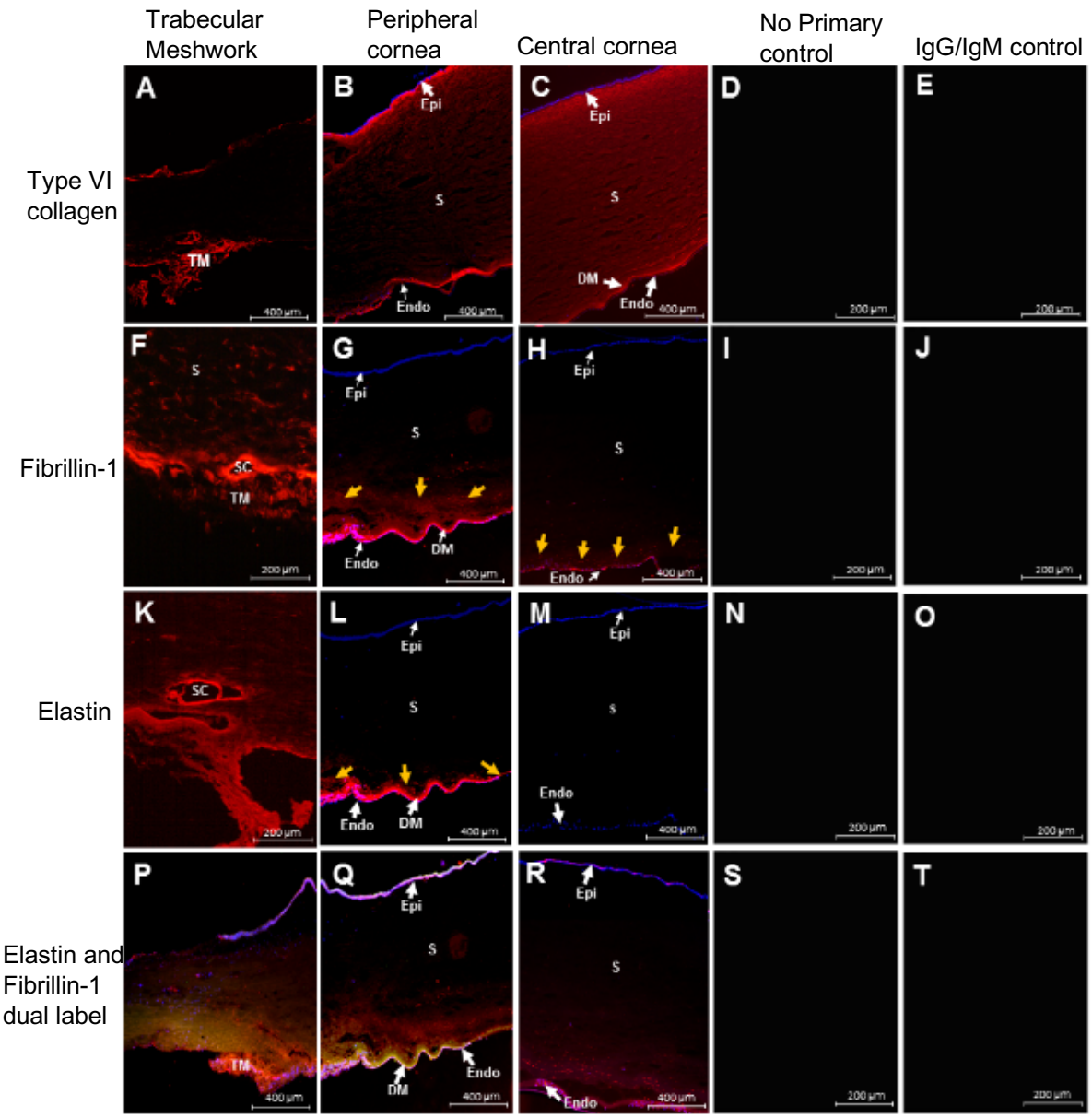
Trabecular Meshwork
Peripheral cornea
Central cornea
No Primary control
IgG/IgM control
Type VI collagen
Fibrillin-1
Elastin
Elastin and Fibrillin-1 dual label
A
B
C
D
E
F
G
H
I
J
K
L
M
N
O
P
Q
R
S
T
Epi
Endo
DM
TM
SC
S
400 µm
200 µm

Figure 5.5. Adult human cornea immunofluorescence

S: stroma; TM: trabecular meshwork; SC: Schlemm's canal; DM: Descemet's membrane. Results shown from cornea 2 (**Fig. 5.5A & Fig. 5.5F**), cornea 4 (K), cornea 6 (**Figs. 5.5B-E),** cornea 7 (**Figs. 5.5G-J, Figs. 5.5 L-T**). **Figs. 5.5A-C**: Type VI collagen expressed within the trabecular meshwork and corneal stroma of all corneal tissue analysed. **Fig. 5.5 D and Fig. 5.5E**: There was no type VI collagen within the no primary and the IgG controls. **Figs. 5.5 F-H**: Fibrillin-1 appeared to be increased within the TM and posterior peripheral cornea. Fibrillin-1 decreased towards the central cornea. Fibrillin-1 showed similar results across all corneal tissue, however, in addition, it presented in the anterior corneal stroma directly inferior to Bowman's membrane in two corneas taken from the same donor (cornea 3 and 4), this was not seen in any other corneal tissue analysed. **Fig. 5.5 I and Fig. 5.5J**: No fibrillin-1 was detected in the no primary control and IgG controls. **Figs. 5.5 K-M**: Elastin within all three corneal tissues was present within the trabecular meshwork and posterior peripheral cornea, where labelling was enhanced anterior to Descemet's membrane (DM). Elastin was absent within the central or anterior corneal stroma. **Fig. 5.5N and Fig. 5.5O**: No positive labels of elastin were seen in the no primary control and with the IgG control. **Figs. 5.5. P-R**: Dual labels shows elastin (green) and fibrillin-1 (red) co-localised (orange) within the TM and peripheral cornea. Fibrillin-1 was found with no elastin in the central cornea. **Fig. 5.5 S and Fig. 5.5T:** No primary control and the IgG controls contained no staining for the dual label results.

5.4. Discussion

This chapter compared the elastic fibre system as well as the trabecular meshwork insertion points between the adult mouse and human cornea, whilst classifying the type of elastic fibres within the corneal stroma. This was investigated to further understand the adult human and mouse elastic fibre system before analysis of the developing elastic fibre system was undertaken. The tannic acid-uranyl acetate method stained the amorphous elastin core and the fibrillin-rich microfibrillar components of elastic fibres (Lewis et al. 2016, Simmons and Avery 1980). Mouse cornea SBF-SEM reconstructions of the elastic fibre system revealed a concentrated network of elastic tissue anterior to Descemet's membrane, with individual elastic fibres across the corneal stroma. Elastic fibres within the mouse cornea were present throughout the stroma, whereas within the human cornea, elastic fibres were abundant only in the posterior stroma and concentrated within the region immediately above Descemet's membrane (Lewis et al. 2016). TEM results suggested the mouse elastic fibre system mainly composed of oxytalan fibres, with no visualisation of the elastin amorphous core. These results have been previously described in the literature, with the identification of microfibrils in the mouse corneal stroma (Hanlon et al. 2015). Interestingly, the presence of microfibrils dispersed throughout the corneal stroma has also been described in the rabbit cornea, which demonstrates a similarity between the rabbit and mouse elastic fibre models (Carlson and Waring 1988). Another difference between the peripheral mouse and human was the presence of an elastin-rich amorphous core that was absent in the mouse elastic fibres, indicating that, in human cornea, they are true elastic fibres. The amorphous core was also identified in previous electron microscopy studies on human corneal elastic fibres (Lewis et al. 2016).

To further classify the type of elastic fibres seen, localised immunofluorescence was used and identified true elastic fibres within the posterior peripheral human cornea. Elastin and fibrillin-1 was expressed within the posterior peripheral corneal stroma and directly anterior to Descemet's

membrane, which extended from the sclera and trabecular meshwork. Elastin was not found within the central cornea, whilst fibrillin-1 was, which further identified the presence of elastin-free microfibrils (oxytalan fibres) in the central cornea. The results generated from this chapter have led to a suggested model of elastic fibre distribution within the human and mouse cornea, similar to the model suggested in a previous study (**Figure 5.6**) (White et al. 2017b).

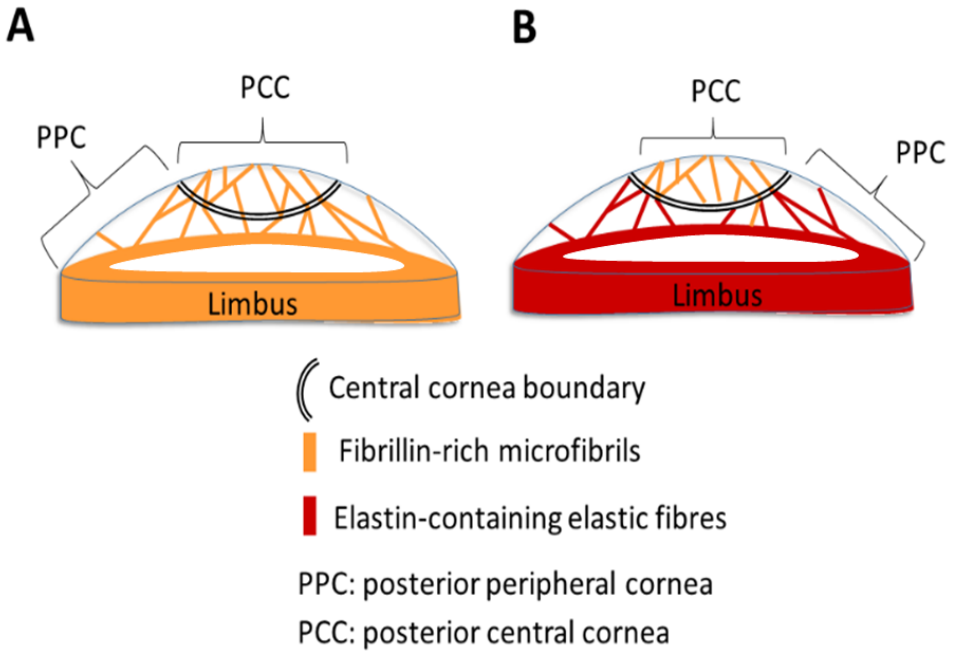

Figure 5.6. Theorised elastic fibre system within the adult mouse cornea (Fig. 5.6A) and adult human cornea (Fig. 5.6B).

The results obtained from this chapter suggest that the mouse cornea consists solely of oxytalan fibres, whilst the human cornea contains true elastic fibres, elaunin and oxytalan fibres. Within the central and peripheral mouse cornea, fibrillin-1 expressed without elastin, which indicates oxytalan fibres. However, tropoelastin within the peripheral mouse cornea suggests a potential for elastin formation when required, possibly during repair. The human cornea had elastin-containing elastic fibres in the posterior peripheral cornea, which could provide elastic properties. A decreased presence of elastin with fibrillin-1 indicated elaunin fibres present towards the central cornea, this transition in the human cornea is probably gradual. When travelling more centrally only fibrillin-1 was seen, which indicates oxytalan fibres. Fibrillin-rich microfibrils likely stiffen the central cornea to preserve corneal shape when small intraocular pressure fluctuations occur.

The confirmation of elastin in the human cornea with an increased quantity in the posterior peripheral cornea, directly anterior to Descemet's membrane, was confirmed by a separate study which identified a clinical significance of corneal elastic fibres in scrolling within endothelial keratoplasty (Mohammed et al. 2018). The mouse cornea had fibrillin-1 throughout the corneal stroma with no presence of elastin. Despite this, tropoelastin within the posterior peripheral cornea indicated the possibility of elastic fibre assembly. Further analysis of older mouse tissue could determine if the tropoelastin becomes cross-linked to form true elastic fibres. However, mice may not live long enough for true elastic fibres to be necessary within the cornea. The negative labelling of tropoelastin within the human cornea illustrates that the tropoelastin has been cross-linked into true elastic fibres by the age of 31 years within the human cornea, to determine when the maturation of tropoelastin is complete, younger corneal tissue would be required.

Fibrillin-rich microfibrils exist throughout the corneal stroma of the mouse cornea and are enhanced within the anterior corneal stroma. In connective tissues, fibrillin microfibrils provide structural support and likely to play a similar role in the cornea, with calcium providing microfibril rigidity through its interactions with cEGF domains (Eriksen et al. 2001, Hansson 1970). In bovine and human corneas, deformations in response to the intraocular pulse occur only within the periphery, allowing the central cornea to retain its shape (Boyce et al. 2008, White et al. 2017b). The elastin component of true elastic fibres would permit slight deformations within the human peripheral cornea. Their presence within the peripheral cornea may also oppose small fluctuations to IOP. True elastic fibres are thought to have developed to reinforce the high pressured circulatory system in vertebrates; true elastic fibres could, therefore, carry out a similar role in containing IOP and thus corneal shape in the human eye (Faury 2001).

Studies which test elastic modulus of the central and peripheral cornea have calculated the peripheral cornea to have a smaller elastic modulus, thus the

peripheral cornea has less resistance to deformation when stress is applied (Mikula et al. 2016). The true elastic fibres could reduce elastic modulus in the peripheral cornea compared with the central cornea. However, the posterior peripheral cornea had a greater elastic modulus than the anterior peripheral cornea, which further implies that other components in the periphery also influence elastic modulus; such as the organisation of the collagen lamellae (Mikula et al. 2016). In addition, Mikula *et al.,* used tissue ages between 85-101 years, and elastic fibres are known to lose their structure and function with increased age, leading to an increase in elastic modulus (Agache et al. 1980, Sherratt 2009). Therefore, the analysis of younger corneas is required to fully understand the impact of elastic fibres on the elastic modulus of the cornea.

Matrix elasticity regulates TGF-β signalling within the trabecular meshwork, which is increased in patients with primary open angle glaucoma (POAG) (Han et al. 2011). Furthermore, elastic fibre proteins are increased within the trabecular meshwork in patients with glaucoma (Umihira et al. 1994), suggesting the elastic fibre system could play a role in maintaining a physiological cornea and aqueous humor outflow or contribute to the pathogenesis of POAG. 3-D SBF-SEM reconstructions within the mouse cornea demonstrated a connection of the elastic fibre system between the trabecular meshwork and peripheral cornea, with no clear insertion point into the corneal stroma. This contrasts with human reconstructions, where the trabecular meshwork inserts between the posterior peripheral corneal stroma and Descemet's membrane 250 μm after Descemet's membrane termination (Lewis et al. 2016). The anatomical differences between the mouse and human could indicate an evolutionary advancement of the human cornea to regulate IOP outflow and corneal physiology. However, the continuation of the elastic fibre system in both models further demonstrated the elastic fibre system could have an important role between the cornea and the trabecular meshwork. The elastic fibre system attachment may anchor the trabecular meshwork into the cornea, holding it taut. If so, this system may be necessary to maintain normal IOP and corneal structure. The elastic fibre system could

provide a potential target for treatment strategies in the future for glaucoma, but more research is needed to determine the role of the corneal elastic fibres.

5.5. Summary

This chapter has shown anatomical variations of the elastic fibre system in the human and mouse adult cornea. True elastic fibres are distributed within the posterior peripheral human cornea and are thought to allow for slight deformations within the peripheral cornea. A fibrillin-rich microfibril system was also identified within the posterior central human cornea, which may add biomechanical strength to reinforce tissue stiffness. The mouse model possessed anatomical differences to the human cornea. Fibrillin microfibrils were dispersed throughout the entire thickness of the mouse corneal stroma. The mouse model also showed no clear insertion of the trabecular meshwork between the corneal stroma and Descemet's membrane. This is the first study to identify true elastic fibres within the human posterior peripheral cornea with immunofluorescence techniques, which localised elastin and fibrillin-1. The differences identified between the elastic fibre system and the trabecular meshwork should be considered when the mouse model is incorporated for trabecular meshwork outflow, glaucoma and elastic fibre studies.

Chapter 6: A 3-D structural study of the developing human corneal stroma

6.1. Introduction

The availability of human embryonic tissue has restricted studies directed to understand the initial events and mechanisms that develop the human cornea. The human cornea begins its development with the surface ectoderm attached to the lens, which separates from the lens to become the corneal epithelium (Barishak 2001, Sevel and Isaacs 1988). The first wave of neural crest-derived mesenchymal cells become the corneal endothelium, followed by a second wave of cells which forms the keratocytes and corneal stroma (Zieske 2004). One crucial difference between the avian model and the current mammalian developmental models analysed is the presence of a primary stroma that drives mesenchymal cell migration into the avian cornea (Haustein 1983, Hay E. D. and Revel 1969). ***Chapter 3*** confirmed previous research that the mouse cornea does not have a collagenous primary stroma (Cintron et al. 1983, Haustein 1983, Pei and Rhodin 1970). Because of the absence of a primary stroma, the mechanisms that control cells to migrate, lay down and organise the mature collagen fibril network remains to be determined. Even though the general consensus in the literature states that the human cornea does not have a primary stroma, one study was found that described the presence of an acellular matrix between the lens vesicle and the surface ectoderm in the human cornea prior to mesenchymal cell migration, which could act as a primary stroma in the human cornea (Wulle and Richter 1978). However, most studies state that a primary stroma is not observed in mammalian and primate corneal development (Cintron et al. 1983, Zieske 2004).

An organised extracellular matrix is imperative to develop a cornea with transparency and biomechanical strength. Previous work has been directed to establish the distribution of collagens and proteoglycans within corneal

development across species. In addition to these extracellular matrix molecules, elastic fibres are also a component of the human adult cornea, concentrated in the posterior peripheral corneal stroma (Lewis et al. 2016). Further experiments, which include the results presented in ***Chapter 5*** of this thesis, have shown elastin-containing elastic fibres distribute through the adult posterior peripheral cornea, associated with Descemet's membrane (Mohammed et al. 2018). Most elastic fibre research in the cornea so far has focused on the adult system, with only one study that identified elastic fibres at week 13 of human corneal development (Lewis et al. 2016). Previous analyses of pathological adult corneas with disrupted shape have also identified a disruption to the elastic fibre system, which led to suggestions that elastic fibres help maintain corneal shape and structure (White et al. 2017a, White et al. 2017b). These results further suggest that elastic fibres may have an important role in corneal development, and further investigations should reveal their functional importance.

This chapter aims to analyse human corneal stromal development using novel 3-D structural imaging techniques to determine if a primary stroma is present within the initial stages of corneal development. Thus, to determine whether or not developmental events in the human cornea follow a similar pattern to other mammalian or avian developmental models described in earlier chapters of this thesis. The second aim of this chapter was to visualise elastic fibres through human corneal development from week 7 to week 17 with the well-established tannic-acid uranyl-acetate electron microscopy method.

6.2. Methods

To note, stages up until week 8 were further referred to with the Carnegie stage system, to identify the specific embryonic ages being analysed (Hill 2012). After week 8, the tissue is no longer embryonic and is referred to as foetal.

6.2.1. Tissue collection

All tissue was obtained from the Human Developmental Biology Resource (HDBR), Newcastle, UK and was used in accordance with the human tissue act 2004. Corneas were obtained from week 7 to week 17 of development, being further dissected into halves and prepared for electron microscopy processing by being placed in Karnovsky's fixative for 3 hours. 2 unpaired samples for each specific age were analysed.

6.2.2. Electron Microscopy

To enhance the elastic fibre system, the tannic acid – uranyl acetate processing method was employed as described in section 2.2.1 of this thesis for serial block-face scanning electron microscopy (SBF-SEM) and transmission electron microscopy (TEM) imaging.

6.3. Results

6.3.1. Week 7

At the start of week 7 (stage CS20), the corneal endothelium and epithelium were present (**Figure 6.1**). Collagen fibrils were deposited directly posterior to the corneal epithelium, which represented the immature Bowman's layer. Collagen fibrils were also deposited within the central corneal stroma, central to the corneal epithelium and endothelium. Corneal stromal cells were absent

from this area in the presumptive central corneal stroma, with mesenchymal cells solely in the periphery (**Figure 6.1**). 3-D reconstructions of the cornea at CS20 showed tortuous cell projections arising from the corneal endothelium to branch anteriorly towards the corneal epithelium (**Figure 6.2**). The 3-D models further demonstrated collagen fibrils to be dispersed in the central cornea, where no mesenchymal cells had migrated between the corneal epithelium and the corneal endothelium (**Figure 6.2 and supplementary video 6**). TEM images of the cornea at CS20 demonstrated collagen fibrils posterior to the corneal epithelium and within the central corneal stroma, with no evidence of mesenchymal cells between the epithelium and endothelium, which further supports the SBF-SEM results (**Figure 6.3 and supplementary video 6**).

With increased maturation during week 7 (stage CS22), collagen fibrils further condensed to the central cornea (**Figure 6.4**). Similar to the previous age analysed, mesenchymal cells were confined to the peripheral cornea (**Figure 6.4**). 3-D reconstructions of the developing cornea at CS22 showed cell projections from the corneal endothelium branching anteriorly towards the condensed collagen matrix situated in the central cornea and with the mesenchymal cells (**Figure 6.5 and supplementary video 6**). The mesenchymal cells in the peripheral region of the 3-D reconstruction also associated with the condensed acellular collagenous matrix (**Figure 6.5 and supplementary video 7**). TEM images displayed a concentrated collagenous matrix between the corneal epithelium and endothelium (**Figure 6.6**). At a later stage of CS22, the mesenchymal cells in the periphery appeared as a single celled layer, with cells located more centrally, compared to younger ages where the cells were only seen in the periphery (**Figure 6.7**). A single cell analysed at an increased magnification with SFB-SEM in the peripheral cornea appeared to associate with the collagenous matrix (**Figure 6.7**). As seen in the other reconstructions, endothelial cell projections extended anteriorly towards the mesenchymal cells. The collagenous matrix further condensed in the central cornea compared to the peripheral cornea.

No heavily stained filaments characteristic of elastic fibres were found within the SBF-SEM and TEM datasets during week 7 of corneal development.

Supplementary video 6 link: *https://figshare.com/s/6adca9177fed6e846f4a*

Supplementary video 7 link: *https://figshare.com/s/64317700de2c0935e384*

6.3.1.1. CS20

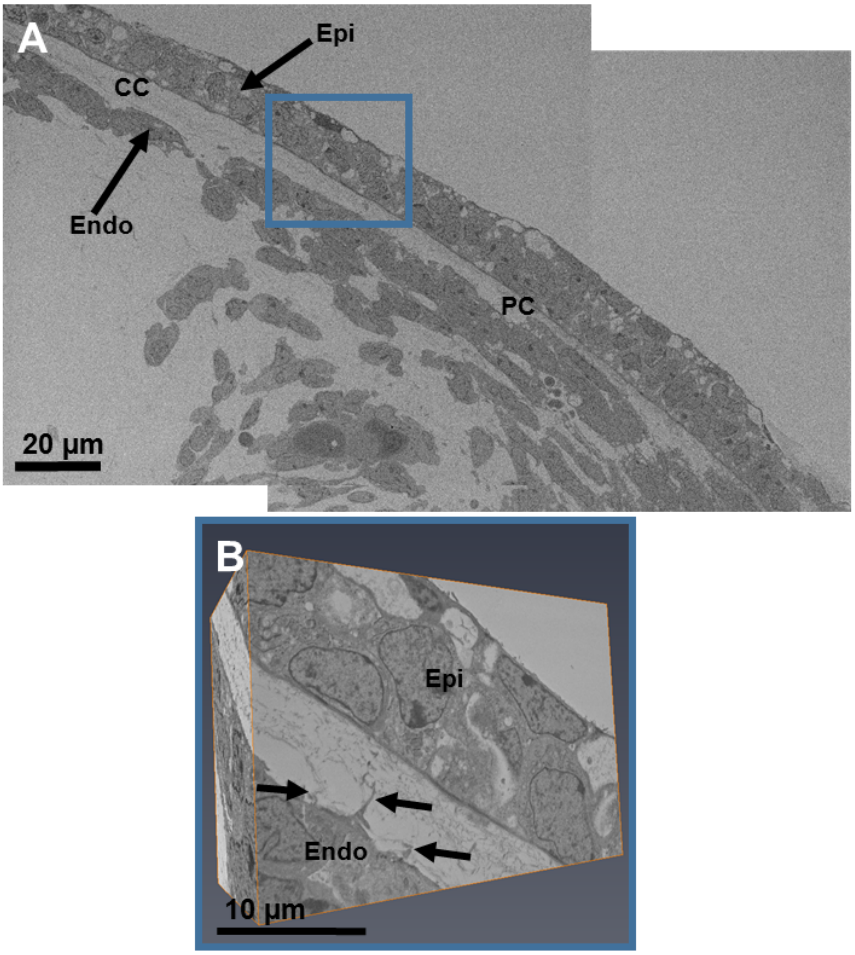

Figure 6.1. Serial block-face scanning electron microscopy (SBF-SEM) images of the embryonic cornea at Carnegie stage 20.

Fig. 6.1A: An SBF-SEM image of the cornea showed the developed corneal epithelium (**Epi**) and endothelium (**Endo**), with collagen fibrils dispersed between both layers. Corneal stromal cells were absent from the central cornea (**CC**), present only in the peripheral corneal regions (**PC**). A high magnification dataset from the region of interest (blue box) was collected in the central cornea. **Fig. 6.1B:** 3-D reconstructions identified cell extensions from the corneal endothelium to extend anteriorly towards the corneal epithelium (black arrows). No mesenchymal cells were present in the 3-D reconstruction of the central cornea.

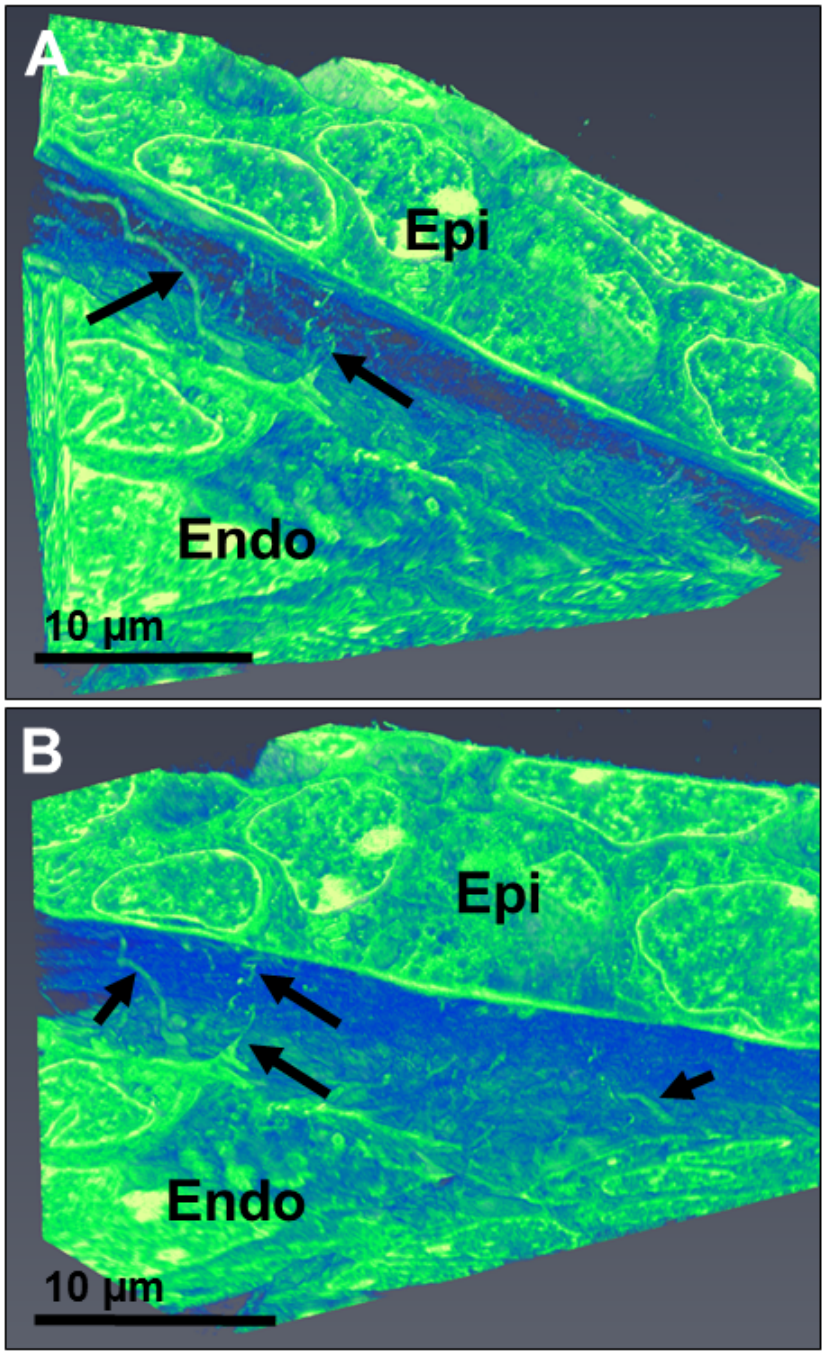

Figure 6.2. Three-dimensional reconstructions of the central embryonic cornea at Carnegie stage 20.

Fig. 6.2A and Fig. 6.2B: The epithelium (**Epi**) and endothelium (**Endo**) were developed, with no mesenchymal cells situated between both layers. Cell projections from the endothelium appeared to extend anteriorly towards the corneal epithelium (black arrows), which suggests a communication network between these cell types. For greater detail of these models, refer to supplementary video 6.

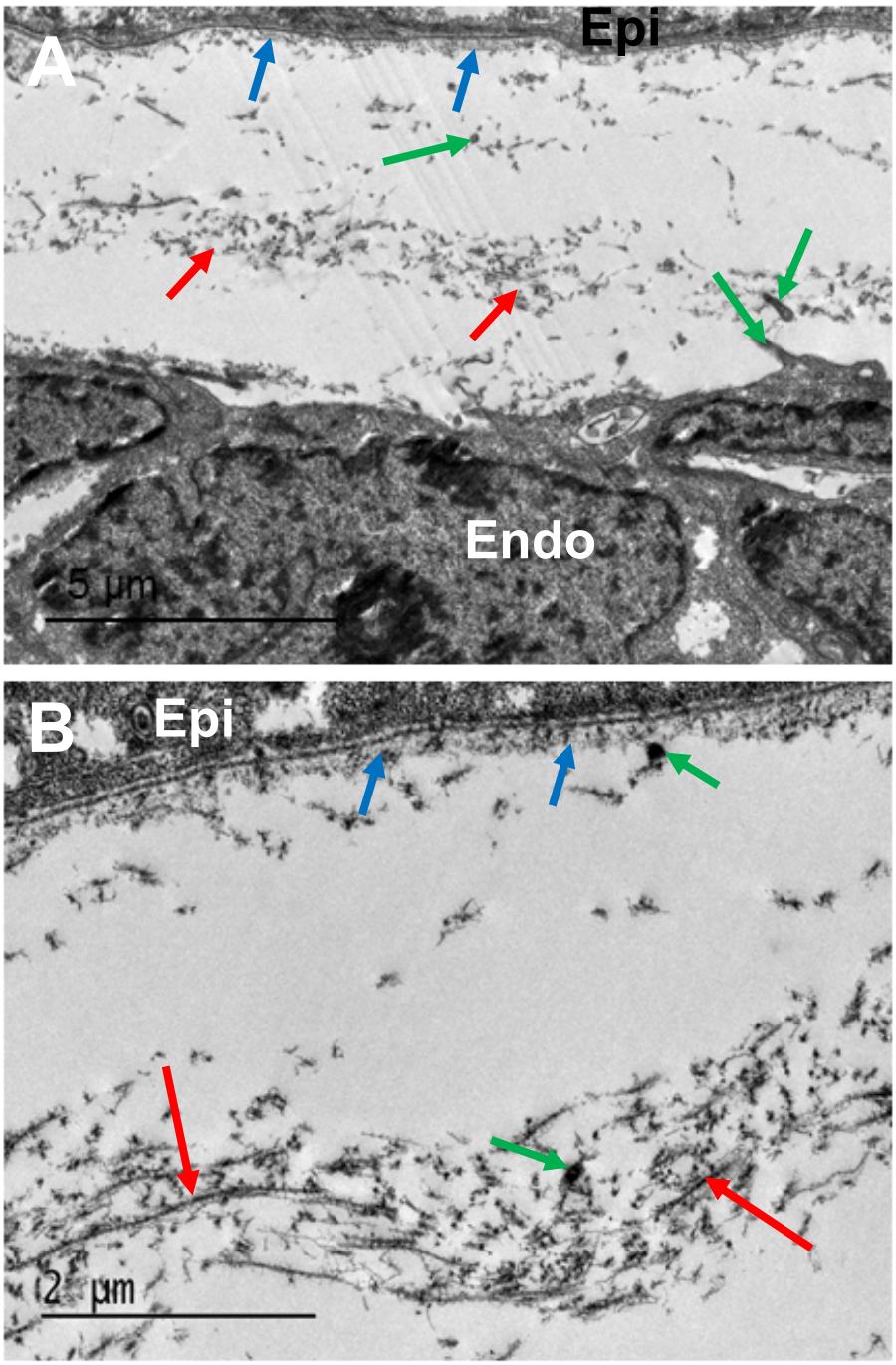

Figure 6.3. Transmission electron microscopy imaging of the embryonic cornea at Carnegie stage 20.

Fig. 6.3A and Fig. 6.3B: A concentration of acellular collagenous matrix was identified between the corneal epithelium (**Epi**) and endothelium (**Endo**) in the central cornea (red arrows). A concentrated extracellular matrix also displayed below the epithelium (blue arrows). It is suggested that cell processes were apparent between the corneal epithelium and endothelium (green arrows). Scale bar in Fig. 6.3A measured 5µm. Scale bar in Fig, 6.3B measured 2µm.

6.3.1.2. CS22

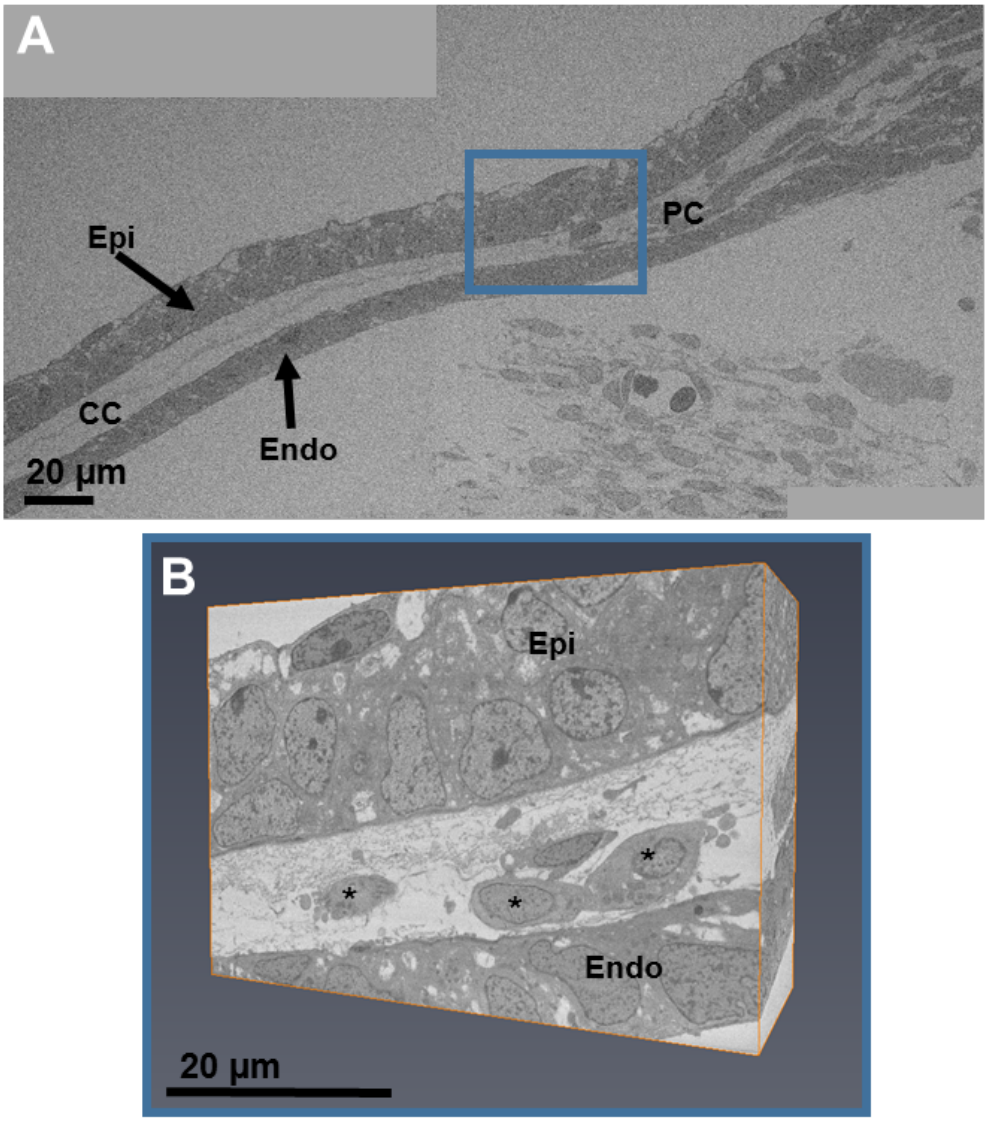

Figure 6.4. Serial block-face scanning electron microscopy (SBF-SEM) imaging of the embryonic cornea at Carnegie stage 22.

Fig. 6.4A: Corneal stromal cells were imaged in the peripheral cornea (**PC**), with a condensed collagenous matrix between the epithelium (**Epi**) and endothelium (**Endo**) of the central cornea (**CC**). A region of interest (blue box) was further imaged at a high magnification in the peripheral cornea. **Fig. 6.4B:** 3-D reconstructions what appears to be a primary stroma concentrated to the central region. Mesenchymal cells (black asterisks) were distributed in the peripheral region of the cornea and associated with the condensed collagenous matrix.

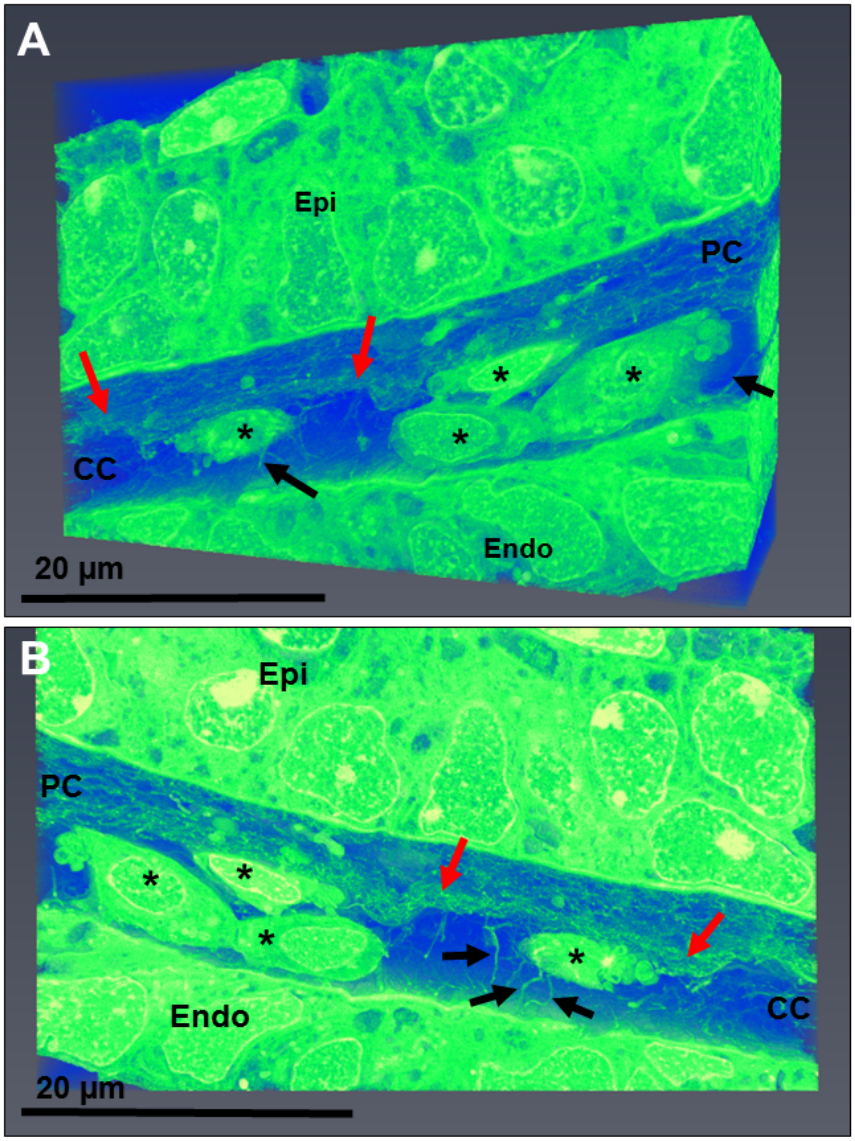

Figure 6.5. Three-dimensional reconstructions of the peripheral embryonic cornea at Carnegie stage 22.

Fig. 6.5A and 6.5B: 3-D reconstructions of the peripheral cornea. A condensed acellular collagenous matrix presented in the central region of the cornea (red arrows), posterior to the corneal epithelium (**Epi**). Cell projections from the endothelium (**Endo**) directed anteriorly towards the collagen layer and mesenchymal cells, with a tortuous path (black arrows). Mesenchymal cells were only situated in the peripheral corneal regions (**PC**), with no mesenchymal cells in the central cornea (**CC**) (black asterisks). For additional material of the 3-D reconstructions refer to supplementary video 7.

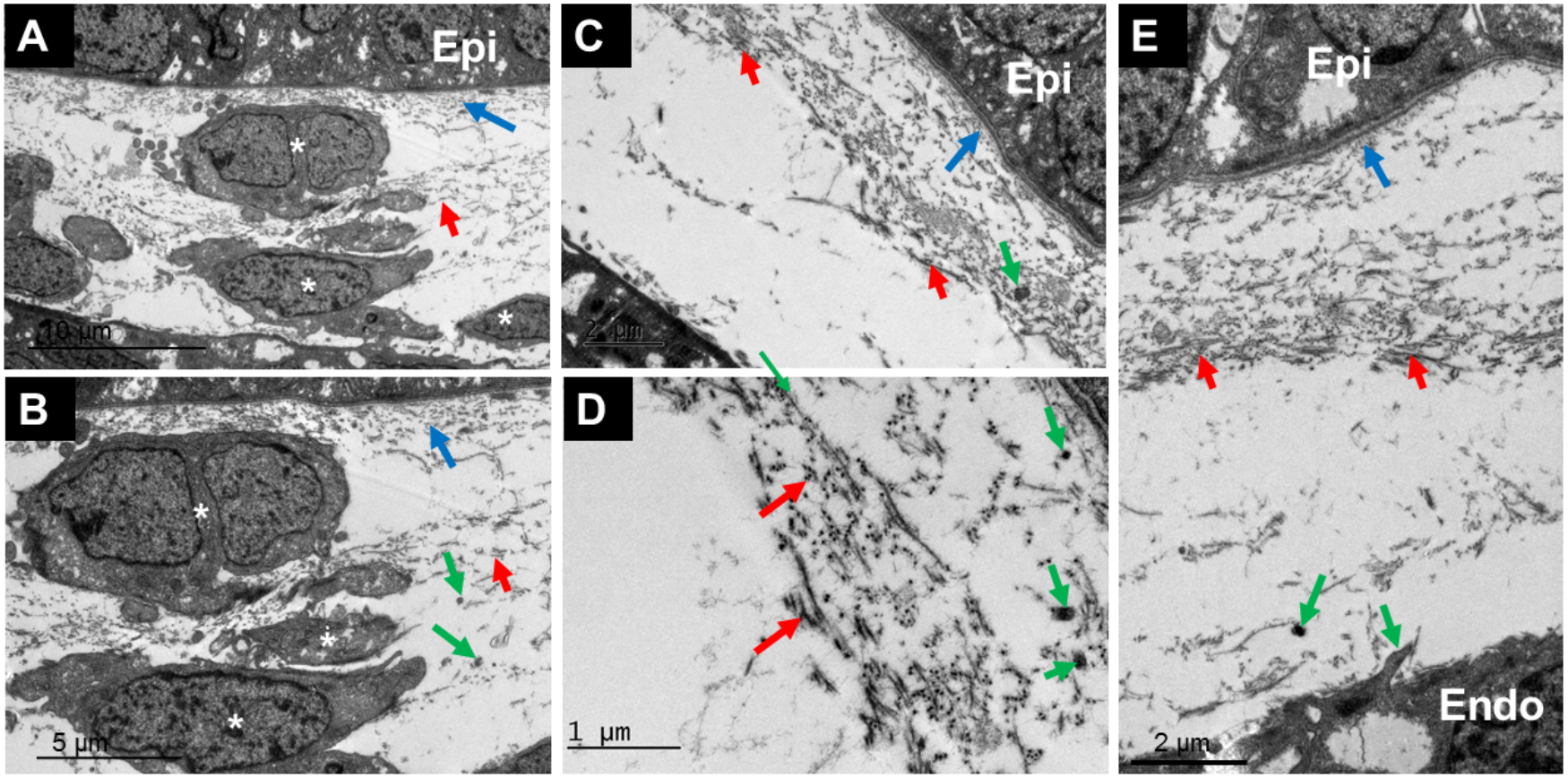

Figure 6.6. Transmission electron microscopy imaging of the embryonic cornea at Carnegie stage 22.

Fig. 6.6A and Fig. 6.6B: Mesenchymal cells (white asterisks) in the peripheral region of the cornea were surrounded by extracellular matrix. **Fig. 6.6C and Fig. 6.6D:** The central cornea contained no mesenchymal cells, with a collagenous matrix concentrated in the anterior central cornea (red arrows) and posterior to the corneal epithelium (**Epi**) (blue arrows). **Figs. 6.6C-E:** The collagenous matrix contained no mesenchymal cells. However, it is suggested that cell projections (green arrows) were observed.

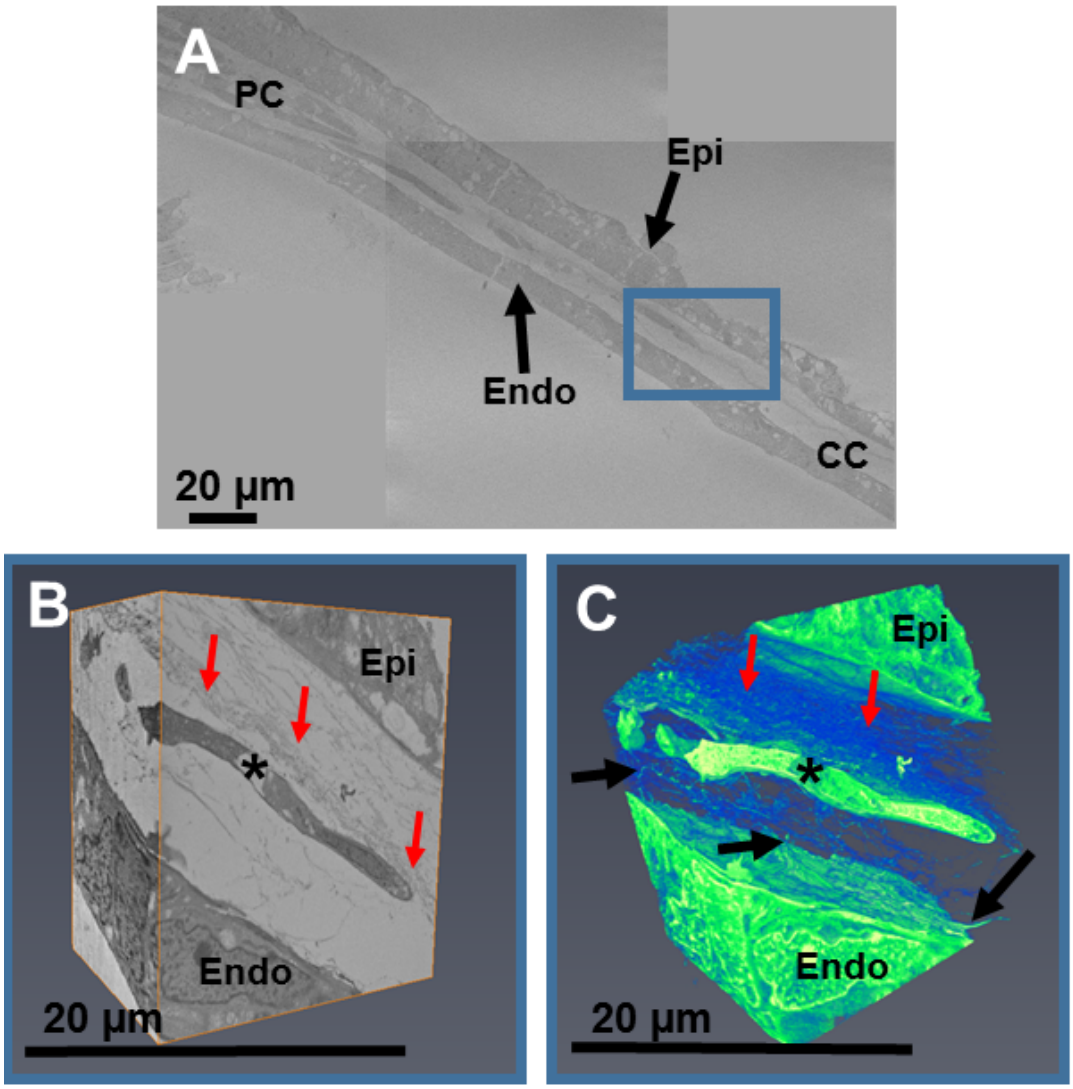

Figure 6.7. Serial block-face scanning electron microscopy (SBF-SEM) imaging of the embryonic cornea at CS22.

Fig. 6.7A: Mesenchymal cells were situated between the corneal epithelium (**Epi**) and endothelium (**Endo**) in the peripheral region of the cornea (**PC**) as a single cell layer. **Fig. 6.7B and Fig. 6.7C:** Analysis of an individual cell (blue box) identified its (black asterisk) association with the collagenous matrix. 3-D reconstructions demonstrated the endothelial cell projections to branch anteriorly towards the corneal cell (black arrows), which was apposed to a collagenous matrix anterior to the cell (red arrows).

6.3.2. Week 8 and 9

The corneal stroma in week 8 dramatically increased in size compared with week 7, with cells dispersed throughout the corneal stroma (**Figure 6.8**). The stromal cells have presumably developed from the mesenchymal cells that migrate into the corneal stroma, previously imaged in younger corneas to be concentrated within the peripheral cornea. Small deposits of collagen fibrils surrounded corneal stromal cells (**Figure 6.8**). High-magnification images further demonstrated collagen fibrils to surround corneal stromal cells. These collagen fibrils ran longitudinally and transversely, to some extent, orthogonally arranged within the corneal stroma (**Figure 6.8E**).

At week 9, collagen deposition was seen throughout the corneal stroma, organised to run longitudinally and transversely with respect to adjacent collagen fibrils between corneal stromal cells (**Figure 6.9**). Collagen fibrils had begun to form lamellae, but extracellular matrix space between the developing cells and collagen fibrils still remained. Cell projections from the endothelium were identified to branch into the corneal stroma, supplementing SBF-SEM and TEM endothelial cell projection data in younger tissues previously described (**Figure 6.9**).

No heavily stained filaments characteristic of elastic fibres were identified within any of SBF-SEM and TEM datasets during week 8 and 9 of corneal development.

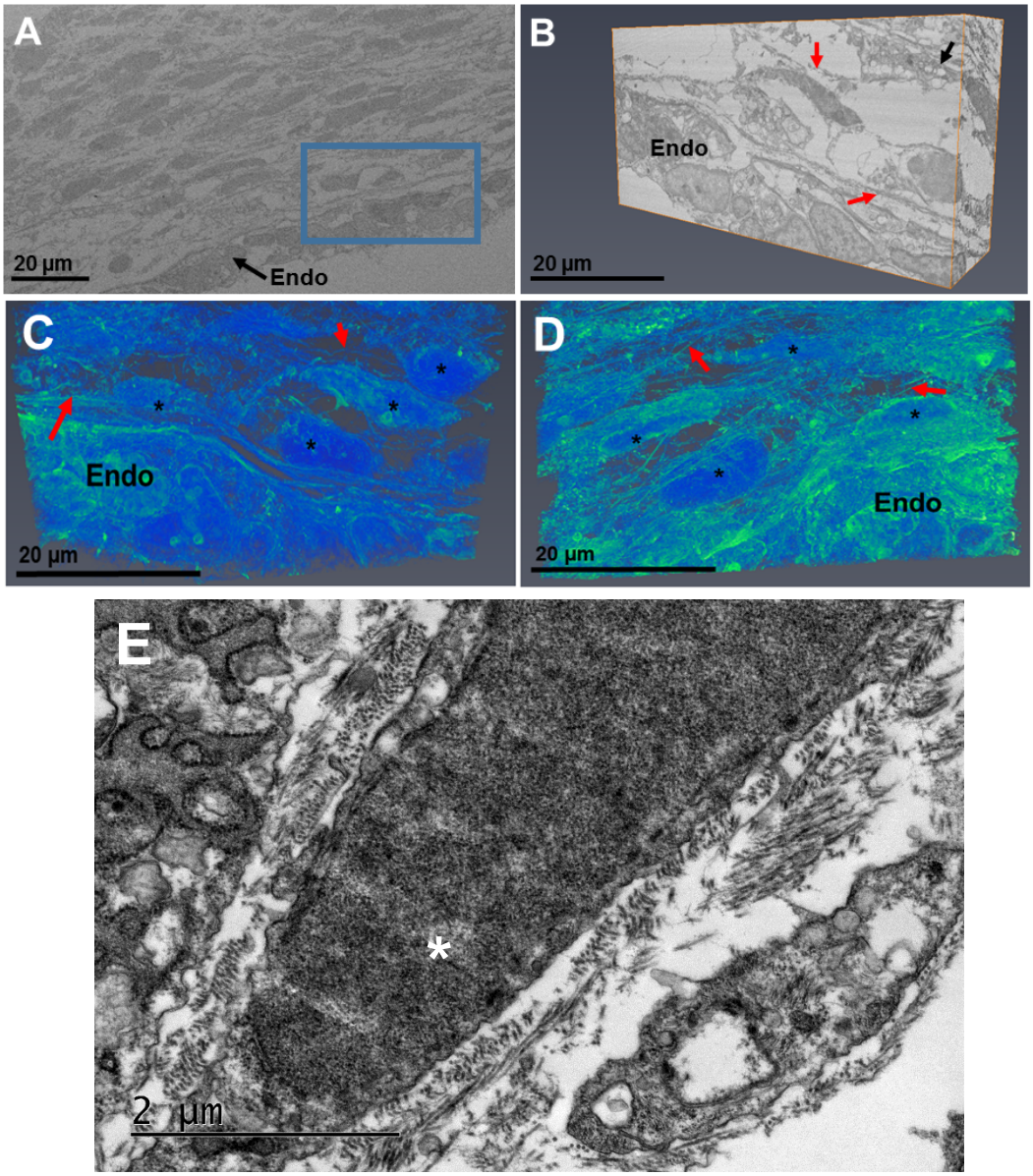

Figure 6.8. Serial block-face scanning electron microscopy (SBF-SEM) and transmission electron microscopy (TEM) images of the foetal cornea at week 8.

Fig. 6.8A: SBF-SEM images revealed cells to have infiltrated into the presumptive stroma. The area of the posterior cornea, directly anterior to the corneal endothelium (**Endo**) was further analysed in 3-D (blue box) **Fig. 6.8B**: Cells presented throughout the corneal stroma, surrounded by small collagen fibril deposits (red arrows). The corneal stromal cells also branched to adjacent cells (black arrows). **Fig. 6.8C and Fig. 6.8D**: 3-D reconstructions identified stromal cells (black asterisks) surrounded by collagen fibrils (red arrows). **Fig. 6.8E:** TEM images further displayed corneal stromal cells (white asterisks) throughout the corneal stroma, surrounded by collagen fibrils running mainly in transverse and longitudinal directions.

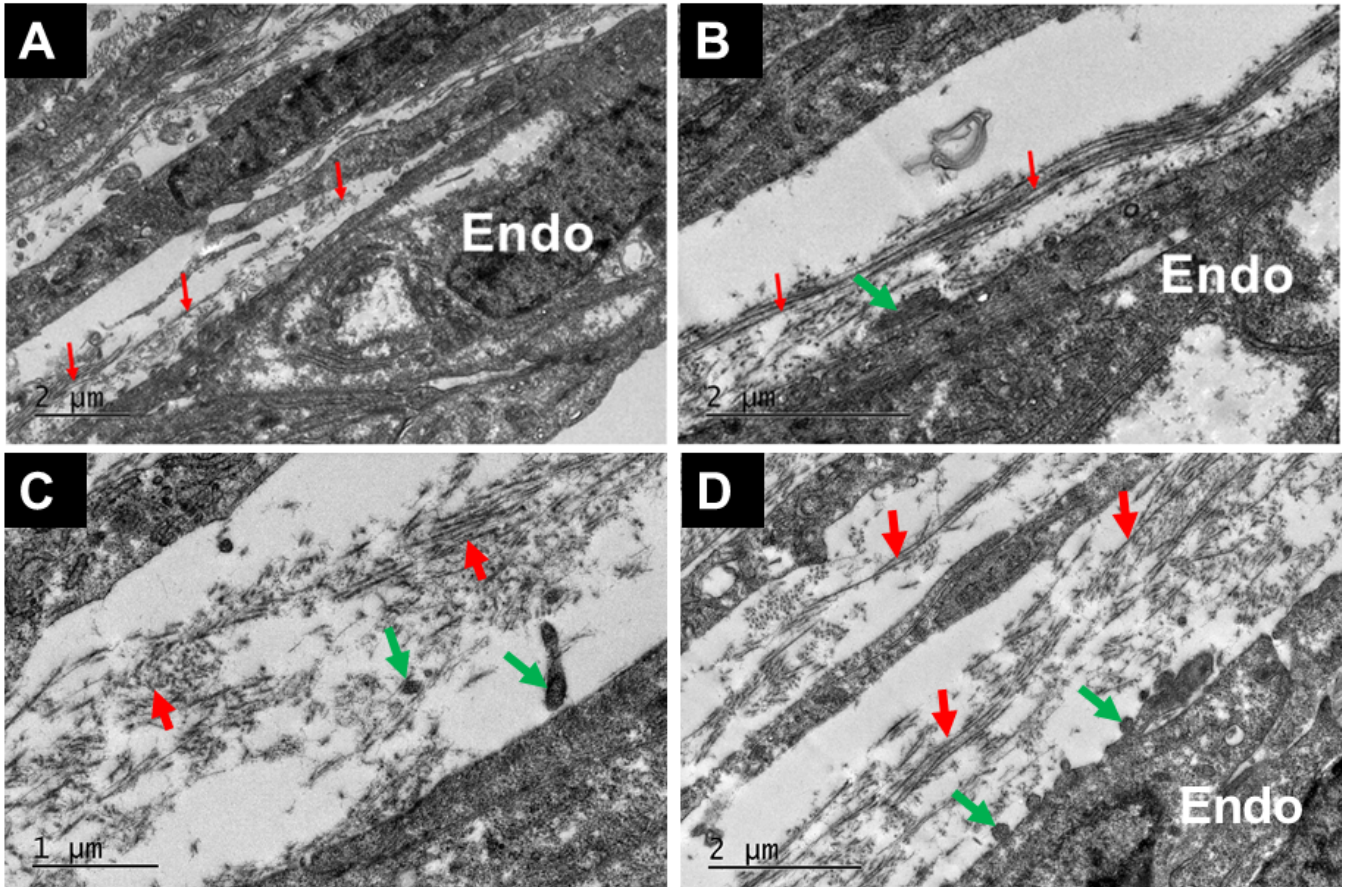

Figure 6.9. Transmission electron microscopy images of the cornea at week 9 of foetal development.

Fig. 6.9A-D: In all images of the posterior peripheral cornea, collagen fibrils were orientated longitudinally or transversely relative to adjacent collagen fibrils (red arrows). Cell projections were seen from the endothelium (**Endo**) (green arrows) to branch anteriorly into the stroma. Scale bar in Fig. 6.9A-B and D measured 2 µm. Scale bar in fig. 6.9C measured 1 µm.

6.3.3. Week 12 and 13

As development progressed to week 12 collagen organisation and the maturation of the cornea increased (**Figure 6.10 and Figure 6.11**). SBF-SEM images showed a concentration of fibres ~2 μm thick anterior to the endothelium, with collagen around the stromal cells (**Figure 6.10**). 3-D segmentation identified individual fibres in the posterior peripheral cornea, with an enhanced concentration of segmented material anterior to the corneal endothelium (**Figure 6.10**). Collagen fibrils had formed lamellae within the corneal stroma, with a moderate orthogonal organisation (**Figure 6.10**). Extracellular space within the corneal stroma still remained, which demonstrated that the entire extracellular matrix had not completely deposited. The cornea at an increased magnification with TEM identified fibres with an enhanced contrast directly anterior to the corneal endothelium (**Figure 6.11**). Images of the anterior cornea at week 12 showed no appearance of these structures with enhanced contrast. The collagen fibrils had regular spacing of transverse fibrils (**Figure 6.11D**).

With increased development to week 13, the corneal stroma had further matured, with an enhanced organisation of collagen fibril bundles into lamellae. SBF-SEM images revealed a concentrated network of fibres directly anterior to the corneal endothelium, contained within sheets. In addition, individual fibres ran longitudinally within the posterior peripheral corneal stroma and branched in different directions that remained in the same horizontal plane of the collagen lamellae (**Figure 6.12**).

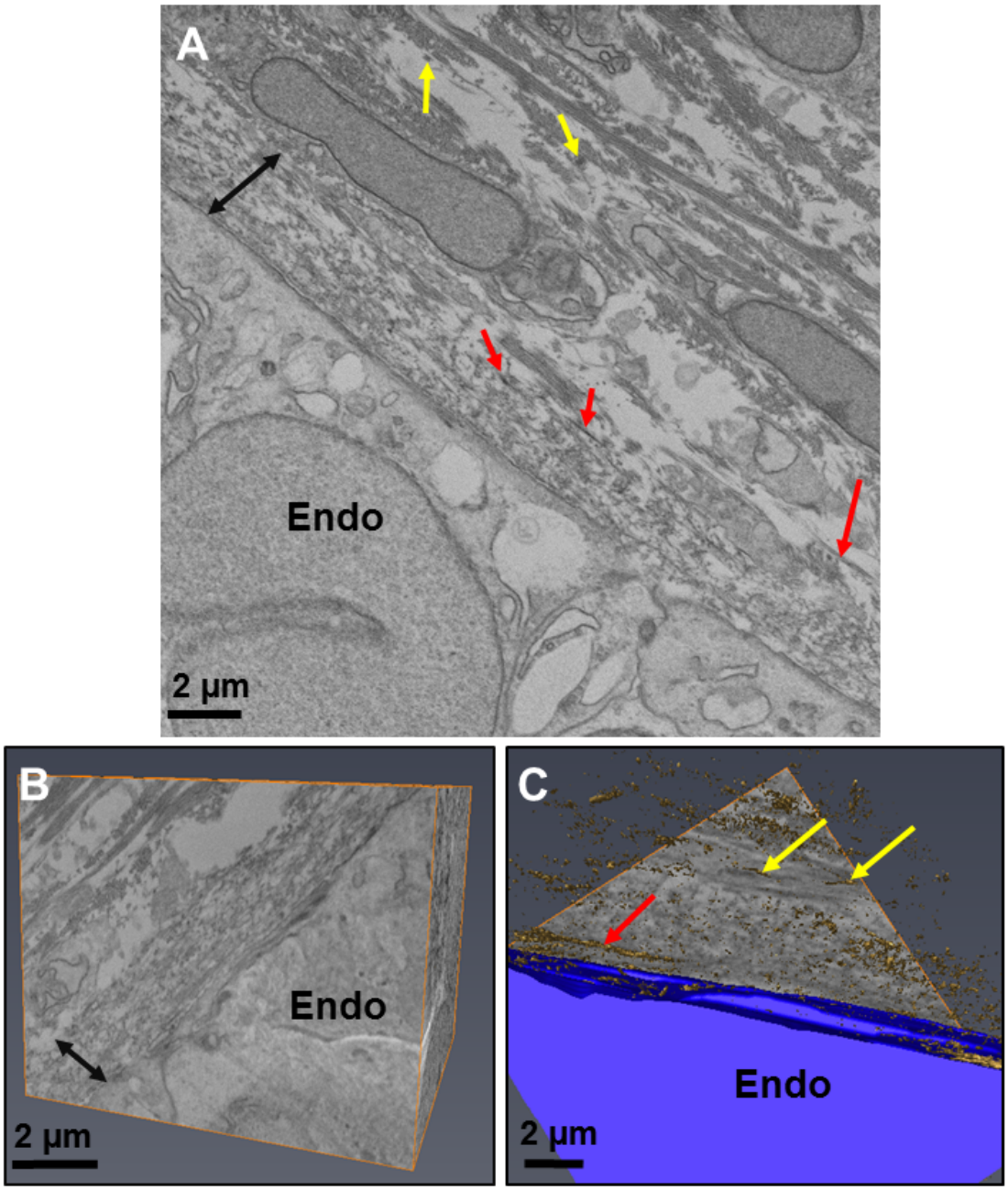

Figure 6.10. Serial block-face scanning electron microscopy (SBF-SEM) image of the week 12 foetal corneal elastic fibre system.

Fig. 6.10A and Fig. 6.10B: A concentration of fibres was identified with SBF-SEM in the posterior stroma, localised to ~2 µm (bidirectional arrow) above the corneal endothelium (**Endo**). **Fig. 6.10C:** Individual lengthened fibres (yellow arrows) were reconstructed in the posterior corneal stroma, as well as a concentration of fibres (red arrows) directly anterior to the corneal endothelium (blue) in 3-D.

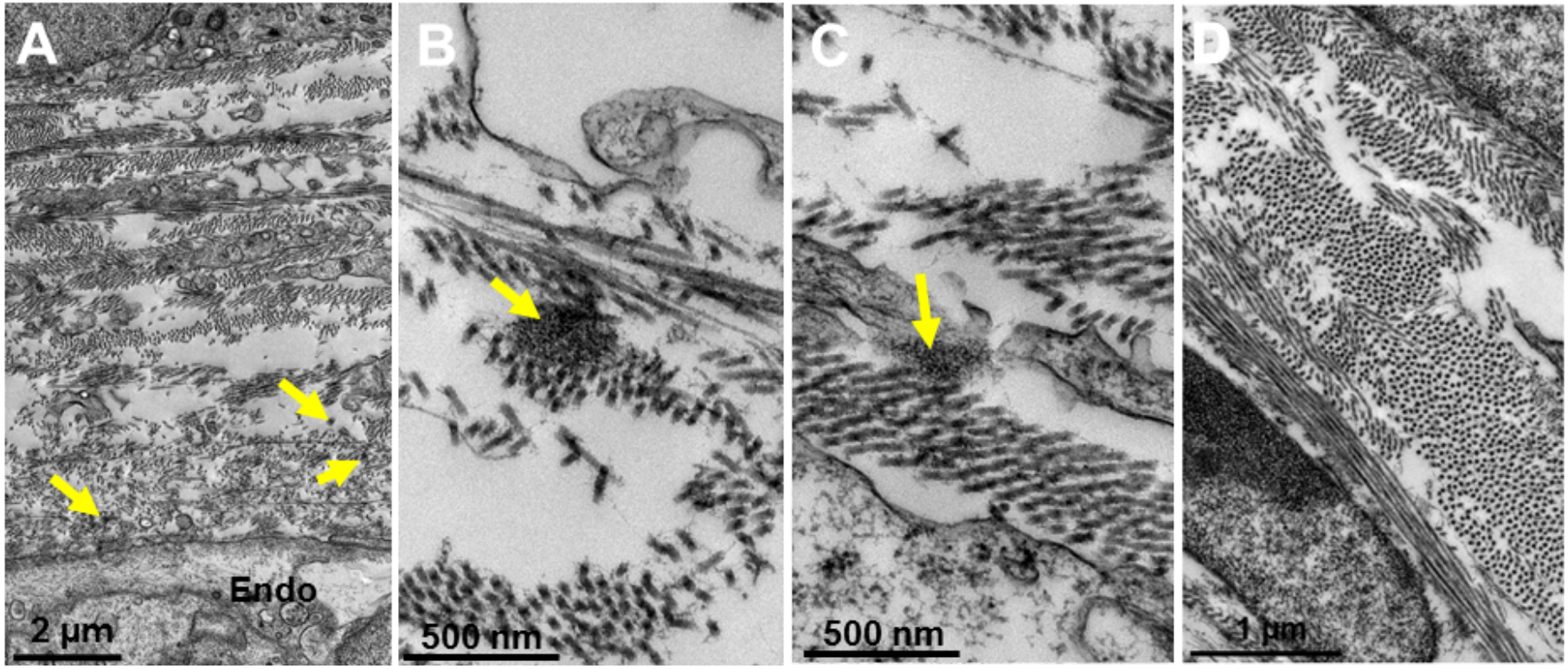

Figure 6.11. Transmission electron microscopy images of the cornea at week 12 of foetal development.

Figs. 6.11A-C: The posterior peripheral cornea contained fibres with an enhanced contrast and a round morphology (yellow arrows). The fibres appeared composed of smaller microfibrils which formed loose bundles of larger fibres **Fig. 6.11D**: There was no presence of these fibres in the anterior or central aspect of the cornea. The collagen fibrils were regularly spaced in the transverse sections. Endothelium (**Endo**).

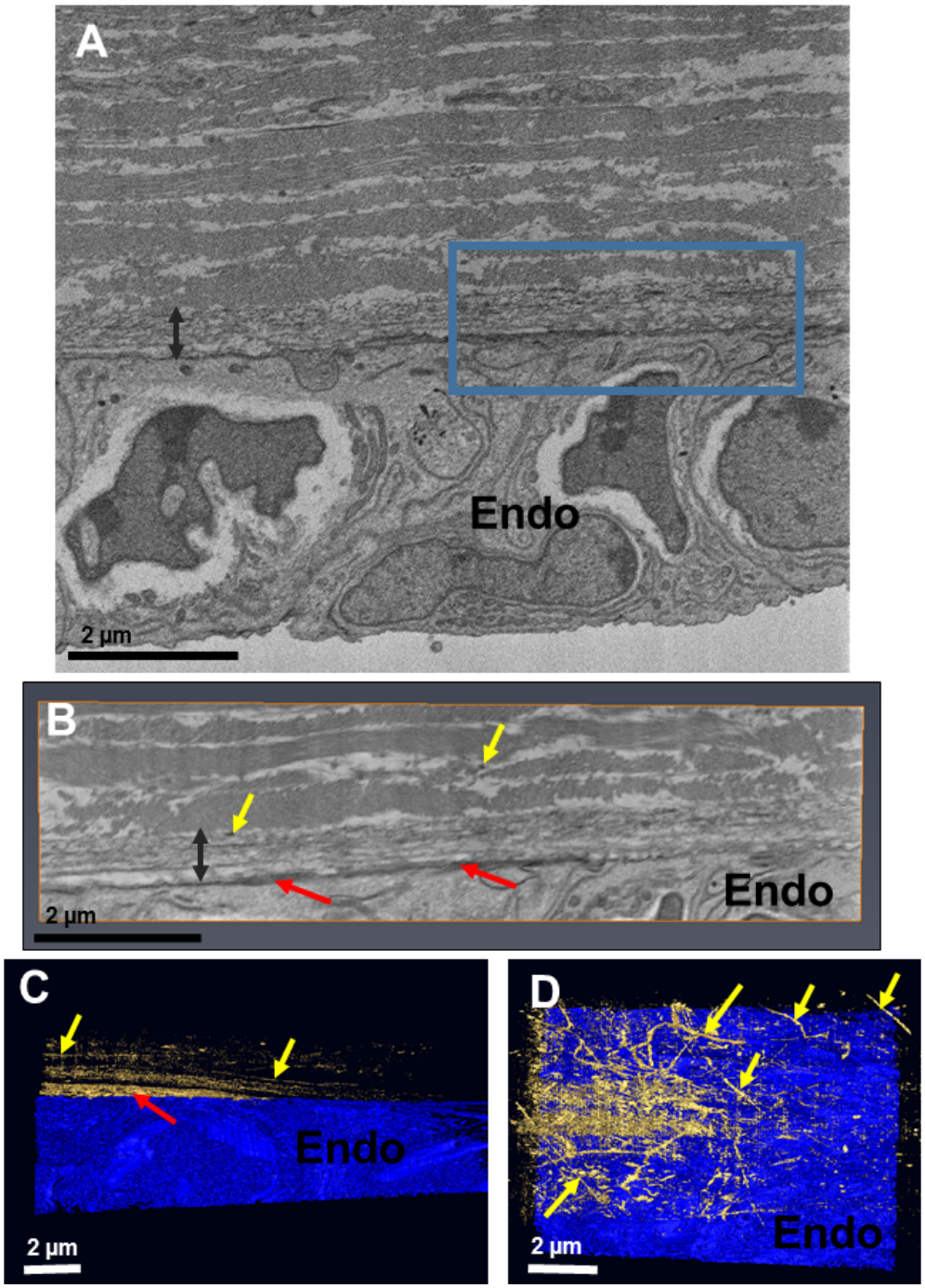

Figure 6.12. Serial block-face scanning electron microscopy images of the developing cornea at week 13.

Figs. 6.12A-C: The posterior peripheral cornea contained an enhanced concentration of fibres within sheets directly anterior to the corneal endothelium (bidirectional arrow) (red arrows). **Fig. 6.12A and Fig. 6.12B**: An area of interest in the posterior peripheral cornea (blue box) was chosen to reconstruct the elastic fibre network. **Fig. 6.12C and Fig. 6.12D**: Elastic fibres (rendered in gold) displayed within sheets (red arrows) anterior to the corneal endothelium and as individual fibres (yellow arrows) running through the posterior corneal stroma. Fig. 6.12C shows the fibres in same orientation as Fig. 6.12A-B. Fig. D is the top down view of Fig. 6.12C, which demonstrates the individual fibres to run in different directions through the plane of the lamellae.

6.3.4. Week 14 and 16

Collagen was packaged within lamellae, and to some extent, orthogonally arranged to adjacent lamellae throughout the corneal stroma (**Figure 6.13 and Figure 6.14**). The fibre network appeared to be enhanced in density and size when compared to younger ages (**Figure 6.13 and Figure 6.14**). TEM images revealed fibre sheets to be contained within a ~2 μm thick layer anterior to the corneal endothelium, as was identified in previous ages (**Figure 6.13 and Figure 6.14**). Individual fibres with enhanced contrast were found within and above the fibre sheets, confined to the posterior corneal stroma. In all ages, the fibres were composed of smaller microfibrils bundled together. Measurements of the individual microfibrils transversely orientated within the fibres measured between approximately 10-12 nm, characteristic of fibrillin microfibrils. These fibres were not seen in the anterior or central aspects of the corneal stroma at this stage of development. At week 16, some fibres contained a dense core surrounded by microfibrils, which displayed different contrasts, characteristic of an elastin amorphous core (**Figure 6.14E**). Furthermore, these fibres were absent from the central cornea of all ages analysed (**Figure 6.13E, Figure 6.13F and Figure 6.14F**).

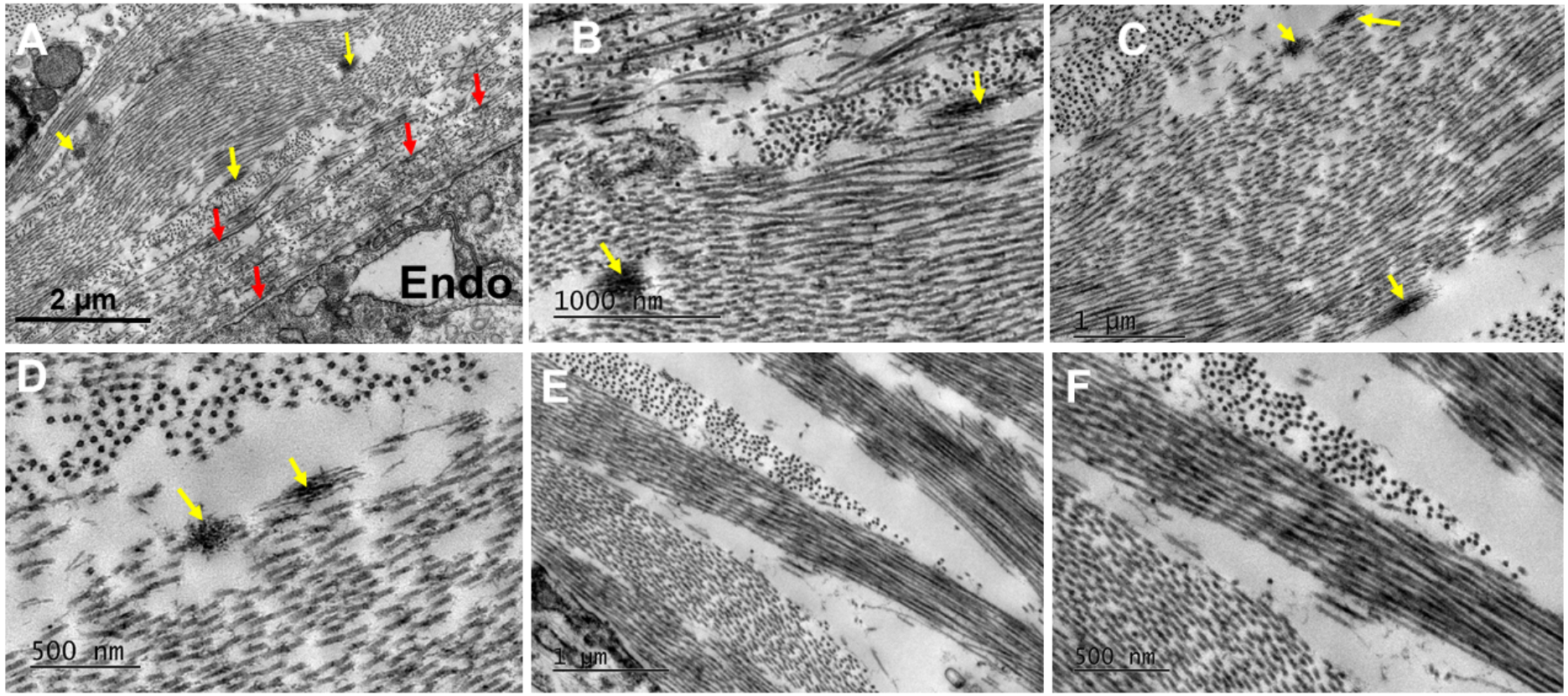

Figure 6.13. Transmission electron microscopy imaging of the foetal cornea at week 14.

Fig. 6.13A: Sheets of fibres were concentrated directly anterior to the corneal endothelium in the posterior cornea (**Endo**) (red arrows). **Figs. 6.13A-D:** Individual fibres were also present within the posterior peripheral corneal stroma (yellow arrow). **Figs. 6.13B-D:** Larger fibres comprised of bundles of microfibrils. **Fig. 6.13E and Fig. 6.13F**: No fibres were identified in the anterior stroma of the cornea at week 14, with only collagen fibrils arranged into orthogonal lamellae seen.

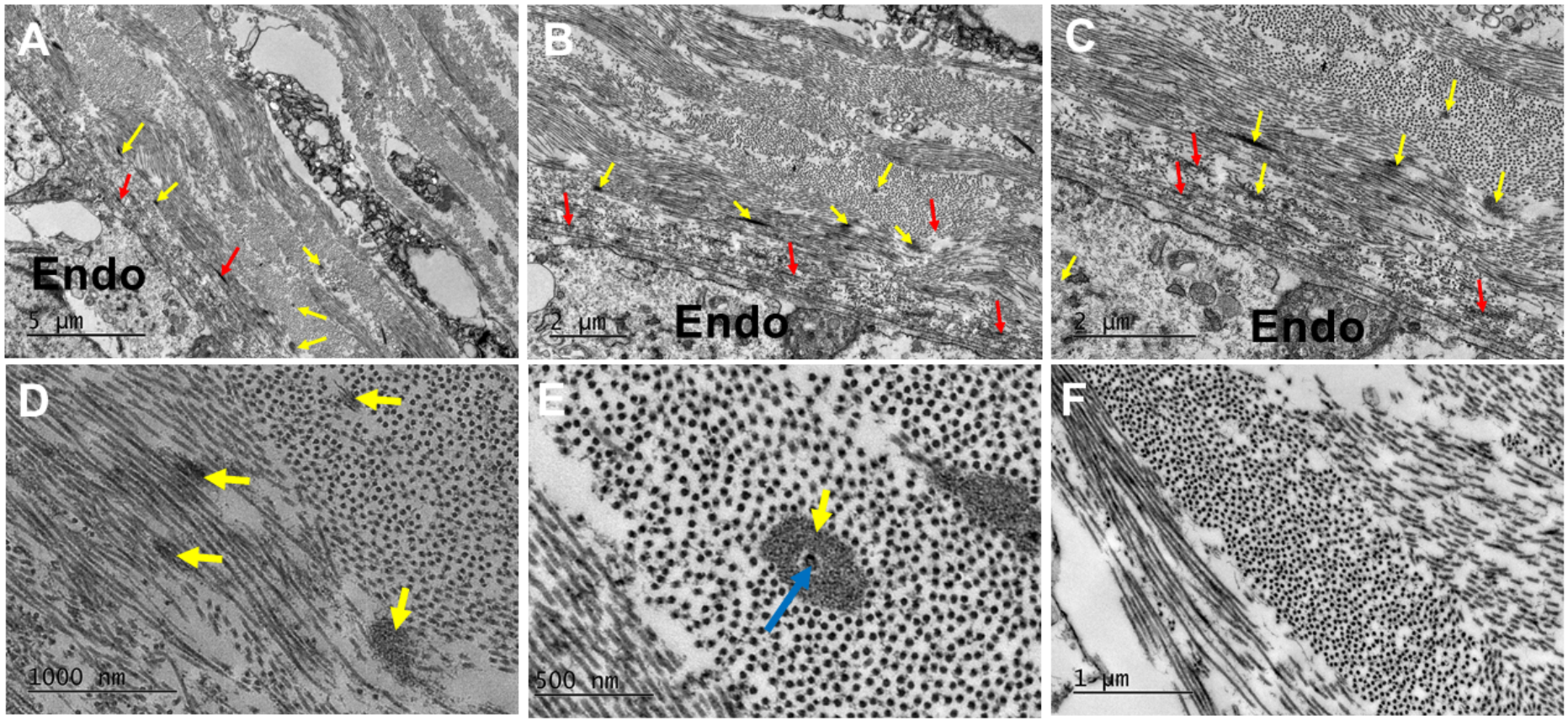

Figure 6.14. Transmission electron microscopy imaging of the foetal cornea at week 16.

Figs. 6.14A-C: The posterior peripheral cornea displayed a concentration of fibres within sheets directly anterior to the corneal endothelium, contained within a ~2 µm region (red arrows). **Figs. 6.14A-E:** Individual fibres also distributed within the posterior peripheral cornea (yellow arrows). **Figs. 6.14E:** Some of the individual fibres within the posterior corneal stroma had a dense core (blue arrow), surrounded by microfibrils (yellow arrow). **Fig. 6.14F:** No fibres were present in the anterior corneal stroma.

6.3.5. Week 17

Collagen fibrils formed lamellae which demonstrated orthogonality at week 17 in the posterior stroma (**Figure 6.15 and Figure 6.16**). SBF-SEM 3-D models showed an enhanced concentration of fibres anterior to the corneal endothelium, and individual fibres displayed within the posterior peripheral corneal stroma (**Figure 6.15**). High-magnification TEM illustrated the high contrast fibres to be situated between and within collagen lamellae (**Figure 6.16**). The anterior corneal stroma did not contain the fibre structures with enhanced contrast, similar to younger ages analysed (**Figure 6.16E and Figure**

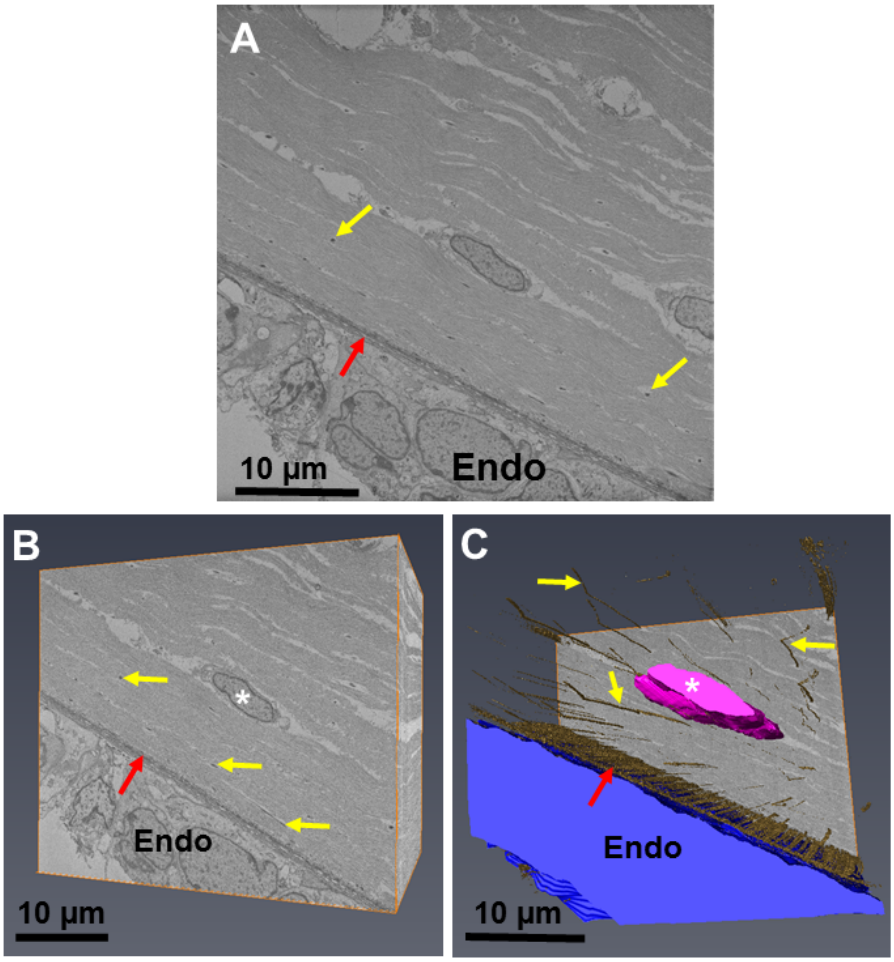

Figure 6.15. Serial block-face scanning electron microscopy images of the week 17 corneal elastic fibre system.

Fig. 6.15A and Fig. 6.15B: A network of fibre sheets (red arrows) concentrated anterior to the corneal endothelium (**Endo**) (blue). **Figs. 6.15A-C:** Individual fibres with an enhanced contrast (gold) displayed within the posterior peripheral cornea (yellow arrow). A corneal stromal cell was also present (pink) (white asterisks).

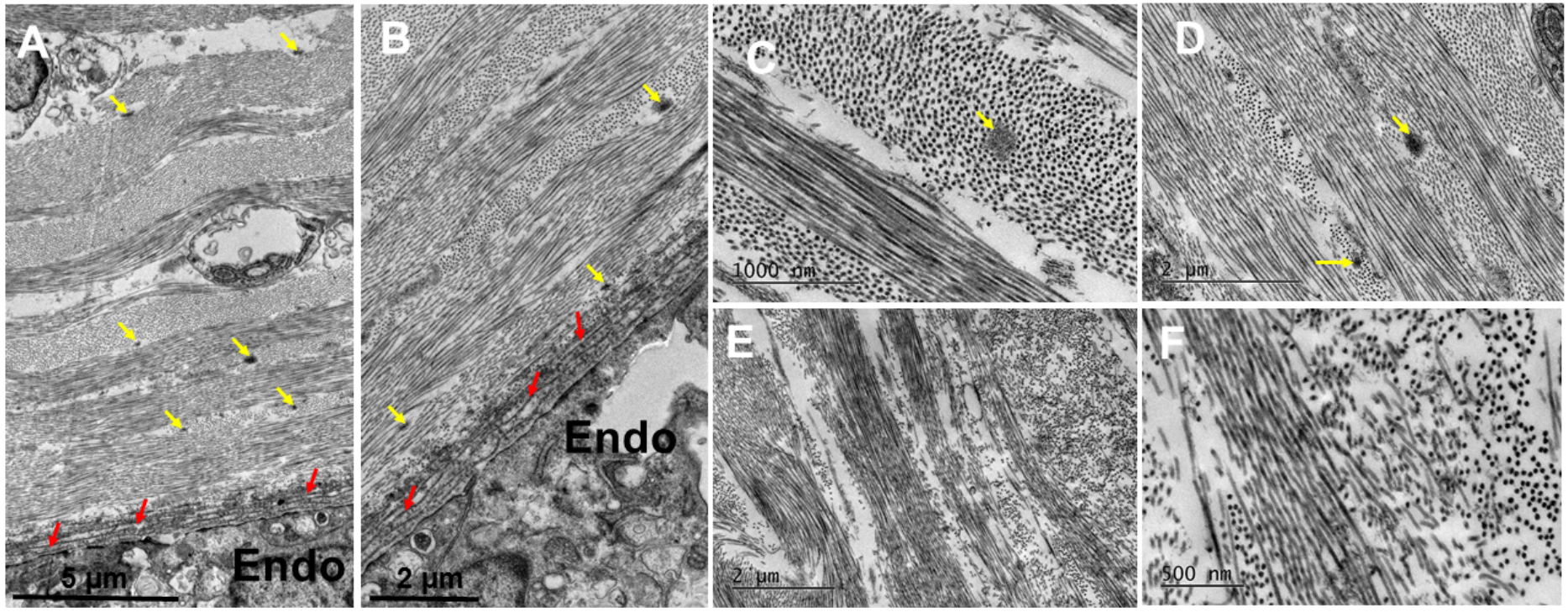

Figure 6.16. Transmission electron microscopy imaging of week 17 foetal corneas.

Figs. 6.16A-D: The posterior peripheral human corneal stroma displayed fibre sheets anterior to the corneal endothelium (**Endo**) (red arrows). Individual fibres were imaged within the posterior peripheral cornea (yellow arrow). Collagen fibrils formed within lamellae throughout the corneal stroma, orthogonally arranged to adjacent collagen lamellae. **Fig. 6.16E and Fig. 6.16F**: No structures represented elastic fibres in the anterior cornea. Scale bar in Fig. 6.16C, 1000 nm; Fig. 6.16D and Fig. 6.16E, 2 µm, Fig. 6.16F 200 nm.

6.4. Discussion

The youngest cornea analysed was at the start of week 7, Carnegie stage (CS) 20. The embryonic cornea at CS20 had a well-developed corneal epithelium and endothelium. Between these cellular layers, an acellular collagen matrix was concentrated in the central anterior corneal stroma and directly posterior to the corneal epithelium. The collagen directly posterior to the corneal epithelium represented developing Bowman's layer. At this age, mesenchymal cells were only seen in the peripheral cornea, absent in the central regions. These results demonstrated the central corneal stroma to be acellular during week 7. These results suggest before mesenchymal cell migration, the human cornea has an acellular condensed collagenous matrix, with collagen fibrils with a transverse and longitudinal arrangement, showing orthogonality. These results provide novel evidence of a collagenous primary stroma in the human cornea. Evidence of a primary stroma has been previously proposed in 1978, but no other studies to my knowledge has reported these findings (Wulle and Richter 1978). The three-dimensional models revealed the endothelium extended cytoplasmic processes anteriorly towards the epithelium, which provides evidence of a communication system between both cell types. Analysis of a further developed cornea at week 7.5 (stage CS22) showed similar results to those at CS20. This included an acellular collagenous matrix between the epithelium and endothelium with mesenchymal cells in the peripheral cornea. However, the collagen matrix had further condensed towards the central corneal stroma at CS22, with increased density of collagen fibrils compared with CS20. Endothelial cell projections were identified again at CS22, directed towards the condensed acellular collagen matrix and mesenchymal cells. This suggests that the endothelium could support or communicate with the acellular collagen matrix. The mesenchymal cells at the periphery are thought to be the cells which will infiltrate the central cornea at a later stage of corneal development. An individual cell analysed in the peripheral cornea laid within the collagenous matrix, which also interacted with the endothelial cell projections. These results suggest that the collagen fibrils support cell migration by acting as a substrate, which occurs in the avian

cornea (Bard and Hay 1975, Hay E. D. and Revel 1969). A schematic summary of the suggested events that develop the human cornea can be found in **Figure 6.17**. This chapter has not classified what extracellular matrix components are present within the substrate, further experiments should investigate the distributions of fibronectin and collagen types to further understand the composition of the acellular collagenous matrix.

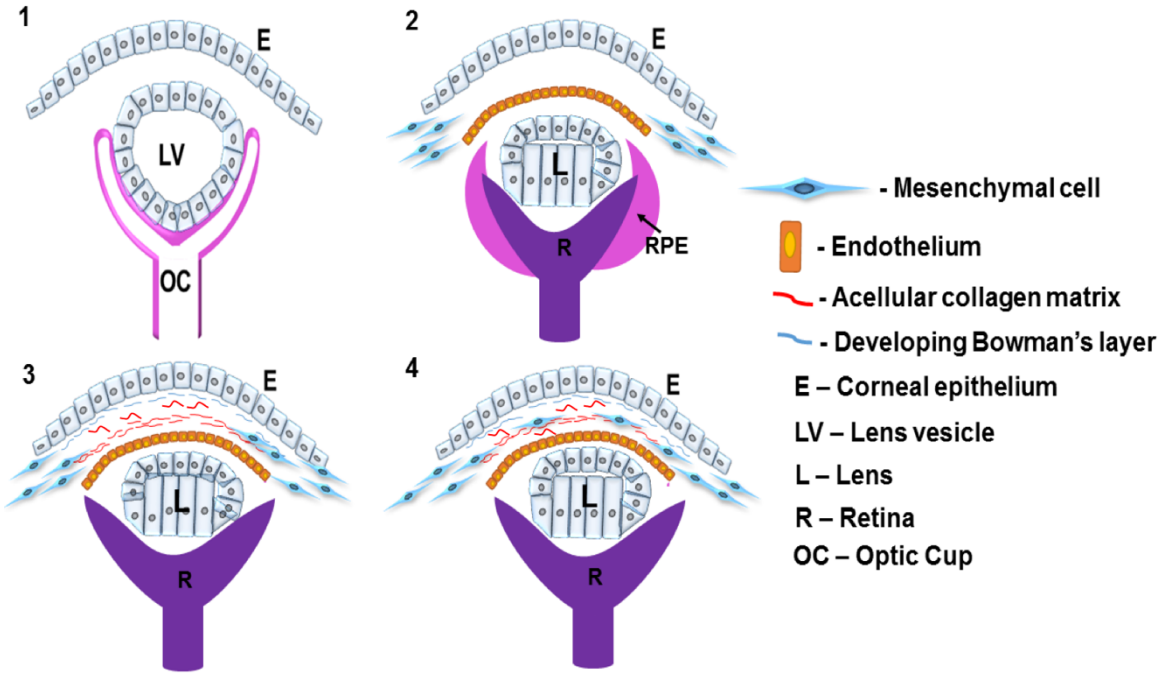

Figure 6.17. The suggested events that develop the human cornea

The surface ectoderm detaches away from the lens vesicle and the surface ectoderm becomes the corneal epithelium prior to week 7 of corneal development (1). A space lies between these structures. The endothelium migrates into the cornea anteriorly to the lens. Mesenchymal cells are in the peripheral aspect of the cornea but are not in the presumptive central corneal stroma at the beginning of week 7 of embryonic development, CS20 (2). Collagen fibrils deposit posterior to the corneal epithelium and within the central cornea at CS20 (3). The collagen fibrils in the central cornea condense and align with the mesenchymal cells in the peripheral cornea at CS21 (3). The cells use the acellular collagen matrix as a substrate for cell migration at CS22 before developing the corneal stroma as development continues (4).

Embryonic cells use other cells and extracellular matrix molecules as a substrate for cell migration in developing tissues (Reig et al. 2014). Cells can utilise extracellular matrix-mediated contact guidance to direct cell migration along a substrate (Reig et al. 2014). Experimental studies have suggested that extracellular matrix fibrils can organise by an exerted mechanical stress, which can further govern cells to migrate by contact guidance mechanisms (Nakatsuji and Johnson 1984). Cell movement has been described in these studies to be aligned along the tension axis, even when the tension axis is perpendicular to the natural axis of alignment (Nakatsuji and Johnson 1984). The results shown in this study suggest that the mesenchymal cells could incorporate contact guidance mechanism with the acellular extracellular matrix to migrate into the central corneal stroma.

Endothelial cell extensions affiliate with the acellular collagenous matrix and mesenchymal cells. In other tissues, endothelial cells have an essential role in cell migration. For example, in leukocyte migration, endothelial cells promote the migration of leukocytes through “outside-in” signals from adhesion molecules (Cook-Mills and Deem 2005). Studies demonstrated that contractile forces in endothelial cells contribute to leukocyte migration by inhibiting endothelial cell control (Garcia et al. 1998, Kielbassa et al. 1998). The cell projections from the corneal endothelium could control mesenchymal cell migration through the interaction of adhesion molecules, contractile forces and signalling pathways. The theory of how mesenchymal cells migrate into the cornea will help understand how the cornea develops. One theory this research has proposed is that the mesenchymal cells use the extracellular matrix as a substrate to migrate into the central corneal stroma. The acellular collagenous network sits in the central aspect of the cornea, adjacent to the mesenchymal cells in the peripheral cornea prior to cell migration from the peripheral cornea. The endothelial cell projections that project anteriorly into the extracellular matrix could adjust to cause the acellular collagenous matrix to move or adjust. This could initiate or stimulate the cells in the peripheral cornea to migrate inwards. Thus, any alterations to the endothelial cell projections e.g. movements, could alter collagenous matrix location and then

assist in directing the cells to migrate inwards along the matrix. The endothelial (Ridley et al. 2003)cell projections could continue to move and influence the collagenous matrix, thus mesenchymal cells, until all cells have infiltrated the cornea. The endothelial cells could also utilise adhesion molecules, contractile forces or signalling molecules to regulate mesenchymal cell migration. Future studies should focus on understanding the mechanisms that generate mesenchymal cell migration and thus develop a functional cornea.

Mediating cell migration is crucial for the development, repair and regeneration of tissues. This chapter has suggested theories that the extracellular matrix and cell extensions could contribute in cell migration. The neighbouring cells and the extracellular matrix environment can alter cell passage and there are many important components of this network that ensures cell migration. For cells to move, signal transduction pathways that encompass lipid second messengers, GTPases, cytoskeleton modifying proteins, motor proteins and kinases must be restricted to areas of a cell (Ridley et al. 2003). The mechanism of cell migration is highly dependent on cell and cell surface receptors, which can assist and alter cell migration. G protein coupled protein receptors activate signalling cascades that can alter cell morphology and regulate actin to assist cell migration (Cotton and Claing 2009). Integrins are adhesive mediated receptors that allow the cell to communicate with the extracellular matrix. Integrins can activate signalling pathways through mechanosensation, by sensing mechanical forces and viscoelastic properties, which can alter the direction in which the cells are migrating (Bershadsky et al. 2006). Focal adhesion detachment of cells from a substratum to assist movement is also altered with epidermal growth factor receptor kinase, which could also act in cell migrations into the corneal stroma (Xie H. et al. 1998). Further studies should analyse the receptors involved in mesenchymal cell migration into the human cornea to understand the processes that might mediate cell migration and thus corneal development.

The results provide novel evidence of a collagenous primary stroma in the human cornea, which shows a similar mechanism of initial development to the avian cornea (Hay E. D. and Revel 1969). In the avian cornea, the epithelium and endothelium secrete the primary stroma (Hay E. D. and Dodson 1973, Hayashi M. et al. 1988). It cannot be confirmed whether or not the epithelium and endothelium secrete the extracellular matrix in the human cornea, however, because no other cells are within the corneal stroma at this stage, it is suggested that the endothelium and epithelium have a role in collagen secretion, similar to the avian cornea (Trelstad and Coulombre 1971). More research needs to be undertaken to determine if this is indeed the case and to identify which collagen types are present, to further determine if there is a similar composition of collagen types to that in the avian developmental model (Birk et al. 1986, Hendrix et al. 1982). Types I, II, V and IX collagen are the main collagen types synthesised in the avian primary stroma, the distribution of these collagens should be explored in the human cornea (Hay E. D. and Revel 1969, Hayashi M. et al. 1988, Hendrix et al. 1982). Furthermore, in avian development, the primary stroma is thought to act as a template to direct cell migration. It is proposed, due to the association of cells with the acellular matrix, that a primary stroma is also required in human corneal development to direct mesenchymal cell migration, whose cells will proceed to become the keratocytes and corneal stroma (Bard and Hay 1975, Hay E. D. and Revel 1969, Trelstad and Coulombre 1971). Further research should help understand the signalling molecules and adhesion components involved to further determine the role that the endothelium has in mesenchymal cell migration. Other developmental models should also be studied to determine if endothelial cells associate with the acellular primary stroma and mesenchymal cells.

Overall, the human results oppose the events demonstrated in the mouse cornea, shown in **Chapter 3** of this thesis, where no primary stroma has been found, similar to what is described in the literature (Haustein 1983). These results show differences between mammalian models. No tissue younger than CS20 was obtained, therefore it was not possible to understand how the

endothelium and epithelium were formed. Despite this, the human endothelium was formed before mesenchymal cell migration, which followed a similar pattern of development to the avian species (Hay E. D. and Revel 1969). The surface ectoderm most probably detached away from the lens to form the corneal epithelium and an initial migration of neural crest derived mesenchymal cells formed the corneal endothelium, followed by the second migration of mesenchymal cells which further develops the corneal stroma (Zieske 2004). These results differ from the mouse cornea, where a single migration of cells forms both the corneal endothelium and corneal stroma. It is the condensation of corneal stromal cells in the posterior peripheral mouse cornea that develops the corneal endothelium (Haustein 1983).

At week 8, cells had already infiltrated the human corneal stroma. The stroma had also increased in thickness and collagen deposition compared with younger ages. Collagen fibrils were found to be associated with the corneal stromal cells. These cells in the chick are well known to synthesise and deposit collagen fibrils that will develop the mature stroma (Birk and Trelstad 1984). Collagen deposition, as described in previous chapters occurs through fibripositors in tendon development and their presence in corneal development has been disputed. In this chapter, evidence of fibripositors which direct collagen fibril deposition was not identified. Therefore, further studies would be needed to analyse collagen fibril organisation. The ages between CS22 and week 8, where collagen fibril synthesis is first seen could not be obtained or analysed.

The tannic acid-uranyl acetate based stain used in this chapter enhances the contrast of elastic fibres and has been undertaken by previous studies to analyse elastic fibre distributions (Lewis et al. 2016, Simmons and Avery 1980). This chapter identified structures with an enhanced contrast to hold a similar morphology to elastic fibres. This was determined by measuring the individual microfibrils within the elastic fibres which measured ~10-12 nm, characteristic of fibrillin-microfibrils (Sakai et al. 1986). The majority of fibres

imaged did not contain an amorphous core, which indicates they are fibrillin-rich microfibril bundles. However, some fibres imaged did contain an amorphous core in the posterior peripheral cornea, which represents similar morphologies to true elastic fibres.

Within this study, elastic fibres representative of microfibrils initially appeared with high-rmagnification TEM analysis as small individual fibres during week 12 of foetal development. Before week 12, elastic fibres were not identified in any of the corneas analysed. These elastic fibres were predominantly present in the posterior cornea, with an absence of the structures in the anterior cornea. These results correlated with previous findings of the elastic fibre network in the adult human posterior cornea (Lewis et al. 2016). The elastic fibre sheets and individual elastic fibres in this study continued to develop with increased age to week 17. Many additional changes to corneal ultrastructure occur after eyelid opening, with corneal maturity being reached approximately 6 months after birth (Lesueur et al. 1994). It would be expected that the elastic fibre system also changes, which most probably enhances with development until maturity. Because of ethical regulations of obtaining tissue in the later stages of development, these later stages could not be analysed.

A concentrated network of sheets imaged in this study has been previously imaged and interpreted as an immature Descemet's membrane (Wulle 1972). These fibres could contribute to Descemet's membrane, however, their structure resembled the elastic fibre system that presents anterior to Descemet's membrane in the adult cornea, which suggests that Descemet's membrane has not yet formed (Lewis et al. 2016). Furthermore, the elastic fibres could support the development of Descemet's membrane in embryogenesis.

The structural distribution of elastic fibres has now been well studied in the cornea, but the functional role of this system still remains unclear. It has

previously been hypothesised that the elastic fibres may help maintain corneal curvature and could allow the peripheral posterior cornea to deform and return to its physiological shape subject to external forces. This chapter has proposed the presence of elastic fibres, which show structures to resemble their morphology with a well-known elastic fibre stain used in electron microscopy (Simmons and Avery 1980). The identification of elastic fibres in corneal development further supports that elastogenesis is important to the development of a functional cornea. In both Marfan syndrome and keratoconus, a loss of corneal structure has been associated with a disruption of the elastic fibre network (White et al. 2017a, White et al. 2017b). Further studies should aim to reveal the biomechanical and functional importance of elastic fibres in both the embryonic and adult cornea.

6.5. Summary

This chapter presented novel evidence to support the existence of a primary stroma within the embryonic cornea. These results led to the proposition that a primary stroma is involved in the mechanism to control mesenchymal cell migration into the human corneal stroma, which develops the mature corneal stroma. This mechanism further follows a similar pattern of development to the events within the avian species. The results also suggest that the endothelium regulates the migration of mesenchymal cells. Further studies should explore the mechanisms that control cell migration and further regulate collagen fibril deposition and arrangement within the corneal stroma.

This chapter also demonstrated a similar distribution and organisation of elastic fibres in the foetal cornea to the mature human cornea. Small deposits of elastic fibres were initially identified in week 12, which matured as fibre sheets and individual fibres in the posterior peripheral cornea with increased age. The presence of elastic fibres at an early stage of development highlights their potential importance which could establish corneal structure in human

development. Further research should understand the function of the elastic fibre network in early corneal development.

Chapter 7: A Structural Study of the Developing Fibrillin-1 Knockout Mouse Cornea

7.1. Introduction

Marfan syndrome (MFS) is a systemic autosomal dominant connective tissue disease caused by mutations in the FBN1 gene located on chromosome 15q15-21, which encodes the glycoprotein fibrillin-1 (Chikumi et al. 2000, Robinson and Godfrey 2000). This mutation impairs the secretion of fibrillin-1 and leads to an increase in the intracellular retention of the mutant fibrillin-1 protein, which disrupts the physiological assembly of true elastic fibres (Zeyer and Reinhardt 2015). Patients with MFS show heterogeneity with their phenotypes, arising from genetic variations (Seo et al. 2018). MFS affects tissues abundant in elastic fibres. The main clinical manifestations involve cardiovascular, ocular and skeletal tissue, and the condition often leads to a shortened life expectancy (Attias et al. 2009).

The most frequent ocular manifestations found in patients with MFS include ectopia lentis and myopia (Gehle et al. 2017). Studies have also identified the corneal structure to be disrupted in MFS, with subjects presenting with a flatter, thinner and opaque cornea compared to control groups (Konradsen and Zetterstrom 2013, Maumenee 1981, Salchow and Gehle 2018, Sultan et al. 2002).

To further understand MFS many mouse models have been developed that alter fibrillin-1 genetically. A mouse model ($mg\Delta^{LoxPneo}$) was developed in the Department of Genetics and Evolutionary Biology, University of São Paulo, Brazil (Lima et al. 2010). The mgΔ mouse model was initially created to analyse the fibrillin-1 mutation displayed in patients with MFS. Exons 19-24 on the FBN1 gene were replaced by a neomycin-resistance expression cassette

(*neoR*), which deletes 272 residues from the protein monomer (Pereira et al. 1997). This initial heterozygous model failed to show significant alterations when compared with the wild type model. The homozygous mouse model did show severe phenotypes, but unfortunately these were lethal and did not survive for analysis. To overcome this limitation, in the heterozygous mice, the mutant FBN1 allele was further modified by being neoR flanked by lox-P sequences, initiating the Cre-recombinase-mediated deletion of the resistance cassette (Sunaga et al. 1997). These alterations developed the heterozygous mgΔ^{LoxPneo} mouse model which presented with some MFS phenotypes (Lima et al. 2010). Corneal structural disruptions were identified within the mgΔ^{LoxPneo} adult mouse model compared to the wild type cornea (White et al. 2017a). The main limitation of this mouse model was that the whole spectrum of phenotypes seen between different sufferers was not represented because of the complexity of MFS. To overcome this limitation, Lima and her colleagues developed a phenotypically severe mouse model by crossing two mgΔ^{LoxPneo} mouse strains that presented with different phenotypes. This led to the production of the F2 mgΔ^{LoxPneo} generation mouse model, by crossing both the B6 and 129 mouse strains (Fernandes K. A. et al. 2015). The mutant FBN1 mgΔ^{LoxPneo} gene allele generated a truncated fibrillin-1 monomer that accumulates inside cells. The resultant fibrillin-1 mutation is unable to regulate transforming growth factor signalling (TGF-β); this then leads to an enhancement of TGF-β levels within the surrounding extracellular matrix. The elevated TGF-β levels results in the phenotypic characteristics that display in patients with MFS (Habashi et al. 2006, Neptune et al. 2003, Ramirez and Rifkin 2009). The F2 mgΔ^{LoxPneo} generation mouse model presents with enhanced pathological severity and contains a wider representation of the different phenotypes within the population of MFS sufferers.

The TGF-β signalling pathway is involved in many cellular processes and regulatory pathways to maintain homoeostasis to tissues and extracellular matrix. Within Marfan syndrome some studies have proposed TGF-β to be involved in its pathology (Habashi et al. 2006, Neptune et al. 2003). However, more recent studies appear to contradict these previous studies and replicating the results previously uncovered in Habashi et al has been difficult.

It has recently been shown that TGF-β might be a repair strategy to try and control or restore the condition ineffectively, with mouse models demonstrating a loss of TGF- β exacerbates MFS symptoms (Wei et al. 2017). If TGF-β signalling is upregulated in MFS, this can subsequently upregulate metalloproteases and elastase, which degrade the extracellular matrix (Booms et al. 2005, Quarto et al. 2012). Components that maintain extracellular matrix organisation, such as the PG decorin, also decrease when TGF-β levels are elevated (Westergren-Thorsson et al. 1993). Decorin is an important component within the corneal stroma; it maintains collagen fibril organisation and if disrupted could contribute to altering collagen organisation, with reduced decorin levels also resulting in corneal scarring (Kahari et al. 1991, Mohan et al. 2011, Reed and Iozzo 2002).

Collagen is known to be the main extracellular component that provides the cornea with its strength, shape and transparency. Whilst the corneal structure has been well studied, the mechanisms that regulate the curved morphology, and hence the refractive power, remain unknown. White *et al.,* previously showed using the first generation mg$\Delta^{LoxPneo}$ mouse model that the adult mouse cornea was thinner in diameter when compared with the wild type model (White et al. 2017a). From this study, it was suggested that the elastic fibre system contributes to the physiological development and maintenance of corneal shape. ***Chapter 6*** of this thesis presented evidence of elastic fibres in the foetal human cornea, which suggested that they may have an important role in the development of a normally functioning mature cornea.

The aim of this chapter was to analyse the structure of the adult and developing cornea within the F2 mg$\Delta^{LoxPneo}$ generation mouse model compared with wild type equivalents. The focus was placed on analysing the overall corneal structure as well as the elastic fibre and collagen fibril ultrastructure. Corneal curvature and thickness were analysed with optical coherence tomography (OCT). Serial block-face scanning electron microscopy (SBF-SEM), transmission electron microscopy (TEM) and small angle X-ray scattering experiments (SAXS) were undertaken to analyse the corneal ultrastructure.

Throughout this chapter the F2 mg$\Delta^{LoxPneo}$ generation mouse model will be referred to as “FBN1$^{+/-}$” and the wild type “WT”.

7.2. Methods

All of the tissue analysed in this chapter was obtained from the Department of Genetics and Evolutionary Biology, University of São Paulo, Brazil. Whole mouse eyes of the FBN1$^{+/-}$ mouse model and equivalent WT were obtained and stored in 0.5% paraformaldehyde before being prepared for the necessary experiments. The F2 mg$\Delta^{LoxPneo}$ generation mouse model was analysed at the developmental ages E12.5, E14.5, E16.5, E18.5 and 6-month adults.

7.2.1. Optical Coherence Tomography (OCT)

Table 7 shows the number of samples used for each age and mouse model analysed.

Table 7. Number (n) of unpaired wild type (WT) and fibrillin-1 knockout mouse (FBN$^{+/-}$) corneas analysed with optical coherence tomography.

Sample	number
Adult WT	6
Adult FBN1$^{+/-}$	6
E18.5 WT	3
E18.5 FBN1$^{+/-}$	6
E16.5 WT	8
E16.5 FBN1$^{+/-}$	11
E14.5 WT	11
E12 WT	6
E12 FBN1$^{+/-}$	6

The OCT methodology was discussed in detail in section 2.3 of the general methods chapter. Please refer back to this method for details on OCT imaging and analysis. For all samples, whole mouse eyes were analysed.

7.2.2. Small Angle X-Ray Scattering (SAXS)

Chapter 2 (section 2.4) details the SAXS methodology used. Adult WT (6 unpaired) and adult FBN1$^{+/-}$ eyes (6 unpaired) were analysed by SAXS to measure collagen interfibrillar spacing and collagen fibril diameter. FBN1$^{+/-}$ (6 unpaired) and WT (3 unpaired) eyes were also analysed at embryonic stage E18.5.

7.2.3. Statistical Analysis

All statistical analyses for OCT and SAXS were calculated in MATLAB R2018a. A Kolmogorov-Smirnov test was performed to test normality. If the data had a normal distribution a two-sample t-test was carried out. If data was skewed a Mann-Whitney U test was carried out to determine statistical significance. Any p-value that was less than 0.05 was determined to be statically significant.

7.2.4. Electron Microscopy

The elastic fibre processing protocol previously described in chapter 2 (section 2.2.1, specifically 2.2.1.1.1) was used with serial block-face scanning electron microscopy (SBF-SEM) and transmission electron microscopy (TEM, section 2.2.2). 3 unpaired corneas for each age of both WT and $FBN1^{+/-}$ tissue were imaged with electron microscopy techniques.

7.2.5. Immunogold electron microscopy

7.2.5.1. Tissue processing

3-unpaired samples for adult WT and $FBN1^{+/-}$ tissue stored in 0.5% paraformaldehyde were low temperature embedded for immunogold labelling experiments. Samples after fixation were stored in 0.2M Sörensen phosphate buffer (pH 7.4). Samples were transferred into 30% ethanol overnight before being placed into the Leica AFS2 automatic freeze substitution system (AFS2) (Leica Microsystems, Wetzlar, Germany) to gradually lower the temperature of the samples using liquid nitrogen (**Figure 7.1**). The initial temperature was selected at -15°C and samples were placed into 55% ethanol for 1 hour within the AFS2. The temperature was gradually reduced to -30°C and samples were placed in 75% ethanol for 1 hour. The temperature was further reduced to -35°C with samples being in 100% ethanol for 1 hour with an additional hour in fresh 100% ethanol. Samples were placed in 30% HM20 for 1 hour,

gradually increasing the concentration of HM20 every hour (60% and 100%). Samples were left in 100% HM20 overnight, placed in a fresh 100% HM20 solution 3 times, and then exposed to ultraviolet light to polymerise the resin blocks for 60 hours. The temperature of the samples was then gradually increased to room temperature.

7.2.5.2. Ultrathin sectioning

Samples were sectioned and collected onto grids as described in the TEM section of chapter 2. However, gold grids were used in replacement of copper grids to prevent the antibodies reacting with the copper grids.

7.2.5.3. Immunogold labelling

The gold grids were rehydrated with an incubation solution that contained Tris-acetate buffer (pH 7.2) in 1% bovine serum album (BSA) plus 1% protease inhibitor plus Chondroitinase ABC for 1 hour. The grids were washed in Tris-acetate buffer for 10 mins, which included 10 changes of solution. The grids were further incubated with phosphate buffered saline (PBS) for 10 mins. The grids were then placed on 50 mM ammonium chloride in PBS (pH 7.4) for 5 mins. Samples were washed 10 times for 10 mins with PBS and then placed in blocking buffer made up of 1% BSA in PBS twice over 10 mins. Grids were incubated with a monoclonal mouse primary antibody to decorin (a gift from Professor Claire Hughes, School of Biosciences, Cardiff University) used at a 1:10 concentration in blocking buffer for 2 hours at room temperature. Grids were washed 6 times for 2 mins with blocking buffer and further incubated with the goat anti-mouse 10 nm gold conjugate secondary antibody (Abcam, Cambridge. England), and was used at a 1:20 concentration diluted in blocking buffer for 1 hour at room temperature. Samples were further washed twice for 2 mins in blocking buffer, 4x in PBS and 10x with double distilled water.

The sections were then counterstained with uranyl acetate (UA) and lead and imaged on the TEM as discussed in ***section 2.2.2***.

7.2.5.4. Immuno-electron microscopy gold analysis

To measure any differences in gold labelling between the WT and $FBN1^{+/-}$ tissue, each gold particle was counted on an image. For both the WT and $FBN^{+/-}$ tissues, gold labelling results were analysed with images taken at x20 magnifications. Statistical analysis between the WT and $FBN1^{+/-}$ tissue was carried out using MATLAB R2018a.

7.3. Results

7.3.1. OCT

7.3.1.1. Adult

Corneal thickness was reduced in the adult FBN1$^{+/-}$ corneas when compared to the WT corneas (**Figure 7.2A and Figure 7.2B**). WT central corneal thickness measurements ranged between 182.27 and 208.78 µm with a mean value of 197.17 ± 9.46 µm. FBN1$^{+/-}$ central corneal thickness ranged between 139.20 and 162.39 µm, with a mean of 148.29 ± 7.33 µm. The corneal thickness across the whole cornea was increased in the WT compared to the FBN1$^{+/-}$ mouse model (**Figure 7.2C**). Statistical analysis revealed central corneal thickness in the WT model to be significantly increased compared with the FBN1$^{+/-}$ corneas (Mann-Whitney U test, p = 0.002200) (**Figure 7.2D**). The mean corneal thickness in the peripheral cornea was 126.41 ± 15.68 in the WT cornea and 109.80 ± 17.34 µm in the FBN$^{+/-}$ mouse model. This difference was not significant (Mann-Whitney U test; p = 0.05670) (**Figure 7.2E**). Corneal radius measurements showed no significant difference between the WT and the FBN1$^{+/-}$ corneas (two-sample t-test; p=0.4551) (**Figure 7.2G**). When central corneal thickness and corneal radius measurements were plotted, the WT cornea had a negative correlation coefficient (-0.54) and the FBN1$^{+/-}$ corneas had a positive correlation (0.29) (**Figure 7.2F**).

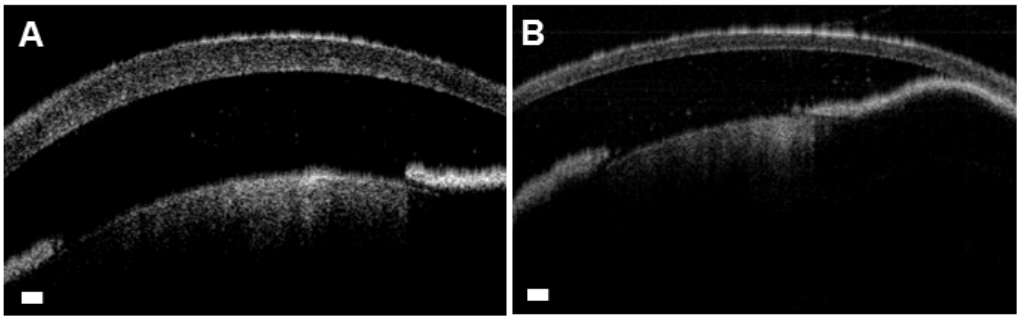
A
B

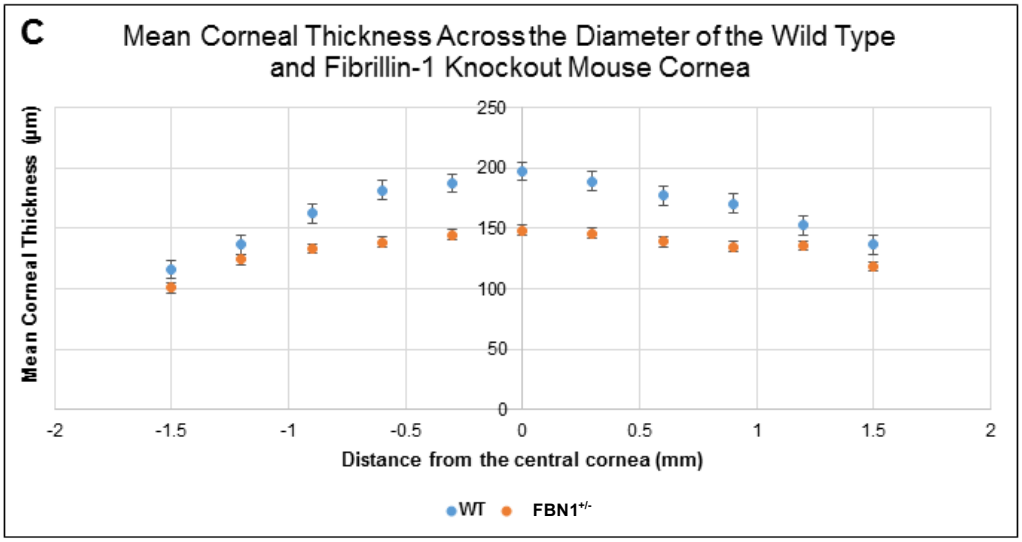
C
Mean Corneal Thickness Across the Diameter of the Wild Type and Fibrillin-1 Knockout Mouse Cornea
Mean Corneal Thickness (µm)
250
200
150
100
50
0
-2
-1.5
-1
-0.5
0
0.5
1
1.5
2
Distance from the central cornea (mm)
WT
FBN1+/-

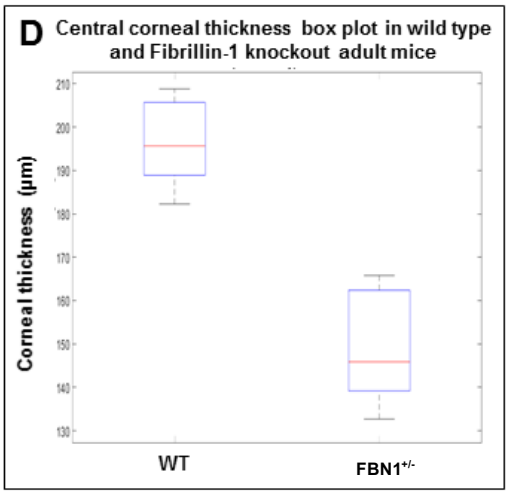
D
Central corneal thickness box plot in wild type and Fibrillin-1 knockout adult mice
Corneal thickness (µm)
WT
FBN1+/-

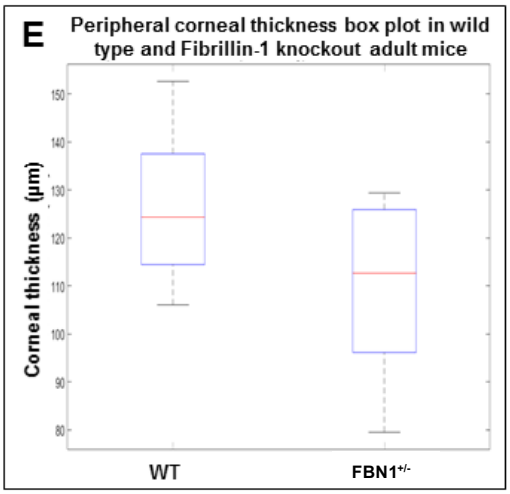
E
Peripheral corneal thickness box plot in wild type and Fibrillin-1 knockout adult mice
Corneal thickness (µm)
WT
FBN1+/-

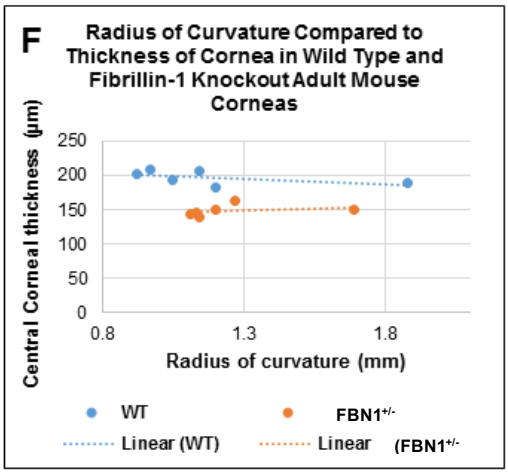
F
Radius of Curvature Compared to Thickness of Cornea in Wild Type and Fibrillin-1 Knockout Adult Mouse Corneas
Central Corneal thickness (µm)
250
200
150
100
50
0
0.8
1.3
1.8
Radius of curvature (mm)
WT
FBN1+/-
Linear (WT)
Linear (FBN1+/-)

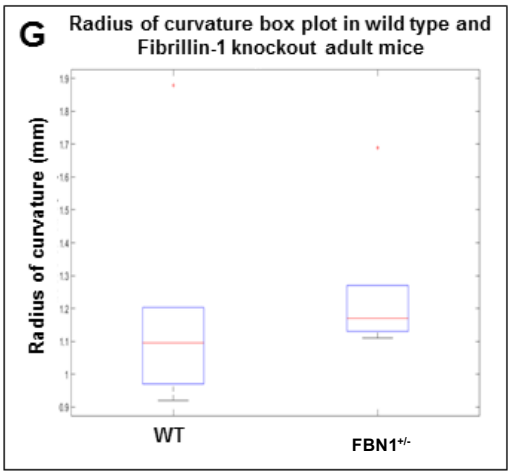
G
Radius of curvature box plot in wild type and Fibrillin-1 knockout adult mice
Radius of curvature (mm)
WT
FBN1+/-

Figure 7.2. Adult wild type (WT) and fibrillin-1 knockout (FBN1$^{+/-}$) mouse cornea optical coherence tomography imaging (OCT) and analysis.

Fig 7.2A: WT cornea OCT analysis (Scale bar = 100 μm). **Fig. 7.2B:** FBN1$^{+/-}$ cornea OCT analysis (Scale bar = 100 μm). **Fig. 7.2C:** Scatter graph plotting WT and FBN1$^{+/-}$ corneal thickness measurements from periphery to periphery. The WT cornea was thicker in all areas measured across the cornea compared to the FBN1$^{+/-}$ cornea. **Fig. 7.2D and Fig. 7.2E:** Central and peripheral corneal thickness boxplots comparing WT and FBN1$^{+/-}$ corneal thickness measurements. **Fig. 7.2F:** Central corneal thickness plotted against radius of curvature measurements. **Fig. 7.2G:** Boxplots for WT and FBN1$^{+/-}$ corneal radius measurements.

7.3.1.2. E18.5

Central corneal thickness within the WT E18.5 cornea ranged between 119.42 and 126.06 μm, with a mean of 124.05 ± 3.28 μm (**Figure 7.3A**). Central corneal thickness within the $FBN1^{+/-}$ mouse model ranged between 61.91 and 96.20 μm, with a mean of 83.28 ± 11.10 μm (**Figure 7.3B**). Corneal thickness within the WT central cornea was significantly increased in comparison to the $FBN1^{+/-}$ (Mann-Whitney U test; $p = 0.02380$) (**Figure 7.3D**). The thickness of the cornea in the peripheral stroma was shown to be significantly increased in the WT cornea compared to the $FBN1^{+/-}$ cornea (Mann-Whitney U test; $p<0.05$) (**Figure 7.3E**). The mean corneal peripheral thickness in the WT cornea was 80.60 ± 3.78 μm. The mean corneal peripheral thickness in the $FBN1^{+/-}$ cornea was 45.59 ± 8.64 μm. The radius of curvature was not significantly different between the WT and $FBN1^{+/-}$ tissues (two-sample t-test; $p>0.05$) (**Figure 7.3G**). When central corneal thickness was plotted against radius measurements, the WT had a weak negative correlation coefficient (-0.01) and the $FBN1^{+/-}$ cornea had a positive correlation coefficient (0.36) (**Figure 7.3F**).

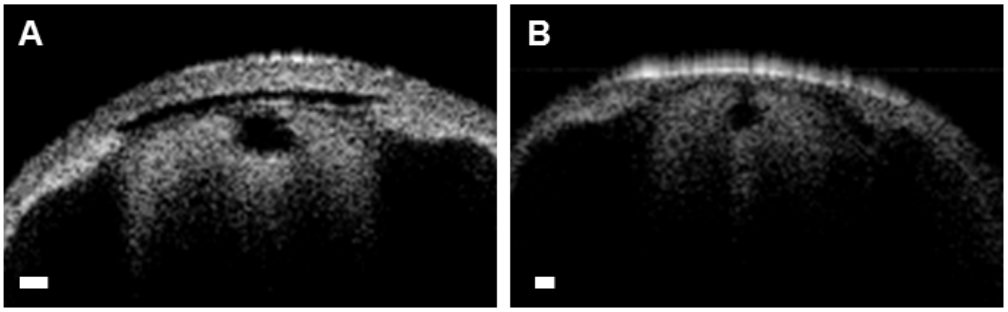
A
B

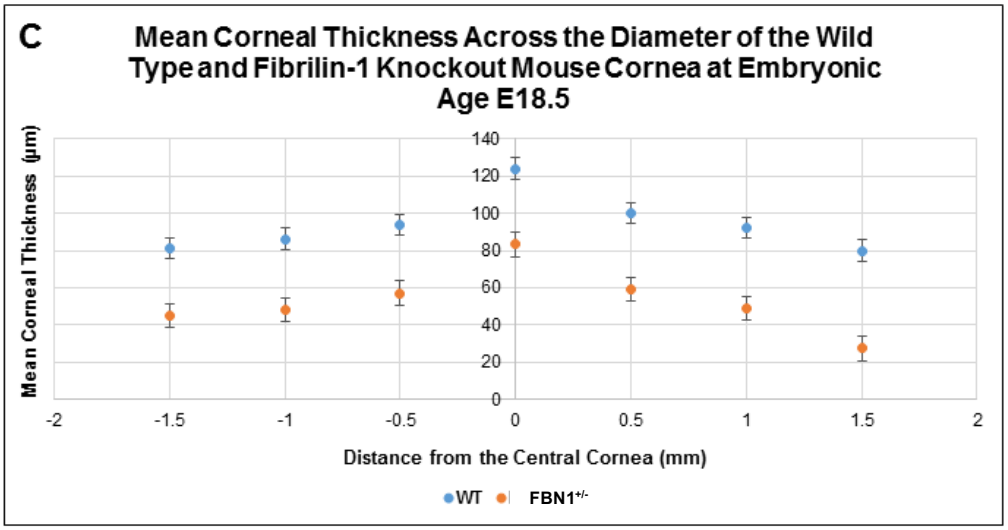
C
Mean Corneal Thickness Across the Diameter of the Wild Type and Fibrilin-1 Knockout Mouse Cornea at Embryonic Age E18.5
Mean Corneal Thickness (µm)
140
120
100
80
60
40
20
0
-2
-1.5
-1
-0.5
0
0.5
1
1.5
2
Distance from the Central Cornea (mm)
WT
FBN1+/-

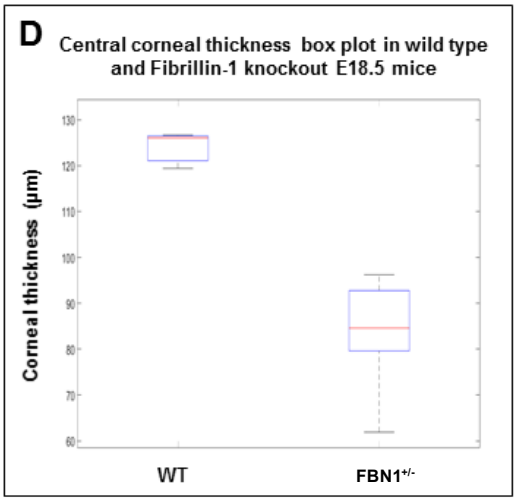
D
Central corneal thickness box plot in wild type and Fibrillin-1 knockout E18.5 mice
Corneal thickness (µm)
WT
FBN1+/-

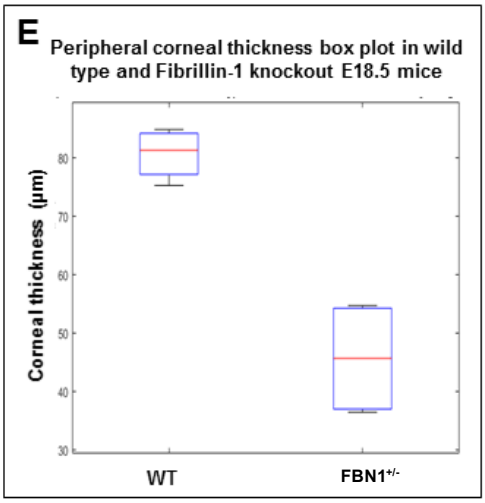
E
Peripheral corneal thickness box plot in wild type and Fibrillin-1 knockout E18.5 mice
Corneal thickness (µm)
WT
FBN1+/-

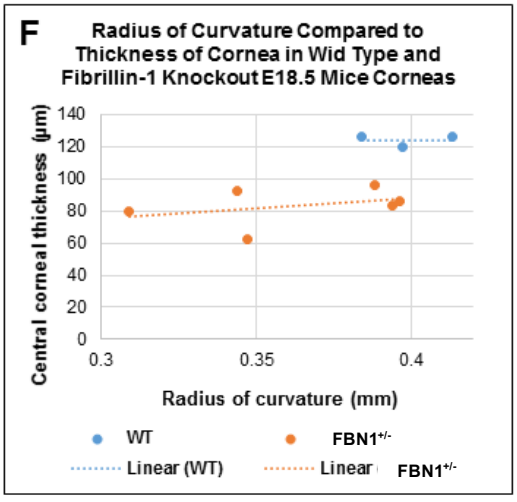
F
Radius of Curvature Compared to Thickness of Cornea in Wid Type and Fibrillin-1 Knockout E18.5 Mice Corneas
Central corneal thickness (µm)
140
120
100
80
60
40
20
0
0.3
0.35
0.4
Radius of curvature (mm)
WT
FBN1+/-
Linear (WT)
Linear
FBN1+/-

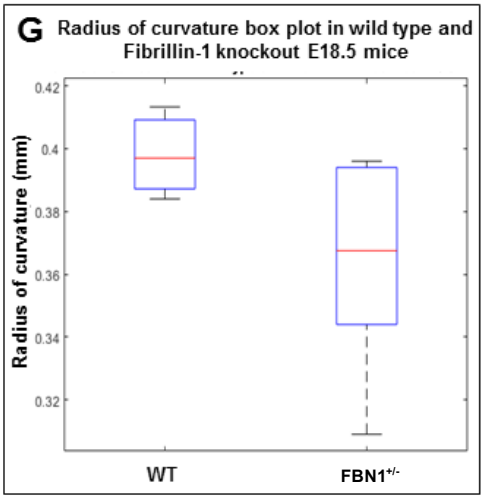
G
Radius of curvature box plot in wild type and Fibrillin-1 knockout E18.5 mice
Radius of curvature (mm)
0.42
0.4
0.38
0.36
0.34
0.32
WT
FBN1+/-

Figure 7.3. E18.5 wild type (WT) and fibrillin-1 knockout (FBN1$^{+/-}$) mouse cornea optical coherence tomography (OCT) imaging and analysis.

Fig 7.3A: WT cornea OCT analysis (Scale bar = 100 μm). **Fig. 7.3B:** FBN1$^{+/-}$ cornea OCT analysis (Scale bar = 100 μm). **Fig. 7.3C:** Scatter graph plotting WT and FBN1$^{+/-}$ corneal thickness measurements across the diameter of the cornea. The WT cornea was thicker in all areas measured across the cornea compared to the FBN1$^{+/-}$. **Fig. 7.3D and Fig. 7.3E:** Central and peripheral corneal thickness boxplots comparing the WT and FBN1$^{+/-}$ corneal thickness measurements. **Fig. 7.3F:** Central corneal thickness plotted against radius of curvature measurements. **Fig. 7.3G:** Boxplots for WT and FBN1$^{+/-}$ corneal radius measurements.

7.3.1.2. E16.5

Corneal thickness was measured across the diameter of the cornea for the E16.5 WT and FBN1$^{+/-}$ mouse corneas (**Figure 7.4A and Figure 7.4B**). Corneal radius measurements were not undertaken as it was difficult to determine the edges of the cornea, a necessary step for accurately measuring the radius. For this reason, radius measurements were not made on corneas younger than E18.5. Central corneal thickness within the E16.5 WT cornea ranged between 30.34 and 52.00 μm, with a mean of 42.68 ± 8.31 μm (**Figure 7.4A**). The central corneal thickness within FBN1$^{+/-}$ corneal tissue ranged between 21.23 and 34.11 μm, with a mean of 26.80 ± 3.58 μm (**Figure 7.4B**). The corneal thickness within the WT central cornea was significantly increased in comparison to the FBN1$^{+/-}$ mouse model (Mann-Whitney U test; p=0.0003175) (**Figure 7.4C**). The peripheral corneal thickness was shown to be significantly increased in the WT cornea compared to the FBN1$^{+/-}$ model when a Mann-Whitney U test was used (p = 0.00008009) (**Figure 7.4E**). The mean peripheral corneal thickness was 37.99 ± 6.07 μm in the WT corneas and 26.67 ± 3.49 μm in the FBN1$^{+/-}$ corneas.

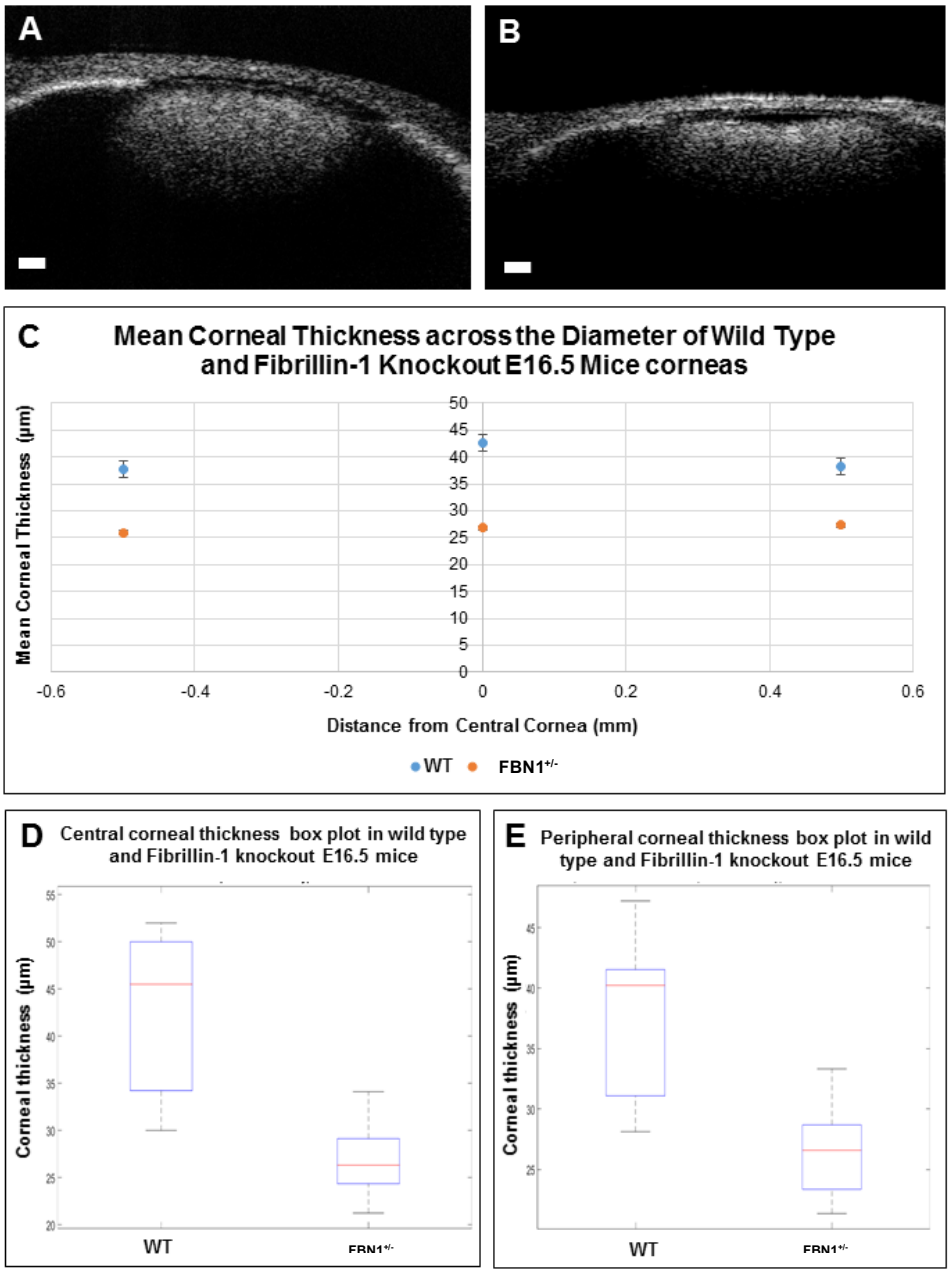

Figure 7.4. E16.5 wild type (WT) and fibrillin-1 knockout (FBN1$^{+/-}$) mouse cornea optical coherence tomography (OCT) imaging and analysis.

Fig 7.4A: WT cornea OCT analysis (Scale bar = 50 µm). **Fig. 7.4B:** FBN1$^{+/-}$ cornea OCT analysis (Scale bar = 50 µm). **Fig. 7.4C:** Scatter graph plotting WT and FBN1$^{+/-}$ corneal thickness measurements across the diameter of the cornea. The WT cornea was thicker in all areas measured across the cornea compared to the FBN1$^{+/-}$ cornea. **Fig. 7.4D and Fig. 7.4E:** Central and peripheral corneal thickness boxplots comparing WT and FBN1$^{+/-}$ corneal thickness measurements.

7.3.1.3. E14.5

Corneal thickness was measured across the diameter of the E14.5 WT and FBN1$^{+/-}$ mice. Central corneal thickness within the WT cornea ranged between 18.67 and 31.78 µm, with a mean of 25.28 ± 4.62 µm (**Figure 7.5A**). Central corneal thickness within FBN1$^{+/-}$ corneas ranged between 21.02 and 25.47 µm, with a mean of 23.13 ± 1.56 µm (**Figure 7.5B**). The central corneal thickness within the WT was not statistically significantly different in comparison to the FBN1$^{+/-}$ mouse model (Mann-Whitney U test; p=0.1564) (**Figure 7.5D**). The mean peripheral corneal thickness in the WT cornea was 21.66 ± 3.42 µm. The mean peripheral corneal thickness in the FBN1$^{+/-}$ mouse cornea was 21.76 ± 1.88 µm. The peripheral corneal thickness was not statistically significantly different between the WT and FBN1$^{+/-}$ corneas (Mann Whitney U test; p = 0.9631) (**Figure 7.5E**).

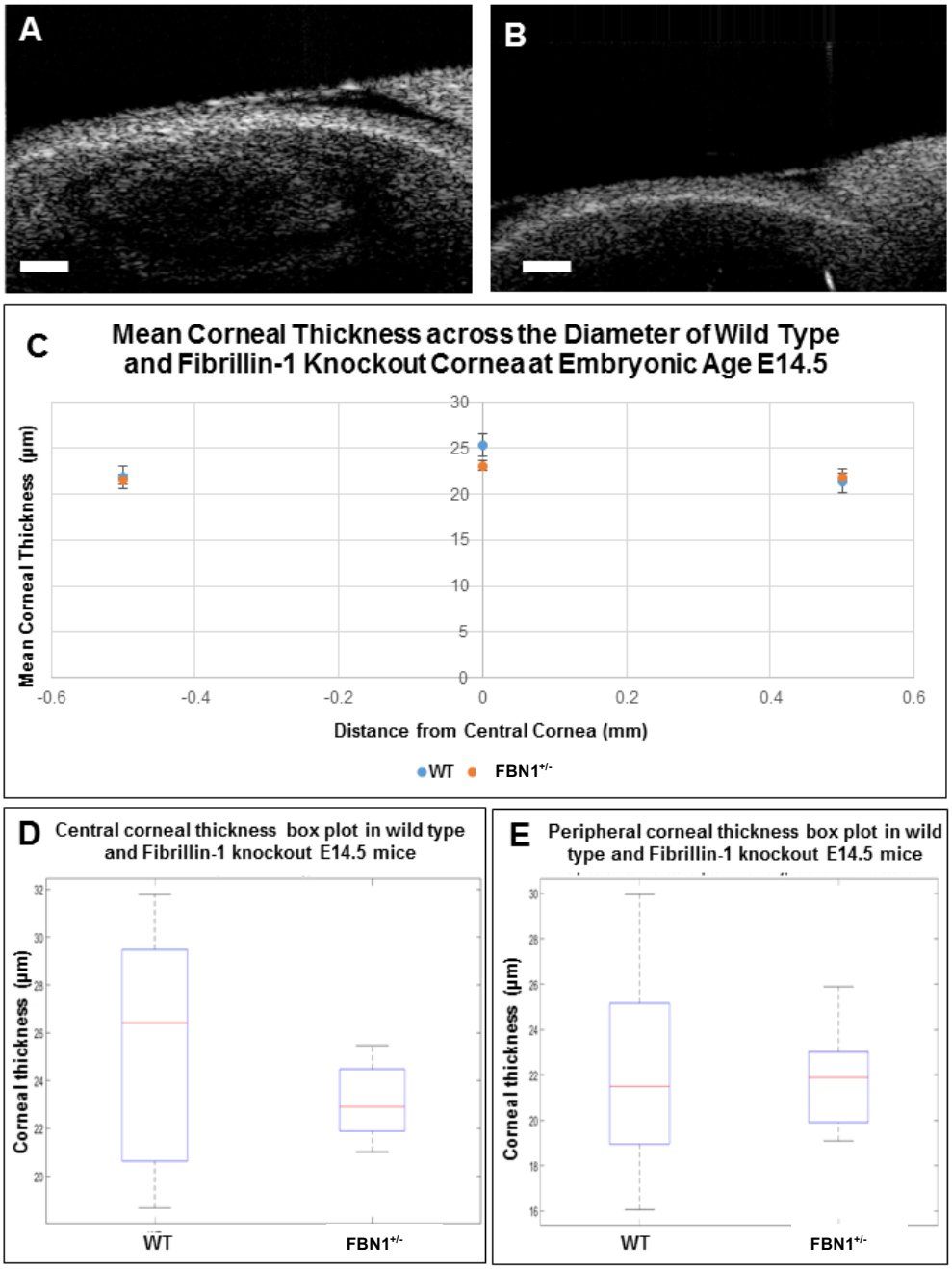

Figure 7.5. E14.5 wild type (WT) and fibrillin-1 knockout (FBN1$^{+/-}$) mouse cornea optical coherence tomography (OCT) imaging and analysis.

Fig 7.5A: WT cornea OCT analysis (Scale bar = 50 µm). **Fig. 7.5B:** FBN1$^{+/-}$ cornea OCT analysis (Scale bar = 50 µm). **Fig. 7.5C:** Scatter graph plotting WT and FBN1$^{+/-}$ corneal thickness measurements across the diameter of the cornea. **Fig. 7.5D and Fig. 7.5E:** Central and peripheral corneal thickness boxplots comparing WT and FBN1$^{+/-}$ corneal thickness measurements.

7.3.1.4. E12.5

OCT was carried out on the WT and FBN1$^{+/-}$ eyes at E12.5 of embryonic development. It was unclear as to where the cornea and the corneoscleral junction was, therefore, no corneal radius or corneal thickness measurements were recorded (**Figure 7.6**).

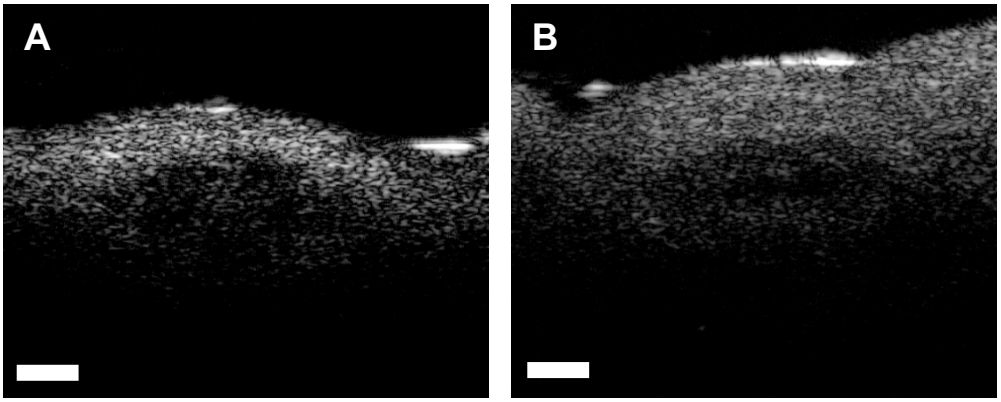

Figure 7.6. Optical coherence tomography (OCT) imaging of the wild type (WT) and fibrillin-1 knockout (FBN1$^{+/-}$) mouse corneas at embryonic age E12.5.

Fig 7.6A: WT eye OCT analysis (Scale bar = 50 μm). **Fig. 7.6B:** FBN1$^{+/-}$ eye OCT analysis (Scale bar = 50 μm). The cornea could not be identified in any of the images.

7.3.2. SAXS Results

7.3.2.1. Interfibrillar spacing

In both the WT and FBN1$^{+/-}$ mouse corneas the interfibrillar spacing (IFS) increased from the central cornea to the periphery, producing a U-shaped distribution on the radial plots (**Figure 7.7A**). IFS ranged between 40.73 and 55.63 nm within the WT central cornea with a mean IFS value of 48.27 ± 5.00 nm (**Figure 7.7B**). IFS ranged between 45.28 and 62.60 nm within the FBN1$^{+/-}$ mouse central corneas with a mean measurement of 55.71 ± 6.03 nm (**Figure 7.7C**). Mean centre-centre spacing was plotted to compare the WT and FBN1$^{+/-}$ corneas. Central cornea IFS was increased within the FBN1$^{+/-}$ corneas, a two-sample t-test showed a statistically significant increase in IFS with the FBN1$^{+/-}$ compared to the WT corneas (p=0.04190) (**Figure 7.7B**). The WT and FBN1$^{+/-}$ corneas had an increased IFS from the central cornea to the peripheral cornea. Peripheral IFS in the WT cornea ranged between 51.28 and 79.60 nm with a mean IFS value of 59.73 ± 7.62 nm. Peripheral IFS in the FBN1$^{+/-}$ corneas showed a large range between 51.52 and 100.13 nm, with a mean of 73.21 ± 14.84 nm (**Figure 7.7C**). Statistical analysis with a two-sample t-test did not show a significant increase in IFS in the peripheral cornea in the FBN1$^{+/-}$ mouse model compared to the WT corneas (p = 0.08070) (**Figure 7.7C**).

SAXS of all tissues at E18.5 did not produce a scatter pattern, therefore only the adult corneas were analysed.

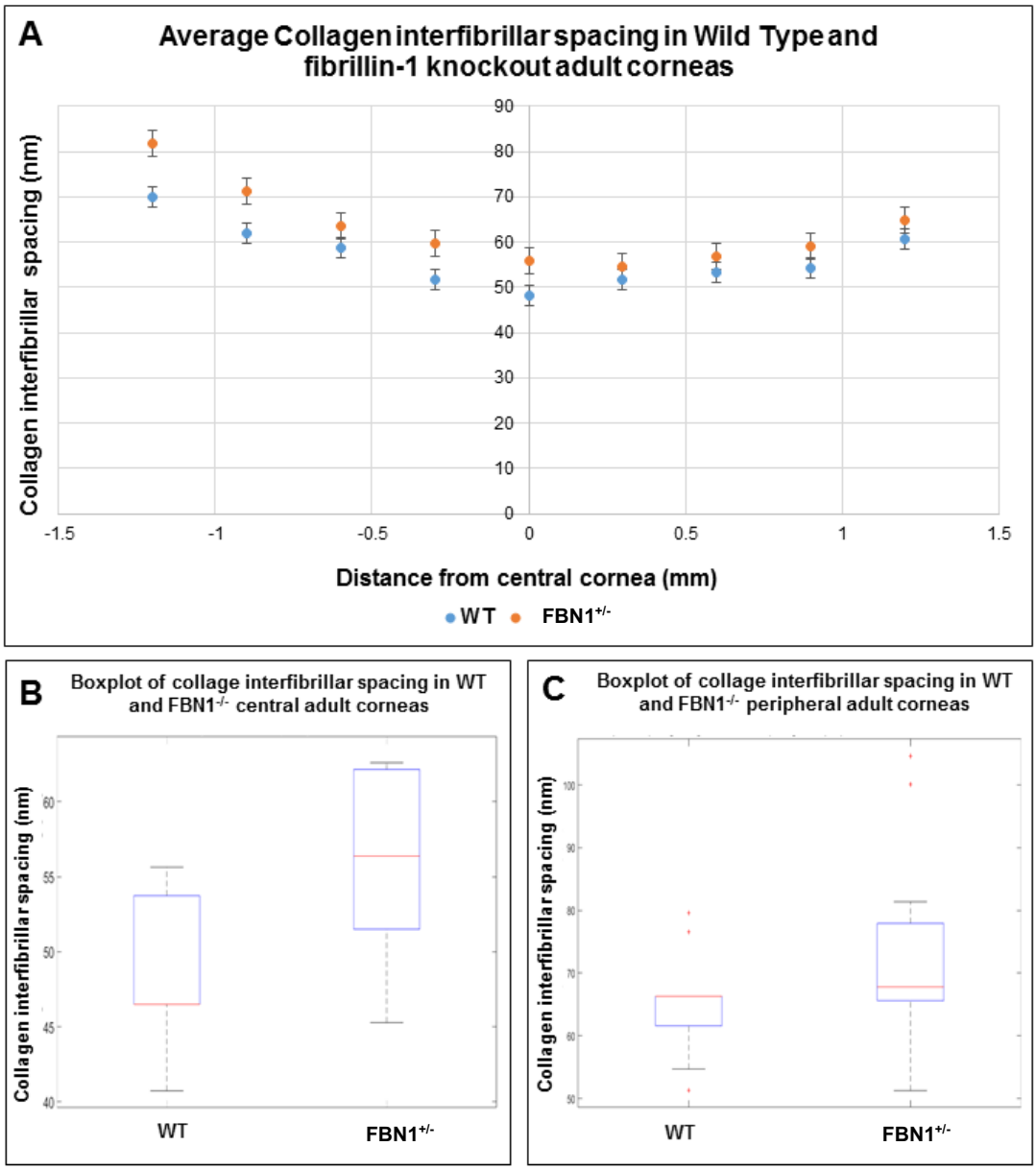

Figure 7.7. Collagen interfibrillar spacing results in the wild type (WT) and fibrillin-1 knockout (FBN1$^{+/-}$) adult mouse corneas.

Fig. 7.7A: Scatter graph of average collagen interfibrillar spacing across the diameter of the cornea in the WT and FBN1$^{+/-}$ cornea; FBN1$^{+/-}$ had increased average interfibrillar spacing measurements compared to the WT cornea. **Fig. 7.7B and Fig. 7.7C:** Boxplots of collagen interfibrillar spacing measurements in WT and FBN1$^{+/-}$ central and peripheral corneas.

7.3.2.2. SAXS Results – Collagen Fibril Diameter

Average collagen fibril diameter measurements increased from the central cornea to the peripheral cornea in both the WT and FBN1$^{+/-}$ mouse corneas (**Figure 7.8A**). The average fibril diameters at different positions across the corneal diameter increased in the FBN1$^{+/-}$ corneal tissue compared to the WT. The central corneal collagen fibril diameter was increased in the FBN1$^{+/-}$ corneas compared to the WT, however, this was statistically insignificant (two-tailed t-test; $p > 0.05$) (**Figure 7.8B**). The central collagen fibril diameter in the WT cornea ranged between 32.93 and 36.01 nm, with an average of 34.35 ± 1.12 nm. The central collagen fibril diameter in the FBN1$^{+/-}$ corneas ranged between 34.71 and 37.21 nm, with an average of 35.88 ± 0.89 nm. The fibril diameter was also increased at the periphery of the FBN1$^{+/-}$ corneas compared to the WT corneal tissue. Peripheral collagen fibril diameters in the FBN1$^{+/-}$ corneas ranged between 35.28 and 41.93 nm, with a mean measurement of 38.07 ± 2.19 nm. Peripheral collagen fibril diameters in the WT cornea ranged between 34.10 and 41.64, with an average measurement of 36.95 ± 2.17 nm. The peripheral collagen fibril diameter measurements were not significantly different between the FBN1$^{+/-}$ and WT corneas (Mann-Whitney U test; $p > 0.05$) (**Figure 7.8C**).

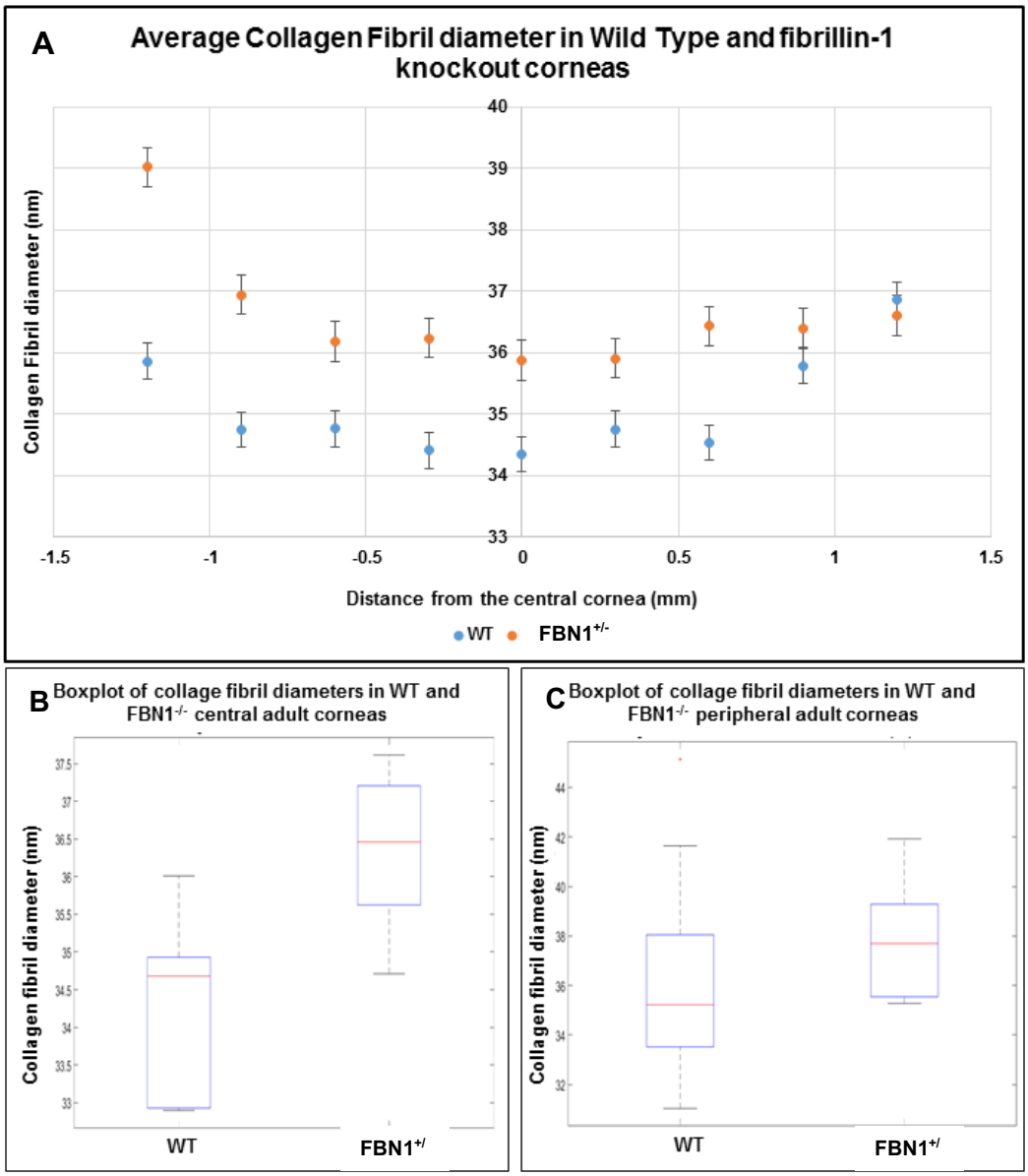

Figure 7.8. Collagen fibril diameter results in wild type (WT) and fibrillin-1 knockout (FBN1$^{+/-}$) adult mouse corneas.

Fig. 7.8A: Scatter graph of average collagen fibril diameters from periphery to periphery of the WT and FBN1$^{+/-}$ cornea; FBN1$^{+/-}$ had increased average collagen fibril diameter measurements compared to the WT cornea. **Fig. 7.8B and Fig. 7.8C:** Boxplots of collagen fibril diameter measurements in WT and FBN1$^{+/-}$ central and peripheral corneas. There was no statistical significance in collagen fibril diameter measurements between WT and FBN1$^{+/-}$ corneas.

7.3.3. Electron Microscopy

7.3.3.1. Collagen ultrastructure analysis by transmission electron microscopy (TEM)

The corneal collagen ultrastructure was imaged and qualitatively assessed with TEM (**Figure 7.9**). The adult and E18.5 $FBN1^{+/-}$ mouse central corneal IFS appeared to be increased compared to the WT tissue. Differences between IFS were not clearly seen in the E14.5 and E16.5 corneas. The diameter of the collagen fibrils in the in $FBN1^{+/-}$ corneas aged E16.5 were larger than the WT cornea, however, this observation was not obvious in other ages analysed. The thicker collagen fibrils in decorin and biglycan knockout mouse models have a cauliflower appearance that is similar to some of the collagen fibrils seen in the results (Zhang G. et al. 2009).

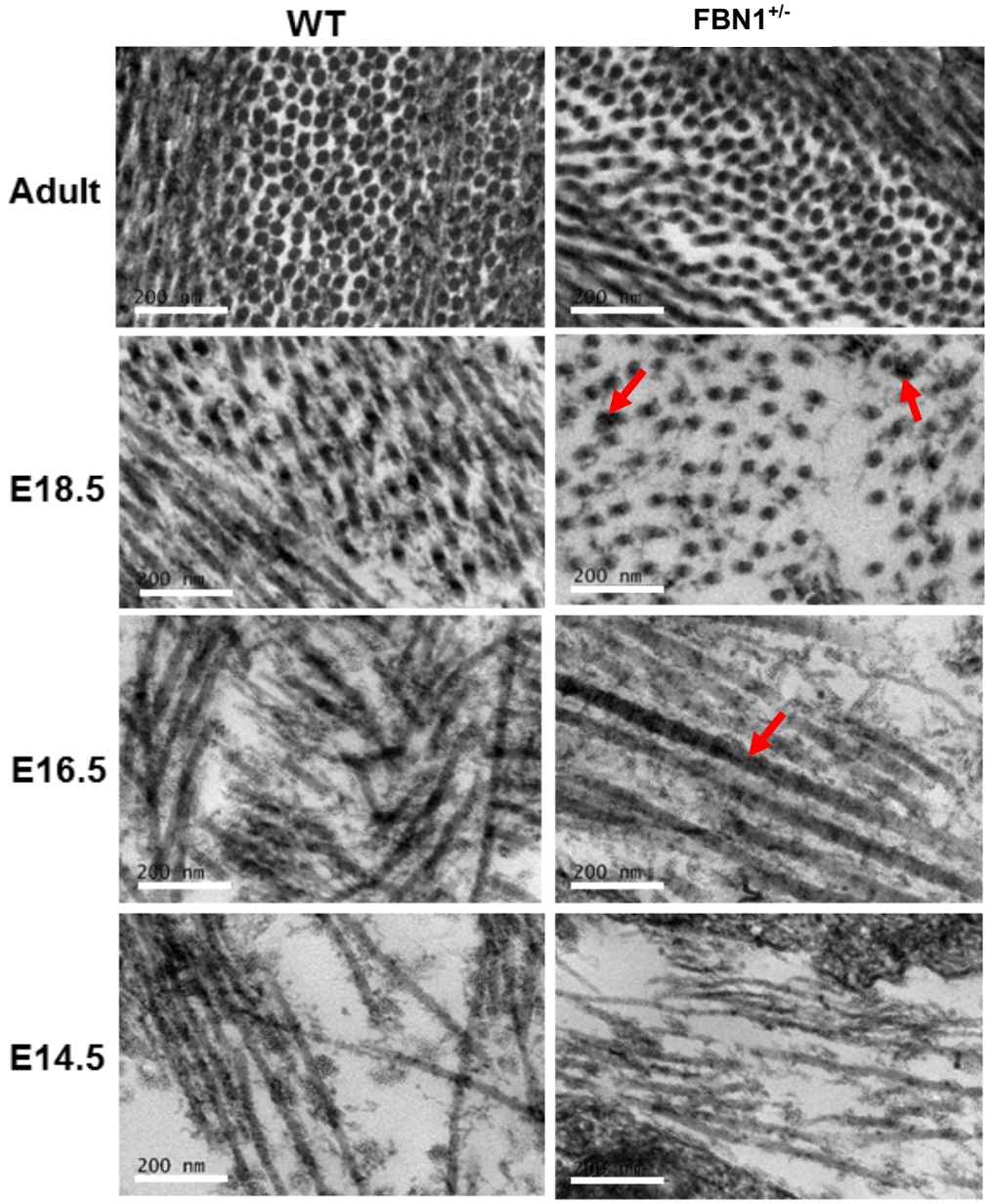

Figure 7.9. Transmission Electron Microscopy (TEM) imaging of the collagen fibrils in the central cornea of wild type (WT) and fibrillin-1 knockout model (FBN1$^{+/-}$).

High magnification imaging with TEM showed greater spacing collagen interfibrillar spacing in the central cornea of the FBN1$^{+/-}$ corneas compared to the WT corneas in the adult and E18.5 embryonic corneas. Some collagen fibril diameters appeared to be increased in the FBN1$^{+/-}$ corneas compared to the WT from E16.5 of corneal development (red arrows). Scale bars = 200 nm.

7.3.3.2. Elastic fibre analysis by serial block-face scanning electron microscopy (SBF-SEM) and transmission electron microscopy (TEM)

SBF-SEM imaging revealed an extensive 3-D network of fibres with increased contrast in both the WT and FBN1$^{+/-}$ adult mouse models (**Figures 7.10**). The area directly anterior to Descemet's membrane, in the posterior periphery of the cornea, was chosen for analysis in both models due to the known abundance of elastic fibres there. As expected, within the adult 3-D WT models, a concentration of fibres was seen anteriorly to Descemet's membrane. Individual fibres were present in the posterior corneal stroma, running in parallel rows and branching within the same plane. Analysis of the FBN1$^{+/-}$ adult mouse cornea also revealed fibres with increased contrast in the posterior peripheral cornea. There was an enhancement of fibres anterior to Descemet's membrane, but this concentration was not as vast as the WT model. The fibres appeared to have some disorganisation compared to the WT cornea, with some individual fibres branching in different directions (**Figure 7.10 and supplementary video 8 and supplementary video 9**). TEM revealed elastic fibres with an increased contrast composed of microfibrils ~10-12 nm in diameter, which bundled together to form larger fibres (**Figure 7.13**). For greater detail of the three-dimensional reconstructions, please refer to supplementary video 8 and supplementary video 9.

SBF-SEM revealed individual fibres with enhanced contrast in the posterior of the developing mouse cornea in both the WT and FBN1$^{+/-}$ mouse models at the embryonic age E18.5 (**Figure 7.11**). 3-D reconstructions did not show a clear difference between the elastic fibre ultrastructure, with fibres appearing to run longitudinally and branch off in the same plane as the lamellae in both the WT and FBN1$^{+/-}$ corneas analysed (**Figure 7.11**). The TEM analysis of the fibres at E18.5 showed bundles of microfibrils ~10-12 nm in diameter within the larger fibre component, typical of fibrillin-rich microfibrillar structures (**Figure 7.13**).

Serial block-face scanning electron microscopy revealed individual elastic fibres in the posterior of the developing mouse cornea in both the WT and the FBN1$^{+/-}$ mouse models at the embryonic age E16.5 (**Figure 7.12**). 3-D elastic fibre reconstructions did not show any obvious differences between the WT and the FBN1$^{+/-}$ mouse models. The fibres could only be reconstructed using manual techniques, this made it difficult to detect all of the fibres. Some of the fibres that were found ran longitudinally in the corneal stroma and branched off, continuing in the same plane as the collagen lamellae (**Figure 7.12**). Transmission electron microscopy imaging of the fibres showed microfibrils ~10-12 nm in diameter bundling to form larger fibres (**Figure 7.13**). At E16.5, the microfibrils formed a loose bundle of fibrils, increasing in density with increased age.

No dense amorphous core was seen in any of the fibres analysed within the cornea in any of the ages analysed, indicating that true elastic fibres were not present (**Figure 7.13**). In addition, no elastic fibres were identified with SBF-SEM and TEM imaging in both the WT and FBN1$^{+/-}$ mouse models at the embryonic age E14.5.

Supplementary video 8 link: *https://figshare.com/s/ede3a79f87dff874bc9f*

Supplementary video 9 link: *https://figshare.com/s/e435cbfd4e10309d81e7*

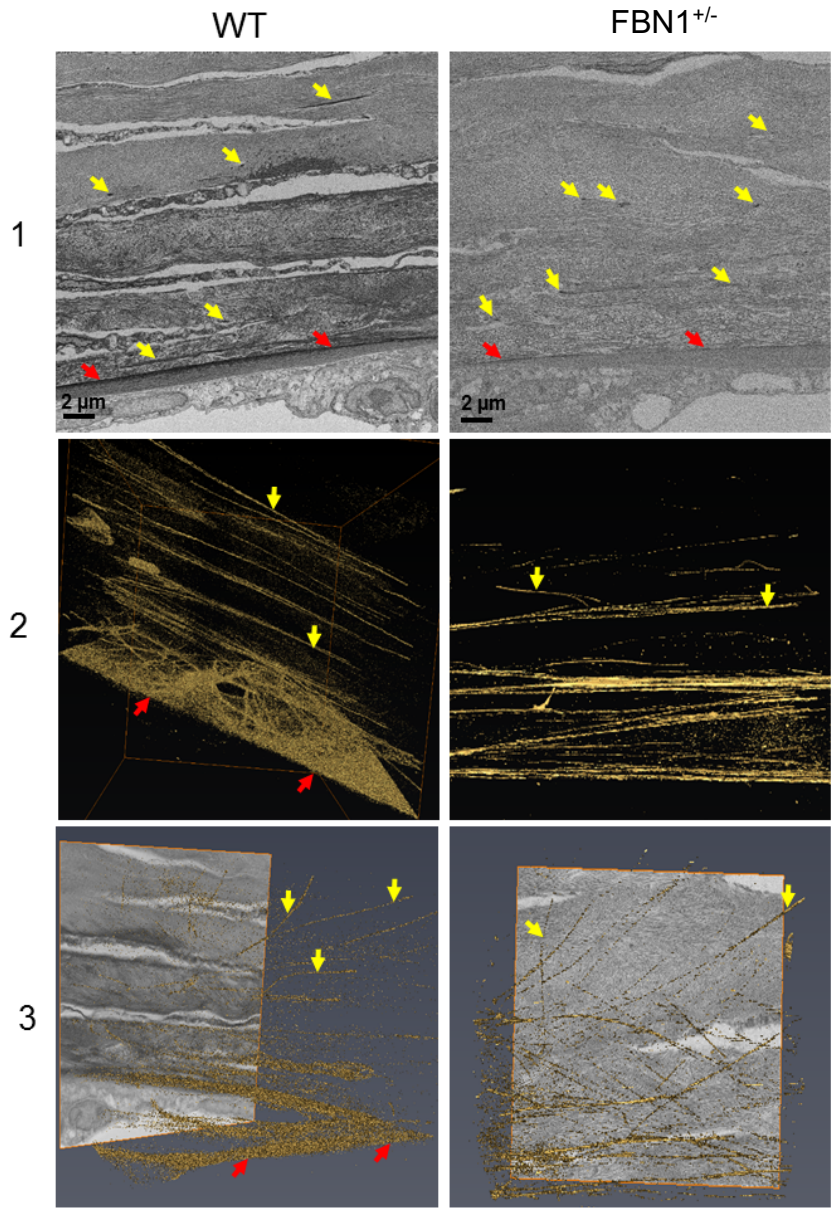

Figure 7.10. Serial block-face scanning electron microscopy (SBF-SEM) dataset of the adult wild type (WT) and fibrillin-1 knockout (FBN1$^{+/-}$) mouse corneas.

SBF-SEM imaging of the adult mouse corneas generated 3-D models of the elastic fibre system. Panel 1 shows the peripheral aspect of the WT and FBN1$^{+/-}$ mouse corneas in the posterior corneal stroma. A concentrated network of elastic fibres was seen anterior to Descemet's membrane (red arrows) more enhanced in the WT cornea, with individual fibres within the posterior corneal stroma (yellow arrows). The 3-D elastic fibre models are seen in panels 2 and 3. The WT and FBN1$^{+/-}$ elastic fibres ran in a parallel orientation throughout the corneal stroma, with some fibres branching and continuing in the same plane as the collagen lamellae. Some of the FBN1$^{+/-}$ elastic fibres appeared to run in different directions, with some disorganisation compared with the WT. Refer to supplementary videos 9 and 10 for greater detail of the WT and FBN1$^{+/-}$ elastic fibre system within the posterior corneal stroma.

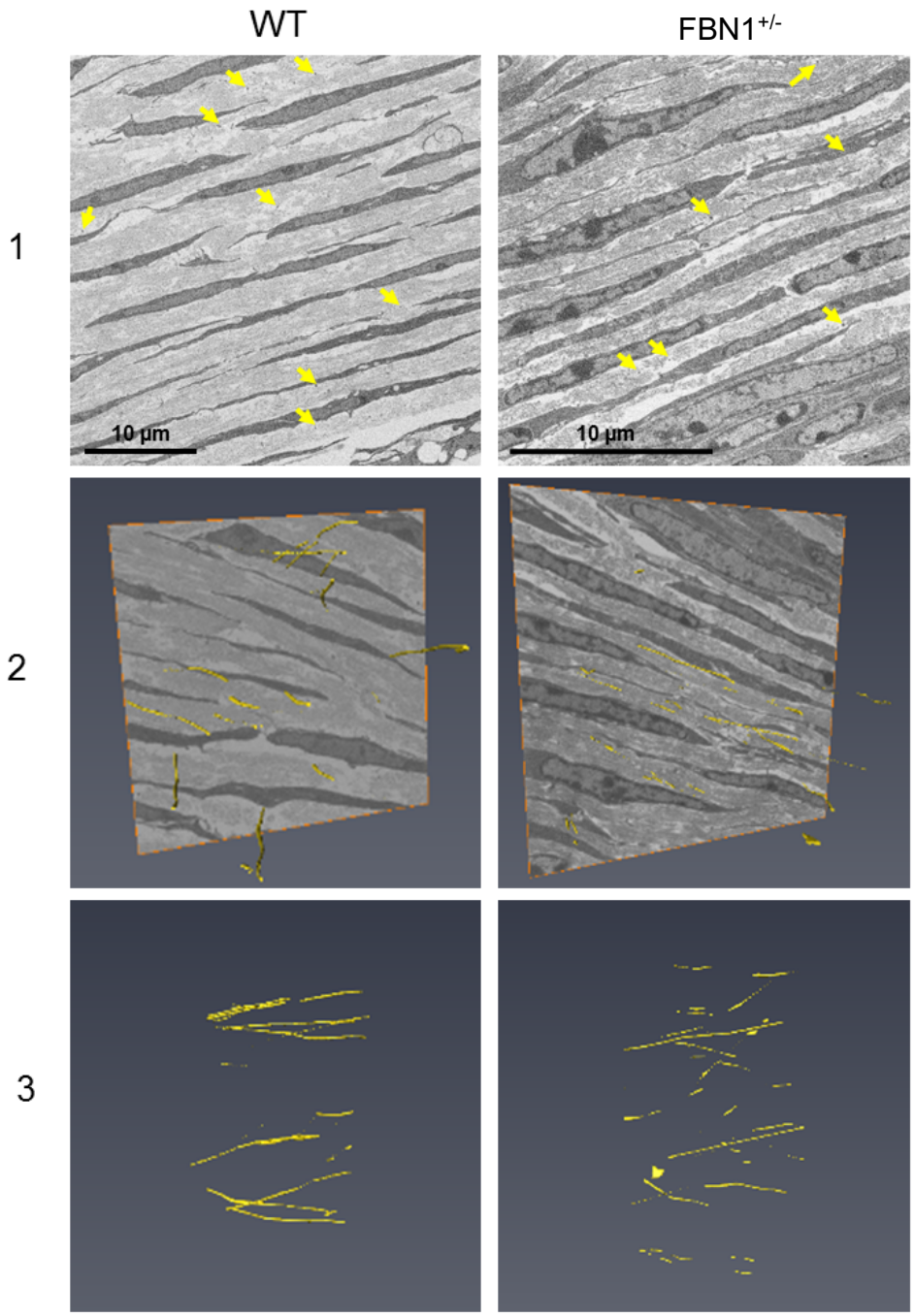

Figure 7.11. Serial block-face scanning electron microscopy (SBF-SEM) dataset of the wild type (WT) and fibrillin-1 knockout (FBN1$^{+/-}$) developing mouse cornea at embryonic age E18.5.

SBF-SEM imaging of the developing E18.5 mouse corneas showed the 3-D elastic fibre system. Panel 1 shows the posterior peripheral region of the developing WT and FBN1$^{+/-}$ mouse corneas. In these images individual elastic fibres were found in the posterior corneal stroma (yellow arrows). 3-D elastic fibre reconstructions are shown in panels 2 and 3. No significant differences between the elastic fibre organisations between the WT and FBN1$^{+/-}$ mouse cornea was identified.

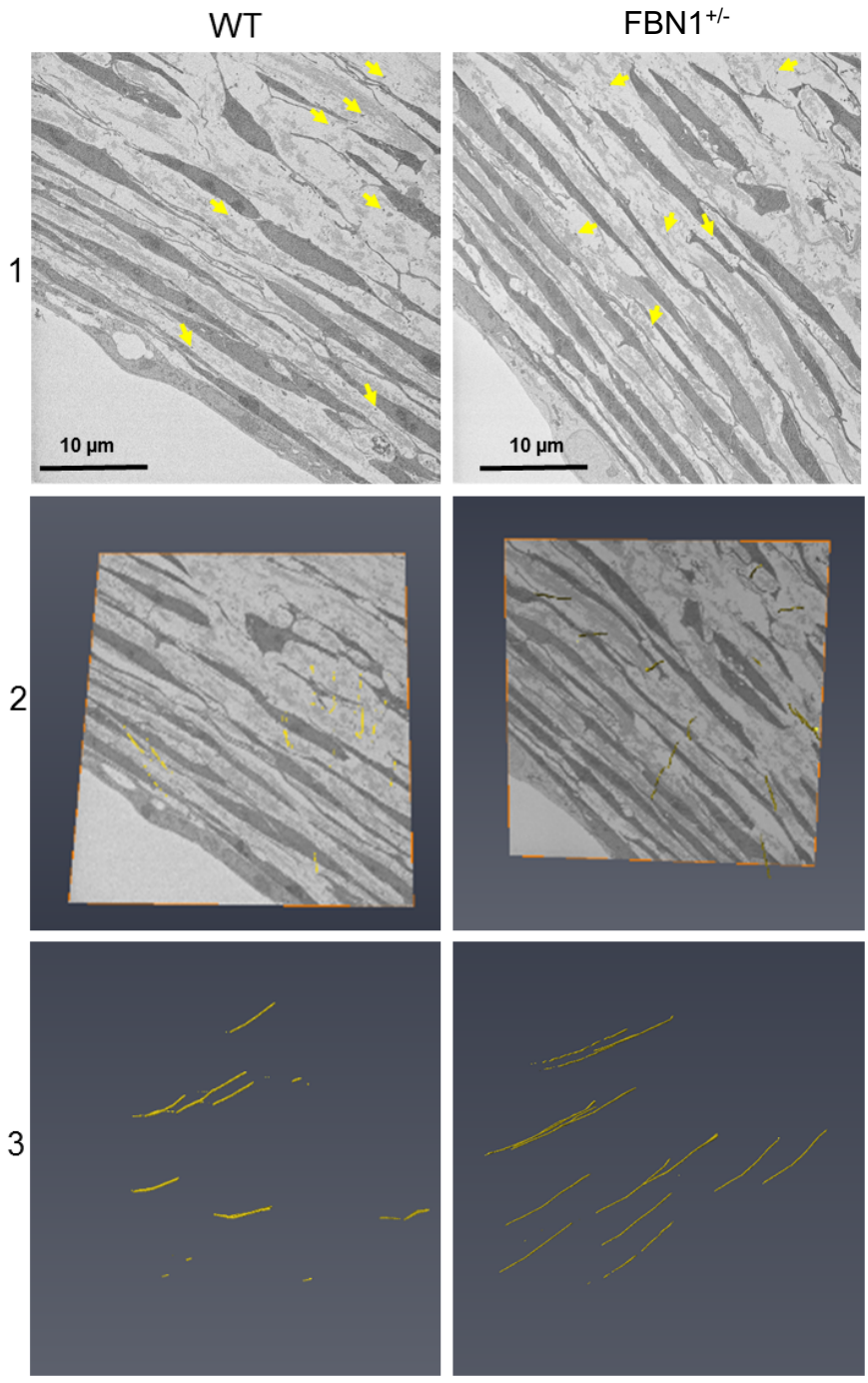

Figure 7.12. Serial block-face scanning electron microscopy (SBF-SEM) dataset of the wild type (WT) and fibrillin-1 knockout (FBN1$^{+/-}$) developing mouse cornea at embryonic age E16.5.

SBF-SEM imaging of the developing E16.5 mouse corneas generated 3-D models of the elastic fibre system. Panel 1 shows the posterior peripheral aspect of the developing WT and FBN1$^{+/-}$ mouse cornea. Individual elastic fibres were present in the posterior corneal stroma (yellow arrows). Elastic fibre reconstructions showed the organisation of the elastic fibre system in panels 2 and 3. The organisation between the WT and FBN1$^{+/-}$ mouse cornea did not show any differences.

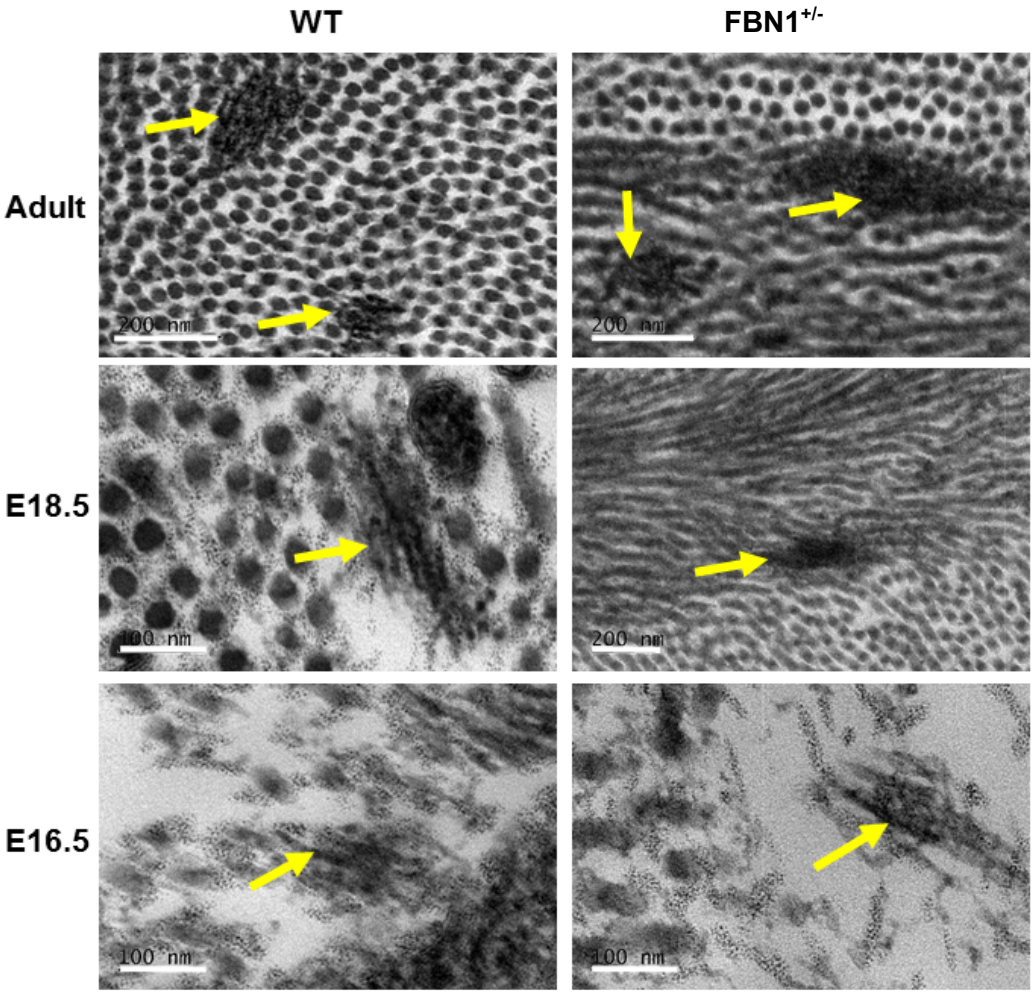

Figure 7.13. Transmission electron microscopy (TEM) imaging of the elastic fibres in the cornea

Elastic fibres were initially seen at E16.5 of mouse corneal development as loose microfibrils ~10-12 nm in diameter, characteristic of fibrillin microfibrils. With increased development the microfibrils appeared to mature, forming bundles of microfibrils with increased density. These fibres were found throughout the corneal stroma in WT and FBN1$^{+/-}$ tissue at E16.5, E18.5 and adult. Scale bars measure 200 nm for all images except the E16.5 and E18.5 WT and the E16.5 FBN1$^{+/-}$ which measure 100 nm.

7.3.4. Immuno-electron microscopy results

Decorin is a small-leucine rich proteoglycan that is known to regulate collagen fibril ultrastructure. In addition, decorin levels are reduced when transforming growth factor beta levels are elevated, as is described in Marfan syndrome. Because of both of these reasons, the localisation of decorin was analysed using immunogold labelling to understand whether reduced decorin levels could be responsible for disrupting the collagen fibril ultrastructure that has been identified in the fibrillin-1 knockout mouse model. The hypothesis is that decorin levels reduce in the fibrillin-1 knockout mouse model compared to the wild type.

7.3.4.1. Decorin

Positive gold-labelling was present in the WT and FBN1$^{+/-}$ adult corneas, with no gold-labelling found on the control sections (**Figure 7.14**). Gold-labelling was identified between the collagen fibrils in the corneal stroma. Quantitative analysis was carried out to determine any significant difference between the staining profiles in the WT and FBN1$^{+/-}$ corneas. The amount of gold labelling was quantified in each image taken at an x20 magnification for both WT and FBN1$^{+/-}$ corneas. A Mann-Whitney U test showed a statistically significant difference between gold particle labelling in the WT and FBN1$^{+/-}$ adult cornea ($p = 0.00007964$) (**Figure 7.15**). This indicates a reduction of the decorin core proteoglycan within the corneal stromal extracellular matrix in the FBN1$^{+/-}$ adult cornea compared to the WT cornea.

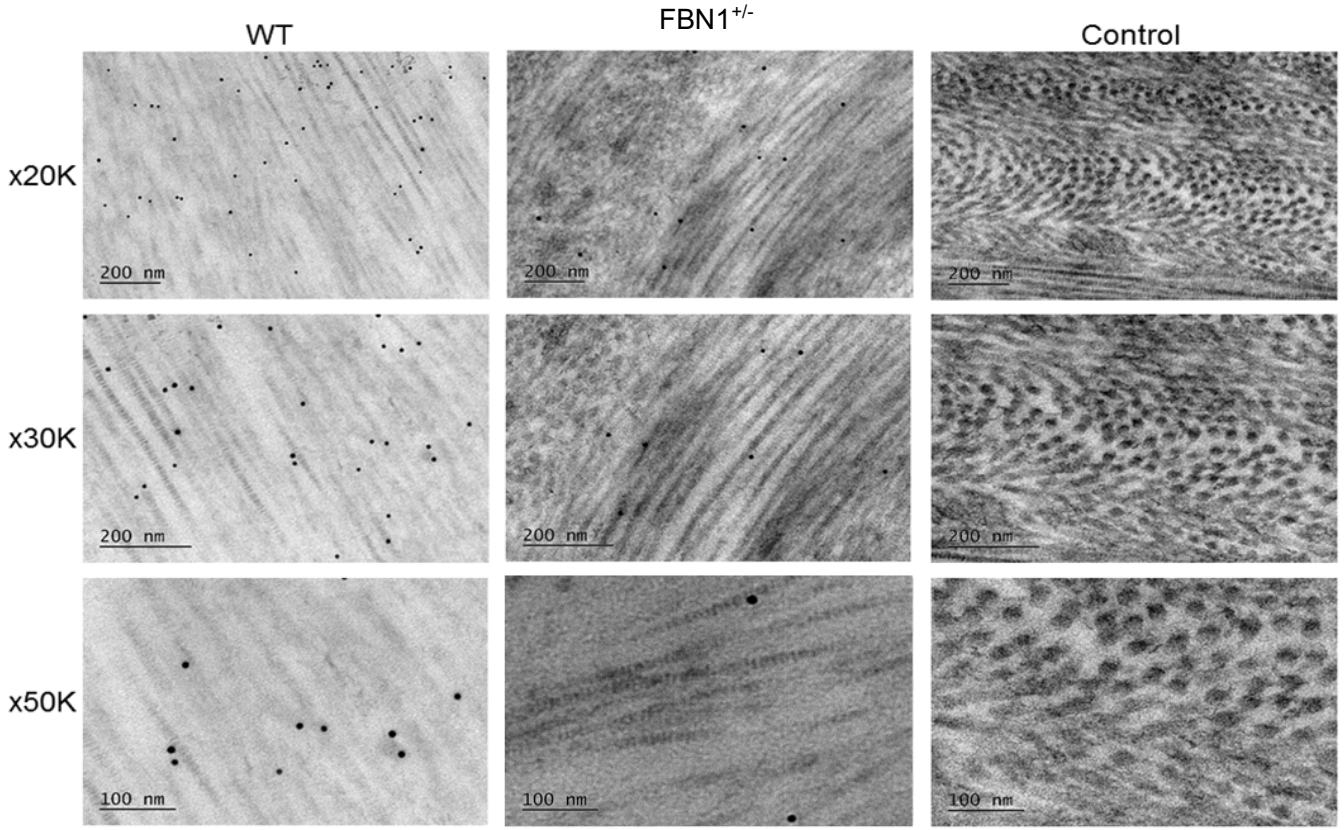

Figure 7.14. Transmission Electron Microscopy (TEM) imaging of the wild type (WT) and fibrillin-1 knockout (FBN1$^{+/-}$) corneas with decorin immuno-gold particle labelling.

Decorin positively labelled in both WT and FBN1$^{+/-}$, with no positive staining being detected in the control sections containing no primary antibody. Decorin mainly labelled between and on top of collagen fibrils in both models. Quantitative analysis of the gold particles was undertaken to determine any differences in staining between the WT and FBN1$^{+/-}$ adult corneas. Scale bars measure 200 nm for x20K and x30K. Scale bars measure 100 nm for x50K.

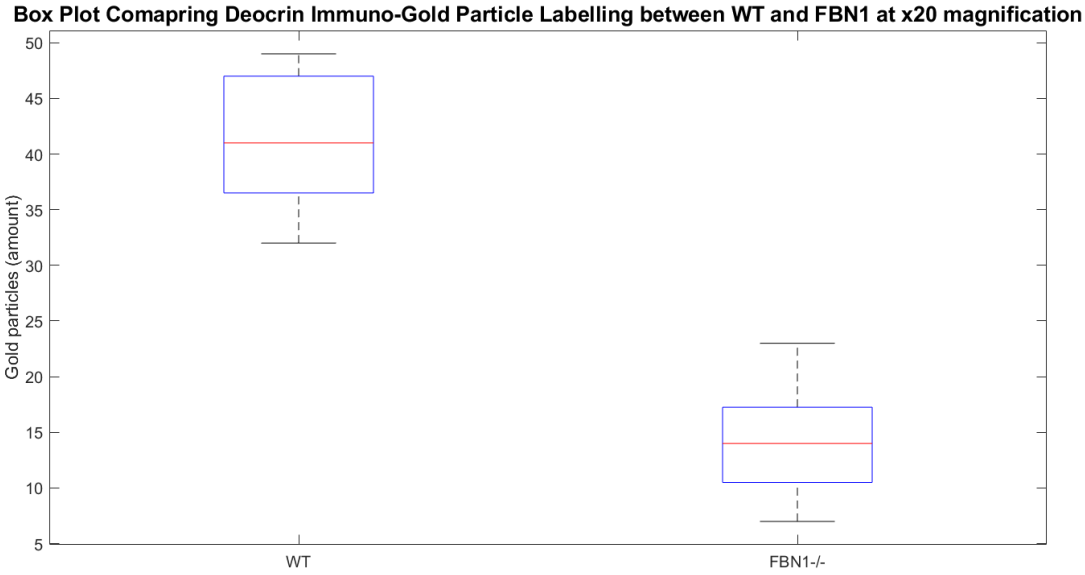

Figure 7.15. Boxplots comparing gold particle labelling of Decorin in Wild type (WT) and Fibrillin-1 knockout mouse corneas ($FBN1^{+/-}$)

There was a statistical significance of the amount of gold labelling particles between the WT and $FBN1^{+/-}$ corneal images at all magnifications analysed ($p < 0.05$). At x20 magnification the average number of particles was 41.18 and 13.73 within WT and $FBN1^{+/-}$ images respectively.

7.4. Discussion

This chapter aimed to analyse the mature and embryonic cornea when the elastic fibre system is disrupted. The development of the wild type cornea was compared to the development of the cornea in a fibrillin-1 knockout mouse model which displayed phenotypic similarities to MFS. The developmental stages E12.5, E14.5, E16.5, E18.5 and 6-month adults were chosen for analysis. This study is the first to have used this specific mouse model to analyse corneal development. For simplicity, the knockout model was referred to as "FBN1$^{+/-}$" and the wild type "WT".

The optical coherence tomography (OCT) data collected in this study showed a significant reduction in corneal thickness in the adult, E18.5 and E16.5 FBN1$^{+/-}$ corneas. Tissue younger than E16.5 had no significant thickness differences compared with the WT data, which suggests that fibrillin-rich microfibrils have a role in tissue architecture from E16.5 of mouse corneal development. The corneal radius of curvature measurements for adult and E18.5 showed no significantly different results; this indicated that corneal curvature was not altered in the FBN1$^{+/-}$ mouse model. This was an interesting observation as corneal curvature reductions have been described in some patients with MFS (Maumenee 1981, Sultan et al. 2002).

The next phase of experiments was carried out to understand, the changes, if any, to corneal stromal ultrastructure that could potentially cause the reduction of stromal thickness. To determine any collagen fibril ultrastructural disruptions within the FBN1$^{+/-}$ model, small X-ray scattering (SAXS) studies were conducted. This experiment was undertaken to measure collagen fibril diameter and collagen interfibrillar spacing. In both the WT and FBN1$^{+/-}$ adult corneas, average collagen interfibrillar spacing and collagen fibril diameter increased between the central and the peripheral cornea. Similar results have previously been reported for the human and mouse cornea that show a U-shaped distribution (Boote et al. 2003, Boote et al. 2012, Young et al. 2009). The mouse cornea is also thinner in the peripheral cornea in comparison to the central cornea, therefore fewer collagen fibrils must be present to

accommodate for the increase in fibril diameter and spacing (Henriksson et al. 2012). Results also revealed that the central collagen interfibrillar spacing was significantly increased in the FBN1$^{+/-}$ model compared to the WT corneas. As corneal thickness is significantly less in the FBN1$^{+/-}$ model, the results suggest that there is overall fewer collagen fibrils present within the FBN1$^{+/-}$ cornea than in the WT cornea. No significant difference was found in fibril diameter measurements, a greater sample number should be analysed in the future to determine significance. Unfortunately, the amount of tissue available to analyse was limited from the source in Brazil and the sample numbers could not be increased.

The embryonic ages analysed with SAXS did not give a strong enough signal to retrieve a SAXS pattern. To generate a SAXS pattern, a significant amount of organised collagen fibrils must be present. The number of organised collagen fibrils within the prenatal mouse cornea was not sufficient to generate a dataset. The mouse corneas continue to develop after birth and these stages could be further analysed by SAXS to identify any changes to the collagen fibril network at a younger age than the adult. To overcome the challenge of analysing collagen fibril ultrastructure with SAXS in the prenatal corneas, electron microscopy techniques were employed to image the embryonic corneal stromal ultrastructure.

TEM imaging showed that the central cornea in the FBN1$^{+/-}$ mouse model has some larger collagen fibril diameters in corneas older than E16.5 compared to the WT mouse corneas. In addition, collagen interfibrillar spacing was greater in the FBN1$^{+/-}$ adult and E18.5 corneas. Interfibrillar spacing decreased as the age of the embryos increased, which eventually appeared to show no difference between the FBN1$^{+/-}$ and WT collagen in the E14.5 and E16.5 corneas. At these very early stages, collagen fibrils were being laid down and there was much extracellular matrix space between them, suggesting that collagen deposition and organisation was not complete. These results correlate with the adult SAXS data, where collagen fibril spacing, and fibril diameter were shown to be greater in the adult FBN1$^{+/-}$ knockout mouse model compared with the WT corneas. SAXS allow the analysis of hydrated tissue

and therefore gives a more accurate measurement of collagen fibril size and arrangement, both of which depend on tissue hydration. Loss of tissue hydration, which occurs during electron microscope preparation, would reduce collagen interfibrillar spacing and collagen fibril diameter measurements. In addition, unlike electron microscopy, X-rays pass through the entire thickness of the cornea, therefore the measurements are averages through the whole corneal stroma (Rawe et al. 1994).

SBF-SEM and TEM techniques were then used to analyse the elastic fibre system with a tannic acid – uranyl acetate based processing method. This method enhances the contrast of elastic fibres for electron microscopy imaging. 3-D visualisation showed the elastic fibres to be concentrated directly anterior to Descemet's membrane in the adult cornea, whilst individual fibres were present throughout the corneal stroma. The elastic fibres had increased disorganisation within the adult $FBN1^{+/-}$ corneas compared to the adult WT corneas. Fibres were also identified within the E16.5 and E18.5 corneas, but they were not easy to detect using the isosurface rendering function. Therefore, it was unclear whether there were any significant changes in the organisation between the embryonic WT and $FBN1^{+/-}$ mouse corneas. TEM was further used to identify the morphology of the fibres. E16.5, E18.5 and adult corneas did not show an amorphous-core within the elastic fibres, which suggests that no elastin was present. Instead, the fibres were composed of many microfibrils which were ~10-12 nm in diameter, characteristic of fibrillin-microfibrils (Wang et al. 2009). Analysis of the corneas aged E14.5 did not identify any fibres, which indicated that the elastic fibre network has not begun to develop or was too sparse to be detected by the method used in this chapter.

The results suggest that the $FBN1^{+/-}$ mouse cornea was not altered until E16.5 of embryonic development. Alterations were also more evident in the adult model, which suggests that the adult tissue has greater corneal disruptions than the developing tissue. Therefore, these results suggest that fibrillin-1 does not have a role in the initial development of the cornea and does not affect the structure of the cornea until E16.5. These results also suggest that

fibrillin-1 has a greater role in the mechanisms that maintain structure in the adult cornea when compared with the embryonic stages. This could be explained by fibrillin-1 having a prominent role in adult tissues for structural support, compared with fibrillin-2, which has a more significant role in embryonic tissues for regulating elastic fibre development (Zhang H. et al. 1995). The localisation of fibrillin-1 in the WT developing mouse cornea has also been shown to increase in E16.5 corneas compared with E12.5 corneas, which further supports that fibrillin-1 has a more prominent role in corneal development from E16.5 (Shi et al. 2013). To further understand whether or not the cornea is affected by the development of elastic fibres, a knockout mouse model of fibrillin-2 could be explored to understand if the initial events of corneal development are disrupted in early elastic fibre assembly (Zhang H. et al. 1995).

The $FBN1^{+/-}$ mouse model analysed in this study has a dysfunctional fibrillin-1 gene, which generates a truncated fibrillin-1 glycoprotein that cannot exit cells to carry out its normal function of extracellular matrix homeostasis. One of these important functions is binding to large latent TGF-β to prevent TGF-β surges which cause pathological alterations to the extracellular matrix structure and function. As the fibrillin-1 glycoprotein cannot exit the cells to carry out this function there is subsequently a surge of latent TGF-β. Previous studies have also shown that an increase in TGF-β in MFS can suppress type I collagen production via the induction of transcription factor CUX1 (Fragiadaki et al. 2011). This pathway could be a potential explanation for the reduction of collagen in the $FBN1^{+/-}$ mouse cornea. A disruption to the collagen fibril network in periodontal ligaments has also been identified in a fibrillin-1 knockout mouse model, which provides evidence of a disrupted collagen fibril network in tissues with MFS (Ganburged 2010). The reduction of collagen can also be explained by a TGF-β surge leading to an enhancement of metalloproteinases 2 and 9, both known to degrade elastic fibres and collagen fibrils (Gomes L. R. et al. 2012). A second study additionally showed metalloproteinases 1 and 3 to be upregulated in cultures when recombinant fibrillin-1 fragments that contained the arginine-glycine-aspartic acid integrin-binding motif is added to understand the pathogenesis of MFS (Booms et al.

2005). The results presented in this chapter also provide evidence that a functional fibrillin-1 system is required to maintain collagen fibril organisation, therefore, an understanding of how and why this organisation is lost is needed.

A pathological increase in latent TGF-β is thought to cause the extracellular matrix changes identified in this chapter. Previous studies have demonstrated this by preventing MFS phenotype progression in a FBN1 mutated mouse model by inhibiting TGF-β signalling (Habashi et al. 2006). However, more recent studies have demonstrated that removal of TGF-β in mouse models exacerbates MFS symptoms, therefore TGF-β could provide a protective function in the pathology (Wei et al. 2017). Furthermore, TGF-β is well known to regulate wound healing and extracellular matrix components, including PGs. Cells that have been incubated with TGF-β for a prolonged time cause decorin levels to decrease; decorin is a PG that plays a crucial role in regulating collagen fibril organisation and fibrillogenesis in the cornea (Kahari et al. 1991, Li et al. 2006, Reed and Iozzo 2002). Animal models have also demonstrated a decrease in decorin levels when TGF-β is upregulated (Westergren-Thorsson et al. 1993). Even though decorin is known to inhibit TGF-β, there is not enough decorin to neutralise the cytokine infiltration in MFS, which leads to a reduction of decorin levels and a potential disruption in an extracellular matrix structure. Immunoelectron microscopy gold particle labelling of the PG decorin demonstrated that there was a significant reduction of decorin labelling in the $FBN1^{+/-}$ when compared to the WT. This reduction of decorin would subsequently disrupt the collagen fibrils within the extracellular matrix.

Future studies should aim to focus on understanding any underlying mechanistic, biomechanical and functional changes that occur in the $FBN1^{+/-}$ mouse model. Understanding changes other than the structural alterations that were identified in this study may further elucidate the role of true elastic fibres and fibrillin-rich microfibrils within the cornea. The study has used some novel techniques to investigate how the cornea is implicated in MFS using a developing mouse model that has not been previously investigated, but future

research could be directed at using these techniques to study the elastic fibres in the corneas of patients with MFS, particularly as MFS patients show a reduction in corneal curvature which was not seen in the mouse model.

7.5. Summary

This study has shown disruptions to the structure of the corneal stroma from stage E16.5 in the F2 mg$\Delta^{LoxPneo}$ mouse model, which presents with phenotypic similarities to patients with severe MFS. Corneal thickness was significantly reduced in this mouse model in E16.5, E18.5 and adult corneas. Furthermore, central corneal collagen fibril diameter and collagen interfibrillar spacing were altered in the developing and adult F2 mg$\Delta^{LoxPneo}$ corneas; this further suggests that the F2 mg$\Delta^{LoxPneo}$ mouse model had alterations to the collagen fibril network. This study has identified a clear disruption to the extracellular matrix of the corneal stroma from E16.5 of embryonic development in the F2 mg$\Delta^{LoxPneo}$ mouse model. It was suggested that a disruption to the fibrillin-1 network alters corneal architecture from early in corneal development and the disorganisation to the stromal network is more severe in adult tissue than the younger embryonic corneas.

Chapter 8: Concluding Discussion

The first mammalian model studied in this thesis was the mouse, because of its easy access and rapid development. This allowed the initial synthesis and organisation of the corneal extracellular matrix to be followed. The aim was to identify whether a primary stroma was present and to elucidate the mechanisms that directed extracellular matrix deposition and alignment. Following this, human corneal embryogenesis was studied, and its developmental events compared to the mouse and avian models.

The prenatal mouse cornea had no collagenous primary stroma to direct mesenchymal cell migration. This has previously been described and was thought to be common across all mammalian species (Haustein 1983, Pei and Rhodin 1970). Contrary to this assumption, this thesis has provided novel evidence of a collagenous acellular matrix in the human cornea. These results implied that the acellular collagenous matrix could act as a primary stroma to initiate mesenchymal cell migration, which occurs in the chick model (Hay E. D. and Revel 1969). The results in this study demonstrated that developmental events in the human cornea were more similar to the avian cornea than the mouse cornea (Haustein 1983, Pei and Rhodin 1970). Another novel finding in the human embryonic cornea was the 3-D visualisation of endothelial cell projections that branched towards the corneal epithelium, collagenous matrix and mesenchymal cells. These results implied that the endothelium has an important communicatory role in human corneal development. Interestingly, endothelial cell projections were not seen in later stages of foetal development, which implied that once mesenchymal cells had differentiated into keratocytes and had established their connections to neighbouring corneal stromal cells, the endothelial cell projections were no longer required. Endothelial cells play a crucial role in the migration of leukocytes (Cook-Mills and Deem 2005) and they may undertake a similar role in the migration of mesenchymal cells into the presumptive corneal stroma. It should also be noted that where a primary stroma was present in the human and avian cornea, the endothelium formed

before mesenchymal cell migration. In mouse development, the endothelium developed after mesenchymal cell infiltration by the subsequent flattening of the posterior mesenchymal cells. Even though endothelial cell extensions were not identified in early mouse development, the 3-D reconstructions did identify extensive corneal stromal cell projections which interacted with adjacent corneal stromal cells and the corneal epithelium. These results demonstrated extensive cell connections in both the human and mouse cornea.

Initial collagen fibril deposition and alignment could not be studied in the human cornea, as the ages that were accessible after CS22 and had already laid down collagen fibrils. Instead, initial extracellular matrix deposition was analysed in the mouse cornea. Deposition commenced in the prenatal anterior stroma, where cells of an active phenotype resided. Immunofluorescence experiments also labelled collagen initially in the anterior corneal stroma before it spread across the whole thickness of the cornea in later development. These results suggest that collagen deposition initially occurs in the anterior cornea of the mouse before it becomes widespread across the whole corneal stroma. The foetal tissue used in this study could not be prepared for conventional immunofluorescence techniques because of the medium in which they had been stored. To overcome this limitation, the tissue was processed with low-temperature embedding to carry out immunogold electron microscopy studies. However, the foetal tissue did not maintain its structure during this processing and could not be analysed with immunofluorescence techniques to determine the extracellular matrix proteins present.

With increased maturation, cell projections aligned with collagen fibrils in the mouse cornea, suggesting that corneal stromal cells have a role in the alignment of collagen fibrils, which was previously described in the avian model (Koudouna et al. 2018a, Young et al. 2014). However, it is still unclear whether or not the cells use the collagen fibrils to migrate, thus exerting forces which in turn regulate the alignment of the collagen fibrils, or if the collagen

fibrils direct cell alignment. Answering these questions could elucidate how corneal stromal architecture is generated.

PGs were observed in the prenatal mouse cornea prior to collagen fibril deposition and were found around corneal stromal cells, linking corneal stromal cells to collagen fibrils and in-between collagen fibrils. PGs were also occasionally organised as longitudinal filaments or transverse punctate dots, with a similar organisation to the collagen fibrils. In the mature cornea, PGs maintain the pseudo-hexagonal arrangement of collagen fibrils within the stroma (Borcherding et al. 1975). Furthermore, PGs have been established in the mouse corneal stroma to regulate collagen fibril diameter (Parfitt et al. 2010). The PGs could also regulate collagen fibril organisation in early corneal development, as they do in the mature cornea. These findings combined with the result that cell projections align with collagen fibrils suggests a possible mechanism in which cells align collagen fibrils through their interactions with PGs.

A recently described extracellular component of the mature human corneal stroma has been the complex organisation of elastic fibres. It was suggested that the elastic fibres may support corneal shape and function, particularly in development (Lewis et al. 2016). Elastic fibres were initially found in the foetal cornea at week 12. These fibres comprised microfibrils ~10-12 nm in diameter, with a morphology characteristic of fibrillin-rich microfibrils (Sakai et al. 1986). As development progressed, the elastic fibres were predominantly found in the posterior peripheral cornea, as in the mature cornea. Some of the elastic fibres imaged contained an amorphous core surrounded by microfibrils, which is characteristic of the elastin component found in true elastic fibres (Baldwin et al. 2013). This result correlated with elastin localised in the posterior human adult cornea, which was further confirmed by a second study (Mohammed et al. 2018). On the other hand, in all elastic fibre studies throughout this thesis, the mouse did not contain elastin. Instead, fibrillin-rich microfibrils were identified across the whole thickness of the stroma, which further demonstrated anatomical variations between the two mammalian species.

The presence of elastic fibres in corneal development, combined with the observations of corneal abnormalities in fibrillinopathies led to the suggestion that elastic fibres could develop corneal stromal shape or provide biomechanical properties to the cornea (Gehle et al. 2017, White et al. 2017a). To explore the functional role of elastic fibres during development, a fibrillin-1 knockout mouse model was studied between E12.5 and E18.5 of embryonic development, along with the knockout adult tissue. The $FBN1^{+/-}$ cornea was thinner compared to the WT and had a disrupted collagen and elastic fibre ultrastructure, which suggested that fibrillin-1 is required to develop a physiological cornea. Dysfunctional fibrillin-1 cannot bind TGF-β in the extracellular matrix which causes large latent TGF-β molecules to elevate and exert a destructive effect on extracellular matrix molecules. Increased levels of TGF-β activates metalloproteinases which break down collagen and elastic fibres and can reduce extracellular matrix components that maintain tissue ultrastructure (Gomes L. R. et al. 2012). Elevated TGF-β is thought to be the main pathway to the breakdown and disrupt the extracellular matrix, which would consequently reduce the corneal thickness and disturb stromal organisation.

8.1. Future Research

From this study, further work is needed to demonstrate whether there is a conventional sequence of events that develops the mammalian cornea across species or if other species also demonstrate developmental differences as established between the mouse and human cornea. It would be interesting to know if other species require a primary stroma for corneal development as in human and avian corneas, or do not, as in mouse corneas. The role of the endothelium in corneal development should be examined, along with the identification of the types of extracellular matrix proteins in the foetal acellular collagenous matrix, and a comparison made with the avian model and other mammalian models.

To further investigate how corneal stromal organisation is achieved, the mechanistic events of collagen and cell alignment should be explored. A common mechanism of collagen deposition and alignment in tendon has been described to occur via fibripositors, which deposit collagen fibrils in a given direction (Canty et al. 2004). The present results did not show any fibripositors during mammalian corneal development, which implies that the collagen fibrils are deposited and aligned differently. The alternative mechanisms that could organise the corneal stroma should be explored. This could involve the analysis of PGs in early prenatal development. To accomplish this, it would be necessary to produce mouse models with genetically mutated PGs, and then analyse the association of PGs with collagen fibrils to determine if there are any alterations in collagen fibril organisation in prenatal mouse development.

Since the structure and localisation of the elastic fibre network in the cornea has now been well documented, future studies should focus on the role of elastic fibres in the cornea. Functional or biomechanical alterations in the F2 mg$\Delta^{LoxPneo}$ mouse cornea compared to the wild type could be investigated. If there are changes to the functional, mechanistic or biomechanical role of the cornea in the F2 mg$\Delta^{LoxPneo}$ mouse model, it may enhance our knowledge of the role elastic fibres have within the cornea. However, it should be noted that this study analysed a very severe phenotypic mouse model of MFS and does not truly replicate the phenotypes seen in the majority of MFS patients. In addition, knockout models can compensate for their loss of a protein by overcompensating others, not giving a true representation of the proteins' function.

To conclude, this thesis has enhanced the knowledge of mammalian corneal stromal development by using novel 3-D and conventional structural imaging techniques to study the embryonic mammalian cornea. This thesis has demonstrated novel findings and observations of the developing mouse and

human cornea. It has also highlighted differences and similarities between the human, avian and mouse cornea, which should be taken into consideration.

References

Abass A, Bell JS, Spang MT, Hayes S, Meek KM, Boote C. 2017. SAXS4COLL: an integrated software tool for analysing fibrous collagen-based tissues. J Appl Crystallogr 50:1235-1240.

Abass A, Hayes S, White N, Sorensen T, Meek KM. 2015. Transverse depth-dependent changes in corneal collagen lamellar orientation and distribution. J R Soc Interface 12:20140717.

Agache PG, Monneur C, Leveque JL, De Rigal J. 1980. Mechanical properties and Young's modulus of human skin in vivo. Arch Dermatol Res 269:221-232.

Aghamohammadzadeh H, Newton RH, Meek KM. 2004. X-ray scattering used to map the preferred collagen orientation in the human cornea and limbus. Structure 12:249-256.

Akhtar S, Almubrad T, Paladini I, Mencucci R. 2013. Keratoconus corneal architecture after riboflavin/ultraviolet A cross-linking: ultrastructural studies. Mol Vis 19:1526-1537.

Alexander RA, Garner A. 1983. Elastic and precursor fibres in the normal human eye. Exp Eye Res 36:305-315.

Attias D, et al. 2009. Comparison of clinical presentations and outcomes between patients with TGFBR2 and FBN1 mutations in Marfan syndrome and related disorders. Circulation 120:2541-2549.

Axelsson I, Heinegard D. 1980. Characterization of chondroitin sulfate-rich proteoglycans from bovine corneal stroma. Exp Eye Res 31:57-66.

Baldock C, Koster AJ, Ziese U, Rock MJ, Sherratt MJ, Kadler KE, Shuttleworth CA, Kielty CM. 2001. The supramolecular organization of fibrillin-rich microfibrils. J Cell Biol 152:1045-1056.

Baldock C, et al. 2006. Nanostructure of fibrillin-1 reveals compact conformation of EGF arrays and mechanism for extensibility. Proc Natl Acad Sci U S A 103:11922-11927.

Baldwin AK, Simpson A, Steer R, Cain SA, Kielty CM. 2013. Elastic fibres in health and disease. Expert Rev Mol Med 15:e8.

Bao F, Geraghty B, Wang Q, Elsheikh A. 2016. Consideration of corneal biomechanics in the diagnosis and management of keratoconus: is it important? Eye Vis (Lond) 3:18.

Bard JB, Bansal MK, Ross AS. 1988. The extracellular matrix of the developing cornea: diversity, deposition and function. Development 103 Suppl:195-205.

Bard JB, Hay ED. 1975. The behavior of fibroblasts from the developing avian cornea. Morphology and movement in situ and in vitro. J Cell Biol 67:400-418.

Bard JB, Hay ED, Meller SM. 1975. Formation of the endothelium of the avian cornea: a study of cell movement in vivo. Dev Biol 42:334-361.

Barishak YR. 2001. Embryology of the eye and its adnexa. Karger.

Bear RS. 1942. Long X-ray Diffraction spacings of collagen. J. Am. Chem. Soc. 64:727.

Beebe DC, Coats JM. 2000. The lens organizes the anterior segment: specification of neural crest cell differentiation in the avian eye. Dev Biol 220:424-431.

Beecher N, Carlson C, Allen BR, Kipchumba R, Conrad GW, Meek KM, Quantock AJ. 2005. An x-ray diffraction study of corneal structure in mimecan-deficient mice. Invest Ophthalmol Vis Sci 46:4046-4049.

Beecher N, Chakravarti S, Joyce S, Meek KM, Quantock AJ. 2006. Neonatal development of the corneal stroma in wild-type and lumican-null mice. Invest Ophthalmol Vis Sci 47:146-150.

Beecher. N. CS, Paul. J., Meek. K.M., Quantock. A.J. 2003. Stromal Structure in the Mouse Cornea at Eye-Opening and the Effect of a Lumican-Null Mutation. Investigative Ophthalmology & Visual Science 44:26-5248.

Bergmanson JP, Horne J, Doughty MJ, Garcia M, Gondo M. 2005. Assessment of the number of lamellae in the central region of the normal human corneal stroma at the resolution of the transmission electron microscope. Eye Contact Lens 31:281-287.

Bershadsky A, Kozlov M, Geiger B. 2006. Adhesion-mediated mechanosensitivity: a time to experiment, and a time to theorize. Curr Opin Cell Biol 18:472-481.

Bettman JW, Jr. 1970. Nature of Bowman's layer. N Engl J Med 282:344.

Beyer EC, Kistler J, Paul DL, Goodenough DA. 1989. Antisera directed against connexin43 peptides react with a 43-kD protein localized to gap junctions in myocardium and other tissues. J Cell Biol 108:595-605.

Birk DE. 2001. Type V collagen: heterotypic type I/V collagen interactions in the regulation of fibril assembly. Micron 32:223-237.

Birk DE, Fitch JM, Babiarz JP, Doane KJ, Linsenmayer TF. 1990. Collagen fibrillogenesis in vitro: interaction of types I and V collagen regulates fibril diameter. J Cell Sci 95 (Pt 4):649-657.

Birk DE, Fitch JM, Linsenmayer TF. 1986. Organization of collagen types I and V in the embryonic chicken cornea. Invest Ophthalmol Vis Sci 27:1470-1477.

Birk DE, Trelstad RL. 1984. Extracellular compartments in matrix morphogenesis: collagen fibril, bundle, and lamellar formation by corneal fibroblasts. J Cell Biol 99:2024-2033.

Birk DE, Trestad RL. 1985. Fibroblasts create compartments in the extracellular space where collagen polymerizes into fibrils and fibrils associate into bundles. Ann N Y Acad Sci 460:258-266.

Birk DE, Zycband E. 1993. Assembly of the collagenous extracellular matrix during tendon development in the chicken limb. Prog Clin Biol Res 383B:523-532.

Booms P, Pregla R, Ney A, Barthel F, Reinhardt DP, Pletschacher A, Mundlos S, Robinson PN. 2005. RGD-containing fibrillin-1 fragments upregulate matrix metalloproteinase expression in cell culture: a potential factor in the pathogenesis of the Marfan syndrome. Hum Genet 116:51-61.

Boote C, Dennis S, Newton RH, Puri H, Meek KM. 2003. Collagen fibrils appear more closely packed in the prepupillary cornea: optical and biomechanical implications. Invest Ophthalmol Vis Sci 44:2941-2948.

Boote C, et al. 2012. Quantitative assessment of ultrastructure and light scatter in mouse corneal debridement wounds. Invest Ophthalmol Vis Sci 53:2786-2795.

Borcherding MS, Blacik LJ, Sittig RA, Bizzell JW, Breen M, Weinstein HG. 1975. Proteoglycans and collagen fibre organization in human corneoscleral tissue. Exp Eye Res 21:59-70.

Bourne WM. 2003. Biology of the corneal endothelium in health and disease. Eye (Lond) 17:912-918.

Boyce BL, Grazier JM, Jones RE, Nguyen TD. 2008. Full-field deformation of bovine cornea under constrained inflation conditions. Biomaterials 29:3896-3904.

Bredrup C, Knappskog PM, Majewski J, Rodahl E, Boman H. 2005. Congenital stromal dystrophy of the cornea caused by a mutation in the decorin gene. Invest Ophthalmol Vis Sci 46:420-426.

Bron AJ, Tripathi RC, Tripathi BJ. 1997. Wolff's Anatomy of the Eye and Orbit. Chapman & Hall Medican.

Bruns RR, Press W, Gross J. 1987. A large-scale, orthogonal network of microfibril bundles in the corneal stroma. Invest Ophthalmol Vis Sci 28:1939-1946.

Bultmann-Mellin I. 2015. Modeling autosomal recessive cutis laxa type 1C in mice reveals distinct functions for Ltbp-4 isoforms. Dis Model Mech 8:403-415.

Cai CX, Fitch JM, Svoboda KK, Birk DE, Linsenmayer TF. 1994. Cellular invasion and collagen type IX in the primary corneal stroma in vitro. Dev Dyn 201:206-215.

Cain SA, Baldwin AK, Mahalingam Y, Raynal B, Jowitt TA, Shuttleworth CA, Couchman JR, Kielty CM. 2008. Heparan sulfate regulates fibrillin-1 N- and C-terminal interactions. J Biol Chem 283:27017-27027.

Canty EG, Kadler KE. 2005. Procollagen trafficking, processing and fibrillogenesis. J Cell Sci 118:1341-1353.

Canty EG, Lu Y, Meadows RS, Shaw MK, Holmes DF, Kadler KE. 2004. Coalignment of plasma membrane channels and protrusions (fibripositors) specifies the parallelism of tendon. J Cell Biol 165:553-563.

Canty EG, Starborg T, Lu Y, Humphries SM, Holmes DF, Meadows RS, Huffman A, O'Toole ET, Kadler KE. 2006. Actin filaments are required for fibripositor-mediated collagen fibril alignment in tendon. J Biol Chem 281:38592-38598.

Carlson EC, Liu CY, Chikama T, Hayashi Y, Kao CW, Birk DE, Funderburgh JL, Jester JV, Kao WW. 2005. Keratocan, a cornea-specific keratan sulfate proteoglycan, is regulated by lumican. J Biol Chem 280:25541-25547.

Carlson EC, Waring GO, 3rd. 1988. Ultrastructural analyses of enzyme-treated microfibrils in rabbit corneal stroma. Invest Ophthalmol Vis Sci 29:578-585.

Carreon TA, Edwards G, Wang H, Bhattacharya SK. 2016. Segmental outflow of aqueous humor in mouse and human. Exp Eye Res.

Carrington SD, Alexander RA, Grierson I. 1984. Elastic and related fibres in the normal cornea and limbus of the domestic cat. J Anat 139 (Pt 2):319-332.

Carter RT. 2009. The role of integrins in corneal wound healing. Vet Ophthalmol 12 Suppl 1:2-9.

Chakravarti S, Magnuson T, Lass JH, Jepsen KJ, LaMantia C, Carroll H. 1998. Lumican regulates collagen fibril assembly: skin fragility and corneal opacity in the absence of lumican. J Cell Biol 141:1277-1286.

Chakravarti S, Petroll WM, Hassell JR, Jester JV, Lass JH, Paul J, Birk DE. 2000. Corneal opacity in lumican-null mice: defects in collagen fibril structure and packing in the posterior stroma. Invest Ophthalmol Vis Sci 41:3365-3373.

Chan FL, Choi HL. 1995. Proteoglycans associated with the ciliary zonule of the rat eye: a histochemical and immunocytochemical study. Histochem Cell Biol 104:369-381.

Chang JH, Gabison EE, Kato T, Azar DT. 2001. Corneal neovascularization. Curr Opin Ophthalmol 12:242-249.

Chen Q, Fitch JM, Gibney E, Linsenmayer TF. 1993. Type II collagen during cartilage and corneal development: immunohistochemical analysis with an anti-telopeptide antibody. Dev Dyn 196:47-53.

Chen S, Birk DE. 2013. The regulatory roles of small leucine-rich proteoglycans in extracellular matrix assembly. FEBS J 280:2120-2137.

Chen S, Mienaltowski MJ, Birk DE. 2015. Regulation of corneal stroma extracellular matrix assembly. Exp Eye Res 133:69-80.

Chen S, Oldberg A, Chakravarti S, Birk DE. 2010. Fibromodulin regulates collagen fibrillogenesis during peripheral corneal development. Dev Dyn 239:844-854.

Chikumi H, et al. 2000. Fibrillin gene (FBN1) mutations in Japanese patients with Marfan syndrome. J Hum Genet 45:115-118.

Choi J, Bergdahl A, Zheng Q, Starcher B, Yanagisawa H, Davis EC. 2009. Analysis of dermal elastic fibers in the absence of fibulin-5 reveals potential roles for fibulin-5 in elastic fiber assembly. Matrix Biol 28:211-220.

Cintron C, Covington H, Kublin CL. 1983. Morphogenesis of rabbit corneal stroma. Invest Ophthalmol Vis Sci 24:543-556.

Cintron C, Covington HI. 1990. Proteoglycan distribution in developing rabbit cornea. J Histochem Cytochem 38:675-684.

Cintron C, Fujikawa LS, Covington H, Foster CS, Colvin RB. 1984. Fibronectin in developing rabbit cornea. Curr Eye Res 3:489-499.

Collinson JM, Quinn JC, Hill RE, West JD. 2003. The roles of Pax6 in the cornea, retina, and olfactory epithelium of the developing mouse embryo. Dev Biol 255:303-312.

Conrad AH, Conrad GW. 2003. The keratocan gene is expressed in both ocular and non-ocular tissues during early chick development. Matrix Biol 22:323-337.

Cook CS, Nowotny AZ, Sulik KK. 1987. Fetal alcohol syndrome. Eye malformations in a mouse model. Arch Ophthalmol 105:1576-1581.

Cook-Mills JM, Deem TL. 2005. Active participation of endothelial cells in inflammation. J Leukoc Biol 77:487-495.

Cornuet PK, Blochberger TC, Hassell JR. 1994. Molecular polymorphism of lumican during corneal development. Invest Ophthalmol Vis Sci 35:870-877.

Cotta-Pereira G, Guerra Rodrigo F, Bittencourt-Sampaio S. 1976. Oxytalan, elaunin, and elastic fibers in the human skin. J Invest Dermatol 66:143-148.

Cotton M, Claing A. 2009. G protein-coupled receptors stimulation and the control of cell migration. Cell Signal 21:1045-1053.

Coulombre AJ. 1965. Experimental Embryology of the Vertebrate Eye. Invest Ophthalmol 4:411-419.

Coulombre AJ, Coulombre JL. 1958. Corneal development. I. Corneal transparency. J Cell Comp Physiol 51:1-11.

Cousins SW, McCabe MM, Danielpour D, Streilein JW. 1991. Identification of transforming growth factor-beta as an immunosuppressive factor in aqueous humor. Invest Ophthalmol Vis Sci 32:2201-2211.

Cox BA, Starcher BC, Urry DW. 1973. Coacervation of alpha-elastin results in fiber formation. Biochim Biophys Acta 317:209-213.

Cui CY, Smith JA, Schlessinger D, Chan CC. 2005. X-linked anhidrotic ectodermal dysplasia disruption yields a mouse model for ocular surface disease and resultant blindness. Am J Pathol 167:89-95.

Cvekl A, Tamm ER. 2004. Anterior eye development and ocular mesenchyme: new insights from mouse models and human diseases. Bioessays 26:374-386.

Daga Gordini D, Castellani I, Volpin D, Bressan GM. 1990. Ultrastructural immuno-localization of tropoelastin in the chick eye. Cell Tissue Res 260:137-146.

De Groef L, et al. 2016. Aberrant Collagen Composition of the Trabecular Meshwork Results in Reduced Aqueous Humor Drainage and Elevated IOP in MMP-9 Null Mice. Invest Ophthalmol Vis Sci 57:5984-5995.

Debelle L, Tamburro AM. 1999. Elastin: molecular description and function. Int J Biochem Cell Biol 31:261-272.

Deerinck TJ, Bushong, E.A., Lev-Ram, V. 2010. Enhancing Serial Block-Face Scanning Electron Microscopy to Enable High Resolution 3-D Nanohistology of Cells and Tissues. Microsc Microanal 16:1138-1139.

DelMonte DW, Kim T. 2011. Anatomy and physiology of the cornea. J Cataract Refract Surg 37:588-598.

Dick JC. 1947. Observations on the elastic tissue of the skin with a note on the reticular layer at the junction of the dermis and epidermis. J Anat 81:201-211.

Doane KJ, Birk DE. 1994. Differences in integrin expression during avian corneal stromal development. Invest Ophthalmol Vis Sci 35:2834-2842.

Doane KJ, Ting WH, McLaughlin JS, Birk DE. 1996. Spatial and temporal variations in extracellular matrix of periocular and corneal regions during corneal stromal development. Exp Eye Res 62:271-283.

Doward W, Perveen R, Lloyd IC, Ridgway AE, Wilson L, Black GC. 1999. A mutation in the RIEG1 gene associated with Peters' anomaly. J Med Genet 36:152-155.

Dua HS, Faraj LA, Said DG, Gray T, Lowe J. 2013. Human corneal anatomy redefined: a novel pre-Descemet's layer (Dua's layer). Ophthalmology 120:1778-1785.

Dublin I. 1970. [Comparative embryologic studies of the early development of the cornea and the pupillary membrane in reptiles, birds and mammals]. Acta Anat (Basel) 76:381-408.

Dudakova L, Jirsova K. 2013. The impairment of lysyl oxidase in keratoconus and in keratoconus-associated disorders. J Neural Transm (Vienna) 120:977-982.

Dunn GA, Heath JP. 1976. A new hypothesis of contact guidance in tissue cells. Exp Cell Res 101:1-14.

Ebendal T. 1976. The relative roles of contact inhibition and contact guidance in orientation of axons extending on aligned collagen fibrils in vitro. Exp Cell Res 98:159-169.

Eriksen TA, Wright DM, Purslow PP, Duance VC. 2001. Role of Ca(2+) for the mechanical properties of fibrillin. Proteins 45:90-95.

Faury G. 2001. Function-structure relationship of elastic arteries in evolution: from microfibrils to elastin and elastic fibres. Pathol Biol (Paris) 49:310-325.

Feneck EM, Lewis PN, Ralphs J, Meek KM. 2018. A comparative study of the elastic fibre system within the mouse and human cornea. Exp Eye Res 177:35-44.

Fernandes GR, Massironi SM, Pereira LV. 2016. Identification of Loci Modulating the Cardiovascular and Skeletal Phenotypes of Marfan Syndrome in Mice. Sci Rep 6:22426.

Fernandes KA, Harder JM, Williams PA, Rausch RL, Kiernan AE, Nair KS, Anderson MG, John SW, Howell GR, Libby RT. 2015. Using genetic mouse models to gain insight into glaucoma: Past results and future possibilities. Exp Eye Res 141:42-56.

Fitch J, Fini ME, Beebe DC, Linsenmayer TF. 1998. Collagen type IX and developmentally regulated swelling of the avian primary corneal stroma. Dev Dyn 212:27-37.

Fitch JM, Birk DE, Linsenmayer C, Linsenmayer TF. 1990. The spatial organization of Descemet's membrane-associated type IV collagen in the avian cornea. J Cell Biol 110:1457-1468.

Fitch JM, Birk DE, Linsenmayer C, Linsenmayer TF. 1991. Stromal assemblies containing collagen types IV and VI and fibronectin in the developing embryonic avian cornea. Dev Biol 144:379-391.

Fitch JM, Kidder JM, Linsenmayer TF. 2005. Cellular invasion of the chicken corneal stroma during development: regulation by multiple matrix metalloproteases and the lens. Dev Dyn 232:106-118.

Fitch JM, Linsenmayer CM, Linsenmayer TF. 1994. Collagen fibril assembly in the developing avian primary corneal stroma. Invest Ophthalmol Vis Sci 35:862-869.

Foellmer HG, Kawahara K, Madri JA, Furthmayr H, Timpl R, Tuderman L. 1983. A monoclonal antibody specific for the amino terminal cleavage site of procollagen type I. Eur J Biochem 134:183-189.

Foster JW, Gouveia RM, Connon CJ. 2015. Low-glucose enhances keratocyte-characteristic phenotype from corneal stromal cells in serum-free conditions. Sci Rep 5:10839.

Fragiadaki M, Ikeda T, Witherden A, Mason RM, Abraham D, Bou-Gharios G. 2011. High doses of TGF-beta potently suppress type I collagen via the transcription factor CUX1. Mol Biol Cell 22:1836-1844.

Frevert CW, Sannes, P.L. 2005. Matrix proteoglycans as effector molecules for epithelial cell function. European Respiratory review 14:137-144.

Friedrichs J, Taubenberger A, Franz CM, Muller DJ. 2007. Cellular remodelling of individual collagen fibrils visualized by time-lapse AFM. J Mol Biol 372:594-607.

Fuhrmann S. 2010. Eye morphogenesis and patterning of the optic vesicle. Curr Top Dev Biol 93:61-84.

Fullmer HM, Lillie RD. 1958. The oxytalan fiber: a previously undescribed connective tissue fiber. J Histochem Cytochem 6:425-430.

Fullwood NJ, Meek KM. 1993. A synchroton X-ray study of the changes occurring in the corneal stroma during processing for electron microscopy. J Microsc 169:53-60.

Funderburgh JL, Caterson B, Conrad GW. 1986. Keratan sulfate proteoglycan during embryonic development of the chicken cornea. Dev Biol 116:267-277.

Funderburgh JL, Corpuz LM, Roth MR, Funderburgh ML, Tasheva ES, Conrad GW. 1997. Mimecan, the 25-kDa corneal keratan sulfate proteoglycan, is a product of the gene producing osteoglycin. J Biol Chem 272:28089-28095.

Ganburged G, Suda, N., Saito, M., Yamazaki, Y., Isokawa, K., Moriyama, K. 2010. Microfibril is Essential for Noraml Development of Peridontal Ligaments (PDLs). Paper presented at IADR General Session 2010.

Ganguli D, Roy IS, Biswas SK, Sengupta M. 1975. Study of corneal power and diameter in simple refractive error. Indian J Ophthalmol 23:6-11.

Garcia JG, Verin AD, Herenyiova M, English D. 1998. Adherent neutrophils activate endothelial myosin light chain kinase: role in transendothelial migration. J Appl Physiol (1985) 84:1817-1821.

Gardner SJ, White N, Albon J, Knupp C, Kamma-Lorger CS, Meek KM. 2015. Measuring the Refractive Index of Bovine Corneal Stromal Cells Using Quantitative Phase Imaging. Biophys J 109:1592-1599.

Ge G, Seo NS, Liang X, Hopkins DR, Hook M, Greenspan DS. 2004. Bone morphogenetic protein-1/tolloid-related metalloproteinases process osteoglycin and enhance its ability to regulate collagen fibrillogenesis. J Biol Chem 279:41626-41633.

Gealy C, Hayes AJ, Buckwell R, Young RD, Caterson B, Quantock AJ, Ralphs JR. 2009. Actin and type I collagen propeptide distribution in the developing chick cornea. Invest Ophthalmol Vis Sci 50:1653-1658.

Gehle P, Goergen B, Pilger D, Ruokonen P, Robinson PN, Salchow DJ. 2017. Biometric and structural ocular manifestations of Marfan syndrome. PLoS One 12:e0183370.

Gelse K, Poschl E, Aigner T. 2003. Collagens--structure, function, and biosynthesis. Adv Drug Deliv Rev 55:1531-1546.

Gibson MA, Finnis ML, Kumaratilake JS, Cleary EG. 1998. Microfibril-associated glycoprotein-2 (MAGP-2) is specifically associated with fibrillin-containing microfibrils but exhibits more restricted patterns of tissue localization and developmental expression than its structural relative MAGP-1. J Histochem Cytochem 46:871-886.

Gipson IK. 1992. Adhesive mechanisms of the corneal epithelium. Acta Ophthalmol Suppl:13-17.

Gipson IK, Argueso P. 2003. Role of mucins in the function of the corneal and conjunctival epithelia. Int Rev Cytol 231:1-49.

Gipson IK, Spurr-Michaud SJ, Tisdale AS. 1987. Anchoring fibrils form a complex network in human and rabbit cornea. Invest Ophthalmol Vis Sci 28:212-220.

Goel M, Picciani RG, Lee RK, Bhattacharya SK. 2010. Aqueous humor dynamics: a review. Open Ophthalmol J 4:52-59.

Goldman JN, Benedek GB. 1967. The relationship between morphology and transparency in the nonswelling corneal stroma of the shark. Invest Ophthalmol 6:574-600.

Gomes JA, Amankwah R, Powell-Richards A, Dua HS. 2004. Sodium hyaluronate (hyaluronic acid) promotes migration of human corneal epithelial cells in vitro. Br J Ophthalmol 88:821-825.

Gomes LR, Terra LF, Wailemann RA, Labriola L, Sogayar MC. 2012. TGF-beta1 modulates the homeostasis between MMPs and MMP inhibitors through p38 MAPK and ERK1/2 in highly invasive breast cancer cells. BMC Cancer 12:26.

Gonzalez G, Sasamoto Y, Ksander BR, Frank MH, Frank NY. 2018. Limbal stem cells: identity, developmental origin, and therapeutic potential. Wiley Interdiscip Rev Dev Biol 7.

Gordon SR. 2014. Fibronectin antibody labels corneal stromal collagen fibrils in situ along their length and circumference and demonstrates distinct staining along the cell and stromal interfaces of Descemet's membrane. Curr Eye Res 39:312-316.

Grant DS, Leblond CP. 1988. Immunogold quantitation of laminin, type IV collagen, and heparan sulfate proteoglycan in a variety of basement membranes. J Histochem Cytochem 36:271-283.

Green EM, Mansfield JC, Bell JS, Winlove CP. 2014. The structure and micromechanics of elastic tissue. Interface Focus 4:20130058.

Grupcheva CN, Laux WT, Rupenthal ID, McGhee J, McGhee CN, Green CR. 2012. Improved corneal wound healing through modulation of gap junction communication using connexin43-specific antisense oligodeoxynucleotides. Invest Ophthalmol Vis Sci 53:1130-1138.

Guillen-Ahlers H, Buechler SA, Suckow MA, Castellino FJ, Ploplis VA. 2008. Sulindac treatment alters collagen and matrilysin expression in adenomas of ApcMin/+ mice. Carcinogenesis 29:1421-1427.

Habashi JP, et al. 2006. Losartan, an AT1 antagonist, prevents aortic aneurysm in a mouse model of Marfan syndrome. Science 312:117-121.

Hamada R, Giraud JP, Graf B, Pouliquen Y. 1972. [Analytical and statistical study of the lamellae, keratocytes and collagen fibrils of the central region of the normal human cornea. (Light and electron microscopy)]. Arch Ophtalmol Rev Gen Ophtalmol 32:563-570.

Han H, Wecker T, Grehn F, Schlunck G. 2011. Elasticity-dependent modulation of TGF-beta responses in human trabecular meshwork cells. Invest Ophthalmol Vis Sci 52:2889-2896.

Hanlon SD, Behzad AR, Sakai LY, Burns AR. 2015. Corneal stroma microfibrils. Exp Eye Res 132:198-207.

Hanlon SD, Patel NB, Burns AR. 2011. Assessment of postnatal corneal development in the C57BL/6 mouse using spectral domain optical coherence tomography and microwave-assisted histology. Exp Eye Res 93:363-370.

Hansson HA. 1970. Scanning electron microscopy of the zonular fibers in the rat eye. Z Zellforsch Mikrosk Anat 107:199-209.

Hassell JR, Birk DE. 2010. The molecular basis of corneal transparency. Exp Eye Res 91:326-335.

Hassell JR, Newsome DA, Krachmer JH, Rodrigues MM. 1980. Macular corneal dystrophy: failure to synthesize a mature keratan sulfate proteoglycan. Proc Natl Acad Sci U S A 77:3705-3709.

Haustein J. 1983. On the ultrastructure of the developing and adult mouse corneal stroma. Anat Embryol (Berl) 168:291-305.

Hay ED. 1980. Development of the Vertebrate Cornea. Int Rev Cytol 63:263-322.

Hay ED, Dodson JW. 1973. Secretion of collagen by corneal epithelium. I. Morphology of the collagenous products produced by isolated epithelia grown on frozen-killed lens. J Cell Biol 57:190-213.

Hay ED, Revel JP. 1969. Fine structure of the developing avian cornea. Monogr Dev Biol 1:1-144.

Hayashi M, Ninomiya Y, Hayashi K, Linsenmayer TF, Olsen BR, Trelstad RL. 1988. Secretion of collagen types I and II by epithelial and endothelial cells in the developing chick cornea demonstrated by in situ hybridization and immunohistochemistry. Development 103:27-36.

Hayashi S, Osawa T, Tohyama K. 2002. Comparative observations on corneas, with special reference to Bowman's layer and Descemet's membrane in mammals and amphibians. J Morphol 254:247-258.

He ZG, Forest F, Gain P, Rageade D, Bernard A, Acquart S, Peoc'h M, Defoe DM, Thuret G. 2016. 3D map of the human corneal endothelial cell. Scientific Reports 6.

Hendrich HJ. 2012. The Laboratory Mouse. Elsevier.

Hendrix MJ, Hay ED, von der Mark K, Linsenmayer TF. 1982. Immunohistochemical localization of collagen types I and II in the developing chick cornea and tibia by electron microscopy. Invest Ophthalmol Vis Sci 22:359-375.

Henriksson JT, Bron AJ, Bergmanson JP. 2012. An explanation for the central to peripheral thickness variation in the mouse cornea. Clin Exp Ophthalmol 40:174-181.

Henriksson JT, McDermott AM, Bergmanson JP. 2009. Dimensions and morphology of the cornea in three strains of mice. Invest Ophthalmol Vis Sci 50:3648-3654.

Herwig MC, Muller AM, Holz FG, Loeffler KU. 2013. Immunolocalization of different collagens in the cornea of human fetal eyes: a developmental approach. Curr Eye Res 38:60-69.

Hill M. 2012. The Carnegie Staged Embryos.

Holmes DF, Gilpin CJ, Baldock C, Ziese U, Koster AJ, Kadler KE. 2001. Corneal collagen fibril structure in three dimensions: Structural insights into fibril assembly, mechanical properties, and tissue organization. Proc Natl Acad Sci U S A 98:7307-7312.

Hoole S. 1798. The Select Works of Antony van Leeuwenhoek, containing his Miscrosopical Discoveries in many of the Works of Nature. G. Sidney.

Huang D. 1991. Optical coherence tomography. Science 254:1178-1181.

Hughes A. 1972. A schematic eye for the rabbit. Vision Res 12:123-138.

Inouye H, Worthington, C.R. 1983. X-ray observations on a collagen fibril lattice structure in peripheral nerve. Int. J. Biol. Macromol., 5:199-203.

Iozzo RV, Schaefer L. 2015. Proteoglycan form and function: A comprehensive nomenclature of proteoglycans. Matrix Biol 42:11-55.

Ito A, Yamamoto M, Ikeda K, Sato M, Kawabe Y, Kamihira M. 2015. Effects of type IV collagen on myogenic characteristics of IGF-I gene-engineered myoblasts. J Biosci Bioeng 119:596-603.

Jacobsen IE, Jensen OA, Prause JU. 1984. Structure and composition of Bowman's membrane. Study by frozen resin cracking. Acta Ophthalmol (Copenh) 62:39-53.

Jastrzebska M, Tarnawska D, Wrzalik R, Chrobak A, Grelowski M, Wylegala E, Zygadlo D, Ratuszna A. 2017. New insight into the shortening of the collagen fibril D-period in human cornea. J Biomol Struct Dyn 35:551-563.

Jensen SA, Robertson IB, Handford PA. 2012. Dissecting the fibrillin microfibril: structural insights into organization and function. Structure 20:215-225.

Jester JV, Moller-Pedersen T, Huang J, Sax CM, Kays WT, Cavangh HD, Petroll WM, Piatigorsky J. 1999. The cellular basis of corneal transparency: evidence for 'corneal crystallins'. J Cell Sci 112 (Pt 5):613-622.

Johnston MC, Noden DM, Hazelton RD, Coulombre JL, Coulombre AJ. 1979. Origins of avian ocular and periocular tissues. Exp Eye Res 29:27-43.

Juarranz A, Ferrer JM, Tato A, Canete M, Stockert JC. 1987. Metachromatic staining and electron dense reaction of glycosaminoglycans by means of cuprolinic blue. Histochem J 19:1-6.

Kadler KE, Hill A, Canty-Laird EG. 2008. Collagen fibrillogenesis: fibronectin, integrins, and minor collagens as organizers and nucleators. Curr Opin Cell Biol 20:495-501.

Kadler KE, Holmes DF, Trotter JA, Chapman JA. 1996. Collagen fibril formation. Biochem J 316 (Pt 1):1-11.

Kahari VM, Larjava H, Uitto J. 1991. Differential regulation of extracellular matrix proteoglycan (PG) gene expression. Transforming growth factor-beta 1 up-regulates biglycan (PGI), and versican (large fibroblast PG) but down-regulates decorin (PGII) mRNA levels in human fibroblasts in culture. J Biol Chem 266:10608-10615.

Kalash R, et al. 2014. Differences in irradiated lung gene transcription between fibrosis-prone C57BL/6NHsd and fibrosis-resistant C3H/HeNHsd mice. In Vivo 28:147-171.

Kamma-Lorger CS, et al. 2010. Collagen and mature elastic fibre organisation as a function of depth in the human cornea and limbus. J Struct Biol 169:424-430.

Kang MH, Oh DJ, Rhee DJ. 2011. Effect of hevin deletion in mice and characterization in trabecular meshwork. Invest Ophthalmol Vis Sci 52:2187-2193.

Kao WW. 2010. Corneal morphogenesis during development and diseases. Eye Contact Lens 36:265-268.

Kao WW, Liu CY. 2002. Roles of lumican and keratocan on corneal transparency. Glycoconj J 19:275-285.

Kasetti RB, Phan TN, Millar JC, Zode GS. 2016. Expression of Mutant Myocilin Induces Abnormal Intracellular Accumulation of Selected Extracellular Matrix Proteins in the Trabecular Meshwork. Invest Ophthalmol Vis Sci 57:6058-6069.

Keene DR, Maddox BK, Kuo HJ, Sakai LY, Glanville RW. 1991. Extraction of extendable beaded structures and their identification as fibrillin-containing extracellular matrix microfibrils. J Histochem Cytochem 39:441-449.

Kidson SH, Kume T, Deng K, Winfrey V, Hogan BL. 1999. The forkhead/winged-helix gene, Mf1, is necessary for the normal development of the cornea and formation of the anterior chamber in the mouse eye. Dev Biol 211:306-322.

Kielbassa K, Schmitz C, Gerke V. 1998. Disruption of endothelial microfilaments selectively reduces the transendothelial migration of monocytes. Exp Cell Res 243:129-141.

Kielty CM, Baldock C, Lee D, Rock MJ, Ashworth JL, Shuttleworth CA. 2002a. Fibrillin: from microfibril assembly to biomechanical function. Philos Trans R Soc Lond B Biol Sci 357:207-217.

Kielty CM, Cummings C, Whittaker SP, Shuttleworth CA, Grant ME. 1991. Isolation and ultrastructural analysis of microfibrillar structures from foetal bovine elastic tissues. Relative abundance and supramolecular architecture of type VI collagen assemblies and fibrillin. J Cell Sci 99 (Pt 4):797-807.

Kielty CM, Sherratt MJ, Shuttleworth CA. 2002b. Elastic fibres. J Cell Sci 115:2817-2828.

Kielty CM, Whittaker SP, Shuttleworth CA. 1996. Fibrillin: evidence that chondroitin sulphate proteoglycans are components of microfibrils and associate with newly synthesised monomers. FEBS Lett 386:169-173.

Kinsey R, Williamson MR, Chaudhry S, Mellody KT, McGovern A, Takahashi S, Shuttleworth CA, Kielty CM. 2008. Fibrillin-1 microfibril deposition is dependent on fibronectin assembly. J Cell Sci 121:2696-2704.

Kivanany PB, Grose KC, Yonet-Tanyeri N, Manohar S, Sunkara Y, Lam KH, Schmidtke DW, Varner VD, Petroll WM. 2018. An In Vitro Model for Assessing Corneal Keratocyte Spreading and Migration on Aligned Fibrillar Collagen. J Funct Biomater 9.

Kocaba V, Damour O, Auxenfans C, Burillon C. 2016. [Limbal stem cell deficiency management. A review]. J Fr Ophtalmol 39:791-803.

Kolliker A. 1860. Manual of Human Microscopic Anatomy. J.W. Parker

Komai Y, Ushiki T. 1991. The three-dimensional organization of collagen fibrils in the human cornea and sclera. Invest Ophthalmol Vis Sci 32:2244-2258.

Konradsen TR, Zetterstrom C. 2013. A descriptive study of ocular characteristics in Marfan syndrome. Acta Ophthalmol 91:751-755.

Koudouna E, Mikula E, Brown DJ, Young RD, Quantock AJ, Jester JV. 2018a. Cell regulation of collagen fibril macrostructure during corneal morphogenesis. Acta Biomater.

Koudouna E, Winkler M, Mikula E, Juhasz T, Brown DJ, Jester JV. 2018b. Evolution of the vertebrate corneal stroma. Prog Retin Eye Res 64:65-76.

Kruse FE. 1994. Stem cells and corneal epithelial regeneration. Eye (Lond) 8 (Pt 2):170-183.

Kume T, Deng KY, Winfrey V, Gould DB, Walter MA, Hogan BL. 1998. The forkhead/winged helix gene Mf1 is disrupted in the pleiotropic mouse mutation congenital hydrocephalus. Cell 93:985-996.

Kuo CL, Isogai Z, Keene DR, Hazeki N, Ono RN, Sengle G, Bachinger HP, Sakai LY. 2007. Effects of fibrillin-1 degradation on microfibril ultrastructure. J Biol Chem 282:4007-4020.

Kutz WE, Wang LW, Bader HL, Majors AK, Iwata K, Traboulsi EI, Sakai LY, Keene DR, Apte SS. 2011. ADAMTS10 protein interacts with fibrillin-1 and promotes its deposition in extracellular matrix of cultured fibroblasts. J Biol Chem 286:17156-17167.

Kwon YH, Fingert JH, Kuehn MH, Alward WL. 2009. Primary open-angle glaucoma. N Engl J Med 360:1113-1124.

Lakshman N, Kim A, Petroll WM. 2010. Characterization of corneal keratocyte morphology and mechanical activity within 3-D collagen matrices. Experimental Eye Research 90:350-359.

Lao T, Tang S. 2014. Cornea Characterization Using a Combined Multiphoton Microscope and Optical Coherence Tomography System. Biomed Opt Express 5:1494-1511.

Last JA, Reiser KM. 1984. Collagen biosynthesis. Environ Health Perspect 55:169-177.

Leivo I, Tani T, Laitinen L, Bruns R, Kivilaakso E, Lehto VP, Burgeson RE, Virtanen I. 1996. Anchoring complex components laminin-5 and type VII collagen in intestine: association with migrating and differentiating enterocytes. J Histochem Cytochem 44:1267-1277.

Lesueur L, Arne JL, Mignon-Conte M, Malecaze F. 1994. Structural and ultrastructural changes in the developmental process of premature infants' and children's corneas. Cornea 13:331-338.

Levy EM. 1980. The ability of horse serum to support an in vitro antibody response. J Immunol Methods 36:181-183.

Levy SG, Mccartney ACE, Moss J. 1995. The Distribution of Fibronectin and P-Component in Descemets-Membrane - an Immunoelectron Microscopic Study. Current Eye Research 14:865-870.

Lewis PN, Pinali C, Young RD, Meek KM, Quantock AJ, Knupp C. 2010. Structural interactions between collagen and proteoglycans are elucidated by three-dimensional electron tomography of bovine cornea. Structure 18:239-245.

Lewis PN, White TL, Young RD, Bell JS, Winlove CP, Meek KM. 2016. Three-dimensional arrangement of elastic fibers in the human corneal stroma. Experimental Eye Research 146:43-53.

Li X, McFarland DC, Velleman SG. 2006. Effect of transforming growth factor-beta on decorin and beta1 integrin expression during muscle development in chickens. Poult Sci 85:326-332.

Liles M, Palka BP, Harris A, Kerr B, Hughes C, Young RD, Meek KM, Caterson B, Quantock AJ. 2010. Differential relative sulfation of Keratan sulfate glycosaminoglycan in the chick cornea during embryonic development. Invest Ophthalmol Vis Sci 51:1365-1372.

Lim SH, et al. 2013. CYP1B1, MYOC, and LTBP2 Mutations in Primary Congenital Glaucoma Patients in the United States. American Journal of Ophthalmology 155:508-517.

Lima BL, et al. 2010. A new mouse model for marfan syndrome presents phenotypic variability associated with the genetic background and overall levels of Fbn1 expression. PLoS One 5:e14136.

Linsenmayer TF, Gibney E, Fitch JM. 1986. Embryonic avian cornea contains layers of collagen with greater than average stability. J Cell Biol 103:1587-1593.

Linsenmayer TF, Gibney E, Gordon MK, Marchant JK, Hayashi M, Fitch JM. 1990. Extracellular matrices of the developing chick retina and cornea. Localization of mRNAs for collagen types II and IX by in situ hybridization. Invest Ophthalmol Vis Sci 31:1271-1276.

Liu CY, Birk DE, Hassell JR, Kane B, Kao WW. 2003. Keratocan-deficient mice display alterations in corneal structure. J Biol Chem 278:21672-21677.

Liu HS, Kao WWY. 2009. A novel protocol of whole mount electro-immunofluorescence staining. Molecular Vision 15:505-517.

Liu W, Atturo F, Aldaya R, Santi P, Cureoglu S, Obwegeser S, Glueckert R, Pfaller K, Schrott-Fischer A, Rask-Andersen H. 2015. Macromolecular organization and fine structure of the human basilar membrane - RELEVANCE for cochlear implantation. Cell Tissue Res 360:245-262.

Llobet A, Gasull X, Gual A. 2003. Understanding trabecular meshwork physiology: a key to the control of intraocular pressure? News Physiol Sci 18:205-209.

Lodish HF. 1988. Transport of secretory and membrane glycoproteins from the rough endoplasmic reticulum to the Golgi. A rate-limiting step in protein maturation and secretion. J Biol Chem 263:2107-2110.

Lu Y, Holmes DF, Baldock C. 2005. Evidence for the intramolecular pleating model of fibrillin microfibril organisation from single particle image analysis. J Mol Biol 349:73-85.

Lunstrum GP, Sakai LY, Keene DR, Morris NP, Burgeson RE. 1986. Large complex globular domains of type VII procollagen contribute to the structure of anchoring fibrils. J Biol Chem 261:9042-9048.

M'Ilroy J H. 1906. On the Presence of Elastic Fibres in the Cornea. J Anat Physiol 40:282-291.

Maddala R, Skiba NP, Rao PV. 2016. Vertebrate Lonesome Kinase Regulated Extracellular Matrix Protein Phosphorylation, Cell Shape and Adhesion in Trabecular Meshwork Cells. J Cell Physiol.

Magrath GB. 1898. Observations Upon the Elastic Tissue of Certain Human Arteries. J Boston Soc Med Sci 3:45-46.

Mantelli F, Mauris J, Argueso P. 2013. The ocular surface epithelial barrier and other mechanisms of mucosal protection: from allergy to infectious diseases. Curr Opin Allergy Clin Immunol 13:563-568.

Marchant JK, Zhang G, Birk DE. 2002. Association of type XII collagen with regions of increased stability and keratocyte density in the cornea. Exp Eye Res 75:683-694.

Mark HH. 2010. Aqueous humor dynamics in historical perspective. Surv Ophthalmol 55:89-100.

Massof RW, Chang FW. 1972. A revision of the rat schematic eye. Vision Res 12:793-796.

Massoudi D, Malecaze F, Galiacy SD. 2016. Collagens and proteoglycans of the cornea: importance in transparency and visual disorders. Cell Tissue Res 363:337-349.

Matic M, Petrov IN, Chen S, Wang C, Dimitrijevich SD, Wolosin JM. 1997. Stem cells of the corneal epithelium lack connexins and metabolite transfer capacity. Differentiation 61:251-260.

Maumenee IH. 1981. The eye in the Marfan syndrome. Trans Am Ophthalmol Soc 79:684-733.

Maurice DM. 1957. The structure and transparency of the cornea. J Physiol 136:263-286.

McNeilly CM, Banes AJ, Benjamin M, Ralphs JR. 1996. Tendon cells in vivo form a three dimensional network of cell processes linked by gap junctions. J Anat 189 (Pt 3):593-600.

Meek KM, Boote C. 2004. The organization of collagen in the corneal stroma. Exp Eye Res 78:503-512.

Meek KM, Knupp C. 2015. Corneal structure and transparency. Progress in Retinal and Eye Research 49:1-16.

Meek KM, Leonard DW. 1993. Ultrastructure of the corneal stroma: a comparative study. Biophys J 64:273-280.

Meek KM, Leonard DW, Connon CJ, Dennis S, Khan S. 2003. Transparency, swelling and scarring in the corneal stroma. Eye (Lond) 17:927-936.

Meek KM, Quantock AJ. 2001. The use of X-ray scattering techniques to determine corneal ultrastructure. Progress in Retinal and Eye Research 20:95-137.

Midura RJ, Hascall VC, MacCallum DK, Meyer RF, Thonar EJ, Hassell JR, Smith CF, Klintworth GK. 1990. Proteoglycan biosynthesis by human corneas from patients with types 1 and 2 macular corneal dystrophy. J Biol Chem 265:15947-15955.

Midwood KS, Schwarzbauer JE. 2002. Elastic fibers: building bridges between cells and their matrix. Curr Biol 12:R279-281.

Mikula ER, Jester JV, Juhasz T. 2016. Measurement of an Elasticity Map in the Human Cornea. Invest Ophthalmol Vis Sci 57:3282-3286.

Mithieux SM, Weiss AS. 2005. Elastin. Adv Protein Chem 70:437-461.

Mo XT, Guo SC, Xie HQ, Deng L, Zhi W, Xiang Z, Li XQ, Yang ZM. 2009. Variations in the ratios of co-cultured mesenchymal stem cells and chondrocytes regulate the expression of cartilaginous and osseous phenotype in alginate constructs. Bone 45:42-51.

Mohammed I, Ross AR, Britton JO, Said DG, Dua HS. 2018. Elastin Content and Distribution in Endothelial Keratoplasty Tissue Determines Direction of Scrolling. American Journal of Ophthalmology 194:16-25.

Mohan RR, Tovey JC, Gupta R, Sharma A, Tandon A. 2011. Decorin biology, expression, function and therapy in the cornea. Curr Mol Med 11:110-128.

Mondrinos MJ, Koutzaki S, Lelkes PI, Finck CM. 2007. A tissue-engineered model of fetal distal lung tissue. Am J Physiol Lung Cell Mol Physiol 293:L639-650.

Moore KL, Agur AMR, Dalley AF. 2013. Clinically Orientated Anatomy Philadelphia: Wolters Kluwer: Lippincott Williams & Wilkins

Morales J, Al-Sharif L, Khalil DS, Shinwari JM, Bavi P, Al-Mahrouqi RA, Al-Rajhi A, Alkuraya FS, Meyer BF, Al Tassan N. 2009. Homozygous mutations in ADAMTS10 and ADAMTS17 cause lenticular myopia, ectopia lentis, glaucoma, spherophakia, and short stature. Am J Hum Genet 85:558-568.

Morishige N, Takagi Y, Chikama T, Takahara A, Nishida T. 2011. Three-dimensional analysis of collagen lamellae in the anterior stroma of the human cornea visualized by second harmonic generation imaging microscopy. Invest Ophthalmol Vis Sci 52:911-915.

Muller LJ, Pels E, Vrensen GF. 2001. The specific architecture of the anterior stroma accounts for maintenance of corneal curvature. Br J Ophthalmol 85:437-443.

Muller-Glauser W, Humbel B, Glatt M, Strauli P, Winterhalter KH, Bruckner P. 1986. On the role of type IX collagen in the extracellular matrix of cartilage: type IX collagen is localized to intersections of collagen fibrils. J Cell Biol 102:1931-1939.

Musselmann K, Alexandrou B, Kane B, Hassell JR. 2005. Maintenance of the keratocyte phenotype during cell proliferation stimulated by insulin. J Biol Chem 280:32634-32639.

Nakatsuji N, Johnson KE. 1983. Comparative study of extracellular fibrils on the ectodermal layer in gastrulae of five amphibian species. J Cell Sci 59:61-70.

Nakatsuji N, Johnson KE. 1984. Experimental manipulation of a contact guidance system in amphibian gastrulation by mechanical tension. Nature 307:453-455.

Neptune ER, Frischmeyer PA, Arking DE, Myers L, Bunton TE, Gayraud B, Ramirez F, Sakai LY, Dietz HC. 2003. Dysregulation of TGF-beta activation contributes to pathogenesis in Marfan syndrome. Nat Genet 33:407-411.

Newsome DA, Gross J, Hassell JR. 1982. Human corneal stroma contains three distinct collagens. Invest Ophthalmol Vis Sci 22:376-381.

Newton RH, Meek KM. 1998. Circumcorneal annulus of collagen fibrils in the human limbus. Invest Ophthalmol Vis Sci 39:1125-1134.

Nicholson SM, Bruzzone R. 1997. Gap junctions: getting the message through. Curr Biol 7:R340-344.

Niederkorn JY. 2009. Role of NKT cells in anterior chamber-associated immune deviation. Expert Rev Clin Immunol 5:137-144.

Nishimura DY. 2001. A spectrum of FOXC1 mutations suggests gene dosage as a mechanism for developmental defects of the anterior chamber of the eye. Am J Hum Genet 68:364-372.

Nishtala K, Pahuja N, Shetty R, Nuijts RM, Ghosh A. 2016. Tear biomarkers for keratoconus. Eye Vis (Lond) 3:19.

Noda K. 2013. Latent TGF-beta binding protein 4 promotes elastic fiber assembly by interacting with fibulin-5. Proc Natl Acad Sci U S A 110:2852-2857.

Norman B, Davis J, Piatigorsky J. 2004. Postnatal gene expression in the normal mouse cornea by SAGE. Invest Ophthalmol Vis Sci 45:429-440.

North AC, Cowan PM, Randall JT. 1954. Structural units in collagen fibrils. Nature 174:1142-1143.

Noske W, Levarlet B, Kreusel KM, Fromm M, Hirsch M. 1994. Tight junctions and paracellular permeability in cultured bovine corneal endothelial cells. Graefes Arch Clin Exp Ophthalmol 232:608-613.

Overby DR, Bertrand J, Schicht M, Paulsen F, Stamer WD, Lutjen-Drecoll E. 2014. The structure of the trabecular meshwork, its connections to the ciliary muscle, and the effect of pilocarpine on outflow facility in mice. Invest Ophthalmol Vis Sci 55:3727-3736.

Pan HT, et al. 2015. Differential proteomic analysis of umbilical artery tissue from preeclampsia patients, using iTRAQ isobaric tags and 2D nano LC-MS/MS. J Proteomics 112:262-273.

Pankov R, Endo Y, Even-Ram S, Araki M, Clark K, Cukierman E, Matsumoto K, Yamada KM. 2005. A Rac switch regulates random versus directionally persistent cell migration. J Cell Biol 170:793-802.

Pankov R, Yamada KM. 2002. Fibronectin at a glance. J Cell Sci 115:3861-3863.

Parfitt GJ, Pinali C, Young RD, Quantock AJ, Knupp C. 2010. Three-dimensional reconstruction of collagen-proteoglycan interactions in the mouse corneal stroma by electron tomography. J Struct Biol 170:392-397.

Patel S, Marshall J, Fitzke FW, 3rd. 1995. Refractive index of the human corneal epithelium and stroma. J Refract Surg 11:100-105.

Patel S, Reinstein DZ, Silverman RH, Coleman DJ. 1998. The shape of Bowman's layer in the human cornea. J Refract Surg 14:636-640.

Pauling L, Corey RB. 1951. The structure of fibrous proteins of the collagen-gelatin group. Proc Natl Acad Sci U S A 37:272-281.

Pei YF, Rhodin JA. 1970. The prenatal development of the mouse eye. Anat Rec 168:105-125.

Pei YF, Rhodin JA. 1971. Electron microscopic study of the development of the mouse corneal epithelium. Invest Ophthalmol 10:811-825.

Pellegata NS, Dieguez-Lucena JL, Joensuu T, Lau S, Montgomery KT, Krahe R, Kivela T, Kucherlapati R, Forsius H, de la Chapelle A. 2000. Mutations in KERA, encoding keratocan, cause cornea plana. Nat Genet 25:91-95.

Pereira L, et al. 1997. Targetting of the gene encoding fibrillin-1 recapitulates the vascular aspect of Marfan syndrome. Nat Genet 17:218-222.

Perveen R, et al. 2000. Phenotypic variability and asymmetry of Rieger syndrome associated with PITX2 mutations. Invest Ophthalmol Vis Sci 41:2456-2460.

Pollard TD, Borisy GG. 2003. Cellular motility driven by assembly and disassembly of actin filaments. Cell 112:453-465.

Pradeepa MM, Grimes GR, Taylor GC, Sutherland HG, Bickmore WA. 2014. Psip1/Ledgf p75 restrains Hox gene expression by recruiting both trithorax and polycomb group proteins. Nucleic Acids Res 42:9021-9032.

Pratt RM, Larsen MA, Johnston MC. 1975. Migration of cranial neural crest cells in a cell-free hyaluronate-rich matrix. Dev Biol 44:298-305.

Provenzano PP, Inman DR, Eliceiri KW, Trier SM, Keely PJ. 2008. Contact guidance mediated three-dimensional cell migration is regulated by Rho/ROCK-dependent matrix reorganization. Biophys J 95:5374-5384.

Puk O, Dalke C, Calzada-Wack J, Ahmad N, Klaften M, Wagner S, de Angelis MH, Graw J. 2009. Reduced corneal thickness and enlarged anterior chamber in a novel ColVIIIa2G257D mutant mouse. Invest Ophthalmol Vis Sci 50:5653-5661.

Puk O, Dalke C, Favor J, de Angelis MH, Graw J. 2006. Variations of eye size parameters among different strains of mice. Mamm Genome 17:851-857.

Qian RQ, Glanville RW. 1997. Alignment of fibrillin molecules in elastic microfibrils is defined by transglutaminase-derived cross-links. Biochemistry 36:15841-15847.

Quantock AJ, Boote C, Siegler V, Meek KM. 2003. Collagen organization in the secondary chick cornea during development. Invest Ophthalmol Vis Sci 44:130-136.

Quantock AJ, et al. 2007. Small-Angle Fibre Diffraction Studies of Corneal Matrix Structure: A Depth-Profiled Investigation of the Human Eye-Bank cornea. J. Appl. Cryst. 40:s335-s340.

Quantock AJ, Kinoshita S, Capel MS, Schanzlin DJ. 1998. A synchrotron x-ray diffraction study of developing chick corneas. Biophys J 74:995-998.

Quarto N, Li S, Renda A, Longaker MT. 2012. Exogenous activation of BMP-2 signaling overcomes TGFbeta-mediated inhibition of osteogenesis in Marfan embryonic stem cells and Marfan patient-specific induced pluripotent stem cells. Stem Cells 30:2709-2719.

Rada JA, Cornuet PK, Hassell JR. 1993. Regulation of corneal collagen fibrillogenesis in vitro by corneal proteoglycan (lumican and decorin) core proteins. Exp Eye Res 56:635-648.

Raghavan D, Starcher BC, Vyavahare NR. 2009. Neomycin binding preserves extracellular matrix in bioprosthetic heart valves during in vitro cyclic fatigue and storage. Acta Biomater 5:983-992.

Ramachandran GN, Kartha G. 1954. Structure of collagen. Nature 174:269-270.

Ramirez F, Rifkin DB. 2009. Extracellular microfibrils: contextual platforms for TGFbeta and BMP signaling. Curr Opin Cell Biol 21:616-622.

Rawe IM, Meek KM, Leonard DW, Takahashi T, Cintron C. 1994. Structure of corneal scar tissue: an X-ray diffraction study. Biophys J 67:1743-1748.

Reed CC, Iozzo RV. 2002. The role of decorin in collagen fibrillogenesis and skin homeostasis. Glycoconj J 19:249-255.

Reig G, Pulgar E, Concha ML. 2014. Cell migration: from tissue culture to embryos. Development 141:1999-2013.

Reinboth B, Hanssen E, Cleary EG, Gibson MA. 2002. Molecular interactions of biglycan and decorin with elastic fiber components: biglycan forms a ternary complex with tropoelastin and microfibril-associated glycoprotein 1. J Biol Chem 277:3950-3957.

Reinstein DZ, Archer TJ, Gobbe M, Silverman RH, Coleman DJ. 2009. Stromal thickness in the normal cornea: three-dimensional display with artemis very high-frequency digital ultrasound. J Refract Surg 25:776-786.

Remington LA, Remington LA. 2012. Clinical anatomy and physiology of the visual system. Elsevier/Butterworth Heinemann.

Reneker LW, Silversides DW, Patel K, Overbeek PA. 1995. TGF alpha can act as a chemoattractant to perioptic mesenchymal cells in developing mouse eyes. Development 121:1669-1680.

Reneker LW, Silversides DW, Xu L, Overbeek PA. 2000. Formation of corneal endothelium is essential for anterior segment development - a transgenic mouse model of anterior segment dysgenesis. Development 127:533-542.

Ricard-Blum S. 2011. The collagen family. Cold Spring Harb Perspect Biol 3:a004978.

Rich A, Crick FH. 1961. The molecular structure of collagen. J Mol Biol 3:483-506.

Richardson SH, Starborg T, Lu Y, Humphries SM, Meadows RS, Kadler KE. 2007. Tendon development requires regulation of cell condensation and cell shape via cadherin-11-mediated cell-cell junctions. Mol Cell Biol 27:6218-6228.

Ridley AJ, Schwartz MA, Burridge K, Firtel RA, Ginsberg MH, Borisy G, Parsons JT, Horwitz AR. 2003. Cell migration: integrating signals from front to back. Science 302:1704-1709.

Rieder CL. 1981. Thick and thin serial sectioning for the three-dimensional reconstruction of biological ultrastructure. Methods Cell Biol 22:215-249.

Robinson PN, Godfrey M. 2000. The molecular genetics of Marfan syndrome and related microfibrillopathies. J Med Genet 37:9-25.

Rones B. 1932. Development of the Human Cornea. Arch Ophthalmol 8:568-275.

Ruberti JW, Hallab NJ. 2005. Strain-controlled enzymatic cleavage of collagen in loaded matrix. Biochem Biophys Res Commun 336:483-489.

Saika S, Shiraishi A, Liu CY, Funderburgh JL, Kao CW, Converse RL, Kao WW. 2000. Role of lumican in the corneal epithelium during wound healing. J Biol Chem 275:2607-2612.

Sakai LY, Keene DR, Engvall E. 1986. Fibrillin, a new 350-kD glycoprotein, is a component of extracellular microfibrils. J Cell Biol 103:2499-2509.

Sakai LY, Keene DR, Glanville RW, Bachinger HP. 1991. Purification and partial characterization of fibrillin, a cysteine-rich structural component of connective tissue microfibrils. J Biol Chem 266:14763-14770.

Sakamoto H, Broekelmann T, Cheresh DA, Ramirez F, Rosenbloom J, Mecham RP. 1996. Cell-type specific recognition of RGD- and non-RGD-containing cell binding domains in fibrillin-1. J Biol Chem 271:4916-4922.

Salchow DJ, Gehle P. 2018. Ocular manifestations of Marfan syndrome in children and adolescents. Eur J Ophthalmol:1120672118761333.

Sawada T, Sugawara Y, Asai T, Aida N, Yanagisawa T, Ohta K, Inoue S. 2006. Immunohistochemical characterization of elastic system fibers in rat molar periodontal ligament. J Histochem Cytochem 54:1095-1103.

Schaefer L, et al. 2007. Decorin-mediated regulation of fibrillin-1 in the kidney involves the insulin-like growth factor-I receptor and Mammalian target of rapamycin. Am J Pathol 170:301-315.

Scott JE. 1980. Collagen--proteoglycan interactions. Localization of proteoglycans in tendon by electron microscopy. Biochem J 187:887-891.

Scott JE. 1988. Proteoglycan-fibrillar collagen interactions. Biochem J 252:313-323.

Scott JE, Haigh M. 1988a. Identification of specific binding sites for keratan sulphate proteoglycans and chondroitin-dermatan sulphate proteoglycans on collagen fibrils in cornea by the use of cupromeronic blue in 'critical-electrolyte-concentration' techniques. Biochem J 253:607-610.

Scott JE, Haigh M. 1988b. Keratan sulphate and the ultrastructure of cornea and cartilage: a 'stand-in' for chondroitin sulphate in conditions of oxygen lack? J Anat 158:95-108.

Segawa K. 1995. [Trabecular meshwork and elastin]. Nippon Ganka Gakkai Zasshi 99:1291-1302.

Sengle G, Charbonneau NL, Ono RN, Sasaki T, Alvarez J, Keene DR, Bachinger HP, Sakai LY. 2008. Targeting of bone morphogenetic protein growth factor complexes to fibrillin. J Biol Chem 283:13874-13888.

Sengle G, Sakai LY. 2015. The fibrillin microfibril scaffold: A niche for growth factors and mechanosensation? Matrix Biol 47:3-12.

Seo GH, Kim YM, Kang E, Kim GH, Seo EJ, Lee BH, Choi JH, Yoo HW. 2018. The phenotypic heterogeneity of patients with Marfan-related disorders and their variant spectrums. Medicine (Baltimore) 97:e10767.

Sevel D, Isaacs R. 1988. A re-evaluation of corneal development. Trans Am Ophthalmol Soc 86:178-207.

Sheppard J, Hayes S, Boote C, Votruba M, Meek KM. 2010. Changes in corneal collagen architecture during mouse postnatal development. Invest Ophthalmol Vis Sci 51:2936-2942.

Sherratt MJ. 2009. Tissue elasticity and the ageing elastic fibre. Age (Dordr) 31:305-325.

Sherratt MJ, Baldock C, Haston JL, Holmes DF, Jones CJ, Shuttleworth CA, Wess TJ, Kielty CM. 2003. Fibrillin microfibrils are stiff reinforcing fibres in compliant tissues. J Mol Biol 332:183-193.

Shi Y, Tu Y, De Maria A, Mecham RP, Bassnett S. 2013. Development, composition, and structural arrangements of the ciliary zonule of the mouse. Invest Ophthalmol Vis Sci 54:2504-2515.

Shoulders MD, Raines RT. 2009. Collagen structure and stability. Annu Rev Biochem 78:929-958.

Siegel RC, Pinnell SR, Martin GR. 1970. Cross-linking of collagen and elastin. Properties of lysyl oxidase. Biochemistry 9:4486-4492.

Simmons TA, Avery JK. 1980. Electron dense staining affinities of mouse oxytalan and elastic fibers. J Oral Pathol 9:183-188.

Simon G, Ren Q, Kervick GN, Parel JM. 1993. Optics of the corneal epithelium. Refract Corneal Surg 9:42-50.

Sinha S, Nevett C, Shuttleworth CA, Kielty CM. 1998. Cellular and extracellular biology of the latent transforming growth factor-beta binding proteins. Matrix Biol 17:529-545.

Smith RS, Sundberg JP, John SWM. 2002. The anterior Segment and Ocular Adnexae. Systematic evaluation of the mouse eye anatomy, pathology and biomethods.

Smolek MK, McCarey BE. 1990. Interlamellar Adhesive Strength in Human Eyebank Corneas. Investigative Ophthalmology & Visual Science 31:1087-1095.

Solanas G, et al. 2008. E-cadherin controls beta-catenin and NF-kappaB transcriptional activity in mesenchymal gene expression. J Cell Sci 121:2224-2234.

Song J, Lee YG, Houston J, Petroll WM, Chakravarti S, Cavanagh HD, Jester JV. 2003. Neonatal corneal stromal development in the normal and lumican-deficient mouse. Invest Ophthalmol Vis Sci 44:548-557.

Spanakis SG, Petridou S, Masur SK. 1998. Functional gap junctions in corneal fibroblasts and myofibroblasts. Invest Ophthalmol Vis Sci 39:1320-1328.

Starborg T, Kadler KE. 2015. Serial block face-scanning electron microscopy: a tool for studying embryonic development at the cell-matrix interface. Birth Defects Res C Embryo Today 105:9-18.

Stepp MA. 2006. Corneal integrins and their functions. Exp Eye Res 83:3-15.

Stramer BM, Zieske JD, Jung JC, Austin JS, Fini ME. 2003. Molecular mechanisms controlling the fibrotic repair phenotype in cornea: implications for surgical outcomes. Invest Ophthalmol Vis Sci 44:4237-4246.

Streilein JW. 2003. Ocular immune privilege: the eye takes a dim but practical view of immunity and inflammation. J Leukoc Biol 74:179-185.

Sultan G, Baudouin C, Auzerie O, De Saint Jean M, Goldschild M, Pisella PJ, Marfan Study G. 2002. Cornea in Marfan disease: Orbscan and in vivo confocal microscopy analysis. Invest Ophthalmol Vis Sci 43:1757-1764.

Sun M, Chen S, Adams SM, Florer JB, Liu H, Kao WW, Wenstrup RJ, Birk DE. 2011. Collagen V is a dominant regulator of collagen fibrillogenesis: dysfunctional regulation of structure and function in a corneal-stroma-specific Col5a1-null mouse model. J Cell Sci 124:4096-4105.

Sunaga S, Maki K, Komagata Y, Ikuta K, Miyazaki JI. 1997. Efficient removal of loxP-flanked DNA sequences in a gene-targeted locus by transient expression of Cre recombinase in fertilized eggs. Mol Reprod Dev 46:109-113.

Svitkina TM. 2016. Filopodia and Lamellipodia. Pages 683-693. Encyclopedia of Cell Biology. Waltham: Academic Press.

Svoboda KK, Nishimura I, Sugrue SP, Ninomiya Y, Olsen BR. 1988. Embryonic chicken cornea and cartilage synthesize type IX collagen molecules with different amino-terminal domains. Proc Natl Acad Sci U S A 85:7496-7500.

Tafti AP, Kirkpatrick AB, Alavi Z, Owen HA, Yu Z. 2015. Recent advances in 3D SEM surface reconstruction. Micron 78:54-66.

Tektas OY, Lutjen-Drecoll E. 2009. Structural changes of the trabecular meshwork in different kinds of glaucoma. Exp Eye Res 88:769-775.

Tervo T, Sulonen J, Valtones S, Vannas A, Virtanen I. 1986. Distribution of fibronectin in human and rabbit corneas. Exp Eye Res 42:399-406.

Theiler K. 1989. The House Mouse - Atlas of Embryonic Development. Springer-Verlag.

Tiedemann K, Batge B, Muller PK, Reinhardt DP. 2001. Interactions of fibrillin-1 with heparin/heparan sulfate, implications for microfibrillar assembly. J Biol Chem 276:36035-36042.

Tisdale AS, Spurr-Michaud SJ, Rodrigues M, Hackett J, Krachmer J, Gipson IK. 1988. Development of the anchoring structures of the epithelium in rabbit and human fetal corneas. Invest Ophthalmol Vis Sci 29:727-736.

Toole BP, Trelstad RL. 1971. Hyaluronate production and removal during corneal development in the chick. Dev Biol 26:28-35.

Torricelli AA, Singh V, Santhiago MR, Wilson SE. 2013. The corneal epithelial basement membrane: structure, function, and disease. Invest Ophthalmol Vis Sci 54:6390-6400.

Trelstad RL, Coulombre AJ. 1971. Morphogenesis of the collagenous stroma in the chick cornea. J Cell Biol 50:840-858.

Umihira J, Nagata S, Nohara M, Hanai T, Usuda N, Segawa K. 1994. Localization of elastin in the normal and glaucomatous human trabecular meshwork. Invest Ophthalmol Vis Sci 35:486-494.

Vecino E, Acera A. 2015. Development and programed cell death in the mammalian eye. Int J Dev Biol 59:63-71.

Vracko R. 1974. Basal lamina scaffold-anatomy and significance for maintenance of orderly tissue structure. Am J Pathol 77:314-346.

Vranka JA, Kelley MJ, Acott TS, Keller KE. 2015. Extracellular matrix in the trabecular meshwork: intraocular pressure regulation and dysregulation in glaucoma. Exp Eye Res 133:112-125.

Wang MC, Lu Y, Baldock C. 2009. Fibrillin microfibrils: a key role for the interbead region in elasticity. J Mol Biol 388:168-179.

Watson ML. 1958. Staining of tissue sections for electron microscopy with heavy metals. J Biophys Biochem Cytol 4:475-478.

Wei H, Hu JH, Angelov SN, Fox K, Yan J, Enstrom R, Smith A, Dichek DA. 2017. Aortopathy in a Mouse Model of Marfan Syndrome Is Not Mediated by Altered Transforming Growth Factor beta Signaling. J Am Heart Assoc 6.

Wenstrup RJ, Florer JB, Brunskill EW, Bell SM, Chervoneva I, Birk DE. 2004. Type V collagen controls the initiation of collagen fibril assembly. J Biol Chem 279:53331-53337.

Wenstrup RJ, Florer JB, Davidson JM, Phillips CL, Pfeiffer BJ, Menezes DW, Chervoneva I, Birk DE. 2006. Murine model of the Ehlers-Danlos syndrome. col5a1 haploinsufficiency disrupts collagen fibril assembly at multiple stages. J Biol Chem 281:12888-12895.

Wentz-Hunter K, Cheng EL, Ueda J, Sugar J, Yue BY. 2001. Keratocan expression is increased in the stroma of keratoconus corneas. Mol Med 7:470-477.

Wess TJ, Purslow PP, Kielty CM. 1997. Fibrillin-rich microfibrils: an X-ray diffraction study of the fundamental axial periodicity. FEBS Lett 413:424-428.

West-Mays JA, Dwivedi DJ. 2006. The keratocyte: corneal stromal cell with variable repair phenotypes. Int J Biochem Cell Biol 38:1625-1631.

Westergren-Thorsson G, Hernnas J, Sarnstrand B, Oldberg A, Heinegard D, Malmstrom A. 1993. Altered expression of small proteoglycans, collagen, and transforming growth factor-beta 1 in developing bleomycin-induced pulmonary fibrosis in rats. J Clin Invest 92:632-637.

White TL, Lewis P, Hayes S, Fergusson J, Bell J, Farinha L, White NS, Pereira LV, Meek KM. 2017a. The Structural Role of Elastic Fibers in the Cornea Investigated Using a Mouse Model for Marfan Syndrome. Invest Ophthalmol Vis Sci 58:2106-2116.

White TL, Lewis PN, Young RD, Kitazawa K, Inatomi T, Kinoshita S, Meek KM. 2017b. Elastic microfibril distribution in the cornea: Differences between normal and keratoconic stroma. Exp Eye Res.

Wiley L, SundarRaj N, Sun TT, Thoft RA. 1991. Regional heterogeneity in human corneal and limbal epithelia: an immunohistochemical evaluation. Invest Ophthalmol Vis Sci 32:594-602.

Williams K, Watsky M. 2002. Gap junctional communication in the human corneal endothelium and epithelium. Curr Eye Res 25:29-36.

Wong MD, van Eede MC, Spring S, Jevtic S, Boughner JC, Lerch JP, Henkelman RM. 2015. 4D atlas of the mouse embryo for precise morphological staging. Development 142:3583-3591.

Wood A, Thorogood P. 1984. An analysis of in vivo cell migration during teleost fin morphogenesis. J Cell Sci 66:205-222.

Wulle KG. 1972. Electron microscopy of the fetal development of the corneal endothelium and Descemet's membrane of the human eye. Invest Ophthalmol 11:897-904.

Wulle KG, Richter J. 1978. Electron microscopy of the early embryonic development of the human corneal epithelium. Albrecht Von Graefes Arch Klin Exp Ophthalmol 209:39-49.

Xie H, Pallero MA, Gupta K, Chang P, Ware MF, Witke W, Kwiatkowski DJ, Lauffenburger DA, Murphy-Ullrich JE, Wells A. 1998. EGF receptor regulation of cell motility: EGF induces disassembly of focal adhesions independently of the motility-associated PLCgamma signaling pathway. J Cell Sci 111 (Pt 5):615-624.

Xie W, Chow LT, Paterson AJ, Chin E, Kudlow JE. 1999. Conditional expression of the ErbB2 oncogene elicits reversible hyperplasia in stratified epithelia and up-regulation of TGFalpha expression in transgenic mice. Oncogene 18:3593-3607.

Yamada K, Young RD, Lewis PN, Shinomiya K, Meek KM, Kinoshita S, Caterson B, Quantock AJ. 2015. Mesenchymal-epithelial cell interactions and proteoglycan matrix composition in the presumptive stem cell niche of the rabbit corneal limbus. Mol Vis 21:1328-1339.

Yamamoto S, Hashizume H, Hitomi J, Shigeno M, Sawaguchi S, Abe H, Ushiki T. 2000. The subfibrillar arrangement of corneal and scleral collagen fibrils as revealed by scanning electron and atomic force microscopy. Arch Histol Cytol 63:127-135.

Yeo GC, Baldock C, Tuukkanen A, Roessle M, Dyksterhuis LB, Wise SG, Matthews J, Mithieux SM, Weiss AS. 2012. Tropoelastin bridge region positions the cell-interactive C terminus and contributes to elastic fiber assembly. Proc Natl Acad Sci U S A 109:2878-2883.

Young RD, Knupp C, Pinali C, Png KM, Ralphs JR, Bushby AJ, Starborg T, Kadler KE, Quantock AJ. 2014. Three-dimensional aspects of matrix assembly by cells in the developing cornea. Proc Natl Acad Sci U S A 111:687-692.

Young RD, Swamynathan SK, Boote C, Mann M, Quantock AJ, Piatigorsky J, Funderburgh JL, Meek KM. 2009. Stromal edema in klf4 conditional null mouse cornea is associated with altered collagen fibril organization and reduced proteoglycans. Invest Ophthalmol Vis Sci 50:4155-4161.

Young RD, Tudor D, Hayes AJ, Kerr B, Hayashida Y, Nishida K, Meek KM, Caterson B, Quantock AJ. 2005. Atypical composition and ultrastructure of proteoglycans in the mouse corneal stroma. Invest Ophthalmol Vis Sci 46:1973-1978.

Yuan X, Chen Z, Yang Z, Gao J, Zhang A, Wu SM, Jacoby R. 2009. Expression pattern of connexins in the corneal and limbal epithelium of a primate. Cornea 28:194-199.

Zaman MH, Trapani LM, Sieminski AL, Mackellar D, Gong H, Kamm RD, Wells A, Lauffenburger DA, Matsudaira P. 2006. Migration of tumor cells in 3D matrices is governed by matrix stiffness along with cell-matrix adhesion and proteolysis. Proc Natl Acad Sci U S A 103:10889-10894.

Zavala J, Lopez Jaime GR, Rodriguez Barrientos CA, Valdez-Garcia J. 2013. Corneal endothelium: developmental strategies for regeneration. Eye (Lond) 27:579-588.

Zeyer KA, Reinhardt DP. 2015. Engineered mutations in fibrillin-1 leading to Marfan syndrome act at the protein, cellular and organismal levels. Mutat Res Rev Mutat Res 765:7-18.

Zhang G, Chen S, Goldoni S, Calder BW, Simpson HC, Owens RT, McQuillan DJ, Young MF, Iozzo RV, Birk DE. 2009. Genetic evidence for the coordinated regulation of collagen fibrillogenesis in the cornea by decorin and biglycan. J Biol Chem 284:8888-8897.

Zhang H, Apfelroth SD, Hu W, Davis EC, Sanguineti C, Bonadio J, Mecham RP, Ramirez F. 1994. Structure and expression of fibrillin-2, a novel microfibrillar component preferentially located in elastic matrices. J Cell Biol 124:855-863.

Zhang H, Hu W, Ramirez F. 1995. Developmental expression of fibrillin genes suggests heterogeneity of extracellular microfibrils. J Cell Biol 129:1165-1176.

Zhang J, Upadhya D, Lu L, Reneker LW. 2015. Fibroblast growth factor receptor 2 (FGFR2) is required for corneal epithelial cell proliferation and differentiation during embryonic development. PLoS One 10:e0117089.

Zhao J, Wang S, Zhong W, Yang B, Sun L, Zheng Y. 2016. Oxidative stress in the trabecular meshwork (Review). Int J Mol Med 38:995-1002.

Zhu H, Mitsuhashi N, Klein A, Barsky LW, Weinberg K, Barr ML, Demetriou A, Wu GD. 2006. The role of the hyaluronan receptor CD44 in mesenchymal stem cell migration in the extracellular matrix. Stem Cells 24:928-935.

Zieske JD. 2004. Corneal development associated with eyelid opening. Int J Dev Biol 48:903-911.